CO_2 Capture by Aqueous Absorption

Summary of 1st Quarterly Progress Reports 2008

Supported by the Luminant Carbon Management Program
and the
Industrial Associates Program for CO_2 Capture by Aqueous Absorption

by Gary T. Rochelle
Department of Chemical Engineering
The University of Texas at Austin
April 20, 2008

Introduction

This research program is focused on the technical obstacles to the deployment of CO_2 capture and sequestration from flue gas by alkanolamine absorption/stripping and on integrating the design of the capture process with the aquifer storage/enhanced oil recovery process. The objective is to develop and demonstrate evolutionary improvements to monoethanolamine (MEA) absorption/stripping for CO_2 capture from coal-fired flue gas. The Luminant Carbon Management Program and the Industrial Associates Program for CO_2 Capture by Aqueous Absorption support 12 graduate students. These students have prepared detailed quarterly progress reports for the period January 1, 2008 to March 31, 2008.

Conclusions

Ethylenediaminetetraacetic acid (EDTA) effectively inhibits oxidative degradation of MEA.

Formaldehyde, acetaldehyde, glyoxal, and hydroxyacetaldehyde have been qualitatively identified in degraded MEA samples using UV detection at 365 nm.

8 M PZ absorbs CO_2 2 to 3 times faster than 7 m MEA.

Elevated viscosity (10 cP) increases the pressure drop and reduces the capacity of Sulzer Mellapak 250Y structured packing. However, it does not affect the effective wetted area.

The effective area of Mellapak 500Y was 15 to 20% greater at low surface tension (~30 dynes/cm) than at high surface tension (~72 dynes/cm).

A pilot plant run with 35% MEA was successfully simulated in RateSep™ using Hilliard's new equilibrium package for MEA. The stripper packing height was adjusted to 5 feet from its real value of 20 feet.

A three-stage flash with solar heating was shown by an Aspen Plus® model to be effective in regenerating an optimized MEA system, giving an equivalent work requirement of 24.5 kJ/gmol CO_2 with compression to 5000 kPa.

Continuous crystallization of potassium sulfate from loaded MEA solution produces large particles of 100 to 250 microns with only 3 to 20 minutes of residence time.

8 m piperazine oxidizes readily to ethylenediamine and formate with 4 mM Cu^{++}. This reaction is effectively stopped by inhibitor A.

8 m piperazine does not oxidize when catalyzed by dissolved iron, chromium, or nickel.

Negligible degradation of 8 m PZ occurs at 135 and150°C. At 175°C measurable degradation results in a significant concentration of formate.

CO_2 solubility in 8 m PZ follows the same correlation with CO_2 loading as Hilliard found with lower PZ. The CO_2 capacity of 8 m PZ should be 1.7 times greater than 7 m MEA.

Piperazine volatility in 8 m PZ follows same correlation with CO_2 loading and total piperazine as Hilliard found at lower PZ. Lean 8 m PZ (0.3 moles CO_2/equiv PZ) should have about 30 ppm of PZ volatility at 40°C.

In the ERCOT utility grid of Texas, CO_2 capture would need to be turned off only 90 hours/year to meet the peak demands for power and save the construction of 4400 MW of capacity to replace the power demand of a total deployment of post-combustion capture.

Thermal degradation of MDEA/PZ (7 m/2 m) occurs at 135°C, with more rapid degradation occurring at 150°C. Within two weeks, over 96% of PZ mass degraded in the presence of MDEA.

1. Oxidative Degradation of Amines *p. 9*

by Andrew Sexton

Aqueous amine solutions were batch loaded into glass jacketed reactors and subjected to oxidative degradation via a high gas flow and low gas flow degradation apparatus. Solutions were degraded in the low gas flow apparatus using 100 mL/min of a 98% O_2/2% CO_2 saturated gas mixture in which mass transfer was achieved by vortexing. Liquid samples were withdrawn from the reactor during the course of the experiment; the samples are analyzed for degradation product formation using anion chromatography and amine losses using cation chromatography. The high gas flow degradation apparatus employed 7.5 L/min of an air/2% CO_2 mixture diluted with N_2 to achieve 15% O_2; oxygen mass transfer in this apparatus takes place by sparging the saturated gas mixture through the solution and by vortexing. A Fourier Transform Infrared Analyzer collects continuous gas-phase data on amine volatility and volatile degradation products.

Anion chromatography analysis on the low gas flow degradation experiment using EDTA as a degradation inhibitor for MEA (catalyzed by iron) yielded promising results. The rate of formation for all anionic species is 0.01 mM/hr or less, and total amine analysis using cation chromatography shows negligible amine losses. However, it is still unknown whether EDTA itself degrades. It is possible that the unknown peak using anion chromatography is a degradation product of EDTA and not MEA – most likely ED3A, EDDA, or EDMA.

In the high gas flow apparatus, MEA losses were approximately 20% for the MEA/Fe/Cu experiment and 30% for the MEA/Fe experiment. This is striking because the degraded MEA/Fe/Cu samples contained greater concentrations of carboxylic acid products. Both of these experiments had some control issues that were still being fixed at that time, so they will both be run again in the next quarter to verify these findings. In the low gas flow apparatus, the addition of formaldehyde or formic acid has a minimal effect on MEA losses. Despite having very little formation of carboxylic acid products, the PZ/Fe solution lost 10% of its original amine concentration. I conclude that there are some volatile products and volatile amine losses that are unaccounted for.

Formaldehyde, acetaldehyde, glyoxal, and hydroxyacetaldehyde have been qualitatively identified in degraded MEA samples using UV detection at 365 nm. In the following quarters I will attempt to quantify the amount of aldehydes in the degraded amines.

2. Thermal Degradation *p. 23*

by Jason Davis

A Ph.D. research proposal has been prepared on thermal degradation of MEA. A number of contributions are expected from this work:

Reaction Kinetics: This project will measure the rates of thermal degradation of amines at stripper conditions and provide insight into the effects of steric hindrance, CO_2 reactivity, nitrogen pKa, and chain length on thermal degradation.

Analytical Methods: This project will help develop a new method for the detection of amines and their ionic degradation products using cation chromatography, and their non-ionic degradation products using HPLC.

Economics: This project will help better define the solvent make-up costs associated with the aqueous amine absorber/stripper system.

System Design: This project will offer engineering controls to reduce thermal degradation and will aid in the design phase in both solvent selection and overall design to balance energy, capital, and operating costs.

Environmental: This project will give some insight into the types and quantities of waste products associated with amine absorber/stripper systems and will allow for the quantification of their environmental impact.

3. Rate Measurements of 8 m PZ *p. 39*

by Ross E. Dugas

Six 8 m piperazine (PZ) rate experiments have been conducted using a wetted wall column at absorber conditions, 40 and 60˚C. Vapor-liquid equilibrium data, allowing for the calculation of CO_2 capacity, were also obtained using the wetted wall column. TheVLE results correspond well with previous VLE data of various aqueous piperazine solvents measured by Hilliard (2008). The 8 m PZ solvent has shown CO_2 mass transfer rates 200-300% higher than 7 m monoethanolamine (MEA) at absorber conditions. The CO_2 capacity of 8 m PZ has been shown to be about 75% greater than 7 m MEA at 40˚C.

4. Influence of Liquid Properties on Effective Mass Transfer Area of Structured Packing *p. 63*

by Robert Tsai
(Also supported by the Separations Research Program}

The influence of viscosity on the hydraulic performance of Sulzer Mellapak 250Y structured packing was measured. Viscosity was increased to approximately 14 cP via the addition of high molecular weight poly(ethylene oxide) – POLYOX™ WSR N750. Slightly elevated pressure

drops relative to the baseline were generally observed. Flooding onset occurred at lower gas F-factors, with the difference becoming more prominent at higher liquid loads. The enhanced viscosity resulted in greater liquid hold-up in the packing; measured values and trends corresponded well with literature data. The effective mass transfer area of Mellapak 250Y was also measured at around 14 cP and was not found to differ appreciably from the base case. Prior work has shown surface tension to have negligible influence as well, indicating that relatively coarse structured packings (250-series) are rather insensitive to fluid property variations. Hydraulic data for Mellapak 500Y were collected. As expected, pressure drop and hold-up were higher than with the 250Y packing. Finally, the effective area of Mellapak 500Y was re-evaluated at high (~72 dynes/cm) and low (~30 dynes/cm) surface tension. While measured values in both cases were greater than those previously reported, the effective area of the packing was still noticeably higher at the reduced surface tension.

5. Modeling Stripper Performance for CO_2 Removal *p. 77*

by David Van Wagener

This quarter focused on continuing two tasks. The first was creating an Aspen Plus® simulation to verify a recent pilot plant run with 35% MEA using a new thermodynamic model developed by Hilliard. Differences between the simulation values and pilot plant data were finally reconciled by implementing side duties in the column to account for heat loss. The five measured column temperatures were matched, and an estimated profile in between the measurements was imposed. The sump split and reboiler duty values were also varied to match plant data. In the final simulation, all of the measured data matched the simulation data within small error, and the calculated heat loss was only 12% greater than the calculated heat loss at the plant. The second stripper task was to investigate flashing stripping as a means of using solar energy to provide the heat for liberating CO_2. The selected solvent was 9 m MEA, and three flashes were used to adiabatically decrease the temperature and pressure and release vapor. A lean stream with a specified loading was used in a previous absorber model to calculate the accompanying rich stream. By varying the temperature step between each flash, the loading of the outlet lean stream was able to be matched to the absorber model specification. Next, the hot temperature was optimized to find the minimum equivalent work for that lean loading. Finally, the lean loading was optimized to further minimize the equivalent work. The minimum equivalent work when compressing the CO_2 to 5000 kPa was 24.47 kJ/mol CO_2. The optimum lean loading was 0.424. In the following quarter, the three stage flash will be further analyzed with new specifications, ensuring equal mole flow in all three vapor streams leaving the flash tanks.

6. CO_2 Absorption Modeling Using Aqueous Amines *p. 89*

by Jorge M. Plaza

Previous work on an absorber model for MEA that incorporates the new thermodynamic model by Hilliard (2008), was continued to obtain kinetic constants in Aspen Plus® in agreement with values calculated assuming a negligible MEA concentration gradient across the liquid film (first order approximation). Forward rates for the formation of carbamate were obtained from the previously set up absorber model that simulates the conditions of the laminar jet used by Aboudheir (2002). Two approaches were used in an effort to troubleshoot the model. Initially, the Aspen regressed kinetic constant was compared to the number obtained directly from

Aboudheir. An additional analysis was done by comparing the flux of CO_2 from Aspen ($CO_{2\ in} - CO_{2\ out}$) and the value obtained using the first order approximation. Absorber and liquid film segmentation was analyzed as part of the troubleshooting effort.

It was determined that there was an error in the first order approximation related to the application of Henry's law for this system. Once this issue was corrected it was possible to obtain Aspen values in complete concordance with the first order approximation at 293 K. Nevertheless, at higher temperatures, Aspen results deviate again from the first order approximation by as much as 25% at 333K. The difference in values might be related to the use of Fick's law in the first order approximation in contrast with the use of Maxwell–Stefan correlations by Aspen which include the effect of other diffusing species in the determination of the flux of CO_2. Results of this analysis are presented in this report.

Additionally, during this period absorber temperature profiles were revisited in an effort to establish a general criterion relating the presence of the temperature bulge and the heat carrying capacity of the liquid and the gas. It was expected that when the bulge is located in the middle of the column the heat carrying capacity of the liquid is equal to the heat carrying capacity of the gas. It was also thought that the inflection point in the solvent capacity vs. lean loading curve was related to this equality in heat carrying capacities. Both of these hypotheses appear to not be correct and results available are still inconclusive.

7. Reclaiming by Crystallization of Potassium Sulfate *p. 101*

by Qing Xu

Potassium sulfate can be crystallized and separated from MEA/PZ solvent by the addition of potassium hydroxide. In this work continuous crystallization of potassium sulfate was conducted with 7 and 11 m MEA at 0.4 CO_2 loading, 8 m PZ at 0.3 CO_2 loading, and with SO_4^{-2}/K^+ in feed from 0.185 to 1. The experiments were conducted at 25, 40, and 60℃, with residence time of 3 min, 10 min, and 20 min, with two different agitators and two different agitation rates. Crystals were vacuum filtered and oven dried and the moisture content in the filter cake varied from 4 wt % to 34 wt %. The particle size distribution was measured by a laser scanner after filtration and desiccation. The mean volume particle size ranges from 110 μm to 260 μm with residence times of 3 to 20 min. SEM and light microscopy were used to analyze the crystal surface micro-morphology, particle size, crystal shape, and habit.

8. Degradation of Concentrated Piperazine *p. 113*

by Stephanie Freeman

Work this quarter focused on oxidative and thermal degradation of 8 m piperazine (PZ). Addition of 4.0 mM of copper was confirmed to catalyze degradation of PZ primarily producing formate, piperazine formamide, ethylenediamine (EDA), oxalate, and oxamide. Small concentrations of iron and vanadium, 0.1 mM each, did not catalyze PZ degradation to a significant degree. The addition of inhibitor A to 8 m PZ solution with copper and iron effectively inhibited the degradation catalyzed by copper. PZ showed appreciable degradation at 175°C while negligible degradation was observed at 135 and 150°C. Copper, iron, inhibitor A, nickel, and chromium do not further catalyze the thermal degradation of 8 m PZ at 175°C.

9. Thermodynamics of Concentrated Piperazine *p. 133*

by Bich-Thu Nguyen

This report presents (1) CO_2 solubility and (2) piperazine volatility data for the PZ-CO_2-H_2O system. CO_2 solubility, measured in terms of partial pressure, is explored as a function of temperature, loading, and amine concentration for systems ranging from 0.9 m up to 8.0 m PZ at temperatures of 40ºC, 60ºC, and 120ºC. New data are included for 8 m PZ. CO_2 partial pressure follows practically the same dependence on loading (mol CO_2/2*mol PZ) with all piperazine concentrations. These data are represented by the empirical equations: ln (P_{CO2}) = 18.54 - 8160.59*(1/T) + 22.32*(Loading) at 40ºC and 60ºC; and ln (P_{CO2}) = -1.12 + 28.82*(Loading) - 34.53*(Loading^2) at 120ºC due to the quadratic shape of the data. PZ partial pressure is higher with greater PZ concentration and with higher system temperature. PZ volatility decreases as CO_2 loading increases because free piperazine is converted to other species. PZ partial pressure is given by ln (P_{PZ}/[PZ]) = 6.73 – 4045.05*(1/T) – 4.21*(Loading).

10. Dynamic Operation of CO_2 Capture *p. 143*

by Sepideh Ziaii Fashami

This work focuses on rate-based dynamic modeling of the stripper with 30 % monoethanolamine in a flow sheet of Aspen Custom Modeler®. The rigorous model of one segment in the stripper is run in steady state mode successfully and the results looks reasonable, however it does not match exactly with simulation results from Aspen Plus® because the respective thermodynamic models do not predict the same CO_2 solubility. In addition a new strategy for on/off operation of CO_2 capture is proposed in which no amine inventory is needed and the dynamic behavior of the stripper can be studied independently.

11. System Level Implications of Flexible CO_2 Capture Operation *p.149*

by Stuart Cohen

To investigate the implications of flexible CO_2 capture, a system model was created to calculate the performance, economics, and CO_2 emissions in the Electric Reliability Council of Texas (ERCOT) grid for several operational strategies of flexible CO_2 capture. The model compares cases with no CO_2 capture and "always on" CO_2 capture with scenarios when capture is "off" during: 1) peak load hours every day of the year, 2) the entire season of system peak load, and 3) system peak load hours only on seasonal peak load days. Assuming installation of MEA absorption at all coal plants in ERCOT and using 2006 grid conditions, flexible operation prevents the need for over 4400MW of new capacity, which amounts to several billion dollars in capital cost savings. CO_2 capture must be "off" for only 99 hours throughout the year, resulting in a 52% system wide CO_2 emissions reduction that is within 1% of that achieved in the "always on" scenario. A system that must remain "off" for the entire peak load season will do so for 76 days, which still reduces emissions by 41%. Average generation costs rise by up to 38% for the "always on" scenario. Costs grow due to the added cost of CO_2 capture as well as the increased use of expensive natural gas generators to replace the base load capacity lost when CO_2 capture is "on." Flexible CO_2 capture is not shown to have a large effect on annual average generation costs or CO_2 avoidance costs, which are calculated as $44-$45 per metric ton of CO_2 in every scenario that uses CO_2 capture. A clear reserve margin specification is important from a policy standpoint because it can be used to define the threshold load above which CO_2 capture must be

"off." Future work will investigate tradeoffs between grid performance, economics, and CO_2 emissions when electricity price variation and CO_2 emissions costs are used to determine operational strategies for flexible CO_2 capture. Much of the results and analysis contained in this report have been submitted to the American Society of Mechanical Engineers 2nd International Conference on Energy Sustainability for dual peer review for publication in the ASME Conference Proceedings and the ASME Journal of Energy Resources Technology.

12. Oxidation-Reduction Potential and Thermal Degradation of MDEA/PZ *p. 165*

by Fred Closmann

In this quarter, we performed oxidation-reduction potential (ORP) experiments on ROC16 solution at a loading of 0.4 moles CO_2/mol PZ. The ORP studies were performed to establish baseline ORP response in PZ solutions under quiescent conditions, and in the presence and absence of reactor agitation and sparging with oxygen and nitrogen. The absence of nitrogen sparging and/or reactor mixing delays ORP response following rapid shutdown of oxygen. When the reactor was brought from a quiescent state to an oxygenated state in rapid fashion, the recovery (increase) of ORP was delayed in the absence of reactor mixing. Thermal degradation of MDEA/PZ (7 m/2 m) occurs at 135°C, with more rapid degradation occurring at 150°C. Within two weeks, over 96% of PZ mass degraded in the presence of MDEA. MDEA and PZ may degrade in an equimolal relationship when thermally degraded as a blended solvent.

Oxidative Degradation of Amines

Quarterly Report for January 1 – March 31, 2008

by Andrew Sexton

Supported by the Luminant Carbon Management Program

and the

Industrial Associates Program for CO_2 Capture by Aqueous Absorption

Department of Chemical Engineering

The University of Texas at Austin

April 18, 2008

Abstract

Aqueous amine solutions were batch loaded into glass jacketed reactors and subjected to oxidative degradation via a high gas flow and low gas flow degradation apparatus. Solutions were degraded in the low gas flow apparatus using 100 mL/min of a 98% O_2/2% CO_2 saturated gas mixture in which mass transfer was achieved by vortexing. Liquid samples were withdrawn from the reactor during the course of the experiment; the samples were analyzed for degradation product formation using anion chromatography and amine losses using cation chromatography. The high gas flow degradation apparatus employed 7.5 L/min of an air/2% CO_2 mixture diluted with N_2 to achieve 15% O_2; oxygen mass transfer in this apparatus takes place by sparging the saturated gas mixture through the solution and by vortexing. A Fourier Transform Infrared Analyzer collected continuous gas-phase data on amine volatility and volatile degradation products.

Anion chromatography analysis on the low gas flow degradation experiment using EDTA as a degradation inhibitor for MEA (catalyzed by iron) yielded promising results. The rate of formation for all anionic species is 0.01 mM/hr or less, and total amine analysis using cation chromatography shows negligible amine losses. However, it is still unknown whether EDTA itself degrades. It is possible that the unknown peak using anion chromatography is a degradation product of EDTA and not MEA – most likely ED3A, EDDA, or EDMA.

In the high gas flow apparatus, MEA losses were approximately 20% for the MEA/Fe/Cu experiment and 30% for the MEA/Fe experiment. This is striking because the degraded MEA/Fe/Cu samples contained greater concentrations of carboxylic acid products. Both of these experiments had some control issues that were still being fixed at that time, so they will both be run again in the next quarter to verify these findings. In the low gas flow apparatus, the addition of formaldehyde or formic acid had a minimal effect on MEA losses. Despite having very little formation of carboxylic acid products, the PZ/Fe

solution lost 10% of its original amine concentration. I conclude that there are some volatile products and volatile amine losses that are unaccounted for.

Formaldehyde, acetaldehyde, glyoxal, and hydroxyacetaldehyde have been qualitatively identified in degraded MEA samples using UV detection at 365 nm. In the following quarters I will attempt to quantify the amount of aldehydes in the degraded amines.

Introduction

This effort is an extension of work by George Goff on the oxidative degradation of MEA. Goff showed that oxidative degradation, under high catalyst conditions, is mass-transfer limited by the physical absorption of O_2 into the amine and not by reaction kinetics. Goff also theorized that the oxidative degradation of MEA produced volatile ammonia as well as a host of other degradation products. The major liquid-phase degradation products among these include the heat stable salts of carboxylic acids, nitrite, and nitrate.

The oxygen stoichiometry necessary to produce these degradation products varies for each individual component; overall, it varies anywhere from 0.5 to 2.5 (Goff, 2004). It is believed that the particular degradation products are specific to certain metal catalysts present in the absorption/stripping system – specifically iron and copper. For example, the following balanced reactions illustrate the differences in oxygen consumption based on the end products:

$$\text{MEA} + 1.5\ O_2 \rightarrow 2\ \text{Formate} + \text{Ammonia}$$
$$\text{MEA} + 3.5\ O_2 \rightarrow 2\ \text{Formate} + \text{Nitrate} + \text{Water}$$
$$\text{MEA} + O_2 \rightarrow \text{Glycolate} + \text{Ammonia}$$

Goff's work on MEA degradation was limited to analyzing MEA degradation rates via the evolution of NH_3. The ammonia evolution rates were measured using a Fourier Transform Infrared (FT-IR) analyzer.

This effort extends Goff's gas-phase analysis by applying various methods of liquid-phase analysis, specifically ion chromatography. These analytical methods will be used to quantify the rate of amine degradation as well as the rate of degradation product formation for amine systems.

Since most gas treating processes using alkanolamines for CO_2 removal are performed in the absence of oxygen, oxidative degradation is a source of solvent degradation that has not been properly quantified. Oxidative degradation is important because it can impact the environment, process economics, and decrease equipment life due to corrosion.

The environmental effects refer to the degradation products themselves: what is being produced, how much of it is being produced, and how can it be disposed of without doing significant damage to the environment. Process economics being impacted are the solvent make-up rate and design of the reclaiming operation. If amine is continually being degraded, then fresh amine must be continually added to the process at a significant cost. In addition, CO_2 loaded amine solutions corrode carbon steel equipment, which catalyzes oxidative degradation even further. It is imperative to quantify how much of this solvent make-up rate is due to oxidative degradation.

Experimental

As stated in prior reports, ion chromatography is the most extensively used liquid-phase analytical method. Anion chromatography utilizes an AS15 (a low-capacity column designed to separate low-molecular weight anions, specifically acetate, glycolate, and formate) IonPac column and an ASRS 4-mm self regenerating suppressor made by Dionex, while cation analysis uses a CS17 and a CSRS 4-mm self-regenerating suppressor. Anion analysis employs a linear gradient of NaOH eluent, while cation analysis uses a step-change from low to high concentration of methanesulfonic acid (MSA) eluent. Refer to prior quarterly reports for detailed descriptions of the Dionex ICS2500 and ICS3000 analytical equipment.

An analytical method has been developed to quantify amides, while analytical methods necessary to quantify concentrations of amino acids and aldehydes in solution are still being modified. While it is believed that anionic products makeup the majority of the amine oxidative degradation products, concentrations for these classes of compounds are needed to further close the material balance.

Aldehydes (specifically formaldehyde, acetaldehyde, glyoxal, and hydroxyacetaldehyde) can be detected using high pressure liquid chromatography (HPLC) with UV detection. These four aldehydes were chosen because they are the precursors to the four carboxylic acids identified using anion chromatography. Aldehyde compounds absorb at a UV wavelength of 200 nm; unfortunately, most classes of compounds absorb at this wavelength as well. In order to separate aldehydes so they can be identified properly, they must be derivatized with 2,4-dinitrophenylhydrazine (DNPH), also known as Brady's reagent. Aldehydes react with DNPH in a condensation reaction to form water and a structure known as a 2,4-dinitrophenylhydrazone. The 2,4-dinitrophenylhydrazone absorbs at a UV wavelength of 365 nm, which does not interfere with any other compounds in solution.

Per Nascimento et al. (1997), calibration standards are derivatized with DNPH and dissolved in acetonitrile. Undiluted experimental samples (4 mL) are derivatized with DNPH (1mL of 0.2 g DNPH dissolved in 100 mL of acetonitrile) and perchloric acid (50 μL), which is used to catalyze the reaction between DNPH and the aldehydes in solution. All calibration standards are diluted from the stock standards using a solution of 45% EtOH/55% H_2O (by volume). Aldehyde analysis is performed on a Waters HPLC (with autosampler) using a Shimadzu C-18 column. The UV lamp is set to detect at a wavelength of 365 nm. An isocratic eluent of 65% methanol/35% water set at 1.0 mL/min for 10 minutes is used to separate the derivatized aldehydes. Post-injection sample analysis is performed using the Xcalibur software package.

Amino acids (specifically glycine and bicine) are detected using an ED electrochemical detector installed on the previously mentioned Dionex ICS3000. The method employs a series of AminoPac PA10 columns with a gradient profile of water/sodium hydroxide/sodium acetate at flowrate of 0.25 mL/min. The cell in the electrochemical detector is a conventional fixed gold electrode, and a waveform using pulsed amperometry is applied to the electrode.

Amides are a class of compounds that were detected in an HPLC-MS screening performed by the Hunstman Chemical analytical department. Amides are formed from

the condensation reaction of an amine with a carboxylic acid. Since both of these species are known to exist in appreciable quantities in degraded amine solutions, it is conceivable that amides are present. Amides can be detected using HPLC with UV detection, but amides absorb at 200 nm, thus making it difficult to separate them from other species in the solution.

Koike et al. (1987) concluded that the addition of excess NaOH was successful at reversing the amide formation reaction back to amine and carboxylic acid. This hypothesis was tested using various concentrations of sodium hydroxide reacted with formamide and N-(hydroxymethyl)acetamide. It was concluded that reacting 1g of sample with 1g of 5 M NaOH at 25^{o}C and allowing the solution to sit for twenty-four hours was sufficient to reverse the amide reaction. Using the anion IC procedure detailed previously, all experimental samples were analyzed pre- and post-addition of NaOH to determine carboxylic acid and amide concentrations. All amide concentrations (as calculated by the difference between the carboxylic acid concentrations prep- and post-NaOH addition) will still be reported as carboxylic acids.

As stated in previous reports, amine solutions in the low gas flow degradation apparatus are oxidized for 12 to 14 days in a low-gas flow jacketed reactor at 55^{o}C. The solutions are agitated at 1400 RPM to produce a high level of gas/liquid mass transfer by vortexing. 98% O_2/2% CO_2 at 100 ml/min is introduced across the vortexed surface of 350 ml of aqueous amine. Samples were taken from the reactor at regular intervals in order to determine how degradation products formed over the course of the experiment. Prior quarterly reports provide a detailed explanation of the low gas flow degradation apparatus.

Four versions of the low gas flow apparatus are now operating in parallel. Two systems operate via the original configuration, which uses an inlet gas of 98% O_2/2% CO_2 premixed in a cylinder provided by Matheson Tri-Gas. A Cole-Parmer rotameter is used to control the flowrate at 100 mL/min. The other two are setup for the modified configuration, which operates with two separate cylinders provided by Matheson Tri-Gas – a pure oxygen cylinder and a pure CO_2 cylinder. The 98% O_2/2% CO_2 mixture is achieved using a 4 channel Brose box made by Brooks and two model 5850E mass flow controllers also manufactured by Brooks. In one setup (Channels 1 and 2), oxygen flowrate is controlled by a 100 cc flow controller, while carbon dioxide is controlled by a 20 cc flow controller. The other setup employs a 250 cc oxygen mass flow controller and a 5cc CO_2 mass flow controller. The control box displays a digital readout corresponding to the % open of the valve on the mass flow controller. The valve % open corresponds to a gas flowrate, which is determined from the calibration curve constructed for each flowmeter.

The original setup is limited by the fact that the partial pressure of CO_2 over the top of the amine solution entering low gas flow apparatus is fixed. Therefore, the loading of each amine solution is fixed and corresponds to 2% CO_2 concentration in the vapor space above the amine solution. The modified setup allows for variations in the CO_2 concentration such that a particular loading in the amine solution can be achieved by adjusting the incoming CO_2 concentration via the flow controllers. Amine loading has become a variable, whereas in the past it was constrained.

Experiments are performed in the high gas flow degradation apparatus by sparging gas through an agitated amine solution in a temperature controlled semi-batch reactor. Reaction gas, consisting of a mixture of house air, nitrogen, and CO_2 is bubbled through water to presaturate the gas before it is sparged through the amine solution in order to minimize water losses in the reactor.

A Parr 1108 Oxygen Combustion Bomb serves as the water presaturator. A 1/8" stainless steel tube on the inside of the presaturator carries the gas mixture into the water reservoir ¼" above the bottom of the presaturator bomb. The gas bubbles through the heated water and out the presaturator bomb. The bomb and its contents are kept at 55^{o}C in a water bath heated by a Lauda Econoline E-100 Series Heating Circulator.

Water level in the presaturator is controlled using a series of Masterflex peristaltic pumps. The inlet pump is a ColeParmer Masterflex Model 7520-50 (range 1-100 RPM). Affixed to the pump is a Masterflex Model 7013-20 pump head. Distilled, deionized water from the Millipore Direct-Q 3 system is contained in an atmospheric reservoir located on top of the inlet pump. The water is pumped into the presaturator through Masterflex 6409-13 Tygon tubing (0.03" ID) at a flowrate of 1 mL/min. This exceeds the rate at which water evaporates from the presaturator, ensuring dry gas will not be sent to the reactor, causing an evaporative cooling effect.

A ColeParmer Masterflex Model 7521-40 (range 6-600 RPM) with an Easy-Load II variable speed drive (Model 77200-50) serves as the outlet pump motor. Affixed to the pump is a Masterflex Model 7016-20 pump head threaded with Masterflex Model 6409-16 Tygon tubing (0.123" ID). The outlet pump is set at a flowrate of 2 mL/min; the outlet flowrate is set at twice the inlet flowrate to ensure that the presaturator does not flood and send water directly to the reactor.

A ¼" stainless steel tube extends 1" down from the top of the presaturator into the reservoir. If the water level in the presaturator is below the bottom of the tube, the outlet pump will only pull the reaction gas mixture at 2 mL/min out of the bomb. Once the water level reaches the bottom of the tube, the outlet pump will begin to pull water out of the reservoir and keep the level in the presaturator bomb constant.

The outlet pump carries the gas/water mixture into a 500 cc flash tank (16 cm OD, 30.5 cm height). Any entrained water drops to the bottom of the tank through a U-tube (¼" ID) and a gate valve, which is cracked open. Static pressure from the water level slowly forces the water through the U-tube and out the valve, where the water falls back into the DDI reservoir. Reaction gas exits the top of the tank and flows through ¼" PE tubing (max 150^{o}F, 120 psig) to a Swagelok tee, where it recombines with saturated gas exiting the presaturator on its way to the reactor.

Temperature is continuously monitored throughout each high gas flow experiment using PicoLog software, and the temperature of the heat baths are adjusted to keep the reactor at a constant temperature of 55^{o}C. Temperature in the jacketed reactor is kept constant using an IsoTemp 3016H temperature bath manufactured by Fisher Scientific International. The heat transfer fluid is dimethyl silicone oil (50 cSt viscosity) purchased from Krayden, Inc. Temperature is controlled within ± 1^{o}C by monitoring the temperature with a PT-100 immersion probe (Class B, 4x150 mm) connected to PicoLog Recorder software (Version 5.13.9) through a PT-104 converter. For this system, in

order to maintain a reactor temperature of 55°C, the temperature bath and presaturator bath are set at a temperature of approximately 63°C (depending on ambient conditions).

Results

Several experiments were conducted using the low gas flow apparatus during the first quarter of 2008. However, using the methods described in the prior section, ion chromatography analysis has been completed on only one low gas flow experiment (MEA/Fe/EDTA). All experiments, listed below, were conducted at 55°C and 1400 RPM and kept at a constant loading using 100 mL/min of a saturated 98% O_2/2% CO_2 gas mixture.

1. 7 m MEA/1 mM Fe/100 mM EDTA (α = 0.40)
2. 3 m EDA (Ethylenediamine)/1 mM Fe (α = 0.30)
3. 3 m EDA/5 mM Cu (α = 0.30)
4. 2.5 m Potassium Glycinate/1 mM Fe (α = 0.40)
5. 2.5 m Potassium Glycinate/5 mM Cu (α = 0.40)

The two sets of experiments using solvents other than MEA were chosen for the purpose of understanding how chemical structure affects susceptibility to oxidative degradation. As has been stated several times before, MEA is an alkanolamine. It has a two-carbon backbone with a hydroxyl group attached at one end and an NH_2 group on the other end. EDA and glycine are two compounds that are structurally similar to MEA.

EDA is a diamine; the hydroxyl group on the α-carbon of the MEA structure is replaced with a second NH_2 group. Because the hydroxyl group is absent from this structure, it is unknown if EDA will degrade into the same sets of intermediates and degradation products as MEA. A concentration of 3.5 molal EDA, loaded to 0.3 mol CO_2/mol EDA, was chosen as a baseline concentration for these experiments.

Glycine is an amino acid; the hydroxyl group of MEA is oxidized to a carboxylic acid functional group while the rest of the structure remains the same. Literature from van Holst (2006) proposes that salts of amino acids are an attractive alternative for CO_2 capture. Sorensen (1998) states that the degradation products of glycinate in the presence of UV and H_2O_2 are glyoxylate, oxalate and formate – at concentrations very close to the minimum detection limit. A 2.5 molal potassium glycinate solution was created using glycine, potassium carbonate, and potassium hydroxide. 1 molal of potassium carbonate was initially dissolved in water. Potassium hydroxide was then added to achieve a concentration of 2.5 molal of potassium ion in solution. Last, 2.5 molal of glycine is dissolved in the mixture, resulting in a 2.5 molal potassium glycinate solution with a loading of 0.4 mol CO_2/mol glycine. Complete liquid phase analysis results for the EDA and potassium glycinate experiments are ongoing and will be included in the next quarterly report.

The MEA low gas flow experiment was conducted because EDTA (ethylenediaminetetracetic acid) has been identified by Blachly and Ravner (1967) and Goff (2005) as an excellent chelating agent. Due to its unique structure, EDTA has four active sites that can react with metals in solution and effectively bind the metal ions, thereby preventing them from catalyzing free radical reactions that promote oxidative degradation. A 1:1 ratio of EDTA:Fe was typically used by Goff, but a 100:1 ratio of EDTA:Fe (representing excess EDTA) was chosen for this experiment.

Figure 1 illustrates the accumulation of degradation products for the MEA/Fe/EDTA experiment. The only detectable oxidative degradation products are formate, nitrite, glycolate, and acetate; glycolate and acetate were detected only after the NaOH derivatization method was performed on the degraded samples. The total formate production rate (formate + formate-MEA amide) is 0.01 mM/hr, while nitrite, glycolate, and acetate production rates are two orders of magnitude lower than that.

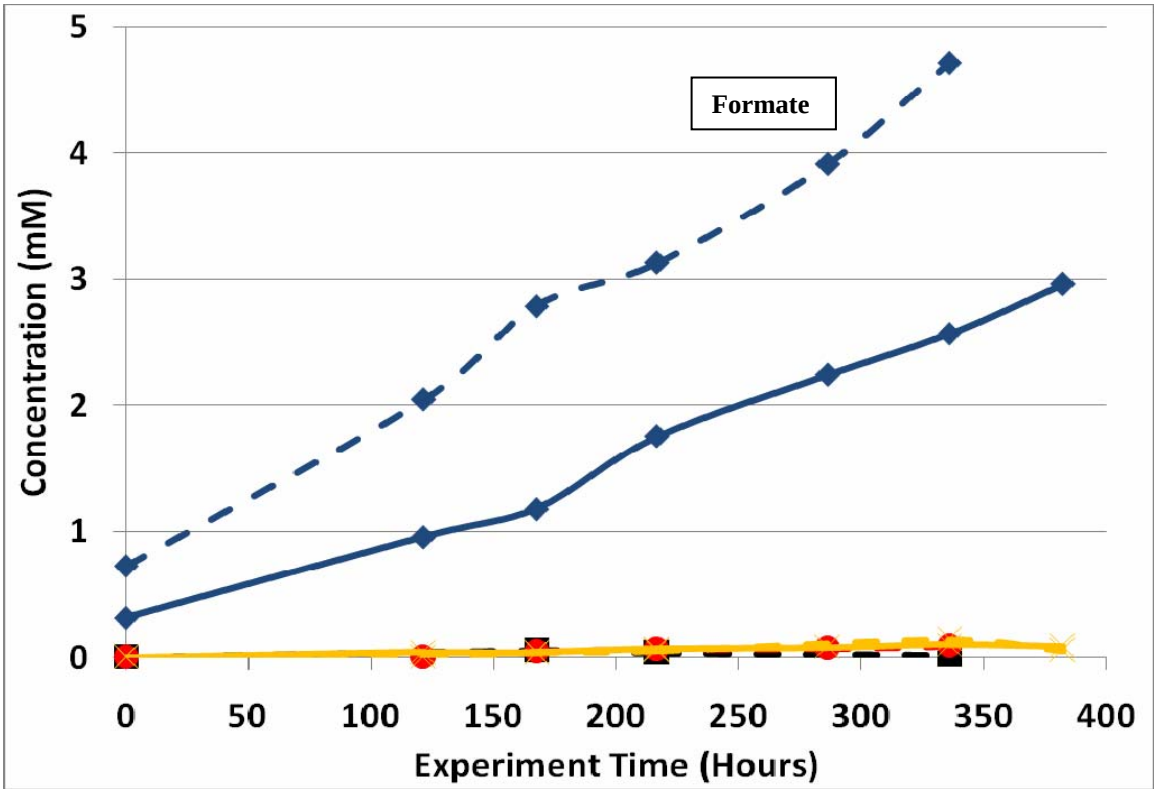

Figure 1: Oxidative Degradation Products of 7 m MEA/1 mM Fe/100 mM EDTA

While the formation of identifiable degradation products is minimal, there is an unknown anion peak that elutes at a retention time of 26.7 minutes, after carbonate but before sulfate. Sorensen (1998) identified iminodiacetic acid (diglycine), glyoxylic acid, and cyanate as anionic degradation products of EDTA in the presence of UV and H_2O_2. All of these anions were tested at the unknown peak, and came back negative. However, Sorensen also states that in oxidation processes where iron is present, EDTA can degrade into ethylenediaminetriacetate (ED3A), ethylenediaminediacetate (EDDA), and ethylenediaminemonoacetate (EDMA). Those compounds are currently being acquired for testing.

It is also important from a cost standpoint to determine if EDTA is being oxidized. EDTA is an expensive additive – an order of magnitude more expensive than MEA, in fact. Even if EDTA is being oxidized very slowly, the cost of continually adding EDTA to a commercial system outweighs its benefits as an amine oxidation inhibitor. EDTA does give a peak using anion chromatography, but it has a very strong response. Concentrations exceeding 25 ppm of EDTA do not give an increased area response using the current method. Therefore, samples containing EDTA will have to be diluted by a factor of 1,000X to 10,000X in order to properly quantify it.

In addition, the 7 m MEA/1 mM Fe high gas flow degradation experiment conducted during the third quarter of 2007 was analyzed using anion chromatography after NaOH derivatization to account for amide concentrations. The experiment was carried out at a temperature of 55°C and an agitation rate of 1400 RPM. A loading of 0.4 was achieved using 7.5 L/min of an air/N_2/CO_2 mixture. Figure 2 illustrates product concentrations as a function of time for the MEA/Fe high gas flow experiment. Both the formate and oxalate amides of MEA are present in greater quantities than formic acid and oxalic acid, respectively. With the exception of formate, all ionic degradation products were observed in concentrations of 6 mM or less at the end of the experiment.

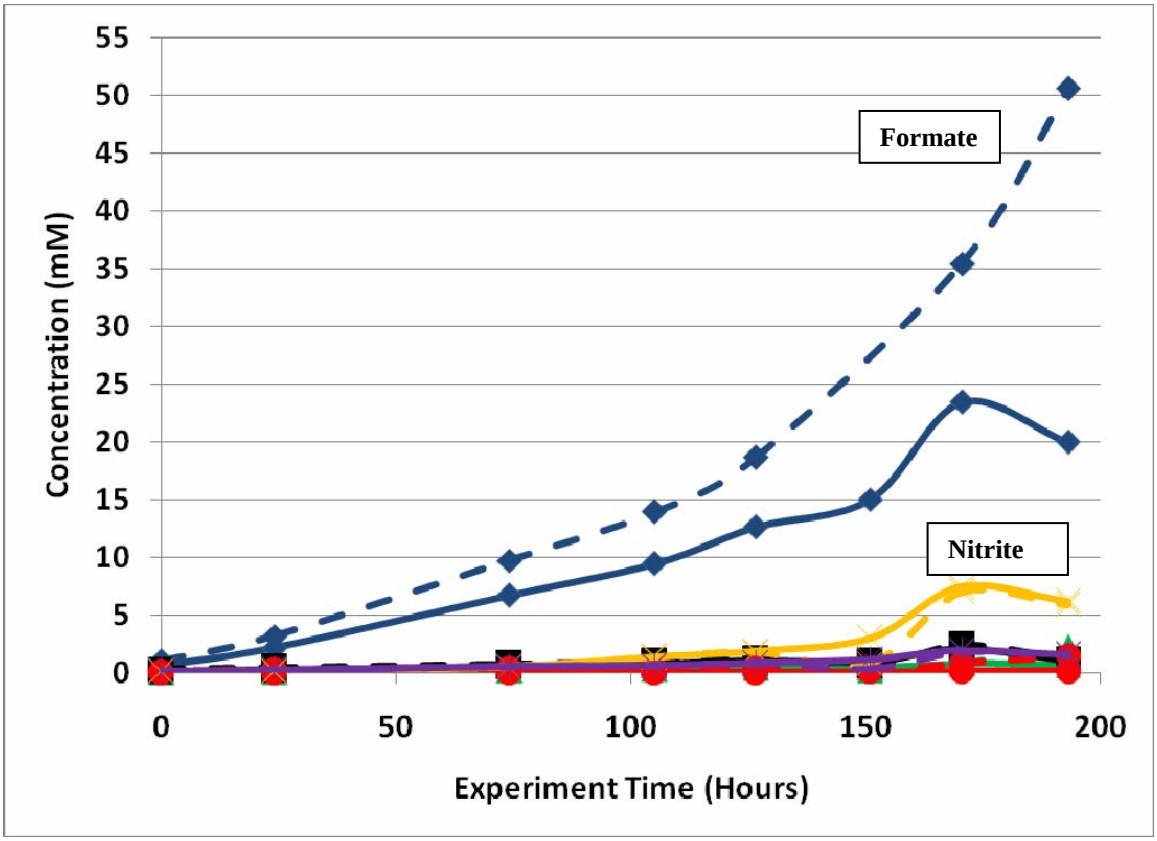

Figure 2: Oxidative Degradation Products of 7 m MEA/1 mM Fe (High Gas)

Table 1 lists rates of formation of liquid-phase oxidative degradation products for the two long-term high gas flow experiments conducted last year. After NaOH was added to all samples taken during these experiments, re-analysis revealed an increase in formate and oxalate concentration, represented by amides formed from the reaction of MEA with formic and oxalic acid. The nitrogen balance is similar for both experiments; since the NO_x is being stripped out from the high gas flow degradation apparatus, the formation of nitrite and nitrate is minimal. However, formate and total carbon formation in the liquid phase is approximately 5X higher in the experiment where 5 mM copper is added.

Table 1: Total Product Rates for 7 m MEA High Gas Flow Degradation Experiments

Iron Conc. (mM)	1		0.1	
Copper Conc. (mM)	-		5	
NaOH Addition	No	Yes	No	Yes
Formate	0.100	0.257	0.455	1.237
Carbon	0.117	0.299	0.513	1.417
Nitrogen	0.039	0.037	0.051	0.043

Using cation chromatography, as discussed in the methods section, amine losses were quantified for several experiments (six MEA experiments and one PZ experiment). Table 2 below tabulates those results, which are reported as % amine loss from the initial sample to the final sample. All samples were treated with NaOH prior to analysis in order to reverse any amide formation back to amine and carboxylic acid so that all amine could be properly accounted for. After amine losses were quantified the first time, the process was repeated a second time to verify the initial results.

In the high gas flow apparatus, the MEA/Fe experiment experienced more MEA losses than the MEA/Fe/Cu experiment, despite having a lower formate and total carbon formation rate in the gas phase. For the low gas flow experiments, the addition of formaldehyde and formic acid did not appear to have much of an effect on the amount of MEA that was preserved during the experiment. However, the addition of 100 mM EDTA kept MEA losses at 4% or lower over the course of a two week experiment. Despite seeing very little formate production, the PZ/Fe low gas flow degradation experiment showed 10% amine losses over two weeks. One possible explanation for the piperazine disappearance is volatile losses.

Table 2: Total Amine Losses from Oxidative Degradation Experiments

Experiment	% Amine Loss	
	Run 1	Run 2
7m MEA/0.1mM Fe/5mM Cu (High Gas	20.7%	18.0%
7m MEA/1mM Fe (High Gas)	30.7%	32.1%
7m MEA/1mM Fe/0.5M Formaldehyde	39.9%	36.1%
7m MEA/1mM Fe/0.5M Formic Acid	26.0%	26.1%
7m MEA / 1mM Fe	36.0%	36.0%
7m MEA/1mM Fe/100mM EDTA	4.2%	1.7%
5m PZ / 5mM Fe	10.8%	10.5%

In an attempt to understand amide formation in the oxidative degradation process, the final sample from every oxidative degradation experiment conducted since 2004 was pulled from the refrigerator and analyzed for anionic degradation products pre and post-NaOH derivatization. For MEA, PZ, and blended MEA/PZ degradation experiments, the amides of formic, acetic, glycolic and oxalic acids with MEA and PZ were detected. In the case of AMP, the amide of glycolic acid with AMP was not detected using the established analytical method; only the amides of formic, acetic, and oxalic acids with

AMP were present. The amides of formic and oxalic acid with amine were the most abundant. On average, the amide of formic acid with amine was just as abundant as formic acid for all amine systems, while the amide of oxalic acid was present in quantities anywhere from equal to oxalic acid concentration to 3X the oxalic acid concentration detected. These results further illustrate the need to continue performing the NaOH treatment to all oxidatively degraded samples.

Significant progress was made in developing the aldehyde analysis method. Calibration curves have been generated for acetaldehyde and formaldehyde by injecting derivatized aldehyde-DNPH using UV detection at a wavelength of 365 nm. The detection limit for both aldehydes is approximately 100 ppm, so a five point calibration curve ranging from 0 ppm to 100 ppm was generated for acetaldehyde and formaldehyde. Figures 3 and 4 show 100 ppm standards of formaldehyde-DNPH and acetaldehyde-DNPH, respectively. Note: All peak areas are reported in units of micro absorbance units (μAU) *min.

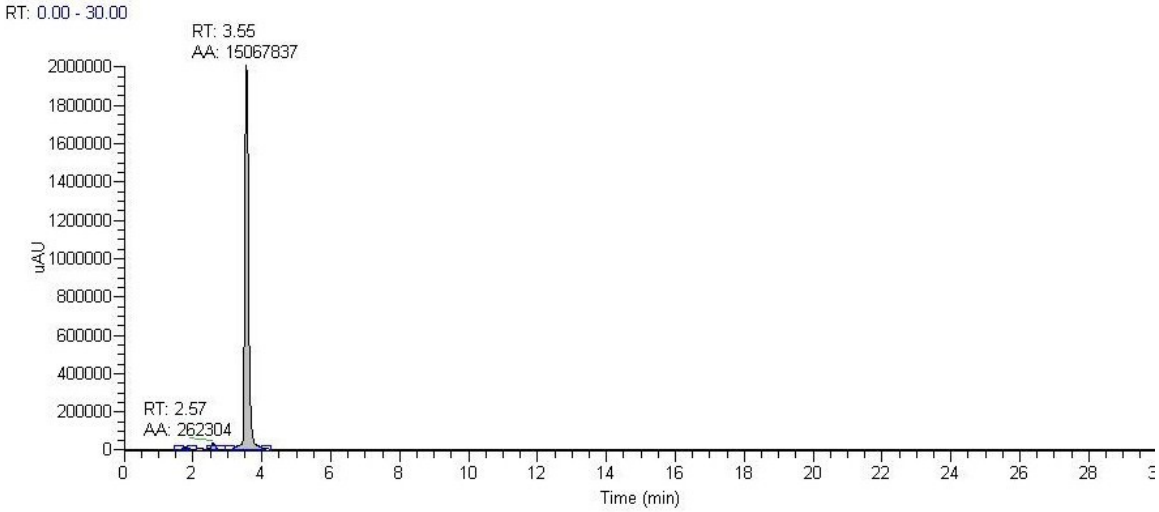

Figure 3: 100 ppm Standard of Formaldehyde-DNPH Detected at 365 nm

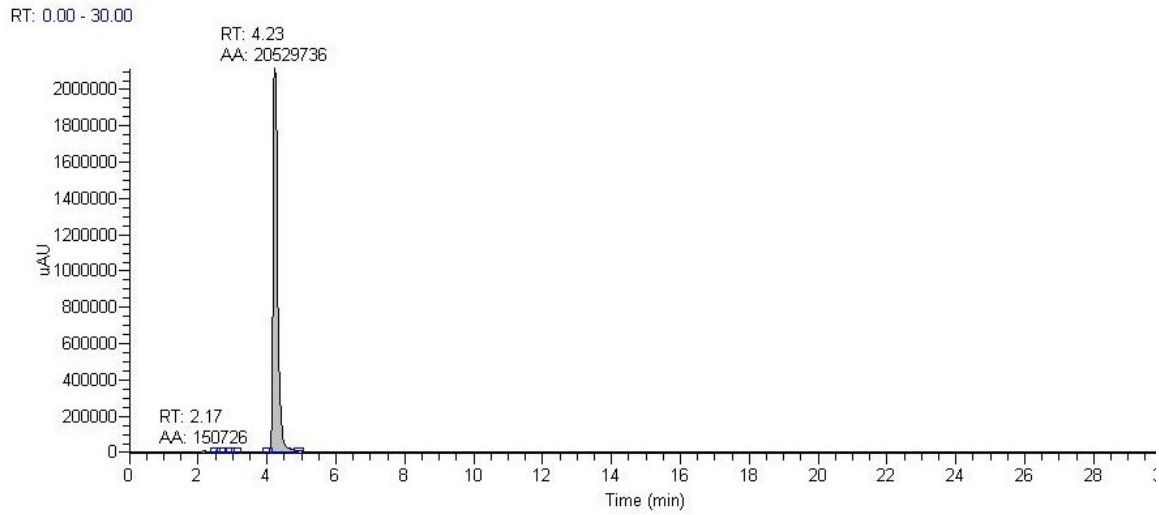

Figure 4: 100 ppm Standard of Acetaldehyde-DNPH Detected at 365 nm

Figures 5 and 6 below show UV analysis for two experiments: Figure 5 shows a UV chromatogram at 365 nm for the MEA/Fe/Formaldehyde low gas flow degradation experiment, while Figure 6 illustrates a UV chromatogram for the MEA/Fe/Cu experiment conducted in the high gas flow apparatus in November 2007. In Figure 5, formaldehyde and glyoxal (the precursors to formic acid and oxalic acid) were identified by adding known quantities of both to the degraded sample. In Figure 6, hydroxyacetaldehyde and acetaldehyde (precursors to acetic acid and glycolic acid) were identified as degradation products using the same method.

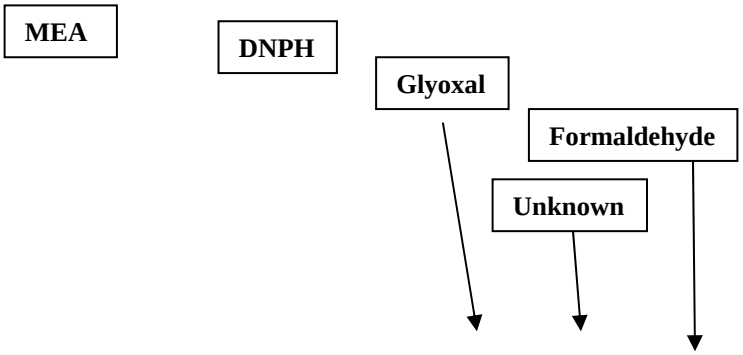

Figure 5: UV Detection of Aldehydes from Degraded MEA/Fe/Formaldehyde

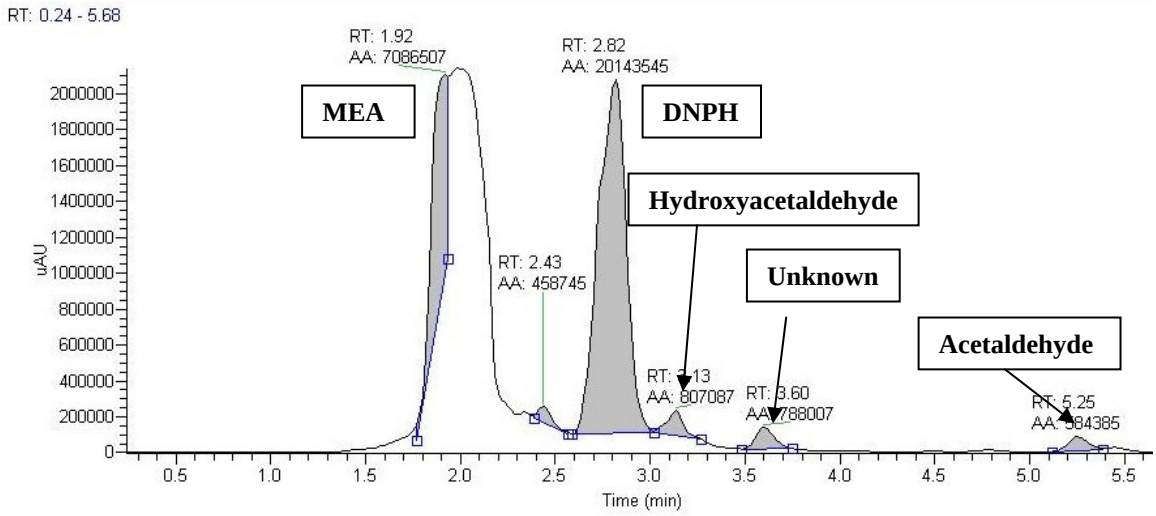

Figure 6: UV Detection of Aldehydes from Degraded MEA/Fe/Cu

In both of the samples, there is an unknown aldehyde peak that appears at approximately 3.60 minutes. The large peak at a retention time of 1.92 minutes is believed to be DNPH-derivatized amine, while the peak at 2.82 minutes is believed to be derivatized acetonitrile or excess DNPH originally added to derivatize the sample. Using the same methods, hydroxyacetaldehyde and glyoxal were qualitatively identified for the MEA/Fe/Formic Acid experiment, while glyoxal and formaldehyde were identified for

the MEA/Fe high gas flow experiment. The derivatized final sample for the EDA/Fe experiment showed no aldehydes to be present in solution.

Minimal progress was made with the amino acid analysis method. Glycine and bicine have maximum detection limits around approximately 30 ppm. Therefore, five point calibration curves were constructed between 0 and 30 ppm for both substances. Diluted final samples were run for several experiments, and it appears that there is a broad peak at a retention time of 6.2 minutes, which is where glycine appears in the calibration standards. However, the peak appears to be at the maximum detection limit because known addition of glycine does not produce any additional peaks, yet does not increase the area of the peak believed to be glycine. Therefore, experimental samples need to be diluted by a factor of 1,000X to 5,000X (instead of 100X, which was tried for previous samples) in order to produce a dilute glycine concentration well below the limits of the electrochemical detector.

Conclusions and Future Work

Anion chromatography analysis on the low gas flow degradation experiment using EDTA as a degradation inhibitor for MEA (catalyzed by iron) yielded promising results. The rate of formation for all anionic species is 0.01 mM/hr or less, and total amine analysis using cation chromatography shows negligible amine losses. However, it is still unknown whether EDTA itself degrades. It is possible that the unknown peak using anion chromatography is a degradation product of EDTA and not MEA – most likely ED3A, EDDA, or EDMA. A larger dilution factor will be used on the anion IC samples to ensure that EDTA concentration in the diluted samples does not exceed the IC detection limit. Since EDTA is so costly, another MEA/Fe/EDTA degradation experiment will be run where a 1:10 ratio of Fe:EDTA will be tested. If a lower concentration of EDTA can achieve the same results, it may be more preferred as a chelating agent in inhibiting degradation.

NaOH derivatization of the MEA/Fe/Cu high gas flow experiment showed significant amounts of MEA-formate and MEA-oxalate amides were present in solution, reinforcing a conclusion that was reached in the last quarter. In both the low and high gas flow degradation apparatus, formate concentration increased by anywhere from a factor of 2 to 4, while oxalate concentration typically increased by a factor of 10. This means that N-formyl MEA is present in solution in similar or greater quantities than formic acid, and oxalic acid amide concentration is an order of magnitude greater than oxalic acid concentration in the analyzed degraded amine solutions. Acetic acid amide and glycolic acid amide are present as well, but in extremely low concentrations.

A suitable method for determining amine concentration in degraded MEA samples has developed using cation chromatography. Water balance issues, which are extremely important in determining amine concentration, have been resolved by analyzing degraded amine solutions for sulfate concentration using anion chromatography analysis. All copper and iron are added to the solutions in the form of inorganic sulfate salts. Since no sulfur is added during the course of the experiment, sulfate concentration should remain the same throughout the experiment and serve as a tracer. Therefore, any fluctuations in sulfate concentration are attributed to changes in water content, and concentrations are adjusted accordingly.

In the high gas flow apparatus, MEA losses were approximately 20% for the MEA/Fe/Cu experiment and 30% for the MEA/Fe experiment. This is striking because the degraded MEA/Fe/Cu samples contained greater concentrations of carboxylic acid products. Both of these experiments had some control issues that were still being fixed at that time, so they will both be run again in the next quarter to verify these findings.

In the low gas flow apparatus, the addition of formaldehyde or formic acid has a minimal effect on MEA losses. This leads me to believe that over the long term neither protects MEA from oxidative degradation. Despite having very little formation of carboxylic acid products, the PZ/Fe solution lost 10% of its original piperazine over the course of the experiment. I conclude that there are some volatile products and volatile amine losses in the low gas flow apparatus that are unaccounted for.

Formaldehyde, acetaldehyde, glyoxal, and hydroxyacetaldehyde have been qualitatively identified in degraded MEA samples using UV detection at 365 nm. In the next quarters I will attempt to quantify the amount of aldehydes in the degraded amines. Since derivatized glyoxal-DNPH and hydroxyacetaldehyde-DNPH do not appear to be commercially available, I may have to make my own standards.

Next quarter, I plan to continue my work on the oxidative degradation of various amine systems (under varying catalyst and inhibitor conditions) using the low as well as the high gas flow degradation apparatus. I plan to perform prolonged experiments so that I can determine total amine losses on the cation IC and pair this with degradation product concentrations (carboxylic acid, nitrite/nitrate, amide, amino acid, and aldehyde). In addition, the preliminary HPLC-MS screening revealed the presence of 2-hydroxyethyl(imidazole) in degraded MEA solution. Analytical methods for quantifying imidazole concentration are still being researched.

Inhibited oxidation conditions will be extensively researched during the next two quarters. Sulfite, EDTA, and other oxygen scavengers/chelating agents will be compared to Inhibitor A in terms of inhibiting degradation. I also plan to screen other alkanolamines such as DEA, DGA, and MDEA, and quantify their resistance to oxidative degradation.

References

Goff GS &GT Rochelle. "Monoethanolamine Degradation: O_2 Mass Transfer Effects under CO_2 Capture Conditions." *Ind & Eng Chem Res* **2004**, 43(20), 6400-6408.

Nascimento RF et al. "Qualitative and quantitative high-performance liquid chromatographic analysis of aldehydes in Brazilian sugar cane spirits and other distilled alcoholic beverages." *J Chromatography A* **1997**, 782(1), 13-23.

Koike L et al. "N-Formyldiethanolamine: a new artifact in diethanolamine solutions." *Chemistry and Industry* **1987**, 626-627.

Sorensen M et al. "Degradation Pathway of the Photochemical Oxidation of Ethylenediaminetetraacetate (EDTA) in the UV/H_2O_2-process." *Acta hydrochim* **1998**, 26(2), 109-115.

Van Holst J et al. "CO_2 Capture from flue gas using amino acid salt solutions." Greenhouse Gas Control Technologies, Proceedings of the 8th International Conference on Greenhouse Gas Control Technologies ,Trondheim, Norway **2006**.

Blachly CH & H Ravner. “Stabilization of monoethanolamine solutions in carbon dioxide scrubbers.” *J Chem Eng Data* **1966**, 11(3), 401-403.

Thermal Degradation of Amines for Carbon Dioxide Removal from Flue Gas

Quarterly Report for January 1 – March 31, 2008

by Jason Davis

Supported by the Luminant Carbon Management Program

and the

Industrial Associates Program for CO_2 Capture by Aqueous Absorption

Department of Chemical Engineering

The University of Texas at Austin

April 18, 2008

Background

Greenhouse gas emissions from manmade sources are a growing environmental concern due to their effects on the global climate. The largest anthropogenic source of greenhouse gas is carbon dioxide which has been steadily increasing in concentration in our atmosphere since recorded measurements started at Mauna Loa Observatory in 1959. Since that time, CO_2 levels have increased by approximately 22% in the atmosphere to 385 ppm at the end of 2007 (NOAA). Ice core samples from Antarctica show that the CO_2 concentrations over the last 400,000 years have naturally varied between 180 and 300ppm, with the current levels being far outside the normal ranges (Barnola, 2003).

Greenhouse gas allows the visible and ultraviolet radiation from the sun to reach the surface of the earth, but prevents some of the energy emitted from the earth as infrared radiation from escaping, thereby increasing the global surface temperature. The National Climatic Data Center has shown that the average land temperatures have increased nearly 1.5^{o}C since 1880 (NCDC, 2006). In fact, 11 of the past 12 years are among the 12 hottest years ever recorded according to the 2007 Intergovernmental Panel on Climate Change's (IPCC) report to the United Nations. In order to reduce the effects of climate change, CO_2 emissions must be reduced. In 2005, coal accounted for 40% of the world's CO_2 emissions (IEA, 2007). Since the majority of this coal is used at point sources for the production of electricity, this makes for an obvious first target for the capture and storage of CO_2 emissions.

Aqueous amine absorption/stripping is a leading technology for the removal of CO_2 from flue gas streams. Compared to other technologies being proposed, it is the most mature technology with over 70 years of use in the natural gas treating industry. Figure 1 shows a diagram of a typical absorber/stripper system. The incoming gas is counter-currently contacted with an aqueous amine solution which absorbs a portion of the CO_2 from the flue gas before it exits at the top of the absorber column. The "rich" amine solution exits the bottom of the absorber column and is preheated by the lean amine in a cross exchanger before going to the stripper

where more heat is applied to liberate the CO_2 and regenerate the solvent before it is returned to the absorber to pick up more CO_2. A slip stream is also generally taken from the hot, lean solution and sent to a reclaiming system to remove product impurities.

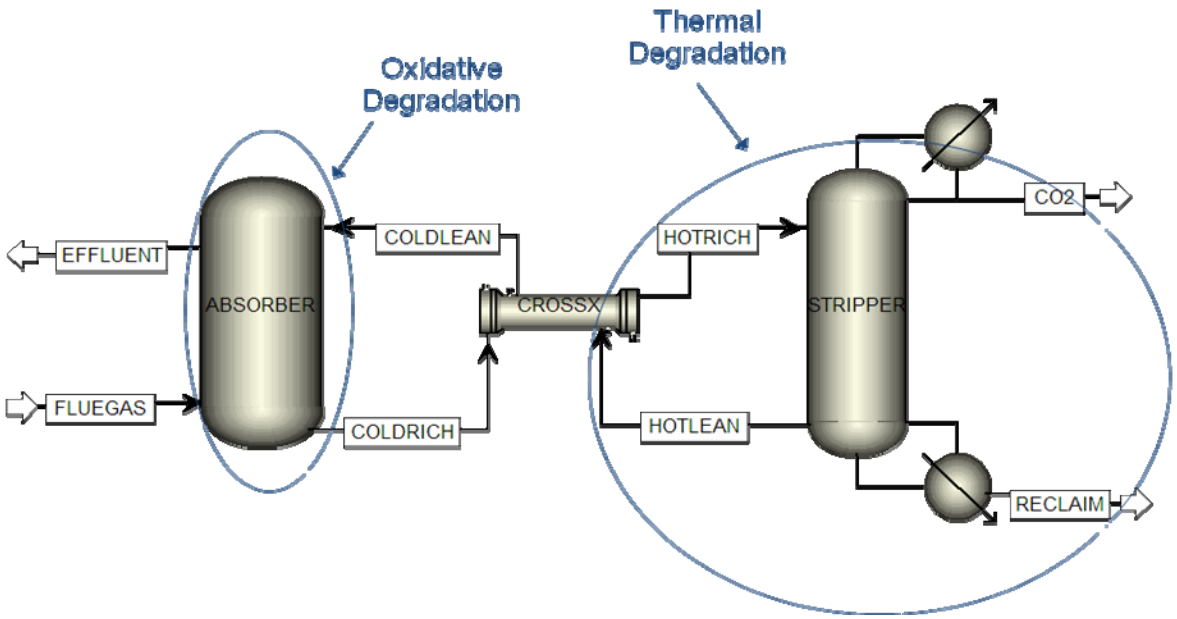

Figure 1: Aqueous absorber/stripper system for the removal of CO_2 from flue gas

In this system, amine solvents are subject to degradation by two main pathways; oxidative degradation and thermal degradation by carbamate polymerization. Oxidative degradation will occur in the absorber where the amine comes in contact with oxygen and will fragment the amine by a free radical mechanism. Thermal degradation will occur in the remainder of the process where temperatures become elevated including the cross exchanger, stripper, and in some cases, the reclaiming unit. The degradation rate will have a direct correlation to amine concentration, CO_2 loading, and temperature. This type of degradation will be the focus of this project.

Monoethanolamine (MEA) is a simple alkanolamine that is being considered for use in the amine absorber/stripper system, and in many ways is the benchmark by which all other amines are compared. Its main advantages are the fast reaction rates at absorber conditions, the relative price compared to other industrially significant amines, the maturity of its use in other gas treating applications, and that it is one of the easiest amines to produce in large quantities. Many researchers are looking for better amine systems including sterically hindered amines, cyclic amines, blended amine systems, and systems with rate promoters and corrosion/degradation inhibitors, but if an amine absorber/stripper system had to be built today it would most likely use MEA.

The current industrial application of the MEA absorber/stripper system is in natural gas sweetening and hydrogen treating applications where it has been employed for over 70 years. Thermal degradation has been identified as a major degradation pathway in this application since oxygen intrusion is kept to a minimum. The main difference between current systems and the new application is that natural gas sweetening processes are performed on a much smaller scale than CO_2 removal from flue gas and are treated as a supplementary unit operation. As such,

these systems are not fully optimized for energy performance or equipment sizing which will both be very important in the newer larger systems.

Oyenekan established that energy requirements for the stripper can be reduced at elevated temperatures and pressures, and the compression train can obviously be reduced in size if the gas enters at a higher pressure. The absorber/stripper system and the compression train for CO_2 are expected to have a 30-40% parasitic load on the power plant from an energy viewpoint, and the equipment is expected to be on the order of one billion dollars for the CO_2 capture unit alone under optimized conditions. Because of this, the operating conditions need to be tested and the limits pushed for optimal design of the entire unit, not just solvent management and corrosion. The first step to being able to test these limits is to have a reliable set of data for conditions that are outside the normal operating ranges of amine concentration, CO_2 loading and temperature/pressure of the stripper unit.

Literature Review

Monoethanolamine

The mechanism for carbamate polymerization was first proposed by Poldermann (1955). In this mechanism, MEA initially reacts with CO_2 to form MEA carbamate (Reaction 1) which is the normal route for CO_2 capture in the absorber.

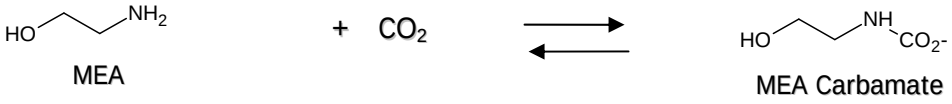

This process is normally reversed in the stripper, but can go through a condensation reaction to form 2-oxazolidone as in Reaction 2.

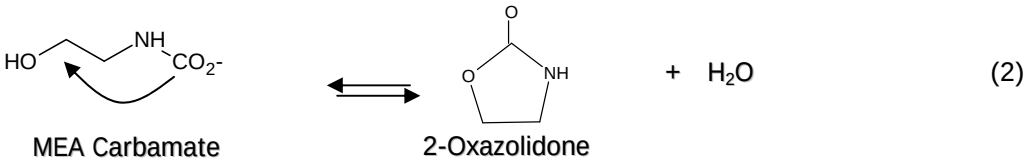

This can react with another molecule of MEA to form 1-(2-hydroxyethyl)imidizolidone(HEIA) as in Reaction 3.

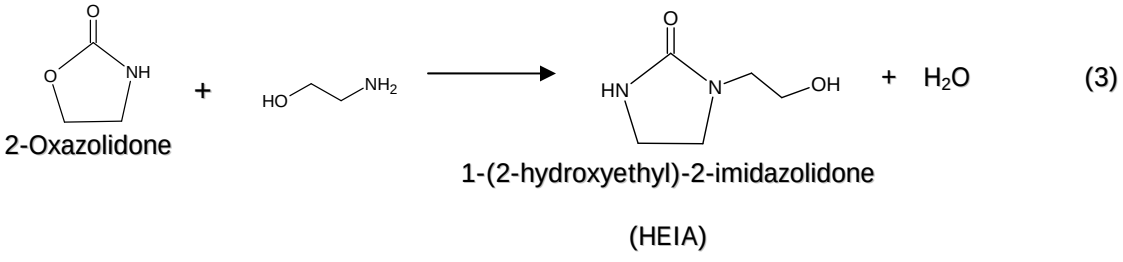

HEIA can then react with a molecule of water and form N-(2-hydroxyethyl)ethylenediamine (HEEDA) as in Reaction 4.

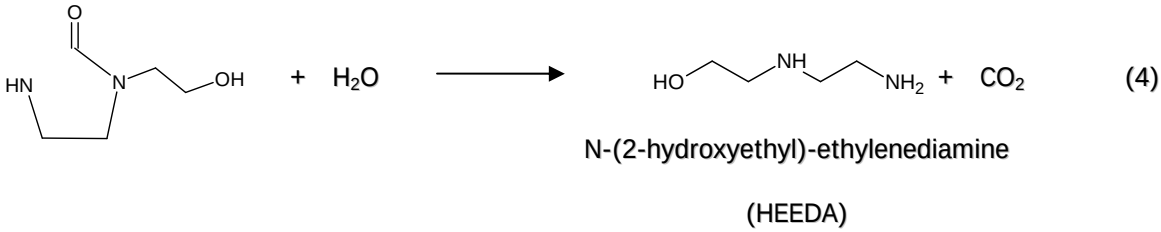

Polderman also took the time to show that this degradation not only decreased the CO_2 absorption capacity of the solution but also increased corrosion of equipment. HEEDA has been shown to play a large part in the corrosion of carbon steel in an amine treating unit with one test showing over 300 times more iron in a solution of HEEDA and MEA compared to a comparable MEA solution (Gillis, 1963).

Yazvikova (1975) found that in lab studies of dehydrated samples of oxazolidone and MEA, a urea was formed initially upon heating instead of HEIA. Upon further heating of the N,N'-di(hydroxyethyl)urea (DHU), HEIA and HEEDA began to form with the sum of their concentrations equal to the amount of DHU disappearance. The molecular formula for DHU is shown below.

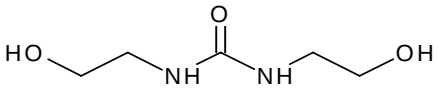

N,N'-di(hydroxyethyl)urea

Talzi (2002 and 2003) focused on thermal degradation of MEA by way of COS and CS_2 as well as CO_2. These papers were both NMR studies from a gas treatment plant in Russia and mainly focused on impurity identification. The basic degradation mechanisms for CO_2 were the same as those described in Polderman and Yazvikova except the path to the urea and HEIA were proposed to be in parallel instead of in series. HEIA and HEEDA concentrations were noted to be very high prior to regeneration of the solvent. Several exotic mechanisms were also proposed for some of the high molecular weight species that were identified.

Strazisar (2003) focused on identification of degradation products found in a flue gas treating unit. A variety of GC methods were used for unknown identification and a large number of degradation products were identified that seem to be a mixture of oxidative and thermal degradation. Most of these products were found in the thermal reclaimer bottoms however, which are subjected to very high amine concentrations, heat and metal content which would not be representative of the degradation occurring at normal stripper conditions. They also noted that no HEEDA was found in the thermal reclaimer bottoms, which is contrary to all of the other papers on the subject.

The remainder of the literature on MEA thermal degradation is limited to industrial experience reported in the Laurance Reid Conference Proceedings for natural gas treating. These proceedings offer a variety of engineering controls for the reduction of corrosion and thermal degradation to manageable levels in natural gas treating conditions.

In order to reduce degradation and corrosion, Dingman et al. (1966) suggest keeping the amine solution strength to 15 wt % or less, maintaining the rich CO_2 loading below 0.35 moles CO_2 per

mole amine, the lean loading around 0.1, and keeping the stripper pressure as low as possible to keep the temperature down. While all of these measures will decrease the amount of thermal degradation, they also increase the energy consumption of the process.

Blake (1962 and 1963) offers advice on how to design and run thermal reclaiming units, including matching the pressure of the unit to the stripper still pressure so the distillate can be used as part of the standard boilup and matching the distillate to the desired amine/water ratio to solve potential water balance issues. These reclaiming units are semi-batch and are run until the reclaimer bottoms reach 150°C at which point some of the contaminating species begin to codistill at appreciable quantities. These systems are the standard reclaiming method in the industry due to simplicity of design and operation.

Wonder et al. (1959) provide a set of analytical methods for the determination of MEA solution composition. A set of titrations is used to determine how much free amine is present in solution and, along with Kjeldahl total nitrogen analysis, provides the amount of amine tied up in nonbasic form. The main test involves separation of all of the species by distillation. Analysis using this method showed an example solution composition of 11.8 wt % MEA, 1.1% HEEDA, 1.9% HEIA and 0.4% higher boiling conversion products. This analysis suggests that this solution is highly degraded as more than 20% of the original amine solution has been converted to other products. The main drawback to this method would be the time involved in the analysis and the accuracy would be highly subject to the skill of the technician. Advances in analytical chemistry would suggest that other methods, such as chromatography, would provide more accurate results in a fraction of the time. This work will offer alternatives for solution analysis.

Diethanolamine

Polderman and Steel proposed a similar thermal degradation mechanism for diethanolamine, DEA (Polderman, 1956). They found that DEA carbamate went through a condensation reaction to form an oxazolidone structure, 3-(2-hydroxyethyl) oxazolidone (HEO).

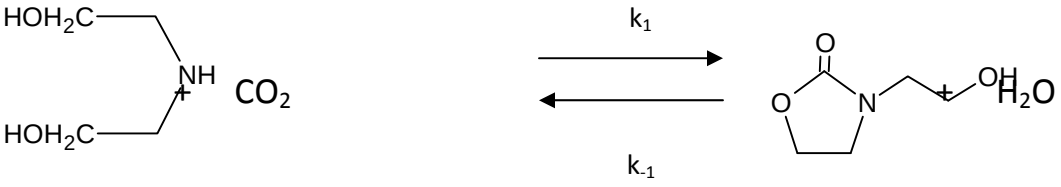

DEA HEO

Kennard and Meissen (1980) showed that the oxazolidone intermediate is attacked by another DEA molecule to form an ethylenediamine intermediate, N,N,N'-tris(2-hydroxyethyl)ethylene-diamine (THEED), analogous to HEEDA formation in the MEA degradation mechanism shown below.

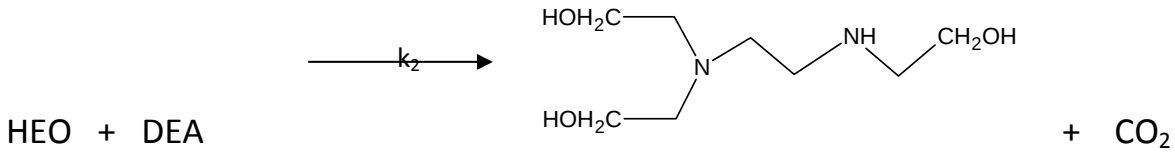

THEED

The THEED molecule then goes through a condensation reaction to form N,N-bis(2-hydroxyethyl) piperazine (HEP) which Polderman and Steele originally defined as the final end product of DEA degradation.

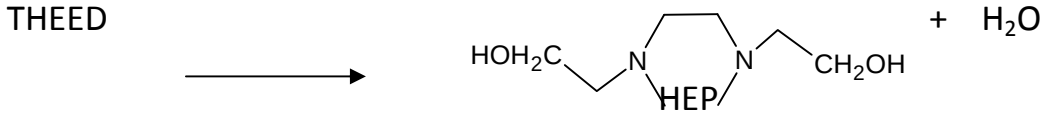

Polderman and Steele started with 25 wt % DEA solutions saturated with CO_2 at 25°C and sealed the solutions in a stainless steel pressurized autoclave. After heating at the desired temperature for 8 hours, the solutions were analyzed for DEA content and higher boiling nitrogenous compounds. Table 1 below shows the results of these experiments.

Table 1: Conversion of 25 wt % DEA in the presence of CO_2 for 8 hours (Polderman and Steele, 1956)

Temperature (°C)	CO^2 Partial Pressure (psig)	DEA Converted (wt %)
100	180	0
110	195	5
120	250	22
135	325	56
150	520	92
175	600	97

They only noticed the formation of HEP in their reactions, but did not have a complete mass balance for their degradation products. In their studies with HEP however, they noticed very little loss in acid gas absorbing capacity as the HEP was found to be competitive with DEA in that respect.

Kennard and Meisen (1980) used 30 wt % DEA solutions at a partial pressure of 600 psia and heated in a pressure vessel to 175°C and 205°C. The elevated temperature and pressure were used to accelerate thermal degradation so an experiment could be completed in a matter of hours rather than weeks. Gas chromatography was used to measure the appearance of degradation products. They reported THEED as a new degradation product but did not report a reaction mechanism for its formation. They also noted that DEA degradation did not follow first order behavior and at higher temperatures, the degradation rate slowed significantly after 5 hours.

Kim and Sartori (1984) used 3.2 M DEA solutions loaded with varying amounts of CO_2 and ran the experiments at industrially significant temperatures of 100°C and 120°C. The results of a typical run can be seen in Figure 2 below.

Figure 2: DEA degradation product formation at 120°C with concentration in wt % on the y-axis and time in days on the x-axis.

From the figure it can be seen that HEO is the initial product of DEA degradation with its concentration quickly approaching steady state with the DEA concentration. THEED appears next after an induction period indicating that it is formed from HEO and eventually starts to decline with DEA concentration. Finally, HEP forms after a long induction period and never reaches a steady state concentration over the time frame of this experiment. From this graphic, it can be concluded that DEA converts to HEO, THEED, and finally HEP. The disappearance of DEA in this work was expressed in terms of the first two reactions as follows:

$$-\frac{d[DEA]}{dt} = \frac{2k_1k_2[DEA]^2[CO_2]_s}{k_{-1} + k_2[DEA]}$$

where:

k_1 and k_{-1} = forward and reverse rate constant of DEA and CO_2 reaction to form HEO
k_2 = rate constant for DEA and HEO reaction to form THEED
$[CO_2]_s$ = steady-state CO_2 concentration at reaction conditions

The rate data obtained in the study were explained by this proposed mechanism.

Kennard and Meisen (1985) developed another mechanism for DEA degradation over a wide range of temperatures (90-250°C), DEA concentrations (1-100 wt %), and total pressures (1500-6900 kPa). The main degradation products were found to be the same as their earlier work in 1980, but the pathway was determined to follow two sets of reactions. The oxazolidone reaction was found to be the same as Kim and Sartori, but the formation of THEED and the eventual formation of HEP was found to proceed directly from DEA and CO_2 without the oxazolidone intermediate.

Other Amines

Kim (1988) gives results for the degradation of diisopropanolamine (DIPA) and found that the primary degradation product was the oxazolidone intermediate which was found to be very stable compared to that of MEA and DEA. The hydrolysis of oxazolidone back to DIPA was very slow and this represented a loss of amine functionality.

Dawodu and Meisen (1996) focused on the degradation of amine blends, specifically, methyl-diethanolamine (MDEA), MDEA+DEA, and MDEA+MEA. They found that in blended systems the degradation of MEA and MDEA were largely independent of the amine concentration suggesting a first order dependence in their degradation, while DEA showed a dependency on concentration. MDEA degraded the least, followed by MEA, and finally DEA with the rate constant for MDEA being an order of magnitude smaller than that of MEA and DEA.

Research Objectives

Thermal degradation, and solvent conservation as a whole, will have to be balanced against energy costs and capital costs. In order to push the system in a more energy efficient manner, the amine system will have to be pushed outside the normal operating ranges used in current applications and therefore degradation of the amine solvent will constitute a significant portion of the day-to-day operating costs of a CO_2 removal facility. The goal of this research will be to better understand thermal degradation of several common amine solvents at proposed stripper conditions and to quantify the amount and cost of thermal degradation in the system as a whole. The specific goals will be as follows:

- Quantify the effects of several process variables including temperature, CO_2 loading, and amine concentration on thermal degradation of monoethanolamine (MEA) and develop a kinetic model over a range of stripper conditions
- Study the effects of amine structure on thermal degradation rates including
  - pKa of the primary nitrogen
  - CO_2 reactivity
  - Steric hindrance of the amine
  - Carbon chain length on oxazolidone stability in alkanolamines
- Study blended amine systems that combine MEA with other commercially relevant amines
- Develop heuristics for amine selection based on thermal degradation findings
- Estimate solvent losses based on ASPEN models currently under development and pilot plant studies
- Determine where in the process degradation will most likely occur and recommend engineering controls to minimize these problem areas

Experimental Design

Thermal degradation experiments will be performed in a set of high pressure sample containers. These containers will be made of 316L SS tubing with ½" Swagelok connections and will be filled with CO_2 loaded amine solutions and placed in forced convection ovens in order to keep the temperature constant. Containers will be removed over the course of time and cooled to room temperature and analyzed by various analytical methods. Cation IC will be used to

measure the disappearance of the amine of interest and to measure any other ionizable species that may have been formed as opposed to the GC methods proposed in the literature. HPLC will be used to look for nonionic degradation products and total inorganic carbon testing will be used to measure the amount of CO_2 that is present in solution.

The method most commonly used for thermal degradation experiments in the literature involves a pressurized reactor where liquid samples are removed through a diptube over time while measuring the temperature and pressure of the solution. The drawback to this method is that only one solution can be run at a time and if there is a leak of any kind, the experiment will need to be repeated. In order to facilitate thermal degradation in a short period of time, these experiments are usually run at temperatures well in excess of standard operating conditions, which could lead to an inaccurate mix of final products, does not give rate data in a usable range of temperatures, and could lead to the formation of products that would not occur at lower temperatures. With the sample containers in an oven method it is possible to run a large number of samples at a time, there are duplicate samples if one leaks, many solutions can be tested at once, and the experiments can be run for extended periods of time at lower temperatures with a higher throughput than the single reactor at higher temperatures.

The main obstacle in these experiments will be analyzing the samples for degradation products and identifying and quantifying the results. Amines are very polar molecules and prove very difficult to separate by traditional chromatographic techniques. In the literature, GC and GC/MS have been the most common methods for quantification and identification of amines and their degradation products, however, these methods have some flaws in that they are generally run at very high temperatures in the column and injection ports and some of the preliminary results have shown that they provide unreliable results when compared to other analytical methods. Due to these drawbacks, it is believed that cation chromatography will provide a simple method for the separation of amines and their ionic degradation products and HPLC can be used more effectively to measure nonionic degradation products in solution.

In order to test the effects of oxazolidone ring structure size on carbamate polymerization, a set of straight chain alkanolamines will be tested under similar conditions. MEA forms a 5-membered oxazolidone ring that is stable, 3-aminopropanol will form a 6-membered ring that should also be stable, and 4-aminobutanol will form a 7-membered ring that in theory should be less stable than the previous two. The amine structures are shown below.

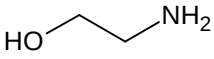

monoethanolamine (MEA)

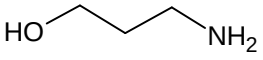

3-aminopropanol

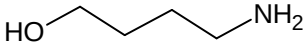

4- aminobutanol

In order to test the effects of steric hindrance, a set of alkanolamines similar to MEA will be tested under similar conditions. The addition of methyl groups to the primary and secondary carbon should provide varying degrees of steric hindrance which should effect the formation of amine carbamates and oxazolidone rings. Preliminary studies have shown that the most hindered

amine on the list (AMP) does degrade at a much slower rate than MEA and the other two amines should provide more insight.

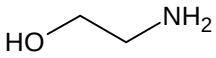

Monoethanolamine (MEA)

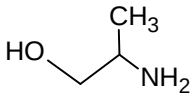

2-amino-1-propanol

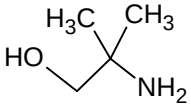

2-amino-2-methyl-1-propanol (AMP)

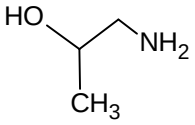

1-amino-2-propanol

A set of blended amine systems with MEA as the primary amine and a variety of thermally stable amines will be screened. Preliminary data obtained in this work suggests amines that are thermally stable in pure form can be reactive in a blended system. Since the pure MEA system will be well understood by the end of this work, it will be used as the main constituent in the blended systems in order to better understand the interaction between the different amines. The thermally stable amines that will be tested with MEA are shown below.

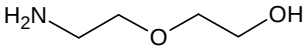

Diglycolamine (DGA)

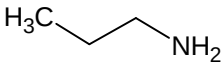

Propylamine

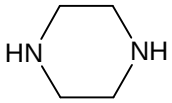

Piperazine (PZ)

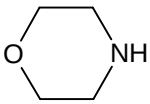

Morpholine

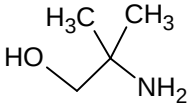

AMP

Other amines that are deemed industrially relevant will also be screened for thermal degradation, but detailed degradation mechanisms will not be pursued in this work.

Preliminary Results

Monoethanolamine Results

A full set of MEA degradation experiments has been performed with concentrations ranging from 3.5 m to 11 m MEA, CO_2 loading from 0.2 to 0.5 moles CO_2 per mole MEA, and temperatures ranging from 100°C to 150°C. Under these conditions, MEA has been shown to thermally degrade in significant quantities such that the degradation can be measured by the disappearance of MEA as opposed to the appearance of degradation products. Figure 3 below is

an IC chromatogram with a fresh 11 m MEA sample and a sample that has been placed in an oven at 135°C for 8 weeks.

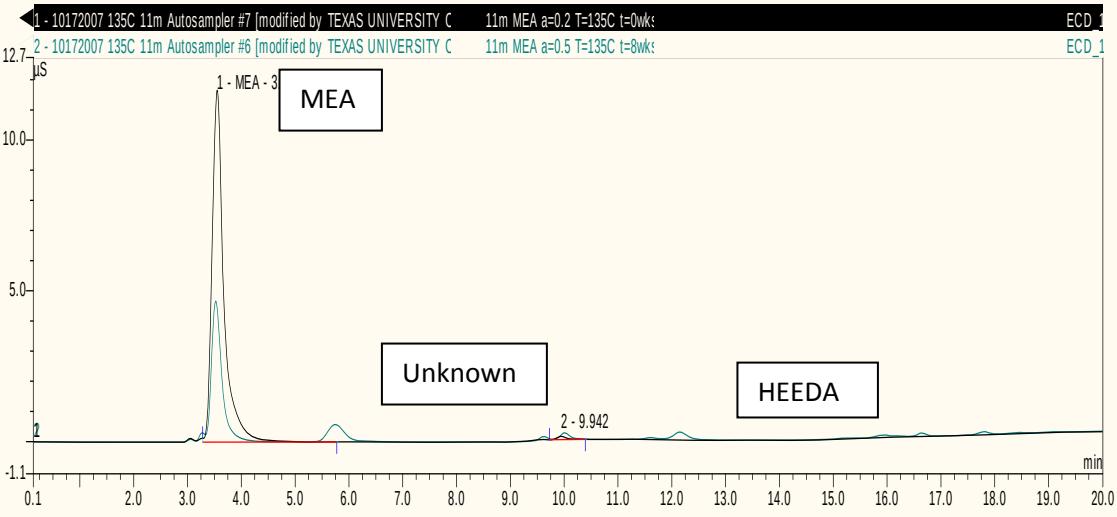

Figure 3: Undegraded 11 m MEA (black line) and a degraded sample (green line) after 8 weeks at 135°C

This chromatogram shows a significant disappearance of MEA (RT 3.5min) and the formation of HEEDA as denoted by the peak at 12 min as well as several unknown ionic degradation products such as the peak at 6 min. Fractionation and further testing such as mass spectroscopy or atomic emission will have to be used to further identify the unknowns before a full kinetic model can be proposed. Figure 4 below shows the effect of temperature on thermal degradation for 7 m MEA with a CO_2 loading of 0.4.

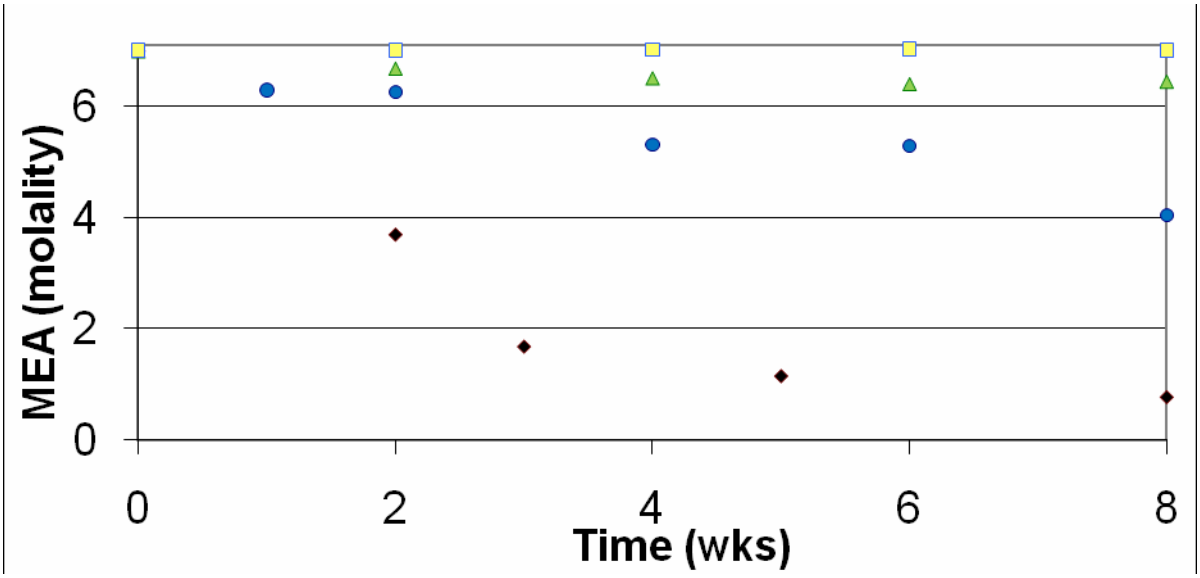

Figure 4: Thermal degradation of 7 m MEA with a CO_2 loading of 0.4 at 100°C( ), 120°C ( ), 135°C ( ) and 150°C ( ).

This graph shows the strong temperature dependence of the thermal degradation rate with an increase of 6.7°C doubling the rate. The 100°C data was found to have minimal degradation with less than 5% MEA loss after 8 weeks. The 150°C data was analyzed using the GC which has been shown to over predict the amount of degradation compared to the IC, which was used for all other samples. Figure 5.3 shows the effect of CO_2 loading on the thermal degradation of 7m MEA at 135°C.

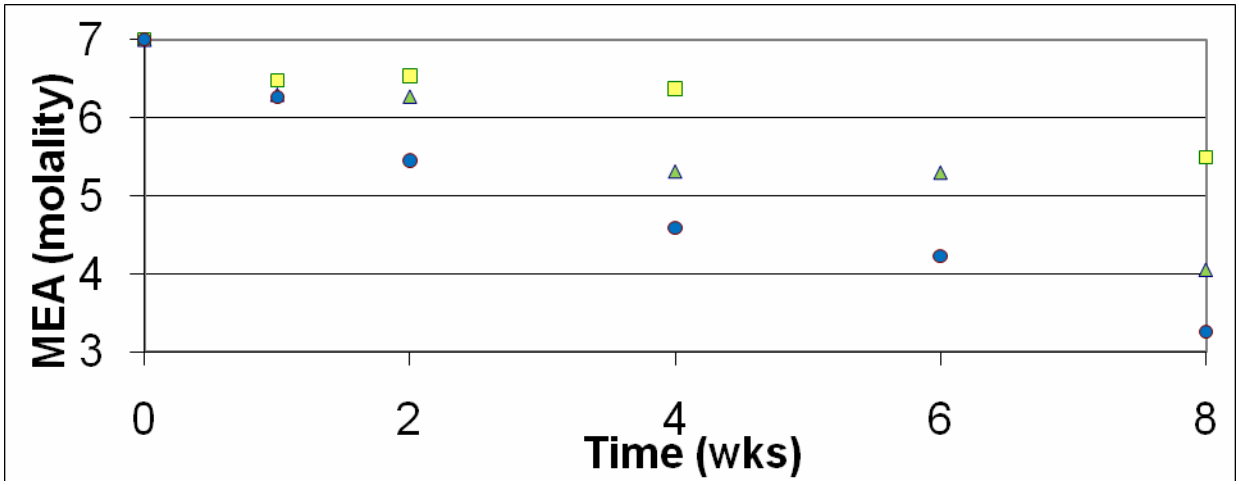

Figure 5: Thermal degradation of 7 m MEA at 135°C at CO_2 loadings of 0.2 (□), 0.4 (△) and 0.5 (○).

This graph shows that the rate is more than first order in CO_2 loading since the amount of degradation more than doubles when the loading doubles. While this is a strong effect, the loading in a typical stripper will not vary widely and will be counteracted by the temperature since the loading will be the highest at the lowest temperatures and lowest at the higher temperature sections. Figure 6 shows the effect of amine concentration on thermal degradation at 135°C and a loading of 0.4.

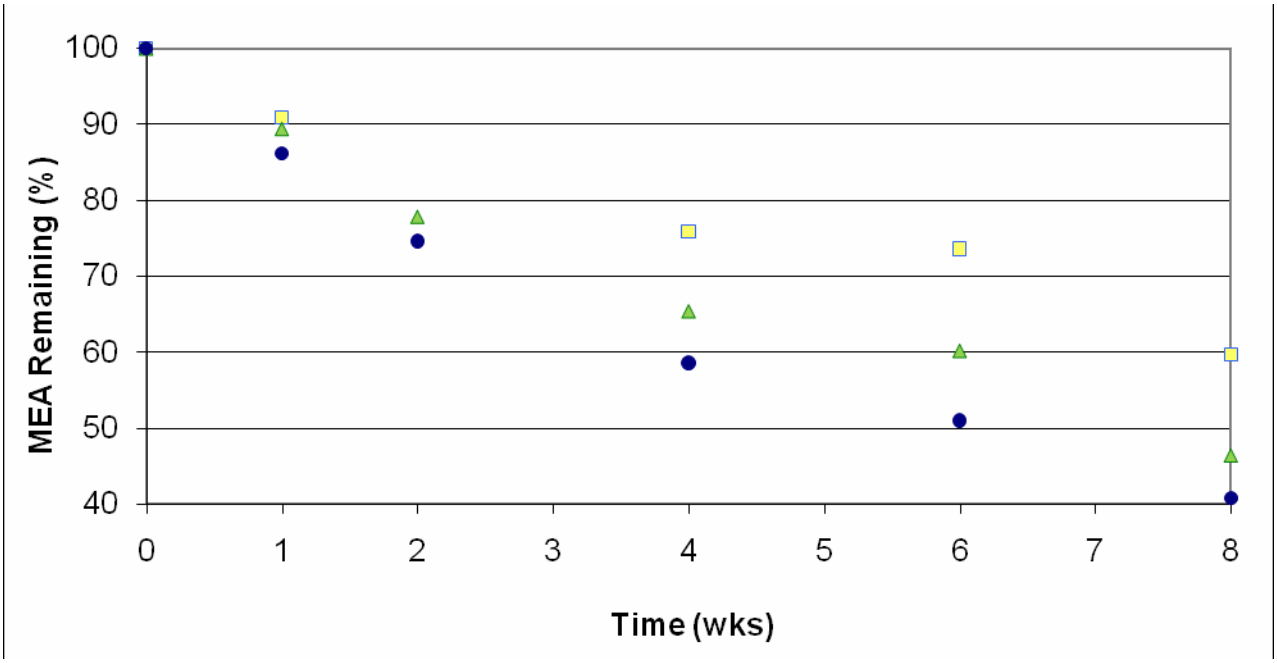

Figure 6: MEA remaining at 135°C and a CO_2 loading of 0.5 with initial concentrations of 3.5 m MEA (□), 7 m MEA (△), and 11 m MEA (○).

Since all of the concentrations do not fall on the same line, the thermal degradation rate is more than first order with respect to MEA concentration. This graph also indicates the rate is not second order either as doubling the concentration from 3.5 m to 7 m MEA only resulted in a slight overall rate increase.

The HEEDA and HEIA concentrations have also been measured for this system. Using this data, the rate constants will be determined and a kinetic model will be developed for the thermal degradation of MEA as a base case for other systems to be measured against. This model will also be used in various stripper designs in Aspen Plus® to determine the effect of system design on thermal degradation, and various design considerations will be offered upon completion.

Blended System Results

Piperazine (PZ) is a cyclic diamine that is used in industry as a promoter to enhance the rates of other amines. It is not an alkanolamine, so carbamate polymerization should not be a viable pathway for thermal degradation. The structure for piperazine is shown below and there is no literature data on thermal degradation of this molecule.

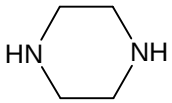

Experiments performed in this work show that aqueous PZ systems do not thermally degrade even at high CO_2 loadings and temperatures as high as 150°C suggesting that it is a thermally stable amine compared to our base case of MEA. A system of MEA and PZ was studied to determine what the combined effects of the two amine system are. A 7 m MEA/2 m PZ solution was made and tested in the same way as the MEA experiments described previously. Table 2 below shows the thermal degradation results for a 5 m PZ system, an 11 m MEA system, and a 7 m MEA/2 m PZ system after 2 weeks at 120°C and 135°C.

Table 2: Solvent Losses in pure and blended MEA and PZ systems after 2 weeks with a loading of 0.4 moles CO_2 per mole of alkilinity.

Solvent	Temp (^oC)	MEA Loss (%)	PZ Loss (%)	Total Alkilinity Loss (%)
5 m PZ	120	-	<2.0	<2.0
11 m MEA	120	4.0	-	4.0
7 m MEA/ 2 m PZ Blend	120	5.0	8.6	6.3
5 m PZ	135	-	<2.0	<2.0
11 m MEA	135	18.1	-	18.1
7 m MEA/ 2 m PZ Blend	135	11.9	31.8	19.1

From the table it can be seen that PZ degradation in the pure system is not detectable at 120^{o}C and 135^{o}C, while MEA loss at these temperatures is measurable. The blended system, however shows significant PZ loss at both temperatures. The total MEA loss is greater than PZ due to the concentration difference, but PZ is a much more expensive solvent and even the fact that such a large percentage of the promoter is degraded is significant in terms of cost.

We are proposing that the degradation pathway involves PZ attacking the oxazolidone intermediate of MEA and that the rate should be a function of the molecule's reactivity with CO_2. We will test this hypothesis by blending other amines with MEA that are thermally stable and have varying CO_2 reaction rates. We hope that this will offer some insight into the reactions between amines in blended systems under stripper conditions and will allow for the selection of better blends of amines.

Contributions

- Reaction Kinetics: This project will measure the rates of thermal degradation of amines at stripper conditions and provide insight into the effects of steric hindrance, CO2 reactivity, nitrogen pKa, and chain length on thermal degradation.
- Analytical Methods: This project will help develop a new method for the detection of amines and their ionic degradation products using cation IC, and their non-ionic degradation products using HPLC.
- Economics: This project will help better define the solvent make-up costs associated with the aqueous amine absorber/stripper system.
- System Design: This project will offer engineering controls to reduce thermal degradation and will aid in the design phase in both solvent selection and overall design to balance energy, capital, and operating costs.
- Environmental: This project will give some insight into the types and quantities of waste products associated with amine absorber/stripper systems and will allow for the quantification of their environmental impact.

References

Barnola, JM, D Raynaud, et al. (2003). "Historical CO_2 Record from the Vostok Ice Core." In *Trends: A Compendium of Data on Global Change*. Carbon Dioxide Information Analysis Center, Oak Ridge National Laboratory, U.S. Department of Energy, Oak Ridge, TN, USA.

Blake, RJ, KC Rothert (1962). "Reclaiming monoethanolamine solutions [for gas purification]." *Proc. Gas Conditioning Conf.*

Blake, RJ (1963). "Why reclaim monoethanolamine solutions?" *Oil & Gas J* **61**(36): 130-4.

Dawodu, OF & A Meisen (1996). "Degradation of alkanolamine blends by carbon dioxide. " *Canadian Journal of Chemical Engineering* **74**(6): 960-966.

Dingman, JC, DL Allen, et al. (1966). "Minimize Corrosion in MEA Units." *Hydrocarbon Processing (1966-2001)* **45**(9): 285-290.

Gillis, GA, LE Hawker & RJ Blake (1963). "N-(2-hydroxyethyl)ethylenediamine, a corrosive contaminant in monoethanolamine gas-treating solutions." *Proc. Gas Conditioning Conf.*

IEA (2007). International Energy Annual 2005, Energy Information Administration.

IPCC (2007). Climate Change 2007, IPCC Fourth Assesment Report (AR4), Intergovernmental Panel on Climate Change.

Kennard, ML & A Meisen (1980). "Control DEA degradation." *Hydrocarbon Processing, International Edition* **59**(4): 103-6.

Kim, CJ & G Sartori (1984). "Kinetics and mechanism of diethanolamine degradation in aqueous solutions containing carbon dioxide." *Int'l J of Chemical Kinetics* **16**(10): 1257-66.

Kim, CJ (1988). "Degradation of alkanolamines in gas-treating solutions: kinetics of di-2-propanolamine degradation in aqueous solutions containing carbon dioxide." *Industrial & Engineering Chemistry Research* **27**(1): 1-3.

Meisen, A & ML Kennard (1985). "Mechanisms and kinetics of diethanolamine degradation." *Industrial & Engineering Chemistry Fundamentals* **24**(2): 129-40.

NCDC (2006). The Annual Global Land Temperature Anomalies, National Climatic Data Center.

NOAA (2008). http://www.esrl.noaa.gov/gmd/ccgg/trends, National Oceanic and Atmospheric Administration.

Polderman, L. D., C. P. Dillon, et al. (1955). "Why monoethanolamine solution breaks down in gas-treating service." *Oil & Gas J.* **54**(No. 2): 180-3.

Polderman, LD & AB Steele (1956). **"**Degradation of diethanolamine in gas treating service." *Proc. Gas Conditioning Conf*: 49-56.

Strazisar, BR, RR Anderson, CM White (2003). "Degradation Pathways for Monoethanolamine in a CO_2 Capture Facility." *Energy & Fuels* **17**(4): 1034-1039.

Talzi, VP & SV Ignashin (2002). "NMR study of decomposition of monoethanolamine under conditions of industrial gas treatment." *Russian Journal of Applied Chemistry* **75**(1): 80-85.

Talzi, VP (2004). "NMR Determination of the Total Composition of Commercial Absorbents Based on Monoethanolamine." *Russian Journal of Applied Chemistry* (Translation of *Zhurnal Prikladnoi Khimii*) **77**(3): 430-434.

Wonder, DK, RJ Blake et al. (1959). "An Approach to Monoethanolamine Solution Control: Chemical Analysis and its Interpretation." *Proc. Gas Conditioning Conf.*

Yazvikova, NV, LG Zelenskaya et al. (1975). "Mechanism of Side reactions During removal of Carbon Dioxide from Gases by Treatment with Monoethanolamine." *Zhurnal Prikladnoi Khimii* **48**(3): 674-676.

Rate and CO_2 Partial Pressure Measurements for 8 m Piperazine at 40 and 60˚C

Progress Report for January 1 – March 31, 2008

by Ross Dugas

Supported by the Luminant Carbon Management Program

and the

Industrial Associates Program for CO_2 Capture by Aqueous Absorption

Department of Chemical Engineering

The University of Texas at Austin

April 18, 2008

Abstract

Six 8 m piperazine (PZ) rate experiments have been conducted using a wetted wall column at absorber conditions 40 and 60˚C. Vapor-liquid equilibrium data, allowing for the calculation of CO_2 capacity, were also obtained using the wetted wall column. TheVLE results correspond well with previous VLE data of various aqueous piperazine solvents measured by Hilliard (2008). The 8 m PZ solvent has shown CO_2 mass transfer rates 200-300% higher than 7 m monoethanolamine (MEA) at absorber conditions. The CO_2 capacity of 8 m PZ has been shown to be about 75% greater than 7 m MEA at 40˚C.

Introduction

The majority of my efforts this quarter was devoted to my Ph.D. research proposal which outlines the scope of my Ph.D. project measuring absorption/desorption rates and diffusion coefficients. That proposal has been attached as an appendix to this report.

This report also contains updated carbon dioxide (CO_2) absorption/desorption rate data for 8 m piperazine. Results were obtained by a wetted wall column at 40 and 60˚C. Many of the methods and procedures used in obtaining this data have been discussed in earlier reports and will not be duplicated here. However, essential information will be duplicated to preserve the continuity of the report.

As in previous work, solution CO_2 loadings are defined on an alkalinity basis. The alkalinity is essentially the number of nitrogen atoms on the amine; 1 for MEA but 2 for PZ. The CO_2 loading definition is shown in Equation 1.

$$CO_2\,Loading = \frac{n_{CO2}}{n_{MEA} + 2n_{PZ}} \qquad (1)$$

Results and Discussion

Aqueous piperazine solvents are being explored for CO_2 capture due to their faster reaction rates and higher CO_2 capacities compared to more common amines systems like 7 m (5 M or 30 wt %) MEA. Rate studies will be performed on a wide range of piperazine concentrations. Thus far, 6 data points have been collected for 8 m PZ at absorber conditions.

Hilliard (2008) explored aqueous amine systems from 0.9 m to 5 m piperazine and showed that the equilibrium CO_2 partial pressure is strictly a function of the solution loading. Hilliard showed that amine concentration did not affect CO_2 partial pressure data. CO_2 partial pressure data at 8 m piperazine obtained on the wetted wall column supports that conclusion. It is possible that at higher piperazine the amine concentration may not remain independent of CO_2 partial pressure due to non-idealities associated with extremely concentrated solutions. At some point piperazine may act like the solvent with water being a solute.

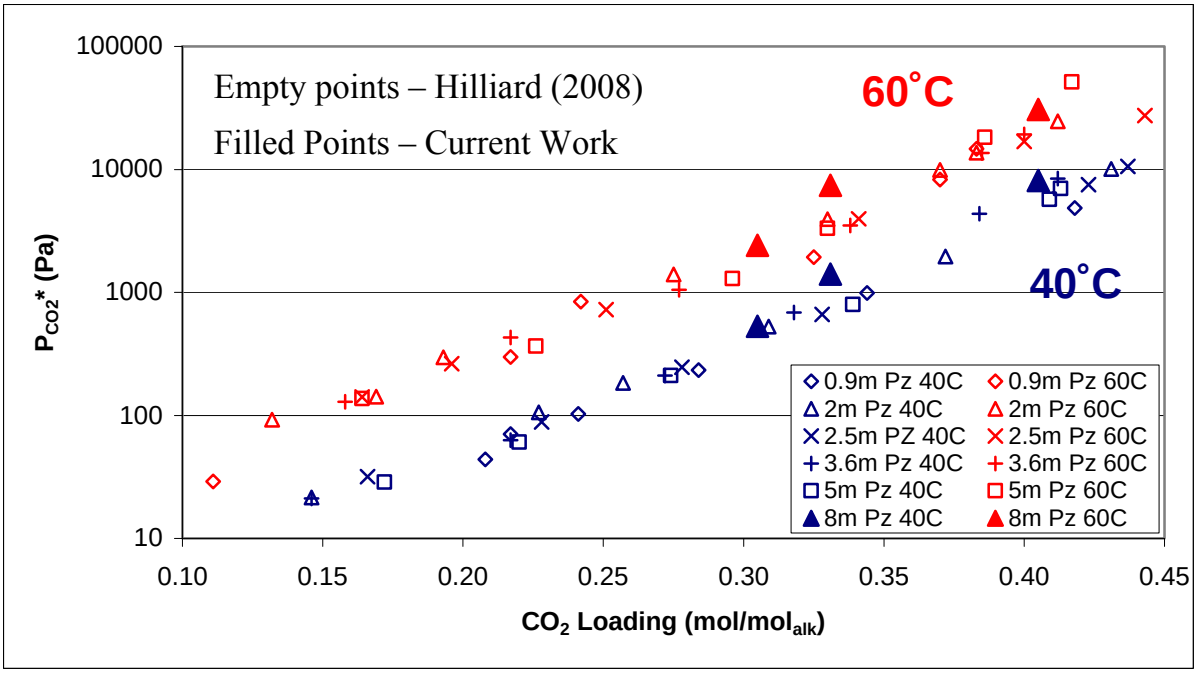

Figure 1: Vapor-Liquid Equilibrium Data for Aqueous Piperazine at 40 and 60˚C

The six data points for the 8 m PZ solvent match well with the partial pressure measurements of Hilliard. There is some disagreement for the two points at 0.33 loading. This reported loading may be underreported here since the solution was estimated at a 0.35 loading in the original CO_2 loading procedure. A 0.35 loading would also bring the data into better agreement with Hilliard. The CO_2 concentration of this solution will be analyzed again to determine the correct CO_2 loading.

The CO_2 partial pressure data also allows for the calculation of the solution capacity, the amount of CO_2 that will be transferred out of the system by a given amount of solvent. Assuming the likely case that 8 m PZ CO_2 partial pressure data continues to correspond with the aqueous

piperazine solvent systems in Figure 1, the CO_2 capacity of 8 m PZ is about 75% greater than 7 m MEA at 40˚C. This means much smaller flow rates can be utilized and significant energy savings can be achieved due to smaller energy requirements associated with heating and cooling the solvent.

8 m piperazine was expected to have faster CO_2 reaction rates than 7 m MEA due to faster kinetics and higher amine concentrations. This hypothesis was verified in the 6 wetted wall column experiments at absorber conditions. The CO_2 absorption/desorption rate data for 8 m PZ can be compared to 7 m MEA on a common partial pressure basis and is shown below in Figure 2.

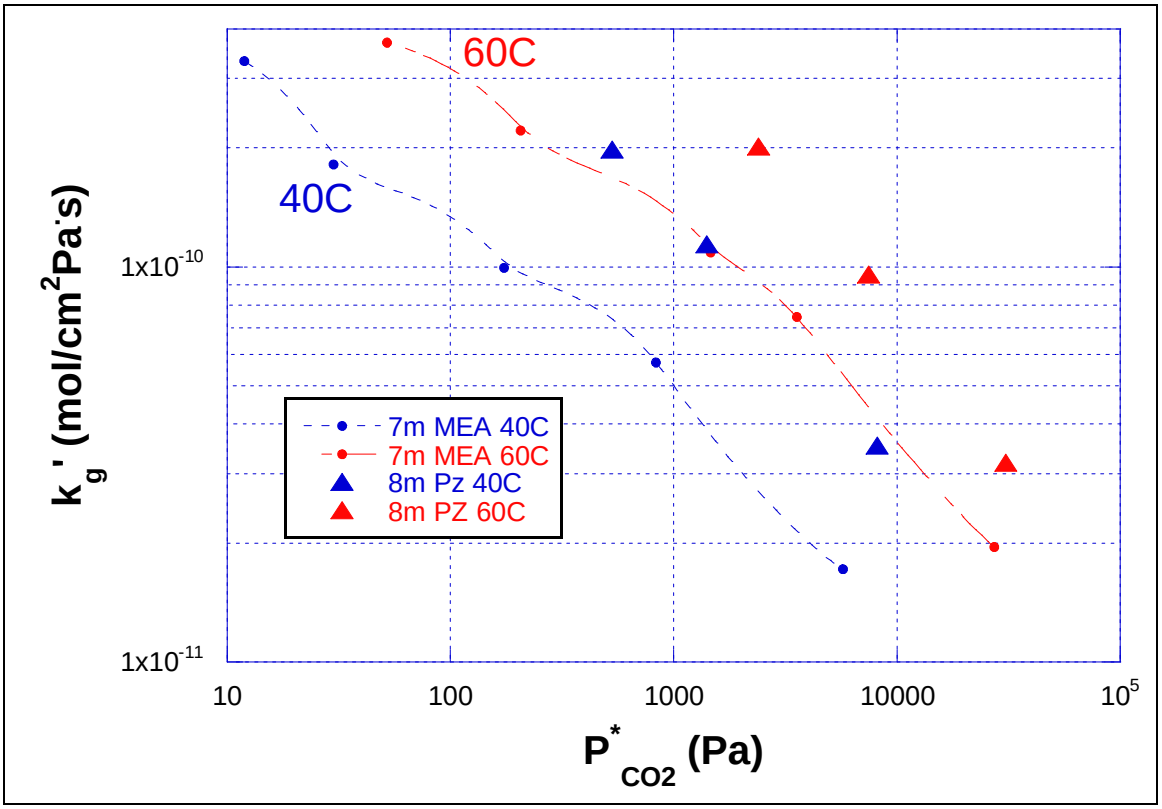

Figure 2: CO_2 Absorption/Desorption Rate Data Comparison for 7 m MEA and 8 m PZ at 40 and 60˚C

Figure 2 shows that the CO_2 reaction rate of 8 m PZ is 2-3 times faster than 7 m MEA at absorber conditions. This means 2-3 times less packing (surface area for reaction) is required for the 8 m PZ solvent. This could in turn allow for the use of much smaller absorbers and thus contribute considerable savings to the CO_2 capture process.

References

Hilliard, M. (2008). A Predictive Thermodynamic Model for an Aqueous Blend of Potassium Carbonate, Piperazine, and Monoethanolamine for Carbon Dioxide Capture from Flue Gas. Chemical Engineering. Austin, The University of Texas at Austin. **Ph.D.:** 1025.

Appendix

Carbon Dioxide Absorption, Desorption and Diffusion in Aqueous Piperazine and Monoethanolamine

Research Proposal

By: Ross Dugas

Advisor: Dr. Gary T. Rochelle

Department of Chemical Engineering

The University of Texas at Austin

February 2008

1. Background

Carbon dioxide emissions into the atmosphere are a growing environmental concern due to the effects of climate change. Continued use of fossil fuels since the industrial revolution in the 1800s has lead to increasing concentrations of CO_2 in the atmosphere. In fact, Keeling (Keeling and Whorf 2005) has shown that atmospheric CO_2 concentrations recorded on Mauna Loa in Hawaii have increased 19.4% from 1959 to 2004, to a 2004 value of 377 ppm. Ice core drilling at Vostok Station in Antarctica has shown that atmospheric CO_2 concentrations have cycled between 180 and 300 ppm dating back about 417,000 years (Barnola, Raynaud et al. 2003).

Increases in atmospheric CO_2 concentrations have affected average temperatures due to the greenhouse gas effect of CO_2. Carbon dioxide effectively reduces the amount of heat which is reflected back into space. The National Climatic Data Center has shown that average land temperatures have risen nearly 1.5˚C since 1880 (NCDC 2006). The rate at which average land temperatures have risen recently is unsettling. Figure 1 shows average global land temperature anomalies with respect to the 20th century average temperature. Temperatures seem to be increasing exponentially. About 1˚C of the 1.5˚C increase has been observed in the last 30 years. In fact, 11 of the past 12 years are among the 12 hottest years ever recorded.

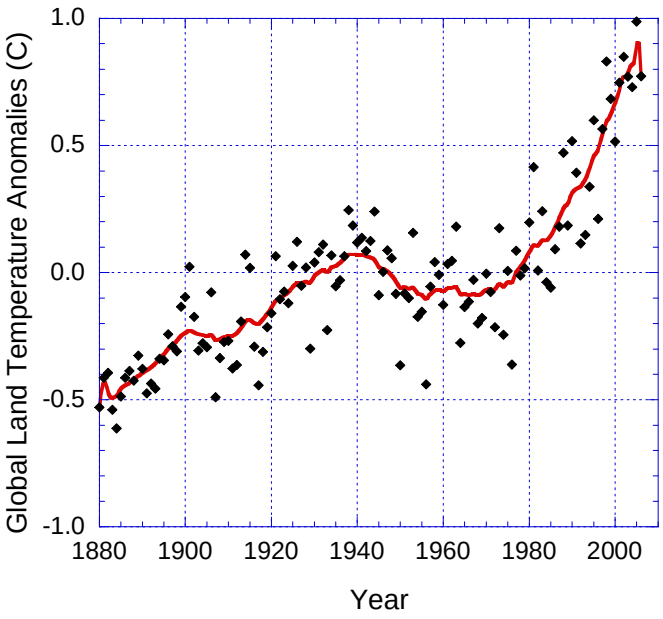

Figure 1. Average Global Land Temperature Anomalies with Respect to the 20th Century Average (NCDC 2006)

Carbon dioxide emissions must be reduced to mitigate the effects of climate change. In 2005, coal accounted for 40% of the world's CO_2 emissions (IEA 2007). Petroleum did account for 39% of CO_2 emissions in 2005 but is a much more difficult target for reductions. Petroleum is used primarily in the transportation sector and includes a very large number of relatively small point sources

(vehicles). Coal, on the other hand, is generally used in power generation sector and contains a relatively small number of large point sources (power plants). Economies of scale make capturing CO_2 from coal the more economically feasible alternative.

Aqueous amine absorption and stripping along with CO_2 sequestration is a leading technology for CO_2 capture from coal fired power plants. A CO_2 absorption stripping system, as shown in Figure 2, uses an aqueous amine to chemically react CO_2 from the flue gas in the absorber. The chemically bound CO_2 is carried to the stripper where conditions are such that the CO_2 is liberated from the amine. Concentrated CO_2 from the stripper can be compressed and sequestered into depleted oil or gas fields or in deep saline reservoirs (IEA 2001). Recent studies show that permanent storage in deep saline aquifers is feasible (Kumar, Ozah et al. 2005).

CO_2 capture using aqueous amine absorption and stripping can be expensive. Estimates

Figure 2. Typical Absorption/Stripping Flowsheet for Aqueous Amine CO_2 Capture with Industrial Temperature Estimates

have suggested that electricity prices would rise about 80% for coal fired power plants with CO_2 capture (Rubin, Rao et al. 2004). About 80% of the price increase would be due to capture and compression while about 20% of the price increase is due to transportation and sequestration (Rao and Rubin 2002). Much of the CO_2 capture research has focused on development of new solvents to decrease CO_2 capture costs. Monoethanolamine is considered the mature, baseline solvent for CO2 capture. Piperazine is a more expensive but much faster reacting amine. Piperazine blends with aqueous MDEA, AMP, MEA and potassium carbonate have all been studied (Bishnoi 2000; Dang 2000; Cullinane 2005; Sun, Yong et al. 2005). The proposed research involves the study of kinetic rates and diffusion characteristics for monoethanolamine (MEA), piperazine (PZ), MEA/PZ blends. A faster solvent would allow for a closer approach to

equilibrium in the absorber and/or facilitate the use of shorter absorbers. Both alternatives could provide substantial cost reductions.

2. Research Objectives

Faster, more concentrated solvents are being explored to reduce the costs of CO_2 capture. A significant amount of rate data is available on some of these amines but almost all the collected rate data is of unloaded (no reacted CO_2) solutions with fairly low amine concentrations. Industrial aqueous amine absorption/stripping systems would likely require the use of highly loaded (high CO_2 concentration), highly concentrated amines. Little data is available for these highly loaded, highly concentrated amines. MEA, an amine with a significant amount of literature data, has only been thoroughly studied at these conditions by one researcher (Aboudheir 2002). No rate data is available on piperazine at these conditions. Obtained MEA rate data by Aboudheir does not seem to coincide with the available literature data, collected at dilute, unloaded conditions. This work seeks to reconcile the work of Aboudheir with the literature data and add another source of highly loaded, highly concentrated data for MEA, piperazine and MEA/PZ systems.

One consequence of using very fast, concentrated solvents is that kinetics can become coupled with diffusion. The more concentrated solvents can transfer more CO_2 resulting in lower flow rates which reduce the energy associated with heating and cooling the solution. If solutions are too concentrated, increased viscosity can severely limit the mass transfer of CO_2 due to diffusion resistances. This work seeks to find optimal amine solvent concentrations to maximize CO_2 transfer, balancing kinetic and diffusion effects.

The proposed work on the amine solvents will entail the following scientific analyses:

1. Measurement of vapor-liquid equilibrium and rate data of highly concentrated, highly loaded MEA, piperazine and MEA/PZ systems from 40 – 100C using a wetted wall column
2. Determination of the effect of ionic strength, amine blends and the addition of heat stable salts and degradation products on the absorption/desorption rates of MEA, piperazine and MEA/PZ systems

3. Increased understanding between the kinetics of highly loaded, highly concentrated amines with literature data consisting of almost exclusively dilute, unloaded amine systems
4. Measurement of diffusion coefficients of CO_2 loaded MEA, piperazine and MEA/PZ solutions likely using a diaphragm cell
5. Measurement of viscosities of MEA, piperazine and MEA/PZ solvents over a range of temperatures and CO_2 concentrations
6. Modeling of kinetic and mass transfer data into Aspen RateSep for the creation of a wetted wall column model

3. Literature Review

3.1. General Chemistry and Mass Transfer

Monoethanolamine and piperazine are both amines which will react with CO_2 due to their amine functional groups. Monoethanolamine and piperazine structures are shown in Equations 1 and 2.

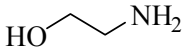

(1)

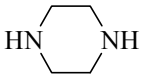

(2)

Aqueous monoethanolamine and piperazine solutions will form carbamates and bicarbonate when reacted with CO_2. The MEA carbamate reaction is shown as Equation 3. The possible piperazine carbamate reactions are listed in Equations 4 – 6. The bicarbonate reaction which can become significant in both MEA and piperazine systems at high CO_2 loading is shown in Equation 7.

$$MEA + CO_2 + B \leftrightarrow MEACOO^- + BH^+ \quad (3)$$

$$PZ + CO_2 + B \leftrightarrow PZCOO^- + BH^+ \quad (4)$$

$$PZCOO^- + CO_2 + B \leftrightarrow PZ\left(COO^-\right)_2 + BH^+ \quad (5)$$

$$PZH^+ + CO_2 + B \leftrightarrow H^+PZCOO^- + BH^+ \quad (6)$$

$$H_2O + CO_2 + B \leftrightarrow HCO_3^- + BH^+ \quad (7)$$

Component B can be any base in the system. Common bases include: MEA, PZ, PZH^+, $PZCOO^-$, H_2O and OH^-.

The CO_2 loading and temperature will determine the speciation of the solution which will control the reaction rates of Equations 3-7. The CO_2 loading is a measurement of the CO_2 concentration in the solution. It is the ratio of CO_2 molecules to amine groups. MEA has one amine group while piperazine has two. The definition of CO_2 loading is expressed mathematically in Equation 8.

$$CO_2 Loading = \frac{n_{CO2}}{n_{MEA} + 2n_{PZ}} \quad (8)$$

Absorption of CO_2 by amines such as MEA and piperazine is typically explained via the zwitterion mechanism, originally proposed by Caplow (1968). The zwitterion is an ionic, but neutrally charged intermediate which is formed from the reaction of CO_2 with an amine. The zwitterion mechanism for carbamate formation is a two step process: the CO_2 reacts with the amine to form a zwitterion, followed by the extraction of a proton by a base. In the following example water acts as the base.

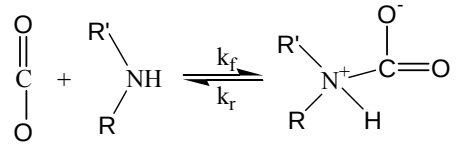

(9)

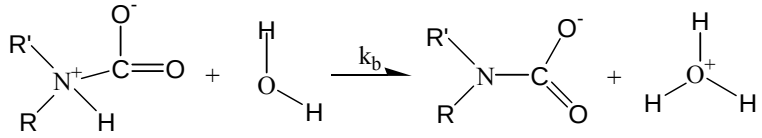

(10)

The two step zwitterion mechanism for a primary amine such as MEA leads to the CO_2 absorption rate shown in Equation 11.

$$r_{CO2} = \frac{[Am][CO_2]}{\frac{1}{k_f} + \frac{k_r}{k_f \sum k_b[B]}} \quad (11)$$

Most researchers have reported that absorption rates of CO_2 are first order with respect to the amine. This suggests that the protonation of the base is an instantaneous process, k_b approaches ∞. This leads to a simplified version of the rate equation for primary amines.

$$r_{CO2} \quad k_f [Am][CO_2] \qquad (12)$$

The overall mass transfer of CO_2 is more complicated than Equation 12. Mass transfer of CO_2 from the gas phase into the liquid phase is a film resistance process. Figure 3 shows a typical film analysis for CO_2 absorption.

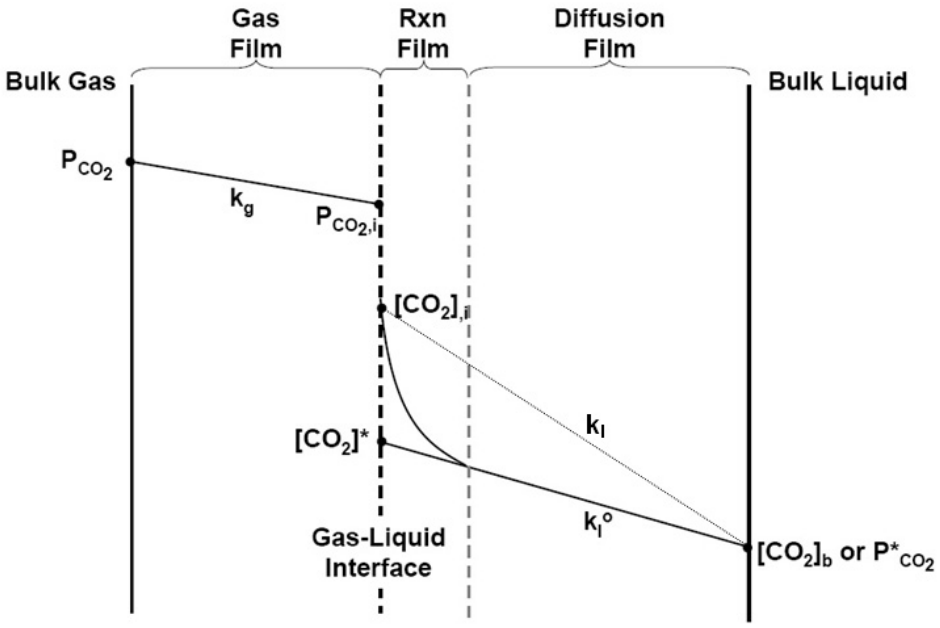

Figure 3. Mass Transfer of CO_2 into the Bulk Liquid with Fast Chemical Reaction

As Figure 3 implies, there can be substantial resistances due to diffusion both in the liquid and gas phases. Often a correlation is used to characterize the gas film mass transfer coefficient, k_g, which is apparatus specific. The liquid phase is more complicated than the gas phase since the diffusion is coupled with the reaction. Typically this complication is solved by performing experiments under conditions where liquid phase diffusion is negligible and mass transfer is dominated by the kinetics. This allows the kinetics to be easily obtained from the experimental data.

Under extreme operating conditions, the absorption of CO_2 could occur in the instantaneous reaction regime. In this regime the kinetics are effectively instantaneous since the mass transfer is completely dominated by the ability of reactants and products to diffuse to and

from the reaction interface, which can shift from the gas-liquid interface. In this case, experimental data is indicative of diffusion coefficients, not reaction kinetics.

Of course it is also possible that measured mass transfer results include a significant contribution from both the kinetic and diffusion forces. This "mixed" regime is not experimentally convenient since separating the kinetic and diffusion contributions can be very difficult. Unfortunately, with faster solvents operating at higher concentrations and CO_2 loadings, this regime may become a necessary complication when measuring mass transfer with apparatuses such as the wetted wall column. This will require an increased understanding of the relationship of the diffusing species. Danckwerts (1970) provides significant mass transfer theory to help understand when diffusion becomes a non-negligible effect in measured mass transfer rates.

3.2. Rate Studies

3.2.1. MEA Systems

A significant amount of data is available on rate studies concerning the reaction of CO_2 and monoethanolamine. Table 1 characterizes the current literature data.

Table 1. Literature Data on the Reaction between CO_2 and Aqueous MEA

Reference	Temp (C)	[MEA] (mol/L)
(Jensen, Jorgensen et al. 1954)	18	0 – 0.2
(Astarita 1961)	21.5	0 – 2.0
(Emmert and Pigford 1962)	25	0.1 - 2.0
(Clarke 1964)	25	1.6 - 4.8
(Sharma 1965)	25 - 30	1.0
(Danckwerts and Sharma 1966)	18 - 35	1.0
(Leder 1971)	80	-
(Sada, Kumazawa et al. 1976a) (Sada, Kumazawa et al. 1976b)	25	0.2 - 1.9
(Hikita, Asai et al. 1977)	5.4 – 35.2	0.02 - 0.18
(Alvarez-Fuster, Midoux et al. 1980)	20	0.2 - 2.0
(Donaldson and Nguyen 1980)	25	0.03 - 0.08
(Laddha and Danckwerts 1981)	25	0.49 - 1.71
(Penny and Ritter 1983)	5 – 30	0 - 0.06
(Sada, Kumazawa et al. 1985)	30	0.5 - 2.0
(Barth, Tondre et al. 1986)	20 - 25	0.02 - 0.05
(Crooks and Donnellan 1989)	25	0.02 - 0.06
(Alper 1990)	5 – 25	0 - 0.45
(Littel, Versteeg et al. 1992)	45 – 60	0 - 3.2
(Hagewiesche, Ashour et al. 1995)	40	-
(Dang 2000)	40 – 60	2.5 – 5.0
(Xiao, Li et al. 2000)	30 – 40	0.1 - 0.4
(Horng and Li 2002)	30 – 40	0.1 - 0.5
(Aboudheir 2002)	20 – 60	3.0 – 9.1
(Jamal, Meisen et al. 2006)	20 – 50 (abs) 60 – 110 (des)	? - 5

Although Table 1 details a large amount of literature data for MEA kinetics, little of it is directly applicable to industrial CO_2 capture systems. The industrial system would likely operate at absorber temperatures ranging from 40 to 70C while the majority of the literature data was collected near ambient conditions. Also, the higher temperature data by Leder (1971) and Littel (1992) are likely erroneous due to experimental or calculation inaccuracies (Versteeg, Van Dijck et al. 1996). The only large data source with supposedly reliable reported kinetics above 40C is Aboudheir (2002). However, laminar jet absorber results from Aboudheir are not easily comparable nor seem to be supported by the literature data.

Industrial CO_2 capture systems would likely operate at high amine concentrations with CO_2 loaded solutions. All of the data with the exception of Dang (2000), Aboudheir (2002) and Jamal (2006) was collected using unloaded solutions. Very little of the data besides these three

data sources was collected at significant MEA concentrations. Industrial operation would likely require at least 5M MEA to reduce operational costs.

Although data by Jamal includes interesting conditions (unloaded absorption experiments up to 50C, high temperature desorption experiments of loaded MEA solutions), it is not particularly useful. Jamal does not report rate constants for MEA nor provide raw data on the experimental conditions of the experiments.

Dang provides useful kinetic results but only provides a total of 7 data points. Three CO2 loadings at 2.5M MEA and 4 CO_2 loadings at 5.0M MEA were examined.

The data collected by Aboudheir is the only valuable major data source applicable to CO_2 capture systems. As previously mentioned, the extracted kinetics do not seem to agree with other literature data. The difference may be due to the highly concentrated, highly loaded or highly non-ideal nature of these solutions. The differences for this ideal versus non-ideal systems highlight the need to perform rate studies on amine systems similar to those expected for industrial systems. In addition to explaining why the Aboudheir data does not seem to agree with the literature data, the current work seeks to add to the current rate data for highly loaded, highly concentrated MEA solutions using a wetted wall column.

3.2.2. PZ Systems

In contrast to more traditional amines such as MEA, DEA, AMP and MDEA, there is very little data published on aqueous piperazine systems. Table 2 summarizes the only four studies in which kinetic data can be extracted.

Table 2. Literature Data on the Reaction between CO_2 and Aqueous Piperazine

Reference	Temp (C)	[MEA] (mol/L)
(Bishnoi and Rochelle 2000)	25	0.2 - 0.6
(Sun, Yong et al. 2004)	30 - 40	0.23 - 0.92
(Derks, Kleingeld et al. 2006)	20 - 40	0.6 - 1.5
(Samanta and Bandyopadhyay 2007)	25 – 40	0.2 – 0.8

The main reason for the lack of aqueous piperazine data is that in industry piperazine is used in combination with other amines, rather than a stand-alone solvent. Piperazine has very fast kinetics and is an effective promoter in some systems. Rigorous flux models for aqueous piperazine or piperazine blend systems both require piperazine reaction kinetics. Since piperazine is typically used in blended systems, low piperazine concentrations have been

examined in past studies. Again, relatively low temperature data has been measured rather than the 40 – 70C conditions more typical of an industrial system.

Recent solid solubility data has shown that piperazine has the capability to be used in very high concentrations possibly making aqueous piperazine economically feasible for industrial CO_2 capture (Hilliard 2008). Aqueous piperazine systems have also shown a very high resistance to thermal degradation which can occur in the reboiler (Rochelle, Seibert et al. 2007).

None of the four rate studies in Table 2 were conducted with CO_2 loaded amines. The current work seeks to explore the piperazine rate data with loaded amines, especially at higher temperatures and much higher amine concentrations.

3.2.3. MEA/PZ Systems

Piperazine has historically been used as a promoter due to its very fast reaction rates. Piperazine activated aqueous MDEA, AMP, MEA and potassium carbonate have all been studied (Bishnoi 2000; Dang 2000; Cullinane 2005; Sun, Yong et al. 2005). Monoethanolamine is the fastest of these four solvents and is being studied in the present work. Previous work on MEA/PZ solvents is scarce and is shown in Table 3.

Table 3. Literature Data on the Reaction between CO_2 and MEA/PZ Blends

Reference	Temp	[MEA]	[PZ]	CO_2 Loading
	(C)	(mol/L)	(mol/L)	(mol/$mol_{alkalinity}$)
(Dang 2000)	40	0.4	0.6	0.06 – 0.14
	40	1.9	0.6	0.01 – 0.44
	40 - 60	3.8	1.2	0.41 – 0.43
(Okoye 2005)	40 - 60	4.4	1.2	0.28 – 0.57

Both literature sources for rate data on MEA/PZ systems study loaded systems. Although Dang (2000) provides data for 3 different MEA/PZ solvent blends, there is little data at each blend composition. Dang provides a total of 7 data points for her MEA/PZ studies. Rate data by Okoye (2005) is similarly scare. Okoye provides a total of 6 data points from his MEA/PZ rate experiments. To complicate matters, data from Okoye does not agree with Dang and seems unreasonable. It is very likely that the Okoye data is erroneous and will be of little value.

The current work seeks to expand the rate data for MEA/PZ blended systems. As usual, an emphasis on highly loaded, highly concentrated (likely industrial) conditions will be explored.

3.3. Diffusion Coefficient and Viscosity Considerations

The current work will use a wetted wall column for rate measurements. The wetted wall column can have significantly longer contact times between the solvent and flue gas than other mass transfer devices such as laminar jet absorbers. These longer contact times reduce the physical mass transfer coefficient of the solvent phase so the measured rates are more likely to be affected by diffusion properties. Some results from the wetted wall column utilizing very fast, highly concentrated, highly loaded amines are likely to be dependent on diffusion properties under some conditions. Therefore, it is very important to understand the diffusion properties to accurately extract kinetics from the obtained mass transfer data.

The wetted wall column should have contact times and liquid film mass transfer coefficients similar, although somewhat lower, to an industrially used packed column. Therefore, some of the wetted wall column observed diffusion effects on mass transfer are likely to be observed in industrial systems.

Some researchers have produced viscosity-diffusion coefficient correlations to account for physical property differences (Versteeg and Van Swaaij 1988; Snijder, te Riele et al. 1993). The empirically regressed correlations do not provide first order dependencies as the Wilke-Chang equation, simplified below, may suggest. Work by Versteeg has shown that the diffusion of N_2O and CO_2 in aqueous amines should follow the viscosity dependence of Equation 14. Snijder has shown that alkanolamine diffusion in aqueous alkanolamine solutions follows the viscosity dependence of Equation 15.

$$D_{AB} \propto \frac{\sqrt{\psi_B M_B} T}{\mu \cdot V_A^{0.6}} \tag{13}$$

$$\left(D_{N2O}\eta^{0.8}\right)_{Amine Solution} = CONSTANT = \left(D_{N2O}\eta^{0.8}\right)_{Water} \tag{14}$$

$$\left(D_{Amine}\eta^{0.6}\right)_{Amine Solution} = CONSTANT = \left(D_{Amine}\eta^{0.6}\right)_{Water} \tag{15}$$

To make matters more complicated, the N_2O and CO_2 diffusivity relationship in Equation 14 was confirmed with MDEA solutions but resulted in less satisfactory results for AMP (Tomcej and Otto 1989; Xu, Otto et al. 1991). If the diffusion relationships are dependent on amines, the relationship in Equation 14 may not directly apply to MEA, piperazine or MEA/PZ systems. The diffusion coefficient must be accurately determined for each system to evaluate

rate data where both diffusion and reaction kinetics affect the total mass transfer. The current work seeks to build and use a diaphragm cell to better understand diffusion coefficients in MEA, piperazine and MEA/PZ systems.

3.4. Ionic Strength and Impurity Additions

For all amine systems it is imperative to detail the significance of the ionic strength of the solution. The ionic strength is dependent on the CO_2 loading of the solution and can drastically affect the kinetics, possibly due to the non-ideality of the solutions. Since very little of the literature data has included loaded amine solutions, the effect of ionic strength on kinetics is still undefined. Reworked MEA rate data from Aboudheir (2002) along with the current work should provide a base to understanding the effects of ionic strength.

Impurities will be introduced into the solvent in industrial CO_2 capture systems due to dirty flue gas, corrosion, oxidative and thermal degradation. The addition of some components (particularly sulfate, formate, zinc and vanadium) into solvent systems will be screened to quantify both kinetic and vapor-liquid equilibrium effects.

4. Outline of Experiments

4.1. Wetted Wall Column

Equilibrium and rate measurements will be obtained via a wetted wall column originally built by Mshewa (1995). The wetted wall column has been used by a number of researchers (Mshewa 1995; Pacheco 1998; Bishnoi 2000; Dang 2000; Cullinane 2005; Okoye 2005). A schematic of the entire apparatus is shown in Figure 4. A detailed view of the wetted wall column cell is shown in Figure 5.

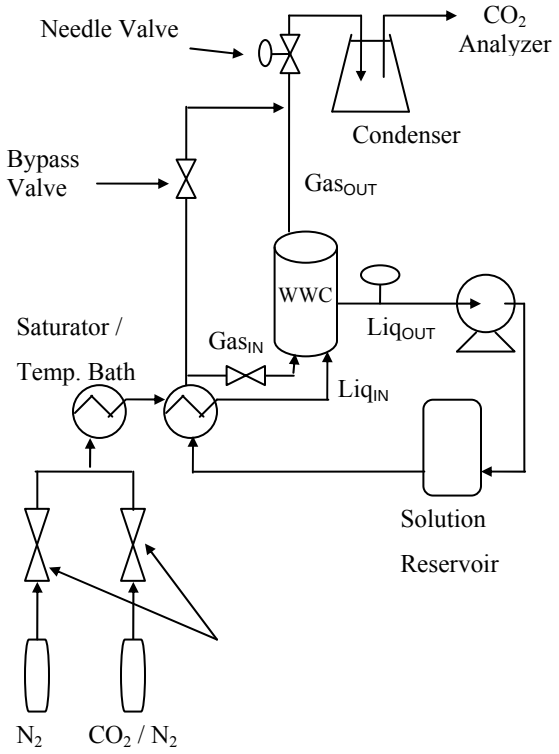

Figure 4. Schematic Diagram of the Wetted Wall Column Apparatus

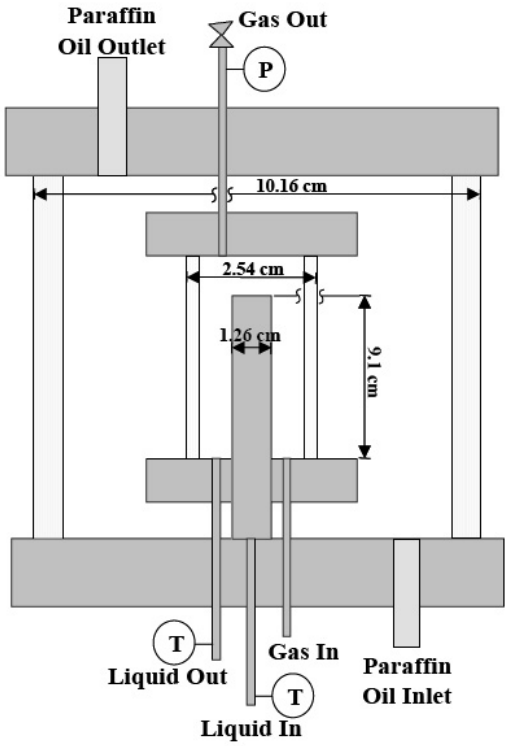

Figure 5. Detailed View of the Wetted Wall Column Cell

Nitrogen and carbon dioxide flows through the system are controlled via mass flow controllers. The resultant N_2/CO_2 blend is then routed to a saturator to saturate the gas at the temperature of the experiment. The gas is then routed through tubing immersed in another temperature bath. The gas enters the wetted wall column and some CO_2 is either absorbed or desorbed by the solvent. The exit gas is routed through a flask immersed in an ice bath before being sent through a desiccant and to the CO_2 analyzer.

Unlike the gas, the solution is recycled though the system. The solution reservoir consists of two 1-liter insulated vessels connected in series. The screw-type positive displacement pump can be controlled to circulate various liquid rates. Liquid rates are controlled around 2 cm^3/s. The large solution reservoir in conjunction with the low liquid flow rate ensures that the absorption/desorption of CO_2 in the column will not appreciably change the CO_2 concentration of the bulk solution throughout an experiment.

The gas-liquid interface occurs on the perimeter of the 9.1 cm tall stainless steel rod. A hole is bored through the middle of the rod. The solution flows upwards through the borehole and overflows down the perimeter of the rod. The upward flowing gas and the downward flowing liquid contact each other and CO_2 mass transfer is achieved over the known surface area of the rod. The wetted area is calculated as 38.52 cm^2 (assuming a hemisphere of liquid is present above the borehole). The annular region for gas flow and the inside diameter of the cell are estimated to be 1.30 cm^2 and 1.70 cm (Pacheco 1998).

Each experiment will measure the flux of CO_2 using about 6 inlet flue gas concentrations. At low CO_2 concentrations, desorption will occur. At high CO_2 concentrations absorption will occur. The CO_2 driving force (CO_2 partial pressure minus equilibrium partial pressure of the solution) can be correlated with flux, as shown in Figure 6. The equilibrium partial pressure of the solution can be extrapolated as the partial pressure which produces no CO_2 flux. The rate at which the flux changes with driving force (slope of the line in Figure 6) is the overall mass transfer coefficient. The overall mass transfer coefficient can be used to calculate the kinetics of the solvent.

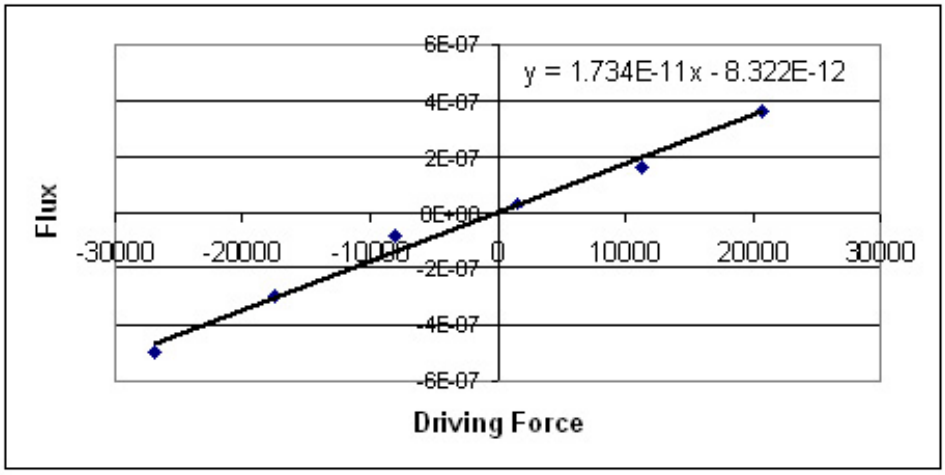

Figure 6. Typical Flux-Driving Force Results for a Wetted Wall Column Experiment

Table 4 shows a matrix of the planned wetted wall column experiments. Some of the conditions will have to be adjusted due to viscosity or solubility limitations. Higher piperazine concentrations can only be tested at relatively high CO_2 loadings due solubility limitations. Both 13m MEA and 16m piperazine are most likely too viscous and slow reacting for industrial CO_2 capture. The observed tradeoffs between rates and capacity will lead to an optimal amine concentration for CO_2 capture.

Table 4. Planned Wetted Wall Column Experiments

Amine Conc (mol/kg_{H2O})		CO_2 Loading	Temp
MEA	PZ	(mol/mol_{alk})	(C)
7 9 11 13	-	0 0.2 0.3 0.4 0.5	40 60 80 100
-	2 5 8 12 16	0 0.2 0.3 0.4 0.5	40 60 80 100
7	2	0 0.2 0.3 0.4 0.5	40 60 80 100

4.2. Diaphragm Cell

Diffusion experiments will likely be performed using a diaphragm cell as shown in Figure 7. It is inexpensive to build and can yield accuracies as high as 0.2% (Cussler 1997). The diaphragm cell contains two compartments separated by a glass frit. Initially the two compartments are filled with different solutions. Over time the two solutions will diffuse into each other. Magnetic stirrers ensure the solution compositions remain homogenous in each compartment. After characterizing the frit using solutions with known diffusion coefficients, diffusion coefficients of unknown solutions can be calculated using mass transfer theory.

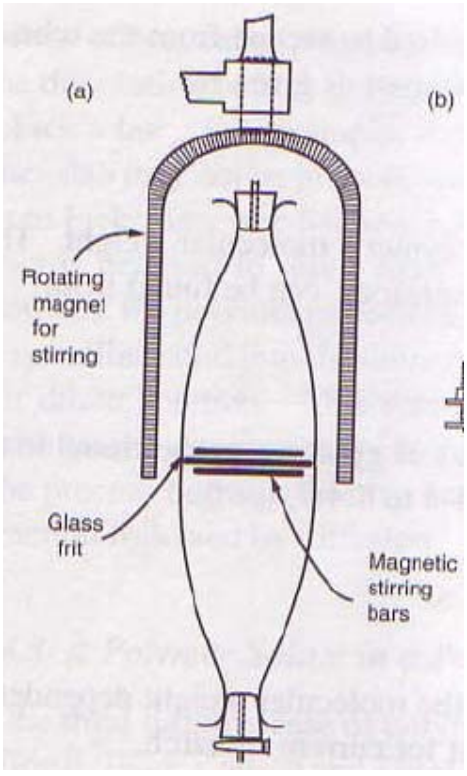

Figure 7. Diaphragm Cell Apparatus (Cussler 1997)

The diffusion cell should be able to determine how the diffusion coefficient of each amine system varies with viscosity and CO_2 loading. Recall, experiment using MDEA and AMP produced different viscosity-diffusion coefficient relationships (Versteeg and Van Swaaij 1988; Tomcej and Otto 1989; Xu, Otto et al. 1991).

5. Summary

The main objective of this work is to determine the optimal amine concentration for CO_2 capture with MEA, piperazine and MEA/PZ solutions. The optimal concentration will depend on tradeoffs between reaction rates (including kinetics and diffusion) and CO_2 capacity. The CO_2 capacity of the solution will increase with increased amine concentration since the CO_2 partial pressure is related primarily to the CO_2 loading. The reaction rate will likely go through a maximum at some amine concentration. The following flux equation shows the relevant terms for mass transfer.

$$N_{CO2} = \frac{\sqrt{D_{CO2} k_2 [Am]_b}}{H_{CO2}} (P_{CO2,i} - P^*_{CO2,b}) \qquad (16)$$

The diffusion coefficient will decrease with increasing amine concentration due to viscosity changes. Obviously the amine concentration term will be higher at higher amine concentrations. It is still unclear whether the rate constant will increase or decrease with increasing amine concentration due to ionic strength effects. This analysis to find an optimal amine concentration will require the use of detailed kinetics and diffusion coefficients in highly loaded, highly concentrated systems. Both wetted wall column and diaphragm cell experiments will be performed to obtain the appropriate kinetic and diffusion data.

6. References

Aboudheir, A. A. (2002). Kinetics, Modeling, and Simulation of Carbon Dioxide Absorption into Highly Concentrated and Loaded Monoethanolamine Solutions. Chemical Engineering. Regina, Saskatchewan, Canada, University of Regina. **Ph.D.:** 364.

Alper, E. (1990). "Reaction Mechanism and Kinetics of Aqueous Solutions of 2-Amino-2-methyl-1-propanol and Carbon Dioxide." Ind. Eng. Chem. Res. **29**: 1725-1728.

Alvarez-Fuster, C., N. Midoux, et al. (1980). "Chemical Kinetics of the Reaction fo Carbon Dioxide with Amines in the Pseudo m-nth Order Conditions in Aqueous and Organic Solutions." Chem. Engr. Sci. **35**(8): 1717-1723.

Astarita, G. (1961). "Carbon Dioxide Absorption in Aqueous Monoethanolamine Solutions." Chem. Engr. Sci. **16**: 202-207.

Barnola, J. M., D. Raynaud, et al. (2003). "Historical CO2 record from the Vostok ice core." In Trends: A Compendium of Data on Global Change. Carbon Dioxide Information Analysis Center, Oak Ridge National Laboratory, U.S. Department of Energy, Oak Ridge, Tenn., U.S.A.

Barth, D., C. Tondre, et al. (1986). "Stopped-Flow Investigations of the Reaction Kinetics of Carbon Dioxide with Some Primary and Secondary Alkanolamines in Aqueous Solutions." Int. J. Chem. Kinetics **18**: 445-457.

Bishnoi, S. (2000). Carbon Dioxide Absorption and solution equilibrium in piperazine activated methyldiethanolamine. Chemical Engineering. Austin, TX, The University of Texas at Austin**:** 270.

Bishnoi, S. and G. T. Rochelle (2000). "Absorption of Carbon Dioxide into Aqueous Piperazine: Reaction Kinetics, Mass Transfer and Solubility." Chem. Engr. Sci. **55**: 5531-5543.

Clarke, J. K. A. (1964). "Kinetic of Absorption of Carbon Dioxide in Monoethanolamine Solutions at Short Contact Times." Ind. and CE Fundamentals **3**(3): 239-245.

Crooks, J. E. and J. P. Donnellan (1989). "Kinetics and Mechanism of the Reaction Between Carbon Dioxide and Amines in Aqueous Solution." J. Chem. Soc. Perkin Trans. II: 331-333.

Cullinane, J. T. (2005). Thermodynamics and Kinetics of aqueous piperazine with potassium carbonate for carbon dioxide absorption. Chemical Engineering. Austin, TX, The University of Texas at Austin**:** 295.

Cussler, E. L. (1997). Diffusion: Mass Transfer in Fluid Systems, Cambridge University Press.

Danckwerts, P. V. (1970). Gas-Liquid Reactions, McGraw-Hill, Inc.

Danckwerts, P. V. and M. M. Sharma (1966). "Absorption of Carbon Dioxide into Solutions of Alkalis and Amines (with Some Notes on Hydrogen Sulphide and Carbonyl Sulphide)." Chem. Engr.: CE244-CE280.

Dang, H. (2000). CO2 absorption rate and solubility in monoethanolamine/piperazine/water. Chemical Engineering. Austin, TX, The University of Texas at Austin. **M.S.E.:** 129.

Derks, P. W. J., T. Kleingeld, et al. (2006). "Kinetics of Absorption of Carbon Dioxide in Aqueous Piperazine Solution." Chem. Engr. Sci. **61**(20): 6837-6854.

Donaldson, T. L. and Y. N. Nguyen (1980). "Carbon Dioxide Reaction Kinetics and Transport in Aqueous Amine Membranes." Ind. Eng. Chem. Fundam. **19**: 260-266.

Emmert, R. E. and R. L. Pigford (1962). "Gas Absorption Accompanied by Chemical Reaction: A Study of the Absorption of Carbon Dioxide in Aqueous Solutions of Monoethanolamine." AlChE Journal **8**(2): 171-175.

Hagewiesche, D. P., S. S. Ashour, et al. (1995). "Absorption of Carbon Dioxide into Aqueous Blends of Monoethanolamine and N-Methyldiethanolamine." Chem. Engr. Sci. **50**(7): 1071-1079.

Hikita, H., S. Asai, et al. (1977). "The Kinetics of Reaction of Carbon Dioxide with Monoethanolamine, Diethanolamine and Triethanolamine by a Rapid Mixing Method." Chem. Engr. **13**: 7-12.

Hilliard, M. (2008). A Predictive Thermodynamic Model for an Aqueous Blend of Potassium Carbonate, Piperazine, and Monoethanolamine for Carbon Dioxide Capture from Flue Gas. Chemical Engineering. Austin, The University of Texas at Austin. **Ph.D.:** 1025.

Horng, S. and M. Li (2002). "Kinetics of Absorption of Carbon Dioxide into Aqueous Solutions of Monoethanolamine + Triethanolamine." Ind. Eng. Chem. Res. **41**: 257-266.

IEA (2001). Putting Carbon Back into the Ground, IEA Greenhouse Gas R&D Programme. **2006**.

IEA (2007). International Energy Annual 2005, Energy Information Administration.

Jamal, A., A. Meisen, et al. (2006). "Kinetics of Carbon Dioxide Absorption and Desorption in Aqueous Alkanolamine Solutions Using a Novel Hemispherical Contactor - I. Experimental Apparatus and Mathematical Modeling." Chem. Engr. Sci. **61**: 6571-6589.

Jensen, M. B., E. Jorgensen, et al. (1954). "Reactions Between Carbon Dioxide and Amino Alcohols." Acta Chem. Scand. **8**(7): 1137-1140.

Keeling, C. D. and T. P. Whorf (2005). "Atmospheric CO2 records from sites in the SIO air sampling network." In Trends: A Compendium of Data on Global Change. Carbon Dioxide Information Analysis Center, Oak Ridge National Laboratory, U.S. Department of Energy, Oak Ridge, Tenn., U.S.A.

Kumar, A., R. Ozah, et al. (2005). "Reservoir simulation of CO2 storage in deep saline aquifers." SPE Journal **10**(3): 336-348.

Laddha, S. S. and P. V. Danckwerts (1981). "Reaction of CO2 with Ethanolamines: Kinetics from Gas Absorption." Chem. Engr. Sci. **36**: 479-482.

Leder, F. (1971). "The Absorption of CO2 into Chemically Reactive Solutions at High Temperature." Chem. Engr. Sci. **26**: 1381-1390.

Littel, R. J., G. F. Versteeg, et al. (1992). "Kinetics of CO2 with Primary and Secondarty Amines in Aqueous Solutions - II. Influence of Temperature on Zwitterion Formation and Deprotonation Rates." Chem. Engr. Sci. **47**(8): 2037-2045.

Mshewa, M. M. (1995). Carbon Dioxide Desorption/Absorption with Aqueous Mixtures of Methyldiethanolamine and Diethanolamine at 40 to 120C. Chemical Engineering. Austin, TX, The University of Texas at Austin. **Ph.D.**

NCDC (2006). The Annual Global Land Temperature Anomalies, National Climatic Data Center.

Okoye, C. I. (2005). Carbon Dioxide Solubility and Absorption Rate in Monoethanolamine/Piperazine/H2O. Chemical Engineering. Austin, TX, The University of Texas at Austin. **M.S.E.:** 57.

Pacheco, M. A. (1998). Mass Transfer, Kinetics and Rate-Based Modeling of Reactive Absorption. Chemical Engineering. Austin, TX, The University of Texas at Austin. **Ph.D.:** 291.

Penny, D. and T. Ritter (1983). "Kinetic Study of Reaction Between Carbon Dioxide and Primary Amines." J. Chem. Soc. Faraday Trans. **79**: 2103-2109.

Rao, A. B. and E. S. Rubin (2002). "A Technical, Economic, and Environmental Assessment of Amine-Based CO_2 Capture Technology for Power Plant Greenhouse Gas Control." Environmental Science and Technology **36**(20): 4467-4475.

Rochelle, G. T., F. Seibert, et al. (2007). CO_2 Capture by Absorption with Potassium Carbonate: Final Report.

Rubin, E. S., A. B. Rao, et al. (2004). Comparative Assessment of Fossil Fuel Power Plants with CO_2 Capture and Storage. 7th International Conference on Greenhouse Gas Control Technologies, Vancouver, Canada.

Sada, E., H. Kumazawa, et al. (1976b). "Gas Absorption with Consecutive Chemical Reaction: Absorption of Carbon Dioxide into Aqueous Amine Solutions." Chem. Engr. **54**: 421-424.

Sada, E., H. Kumazawa, et al. (1976a). "Simultaneous Absorption of Carbon Dioxide and Hydrogen Sulphide into Aqueous Monoethanolamine Solutions." Chem. Engr. Sci. **31**: 839-841.

Sada, E., H. Kumazawa, et al. (1985). "Chemical Kinetics of the Reaction of Carbon Dioxide with Ethanolamine in Non-aqueous Solvents." AlChE Journal **31**(8): 1297-1303.

Samanta, A. and S. S. Bandyopadhyay (2007). "Kinetics and Modeling of Carbon Dioxide Absorption into Aqueous Solutions of Piperazine." Chem. Engr. Sci. **62**(24): 7312-7319.

Sharma, M. M. (1965). "Kinetics of Reactions of Carbonyl Sulphide and Carbon Dioxide with Amines and Catalysis by Bronsted Bases of the Hydrolysis of COS." Trans. Faraday Soc. **61**: 681-688.

Snijder, E. D., M. J. M. te Riele, et al. (1993). "Diffusion Coefficients of Several Aqueous Alkanolamine Solutions." J. Chem. Eng. Data **38**(3): 475-480.

Sun, W.-C., C.-B. Yong, et al. (2005). "Kinetics of the Absorption of Carbon Dioxide into Mixed Aqueous Solutions of 2-amino-2methyl-1-propanol and Piperazine." Chem. Engr. Sci. **60**(2): 503-516.

Tomcej, R. A. and F. D. Otto (1989). "Absorption of Carbon Dioxide and Nitrous Oxide into Aqueous Solutions of Methyldiethanolamine." AIChE Journal **35**(5): 861-864.

Versteeg, G. F., L. A. J. Van Dijck, et al. (1996). "On the Kinetics Between CO_2 and Alkanolamines Both in Aqueous and Non-aqueous Solutions. An Overview." Chem. Engr. Comm **144**: 113-158.

Versteeg, G. F. and W. P. M. Van Swaaij (1988). "Solubility and diffusivity of acid gases (carbon dioxide, nitrous oxide) in aqueous alkanolamine solutions." J Chem Eng Data **33**(1): 29-34.

Xiao, J., C. Li, et al. (2000). "Kinetics of Absorption of Carbon Dioxide into Aqueous Solutons of 2-Amino-2-methyl-1-propanol + Monoethanolamine." Chem. Engr. Sci. **55**: 161-175.

Xu, S., F. D. Otto, et al. (1991). "Physical Properties of Aqueous AMP Solutions." J Chem Eng Data **36**(1): 71-75.

Appendix A

Table A. Schedule of Proposed Experimental and Modeling Work

	2008									2009				
	Mar	Apr	May	Jun	Jul	Aug	Sep	Nov	Dec	Jan	Feb	Mar	Apr	May
Wetted Wall Column - MEA Systems														
Wetted Wall Column - PZ Systems														
Wetted Wall Column - MEA/PZ Systems														
Wetted Wall Column - Impurities in Systems														
Characterize and Troubleshoot Diaphragm Cell														
Perform Diffusion Experiments														
Model WWC with Aspen RateSep														
Dissertation														

Influence of Liquid Properties on Effective Mass Transfer Area of Structured Packing

Quarterly Report for January 1 – March 31, 2008

by Robert Tsai

Supported by the Luminant Carbon Management Program

and by the

Separations Research Program

Department of Chemical Engineering

The University of Texas at Austin

April 18, 2008

Abstract

The influence of viscosity on the hydraulic performance of Sulzer Mellapak 250Y structured packing was measured. Viscosity was increased to approximately 14 cP via the addition of high molecular weight poly(ethylene oxide) – POLYOX™ WSR N750. Slightly elevated pressure drops relative to the baseline were generally observed. Flooding onset occurred at lower gas F-factors, with the difference becoming more prominent at higher liquid loads. The enhanced viscosity resulted in greater liquid hold-up in the packing; measured values and trends corresponded well with literature data. The effective mass transfer area of Mellapak 250Y was also measured at around 14 cP and was not found to appreciably differ from the base case. Prior work has shown surface tension to have negligible influence as well, indicating that relatively coarse structured packings (250-series) are rather insensitive to fluid property variations. Hydraulic data for Mellapak 500Y were collected. As expected, pressure drop and hold-up were higher than with the 250Y packing. Finally, the effective area of Mellapak 500Y was re-evaluated at high (~72 dynes/cm) and low (~30 dynes/cm) surface tension. While measured values in both cases were greater than those previously reported, the effective area of the packing was still noticeably higher at the reduced surface tension.

Introduction

Packing is commonly used in industrial processes as a means of promoting efficient gas-liquid contact. One important application for which packed columns are being considered is treating flue gas for CO_2 capture. The conventional method consists of an aqueous amine solvent such as monoethanolamine (MEA) contacting the gas, resulting in the absorption of CO_2 (Kohl and Nielsen, 1997). The enriched solvent is sent to a stripper for regeneration and is then recycled back to the absorber. Gas-liquid contact in both the absorber and stripper is enhanced through the use of packing.

Reliable mass transfer models are necessary for design and analysis purposes. A critical factor involved in modeling is the prediction of the effective interfacial area of packing (a_e), which can be considered as the total gas-liquid contact area that is actively available for mass transfer. The current research effort is focused on this parameter. Characterization of effective areas is vital to amine-based CO_2 capture at the industrial level, because absorption rates actually become independent of conventional mass transfer coefficients (k_G or k°_L) but remain directly proportional to the effective area. Thus, it is especially desirable to have an accurate area model.

Numerous empirical or semi-empirical packing area correlations have been presented in the literature, but none has been shown to be truly predictive over a wide range of conditions. Wang et al. (2005) performed a comprehensive review of the available models. The various correlations predict different and sometimes even contradictory effects of liquid viscosity and surface tension, properties that would be expected to fundamentally influence the wetted area of packing. It is evident that their role is not well understood, and there is a definite need for work in this subject matter.

The Separations Research Program (SRP) at the University of Texas at Austin has the capability of measuring packing mass transfer areas. Measurements are performed by absorbing CO_2 from air with 0.1 M NaOH in a 430 mm (16.8 in) ID column. Unfortunately, physical parameters are limited to those of water, making it potentially inaccurate to extend these results to other fluids of interest, such as amine solvents, due to the differences in viscosity and surface tension.

Limited understanding of the fluid mechanics and mass transfer phenomena in packed columns has been noted, and the need for experiments over a broader range of conditions has been identified (Wang et al., 2005). The goal of this research is to address these shortcomings and ultimately develop an improved effective area model for structured packing. The general objectives are to:

- Develop a fundamental understanding of the fluid mechanics associated with structured packing operation;
- Determine suitable chemical reagents to modify the surface tension and viscosity of the aqueous caustic solutions employed to make packing area measurements, and characterize potential impacts of such additives on the CO_2-NaOH reaction kinetics;
- Expand the SRP database by measuring the mass transfer areas of several different structured packings over a range of liquid viscosities and surface tensions;
- Combine the data and theory into a semi-empirical model that captures the features of the tested systems and adequately represents effective area as a function of viscosity, surface tension, and liquid load.

Experimental

430 mm ID Packed Column

The packed column had an outside diameter of 460 mm (18 in), inside diameter of 430 mm (16.8 in), and a 3 m (10 ft) packed height. For details regarding the apparatus and procedure for mass transfer or hydraulic tests, earlier quarterly reports may be consulted.

Wetted-Wall Column (WWC)

The wetted-wall column (WWC) is a vapor-liquid contactor with a known interfacial area and is the same apparatus that Mshewa (1995), Bishnoi (2000), and Cullinane (2006) employed to

measure the kinetics of various CO_2-amine systems. The associated equipment and experimental protocol are archived elsewhere (e.g. Q3 2006 report).

Goniometer

The goniometer (ramé-hart Inc., Model #100-00) was equipped with an adjustable stage; the overall setup included a computer-linked camera for live image display and a light source (see Q3 2006 report). The apparatus was utilized in conjunction with FTA32 Video 2.0 software (developed by First Ten Angstroms, Inc.) to make surface tension measurements via the pendant drop method.

Rheometer

The rheometer employed for viscosity measurements was first described in the Q4 2006 report. The apparatus (Physica MCR 300) was manufactured by Anton Paar USA. Temperature was regulated with a Peltier TEK 150P-C unit and a Julabo F25 water bath unit. Measurement profiles consisted of a linearly or logarithmically increased or decreased shear rate (ranging from 100 to 2000 s^{-1}), with 10-20 data points recorded at 15 second intervals. Viscosity was determined from a plot of shear stress (measured) vs. shear rate.

Materials

0.1 M NaOH solution for WWC experiments was purchased from Fisher Scientific (certified grade). The solid NaOH pellets (ACS grade) used in packed tower experiments were obtained from either EMD Chemicals, Inc or PHARMCO-AAPER. POLYOX™ WSR N750 (pharmaceutical (NF) grade) was procured from Dow Chemical. Antifoam agent (Dow Corning® Q2-3183A) was supplied by Dow Corning®.

Results and Discussion

Theoretical Analysis of Data

The primary equation used to interpret both the WWC and packed column results is presented in equation 1. The overall mass transfer resistance is expressed as a series relationship of the gas and liquid contributions. K_G, k_G, and k_g' represent the overall, gas-side, and liquid-side mass transfer coefficients, respectively.

$$\frac{1}{K_G} = \frac{1}{k_G} + \frac{1}{k_g'} \qquad (1)$$

For the WWC, the overall mass transfer coefficient is calculated from the CO_2 flux and the partial pressure driving force.

$$K_G = \frac{N_{CO_2}}{P_{CO_2\,LM}} = \frac{N_{CO_2}}{P\left(y_{CO_2\,in} - y_{CO_2\,out}\right)} \ln\left(\frac{y_{CO_2\,in}}{y_{CO_2\,out}}\right) \qquad (2)$$

A gas-side mass transfer coefficient correlation for the WWC was developed by absorption of SO_2 into 0.1 M NaOH, an entirely gas-film controlled process (Bishnoi, 2000). Equation 3 is a rearrangement of this correlation, which involved the Sherwood, Reynolds, and Schmidt numbers and the physical dimensions of the system.

$$k_G = 1.075\left(\frac{u_G\, d^2}{L\, D_{CO_2,G}}\right)^{0.85}\left(\frac{D_{CO_2,G}}{RTd}\right) \qquad (3)$$

Equations 1-3 are used to calculate k_g', which has been defined as a liquid-side mass transfer coefficient expressed in terms of a CO_2 partial pressure driving force.

$$k_g' = \frac{\sqrt{k_{OH^-}[OH^-]D_{CO_2,L}}}{H_{CO_2}} \qquad (4)$$

For comparison, equation 4 can be evaluated using literature correlations for the diffusivity of CO_2 in electrolyte solutions ($D_{CO2,L}$), the Henry's constant of CO_2 in electrolyte solutions (H_{CO2}), and the rate constant (k_{OH-}) (Pohorecki and Moniuk, 1988).

Equation 1 is also central to the analysis of data gathered using the 430 mm ID packed column. Gas-side resistance is intentionally limited by using dilute caustic solution (0.1 M) and operating at high superficial air velocities (usually 1 or 1.5 m/s). Even under the worst circumstances, this resistance (estimated using the correlation for k_G proposed by Rocha et al. (1996)) should be accountable for no more than 1.5% of the overall mass transfer resistance. Therefore, gas-side resistance is ignored in the analysis, and K_G is assumed to be equal to k_g'. This approximation enables the effective packing area (a_e) to be determined, by separating it from the volumetric mass transfer coefficient, $K_G a_e$, as shown in equation 5.

$$a_e = \frac{u_G \ln\left(\frac{y_{CO_2\,in}}{y_{CO_2\,out}}\right)}{ZK_G RT} \approx \frac{u_G \ln\left(\frac{y_{CO_2\,in}}{y_{CO_2\,out}}\right)}{Zk_g' RT} \qquad (5)$$

Wetted-Wall Column

The purpose of the WWC was two-fold. First, it served to verify the literature correlations (Pohorecki and Moniuk, 1988) historically employed to interpret the packed column data. Second, it was utilized to evaluate the impact of additives on the CO_2-NaOH kinetics. The data from these studies have been discussed in other quarterly reports. In short, the correlations of Pohorecki and Moniuk have been deemed to be acceptable. Furthermore, the particular additives selected for use in this body of work (POLYOX or surfactant) have been concluded to have limited-to-no impact on k_g'.

Mellapak 250Y – Hydraulics

The hydraulic behavior of Sulzer Mellapak 250Y structured packing was measured under viscous ($\mu_L \sim 14$ cP) conditions. The test solution consisted of POLYOX WSR N750 and a small quantity of antifoam (25 $ppm_{w/v}$) dissolved in water. Figure 1 displays the pressure drop data at various liquid loads. The highest liquid loads (15 and 20 gpm/ft^2) were especially sensitive, exhibiting "spiking" behavior indicative of flooding at fairly low F-factors.

Figures 2-4 present the results together with past SRP data (some of which was shown in the previous quarterly report). The influence of viscosity on pressure drop at a given L/G ratio was small in comparison to the dry-vs.-irrigated pressure drop difference. Nevertheless, the viscosity augmentation clearly promoted the onset of flooding at lower F-factors relative to the base case.

The difference is minimal at 5 gpm/ft^2 (Figure 2) but becomes more noticeable at 10 gpm/ft^2 (Figure 3) and much more so at 20 gpm/ft^2 (Figure 4).

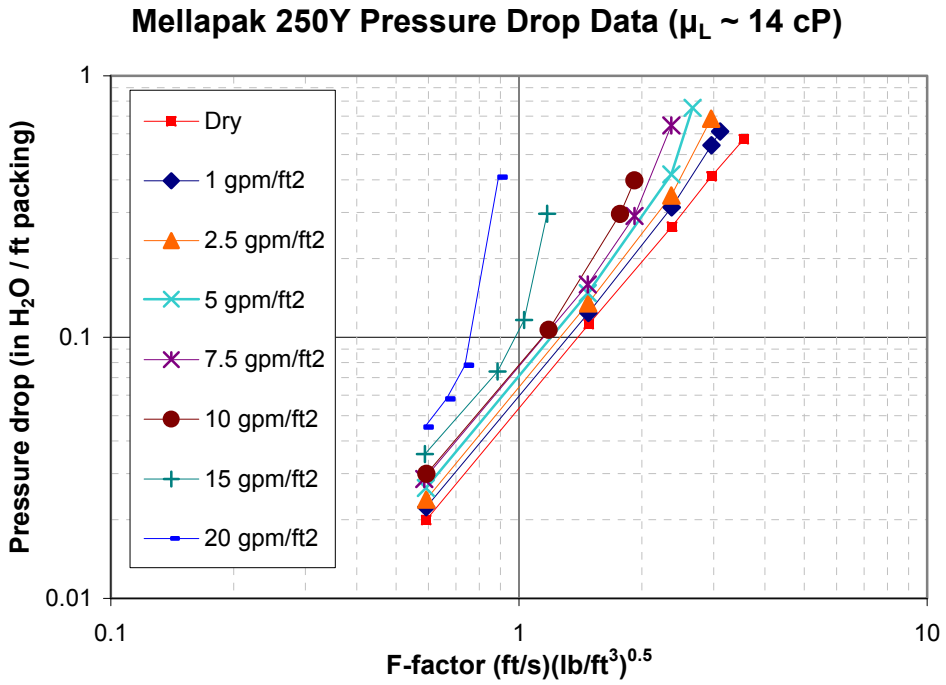

Figure 1: Mellapak 250Y pressure drop data (μ_L ~ 14 cP). Solution contained small quantity of antifoam (~25 $ppm_{w/v}$).

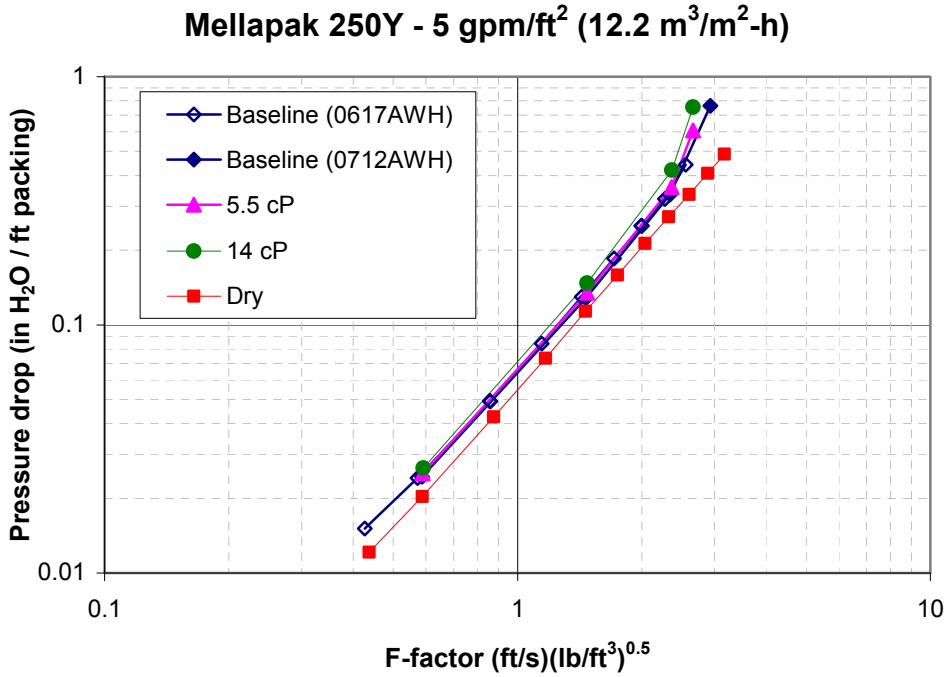

Figure 2: Mellapak 250Y pressure drop data at liquid load of 5 gpm/ft^2. Viscous solutions contained small quantities of antifoam (~10-25 $ppm_{w/v}$).

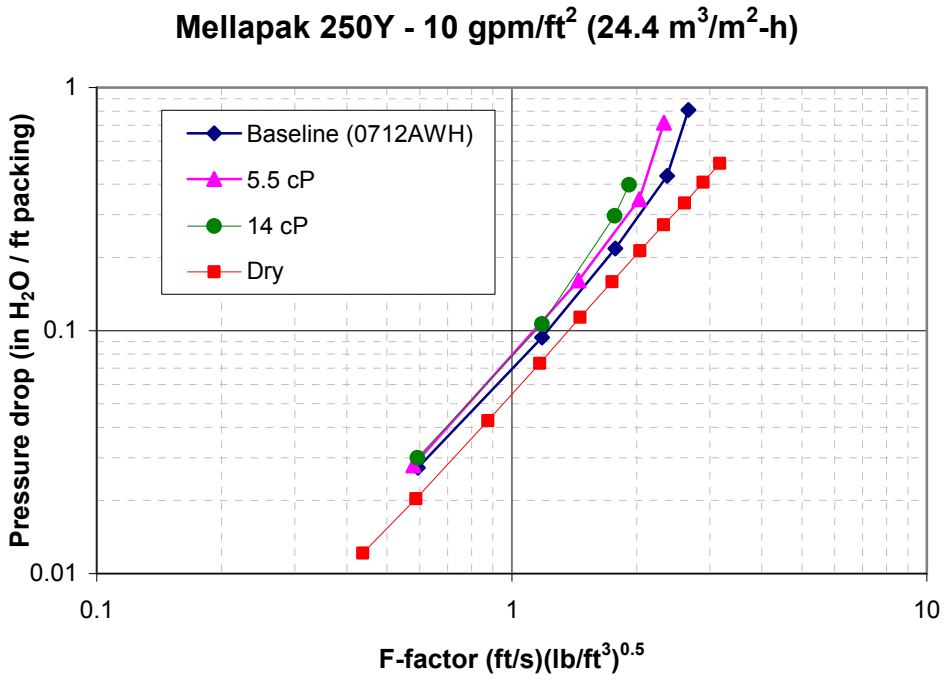

Figure 3: Mellapak 250Y pressure drop data at liquid load of 10 gpm/ft^2. Viscous solutions contained small quantities of antifoam (~10-25 ppm$_{w/v}$).

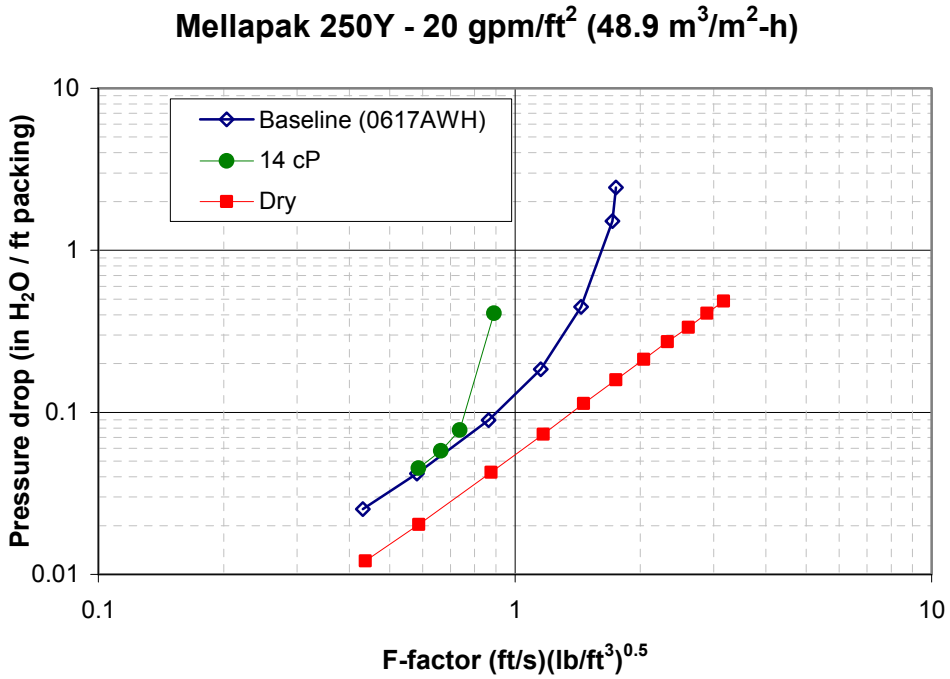

Figure 4: Mellapak 250Y pressure drop data at liquid load of 20 gpm/ft^2. Viscous solution contained small quantity of antifoam (~25 ppm$_{w/v}$).

In Figure 5, liquid hold-up data obtained at an F-factor of around 0.6 (ft/s)(lb/ft^3)$^{0.5}$ (i.e., well below the loading region) are plotted against the model of Suess and Spiegel (1992). Suess and Spiegel used a gamma ray absorption technique to measure hold-up in various Sulzer Mellapak packings. The packed height in their setup (3.5 m) was similar to ours (3 m), which may be important to note for comparative purposes. Their results were correlated into the form shown below.

$$h_L(\%) = c a_p^{0.83} u_L^{x} \left(\frac{\mu_L}{\mu_{L,0}} \right)^{0.25} \quad \text{(applies below loading point)} \qquad (6)$$

$c = 0.0169$, $x = 0.37$ for $u_L < 40$ m^3/m^2-h
$c = 0.00075$, $x = 0.59$ for $u_L > 40$ m^3/m^2-h

Equation 6 was over-predictive at the lowest liquid loads but coincided with the data quite well at higher loads. The discrepancy could perhaps be related to liquid distribution issues; Suess and Spiegel unfortunately did not specify what type of distributor they utilized. Increased viscosity expectedly resulted in greater hold-up, and the impact was in accordance with that predicted by equation 6 (exponent of 0.25).

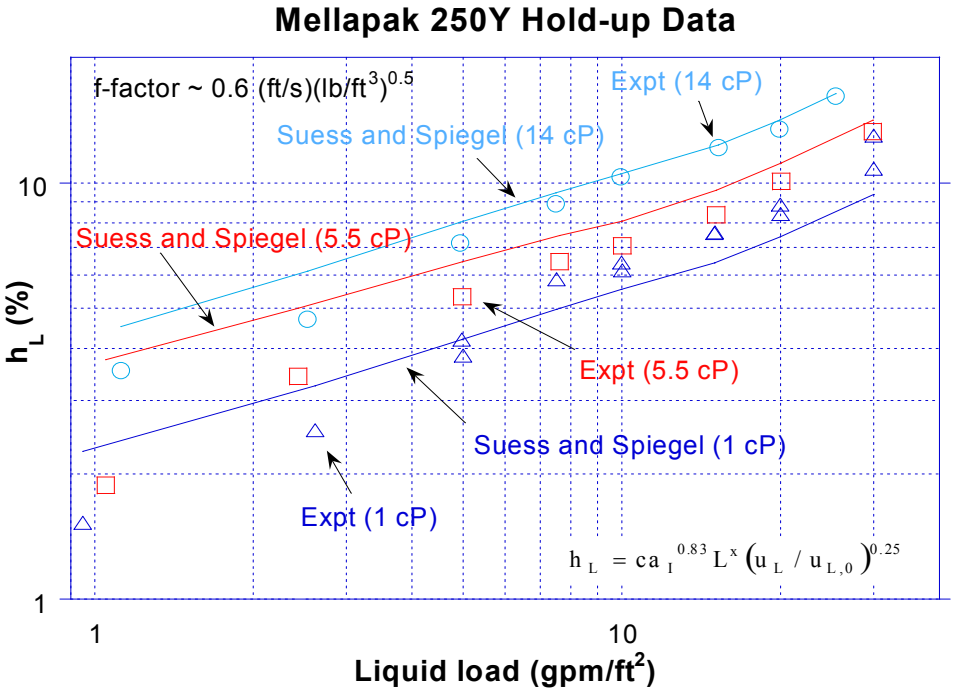

Figure 5: Comparison of Mellapak 250Y hold-up data with predicted values from equation 6. Viscous solutions contained small quantities of antifoam (~10-25 ppmw/v).

Mellapak 250Y – Mass Transfer

The effective mass transfer area of Mellapak 250Y (a_p = 250 m^2/m^3) was measured at approximately 14 cP and 40 dynes/cm. The reduced surface tension was due to both the POLYOX in solution and antifoam agent that was added to control foaming.

Three sets of data were collected at superficial air velocities of 0.6, 1, and 1.5 m/s. The results were found to be approximately the same regardless of air rate. Figure 6 compares the high viscosity data with baseline measurements. In previous work, a reduction in surface tension (~30-35 dynes/cm) was concluded to have no effect on the mass transfer area of 250Y. Therefore, it was assumed that the current results could be considered primarily in the context of viscosity. As can be seen, there was no appreciable difference between the baseline and viscous data sets, aside from possibly the data point at 10 gpm/ft^2. However, this point was not necessarily comparable, since the viscous solution was near its flooding limit.

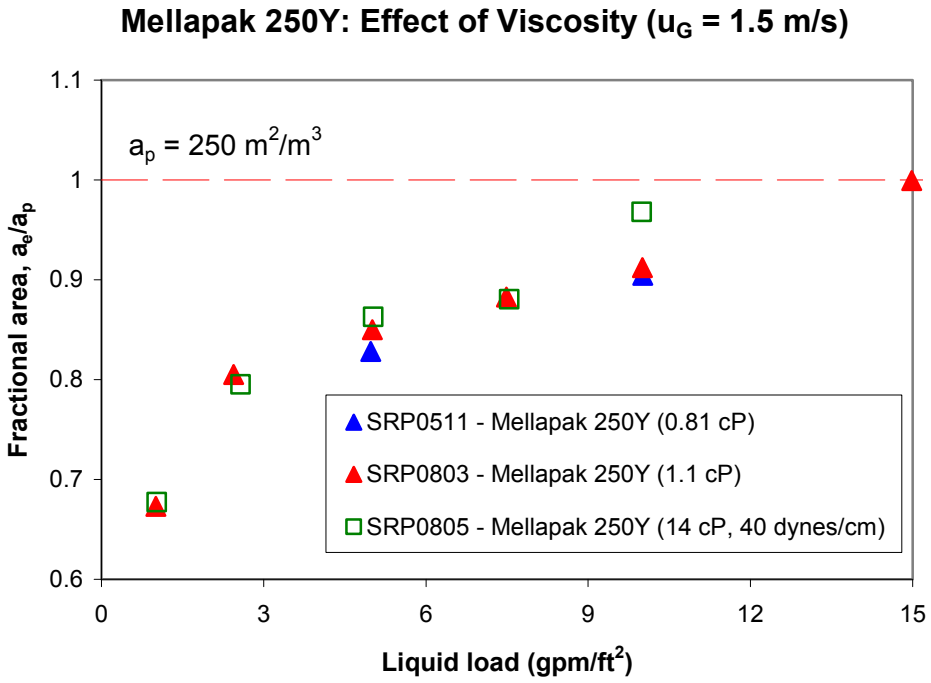

Figure 6: Fractional area measurements for Mellapak 250Y packing, compared at approximately 1 and 14 cP. u_G = 1.5 m/s for all data sets. Viscous solution contained small quantity of antifoam (~25-50 ppm$_{w/v}$).

Mellapak 500Y – Hydraulics

Figure 7 displays the baseline (water) hydraulic behavior of Mellapak 500Y (SRP file: 0806AWH). Pressure drops matched well with a previous study (SRP file: 0625AWH), although the more recent data appeared to tend towards flooding at slightly lower F-factors. Figure 8 is shown to illustrate this fact. This result was not completely surprising, given that exact flooding conditions can be difficult to pinpoint. This may hold especially true for a highly sensitive, fine packing like Mellapak 500Y. In this regard, it is possible that trace contaminants (e.g. from earlier experiments) were a factor, although the system was cleaned thoroughly via repeated flushings with water before beginning these studies.

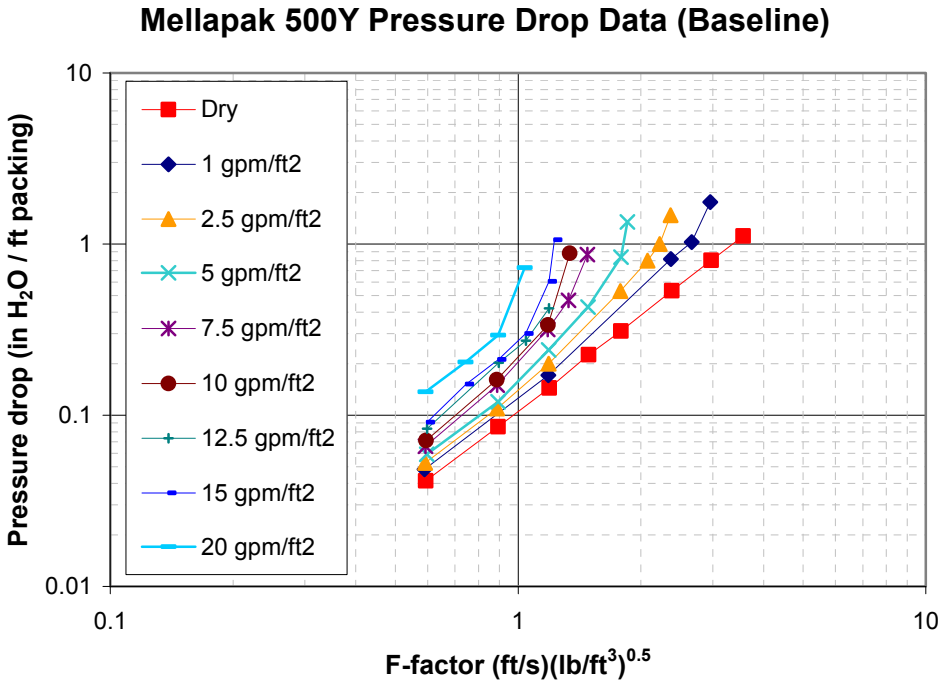

Figure 7: Mellapak 500Y pressure drop data (0806AWH).

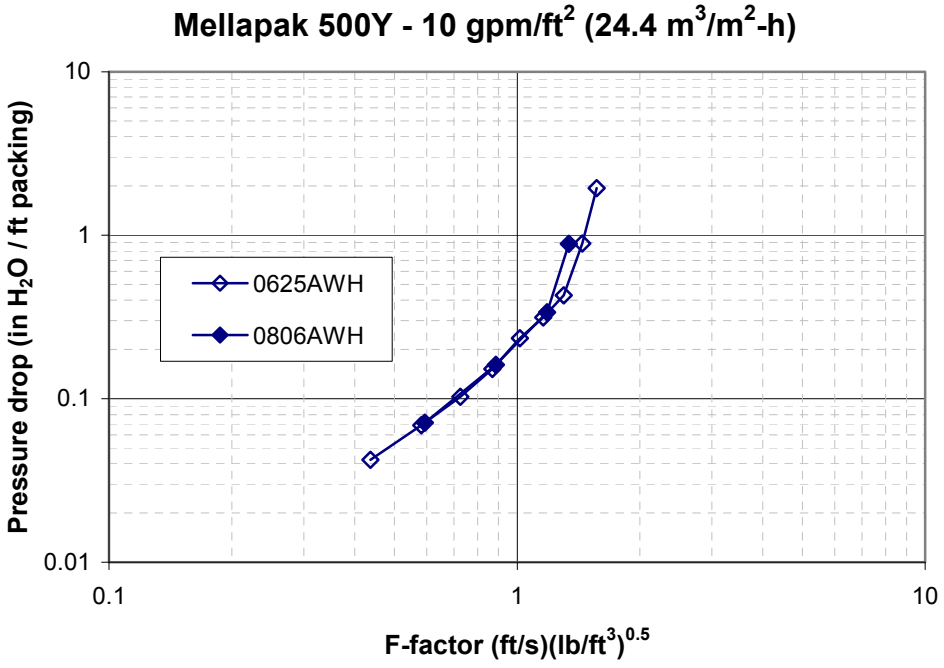

Figure 8: Comparison of Mellapak 500Y baseline pressure drop data (0625AWH and 0806AWH) at liquid load of 10 gpm/ft^2.

Figures 9 and 10 compare the hydraulics of Mellapak 250Y and 500Y. As anticipated, consistently higher pressure drop and liquid hold-up were associated with the higher surface area 500Y packing. Hold-up values calculated from equation 6 agreed with the obtained data.

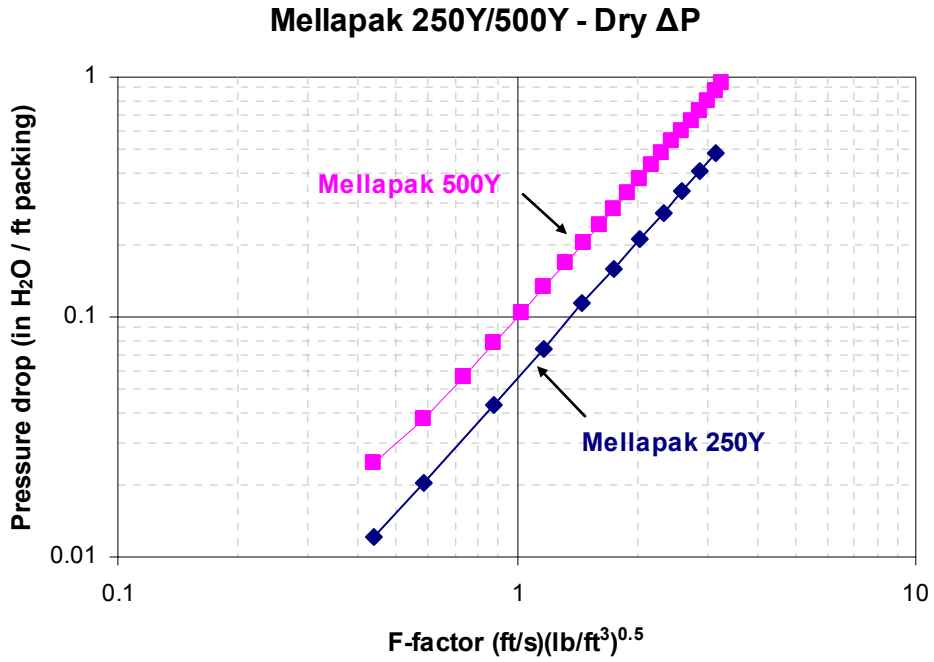

Figure 9: Comparison of Mellapak 250Y and 500Y dry pressure drop data.

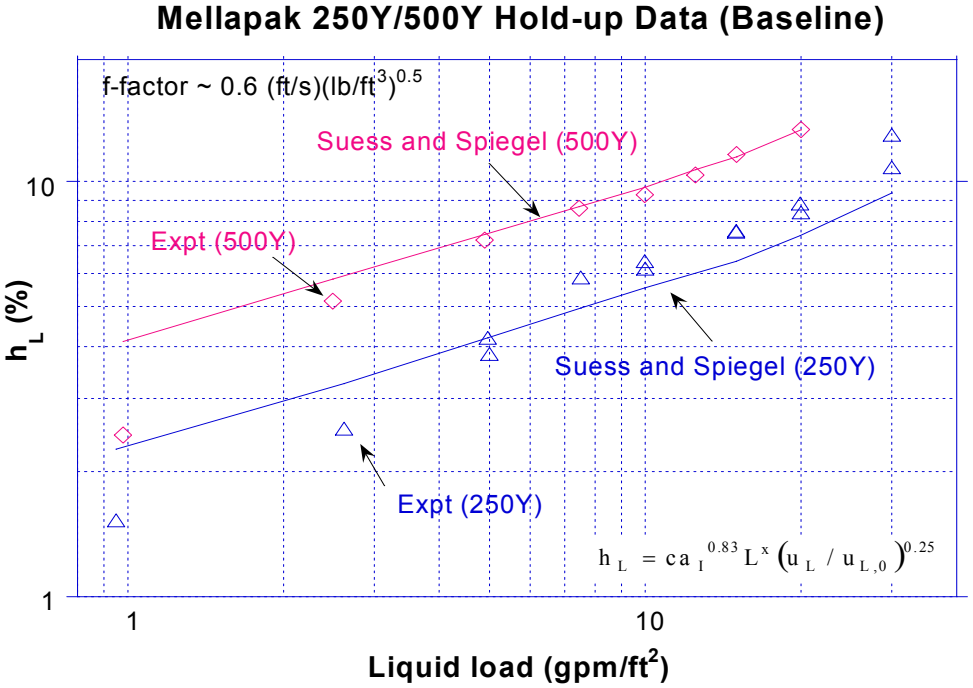

Figure 10: Comparison of Mellapak 250Y and 500Y hold-up data (obtained with water), along with predicted values from equation 6.

Mellapak 500Y – Mass Transfer

Prior to engaging in a high viscosity study with Mellapak 500Y, a baseline experiment was performed. Oddly, the mass transfer areas were significantly higher (>20%) than measured in a previous experiment (Tsai, 2008). Sample analysis ruled out the presence of physical property-altering contaminants, and the "new" results were further validated by repeat testing. The operational sensitivity of the packing was readily apparent; foaming was a problem in a few (but not all) cases, even with just caustic solution in the system. In these situations, a sparse (<5 $ppm_{w/v}$) amount of antifoam was added to the system. The impact on surface tension was verified to be negligible.

It is possible that the "old" data may have been affected by a systematic error – a leak in the sample pump, for instance – although there is no proof of this. An experiment with surfactant (~35 dynes/cm) was also carried out at the time, which showed surface tension to have a very important effect for Mellapak 500Y. To confirm that this conclusion remained true, a reduced surface tension test was conducted with the current system. Figures 11 and 12 respectively compare the older and more recent baseline/surfactant data obtained at an air velocity of 1 m/s. As can be seen, the low surface tension still resulted in a notable increase in mass transfer area, although the effect was not as dramatic as was once believed.

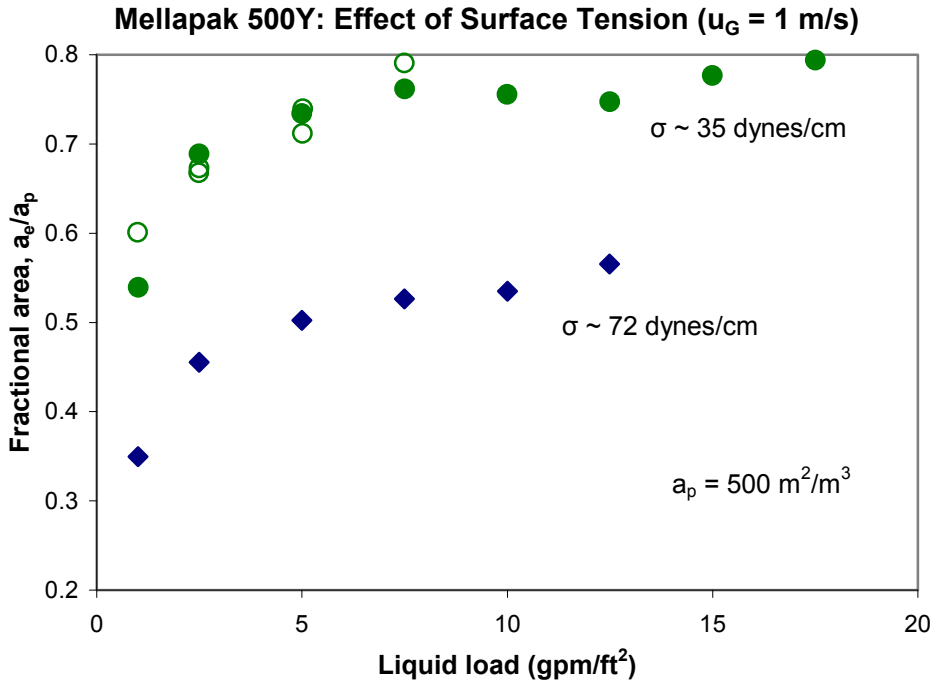

Figure 11: Fractional area measurements for Mellapak 500Y packing, compared at approximately 72 and 35 dynes/cm (Tsai, 2008). u_G = 1 m/s for all data sets. Surfactant solution contained antifoam (~50 $ppm_{w/v}$).

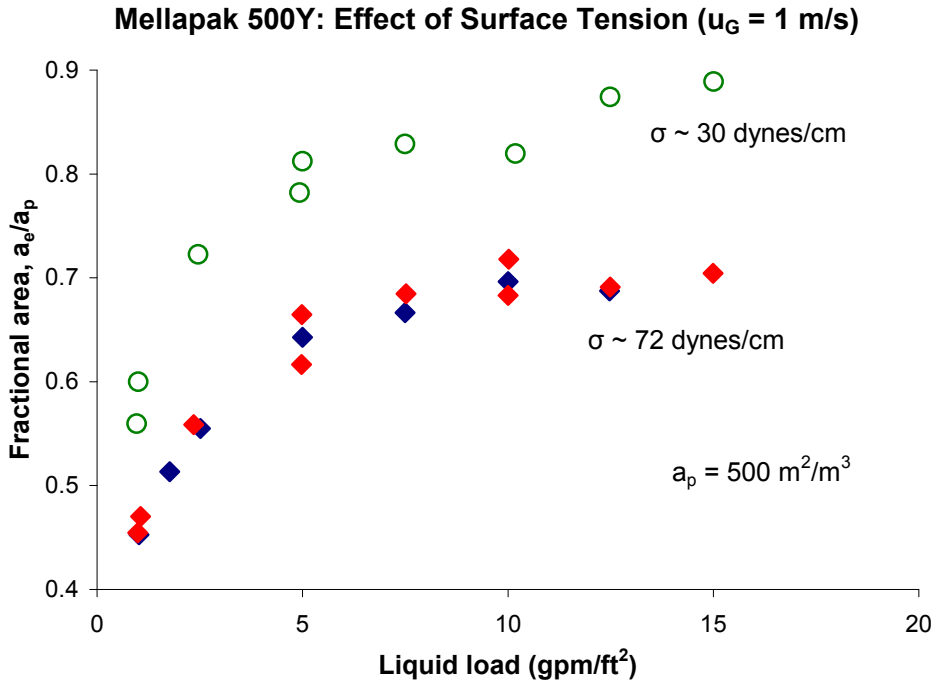

Figure 12: "New" fractional area measurements for Mellapak 500Y packing, compared at approximately 72 and 30 dynes/cm. uG = 1 m/s for all data sets. Surfactant solution contained antifoam (~50 ppmw/v).

Conclusions

Viscosity (~14 cP) did not affect the mass transfer area of Sulzer Mellapak 250Y packing but did impact the hydraulics, reducing the operational capacity of the packing. Mellapak 500Y displayed consistently higher pressure drop and liquid hold-up relative to 250Y. It would appear that the correlation of Suess and Spiegel is satisfactory for the prediction of hold-up in both 250 and 500-type Mellapak packings. For reasons unknown, previous measurements of the effective area of 500Y erred on the low side. Nevertheless, the "original" conclusion that was reached regarding the effect of surface tension on Mellapak 500Y (significant improvement in mass transfer area with a reduction in surface tension) was still found to be valid.

Future Work

The hydraulic behavior and mass transfer performance of Mellapak 500Y will be tested at high viscosity (~10 cP). Experiments with 250Y and 500Y at liquid property conditions that more closely resemble MEA (i.e. μ_L ~ 3-4 times water) will also be conducted.

Nomenclature

a_e = effective area of packing, m^2/m^3
a_p = specific (geometric) area of packing, m^2/m^3
D_{CO2} = diffusivity of CO_2, m^2/s
d = estimated hydraulic diameter of WWC reaction chamber, m
H_{CO2} = Henry's constant of CO_2, m^3·Pa/kmol
h_L = (total) liquid hold-up, dimensionless

K_G = overall gas-side mass transfer coefficient, kmol/(m^2·Pa·s)
k_G = gas-side mass transfer coefficient, kmol/(m^2·Pa·s)
k_g' = liquid-side mass transfer coefficient, kmol/(m^2·Pa·s)
k°_L = physical liquid-side mass transfer coefficient, m/s
k_{OH^-} = second-order reaction rate constant, m^3/(kmol·s)
L = exposed length of WWC, m
N_{CO2} = molar flux of CO_2, kmol/(m^2·s)
P = pressure, Pa
R = ideal gas constant, (m^3·Pa)/(kmol·K)
T = absolute temperature, K
u = superficial velocity, m/s
$y_{CO2\ in/out}$ = mole fraction of CO_2 at inlet/outlet
Z = packed height, m

Greek Symbols
μ = dynamic viscosity, Pa·s
$\mu_{L,0}$ = dynamic viscosity of water at 20˚C, Pa·s
σ = surface tension, N/m

Subscripts
G = gas phase
L = liquid phase

Dimensionless Groups
a_f = fractional area of packing, a_e/a_p

References

Bishnoi, S. Absorption of Carbon Dioxide into Aqueous Piperazine: Reaction Kinetics, Mass Transfer, and Solubility. *Chem. Eng. Sci.* **2000**, *55* (22), 5531-5543.
Cullinane, JT. Kinetics of Carbon Dioxide Absorption into Aqueous Potassium Carbonate and Piperazine. *Ind. Eng. Chem. Res.* **2006**, *45* (8), 2531-2545.
Kohl, A, R Nielsen. *Gas Purification*; Gulf Publishing Co.: Houston, 1997.
Mshewa, MM. Carbon Dioxide Desorption/Absorption with Aqueous Mixtures of Methyldiethanolamine and Diethanolamine at 40 to 120°C. Ph.D. Thesis, University of Texas at Austin, Austin, TX, 1995.
Pohorecki, R, W Moniuk. Kinetics of Reaction between Carbon Dioxide and Hydroxyl Ions in Aqueous Electrolyte Solutions. *Chem. Eng. Sci.* **1988**, *43* (7), 1677-1684.
Rocha, JA, JL Bravo, JR Fair. Distillation Columns Containing Structured Packings: A Comprehensive Model for Their Performance. 2. Mass-Transfer Model. *Ind. Eng. Chem. Res.* **1996**, *35* (5), 1660-1667.
Suess, P, L Spiegel. Hold-up of Mellapak Structured Packings. *Chem. Eng. Process.* **1992**, *31* (2), 119-124.
Tsai, RE, P Schultheiss. A Kettner, JC Lewis, AF Seibert, RB Eldridge, GT Rochelle. Influence of Surface Tension on Effective Packing Area. *Ind. Eng. Chem. Res.* **2008**, *47* (4), 1253-1260.
Wang, GQ, XG Yuan, KT Yu. Review of Mass-Transfer Correlations for Packed Columns. *Ind. Eng. Chem. Res.* **2005**, *44* (23), 8715-8729.

Modeling Stripper Performance for CO_2 Removal

Quarterly Report for January 1 – March 31, 2008

by David Van Wagener

Supported by the Luminant Carbon Management Program

and the

Industrial Associates Program for CO_2 Capture by Aqueous Absorption

Department of Chemical Engineering

The University of Texas at Austin

April 18, 2008

Abstract

This quarter focused on continuing two tasks. The first was creating an Aspen simulation to verify a recent pilot plant run with 35% MEA using a new thermodynamic model developed by Hilliard. Differences between the simulation values and pilot plant data were finally reconciled by implementing side duties in the column to account for heat loss. The five measured column temperatures were matched, and an estimated profile in between the measurements was imposed. The sump split and reboiler duty values were also varied to match plant data. In the final simulation, all of the measured data matched the simulation data within small error, and the calculated heat loss was only 12% greater than the calculated heat loss at the plant. The second stripper task was to investigate flashing stripping as a means of using solar energy to provide the heat for liberating CO_2. The selected solvent was 9 m MEA, and three flashes were used to adiabatically decrease the temperature and pressure and release vapor. A lean stream with a specified loading was used in a previous absorber model to calculate the accompanying rich stream. By varying the temperature step between each flash, the loading of the outlet lean stream could be matched to the absorber model specification. Next, the hot temperature was optimized to find the minimum equivalent work for that lean loading. Finally, the lean loading was optimized to further minimize the equivalent work. The minimum equivalent work when compressing the CO_2 to 5000 kPa was 24.47 kJ/mol CO_2. The optimum lean loading was 0.424. In the next quarter, the three stage flash will be further analyzed with new specifications, ensuring equal mole flow in all three vapor streams leaving the flash tanks.

Introduction

The pilot plant facility at the J. J. Pickle Research Campus has been used in the past to investigate the feasibility of proposed solvents and verify the accuracy of solvent models in Aspen (Oyenekan, 2007; Chen, 2007). Generally, agreement between the pilot plant data and Aspen predictions has proved to be difficult to accomplish, especially in the stripper section. Previous thermodynamic models developed for the CO_2 removing amines have only been valid within the range of absorber operating conditions because the data from which they were regressed were in that range.

Recently, however, Hilliard has developed a new thermodynamic model for H_2O-MEA-CO_2. This model was made using a large collection of data points from a wide range of conditions. The Electrolyte-NRTL model was used to represent the behavior of the solvent. This solvent model is novel because it relates the speciation of the solvent to its heat properties (ΔH_{abs}, C_p) in the hope of making it more accurate (Hilliard, 2008). This new model will be the standard for the Rochelle group, replacing the previous VLE model by Freguia.

In this quarter, work on flashing strippers as a method of solvent regeneration has continued. Flashing strippers operate by sending the rich solvent through the typical cross exchanger and then an additional preheater. The solvent reaches a higher temperature compared to that in a simple stripper configuration. The solvent is then passed through sequential adiabatic flash tanks, each reducing the temperature and pressure of the liquid. Carbon dioxide and water vapor are released in each flash, and the liquid decreases in loading. In this work, a three-step flash is used. A four-step flash was considered, but the increase in complexity was determined to be prohibitive. The three-step flash configuration results in a pressure ratio between each stage which falls close to the optimal compression ratio for vapor compressors, whereas the difference in pressure between each stage for a four-stage configuration would be too small.

The benefit of the flashing stripper configuration is that solar energy can be used where the heat is applied over a range of temperatures. Steam heating in traditional reboilers is provided at one temperature level, the condensation temperature of water at the source pressure. When converting the heat to an equivalent work, a 75% Carnot efficiency is calculated with a 10° approach at the reboiler:

$$W_{eq} = \sum_{i=1}^{n_{reboilers}} 0.75 * Q_i \left(\frac{T_i + 10K - T_{\text{sink}}}{T_i + 10K} \right) \qquad (1)$$

where T_{sink} is 313K, the sink temperature for the turbines converting the coal generated steam into electricity in the power plant. When using a heating medium besides steam, its temperature is not constant throughout heating, so the temperature driving force is decreased. The smaller temperature driving force reduces the lost work and equivalent work for heating. The new equivalent work can be calculated by integrating equation 1 from the initial to final temperature in the case where there is only one heater:

$$W_{eq} = 0.75 * Q \left(\frac{T_f - T_o - T_{\text{sink}} \ln\left(\frac{T_f}{T_o}\right)}{T_f - T_o} \right) \qquad (2)$$

Flashing is not a common approach for stripping of solvents. One reason it is generally avoided is because the CO_2/H_2O selectivity can be very low. However, by using three flashes, some of the stripping is done at high pressure, and high-pressure stripping has been shown to be beneficial for CO_2 selectivity in the multi-pressure and double matrix stripper configurations (Oyenekan, 2007).

Methods and Results

Pilot Plant Stripper Simulation

A run was performed at the pilot plant using 35% MEA for CO_2 removal on October 5, 2007. The stripper was operated at approximately 1 atm. A thermodynamic model for H_2O-MEA-CO_2 was recently completed by Hilliard, and this pilot plant run is an excellent opportunity to compare simulation results using the new model with physical data. Table 1 summarizes important data and calculations from the process. There were six thermocouples in the column at various heights, each indicated by *Temperature i* in Table 1.

Table 1: Pilot Plant Run Results

Lean stream		*Column data*	
Temperature (°F)	112.8	Temperature 1 (°F)	189.6
Flow (GPM)	17.4	Temperature 2 (°F)	187.3
Density (lb/ft³)	69.35	Temperature 3 (°F)	190.2
Loading (mol/mol)	0.36	Temperature 4 (°F)	194.7
Rich stream		Temperature 5 (°F)	195.8
Temperature (°F)	122.3	Temperature 6 (°F)	203.5
Flow (GPM)	17.1	Reboiler vapor T (°F)	216.8
Density (lb/ft³)	67.97	Reboiler duty (MMBTU/h)	0.488
Loading (mol/mol)	0.48	Heat loss (MMBTU/h)	0.077
Heat cross exchanger temperatures		Sump T (°F)	208.8
Lean in (°F)	112.8	Column pressure, bot (psia)	15.23
Lean out (°F)	196.9	Pressure drop, top (inH_2O)	0.57
Rich in (°F)	209.5	Pressure drop, bot (inH_2O)	0.6
Rich out (°F)	122.3	Outlet vapor T (°F)	189.3

As discussed in the previous quarter, not only was the CO_2 removal low, but the equivalent work was also very high. The new model in Aspen was used to attempt to validate this performance. A simulation was built in Aspen to reflect the pilot plant operation, shown in Figure 1. During the run, selected data was collected from the stripping column, and complete data was collected for the rich solvent entering the section and the lean solvent leading to section. Unfortunately,

the feed and product are not directly connected to the stripper, so additional process units besides the column must be simulated. The simulation also includes the reflux section (a cross exchanger, 2-phase flash, and pump). The solvent cross heat exchanger is also included to reproduce the streams for which data was collected in the run. Finally, the pilot plant reboiler was not what would normally be encountered in a separation column. The reboiler was separate from the column, and only a portion of the column sump passed through the reboiler and only a fraction of that liquid was vaporized and circulated back to the column. For this reason, an alternate reboiler section was designed, shown in the bottom right of Figure 1.

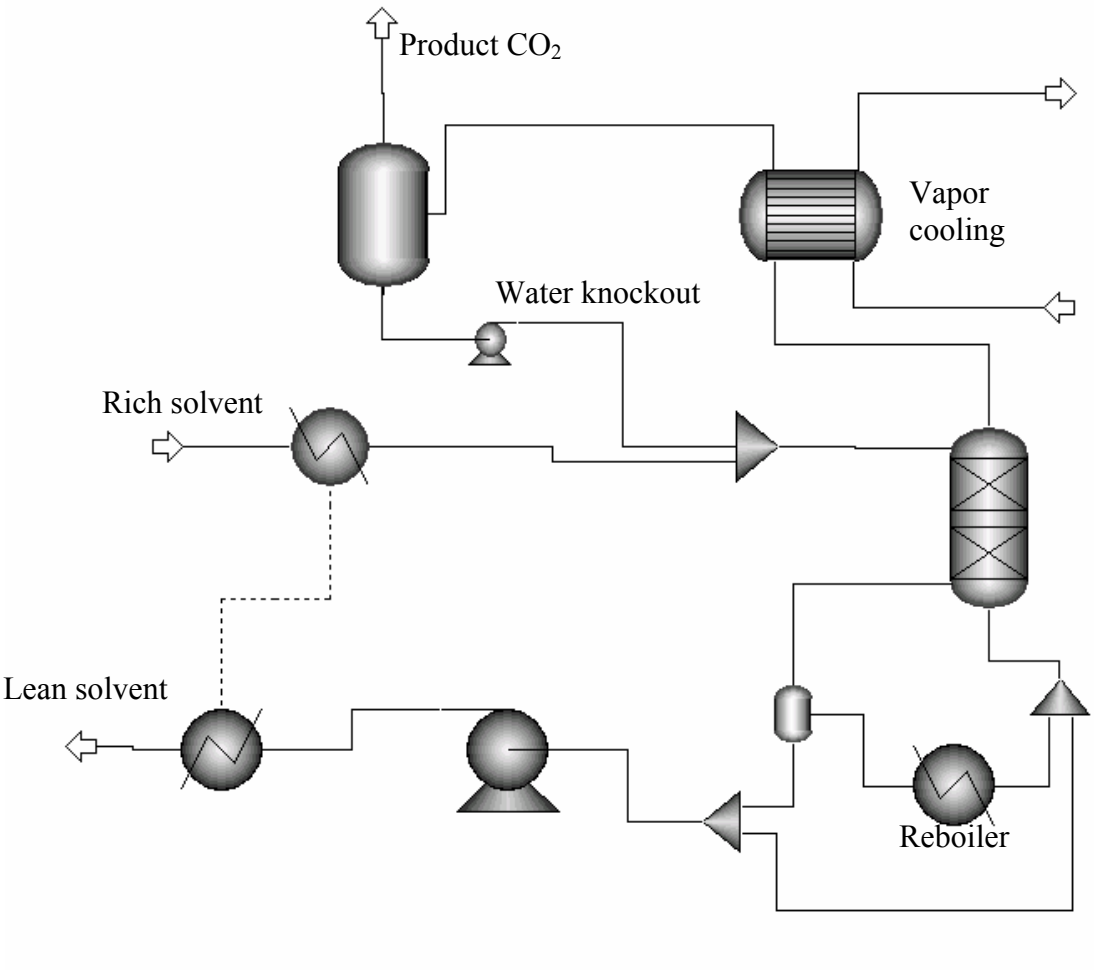

Figure 1: Aspen PFD of Pilot Plant Stripper Section

This Aspen simulation uses the recently completed H_2O-MEA-CO_2 thermodynamic model by Hilliard. The simulation assumes equilibrium reactions in the stripping column: RateSep is activated within RadFrac to calculate accurate mass transfer rates, but only the equilibrium-based reactions are entered.

The simulation was first run using the recorded data from the pilot plant run. The fraction of the sump drawoff was not recorded in the run, so it was estimated to be 75%. Additionally, the heat loss was assumed to be distributed evenly throughout the column. The performance of the column was predicted with acceptable accuracy, giving a lean loading and a lean mass flow rate close to their measured values. However, the temperatures predicted in the simulation were 4°F-

10°F above the measured values, with the exception of the stripper vapor temperature which was 4°F lower than the measured value.

Regressions were used to adjust variables and reduce the differences between the simulation and the pilot plant data. However, none of the regressions yielded perfect results. First, a regression of the data around the reboiler was used. The temperatures of the surrounding streams were corrected to match the plant data by adjusting the reboiler duty and reboiler split ratio, but the accuracy of the column profile and performance suffered. Next, the data was regressed to match the actual performance, but the column profile again did not match the plant data. Finally, a regression was developed to match the column profile, but the variables in the simulation were not adequate to match the values. It was determined that another method was needed to match all the data. Figure 2 displays the temperature in the column as a function of the height. Stage 0 was the top of the column, and stage 20 was the bottom of the column. In this simulation, there was no heat loss and all of the inputs were taken from the pilot plant results.

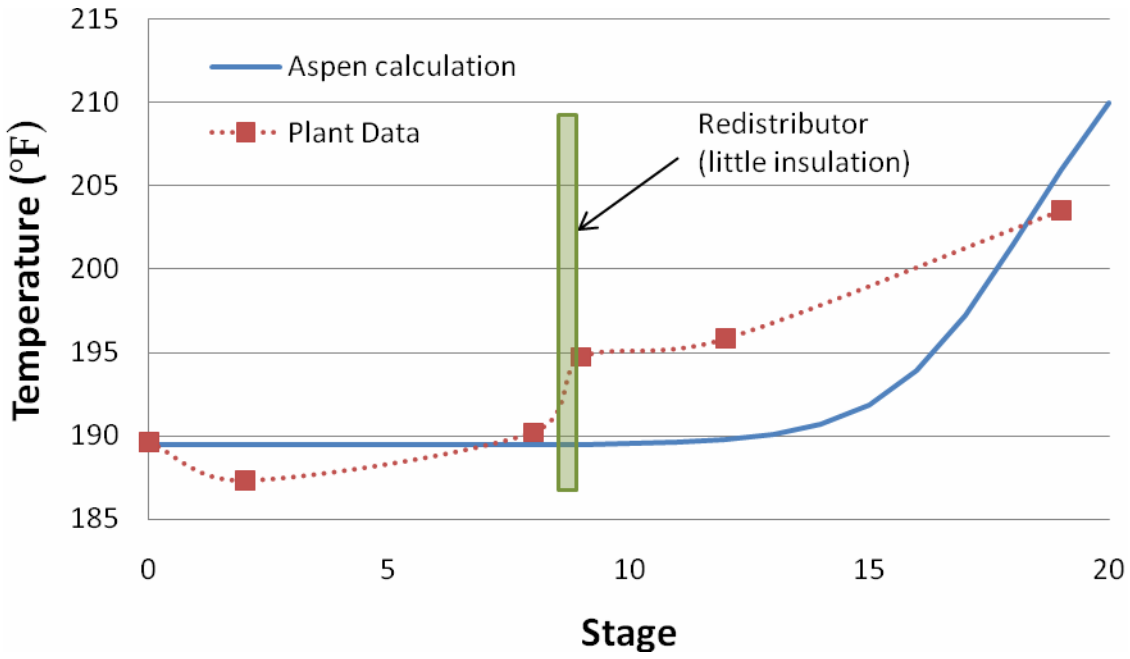

Figure 2: Temperature profiles in pilot plant and Aspen simulation stripper column (20 ft IMTP #40 packing, no heat loss, rich ldg = 0.48, reb duty = 0.488 MMBTU/hr, 63% removal).

Contrary to the simulation assumption, heat loss would not be expected to be uniform throughout the column height for several reasons. First, the insulation on the column was better in some areas than others. For example, the section around the redistributor had very poor insulation. Second, the driving force for heat loss would vary as the column temperature changed from 187°F to 216°F. Since heat loss would not be uniform, the next simulation included heat duties placed in approximately half of the stages of the column to simulate the heat loss. Additionally, the column was simulated with only 5 feet of packing because the majority of change in temperature and composition in the column occurred in the bottom quarter of 20 feet of packing. Figure 3 shows the simulation results with the new specifications. The placed heat duties were adjusted to match the simulation temperature profile with the pilot plant data. The reboiler duty

was adjusted to match the lean loading value. Finally, the sump split was adjusted to match the reboiler temperature.

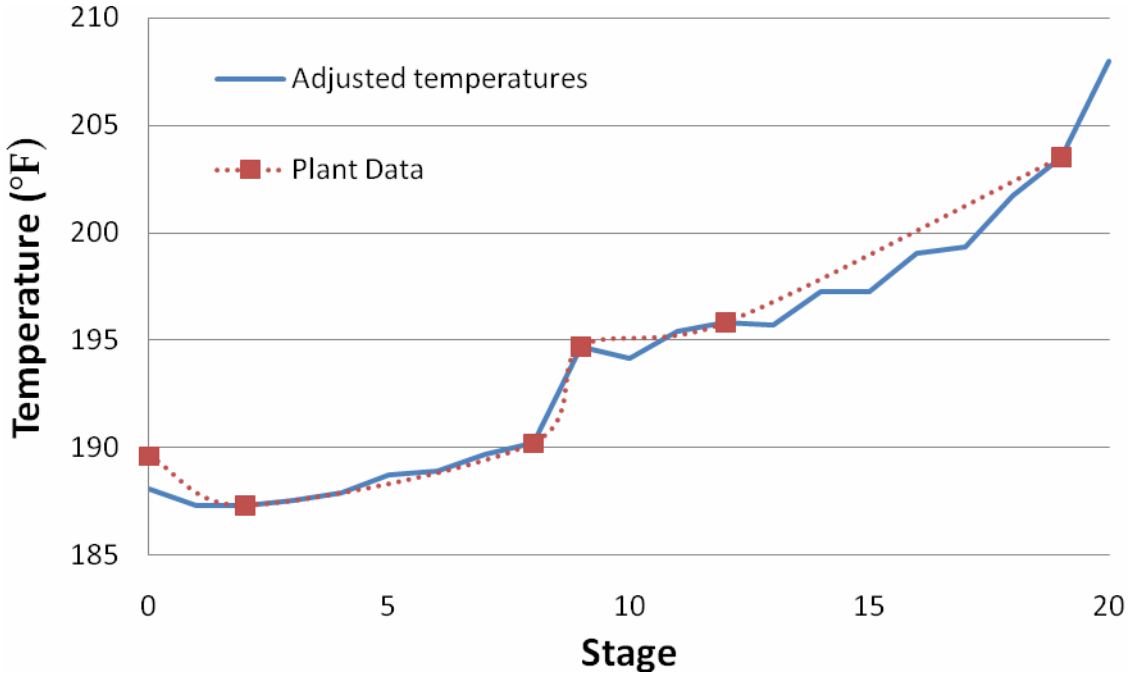

Figure 3: Temperature profiles in pilot plant and Aspen simulation stripper column (5 ft IMTP #40 packing, heat duties to match temperature profile, rich ldg = 0.48, reb duty = 0.488 MMBTU/hr, 63% removal)

Figure 4 displays the impact of changing packing height on the amount of heat applied. The total amount of energy put into the column must be relatively constant for all cases because the output stream temperatures did not change drastically, and the same amount of CO_2 was liberated for each instance. The only variable was the water vapor fraction in the product vapor. Since the total energy input was constant, when the reboiler duty decreased at smaller packing heights due to insufficient mass transfer area, the heat loss in the column increased, corresponding to a decrease in the total side duty of the column. A point worth noting is that at a packing height of approximately 9 feet, the total side duty is positive, indicating a net heat gain by the column. This scenario would not be realistic. The packing height of 5 feet was determined to be the best choice because the heating values best matched the pilot plant data at that height.

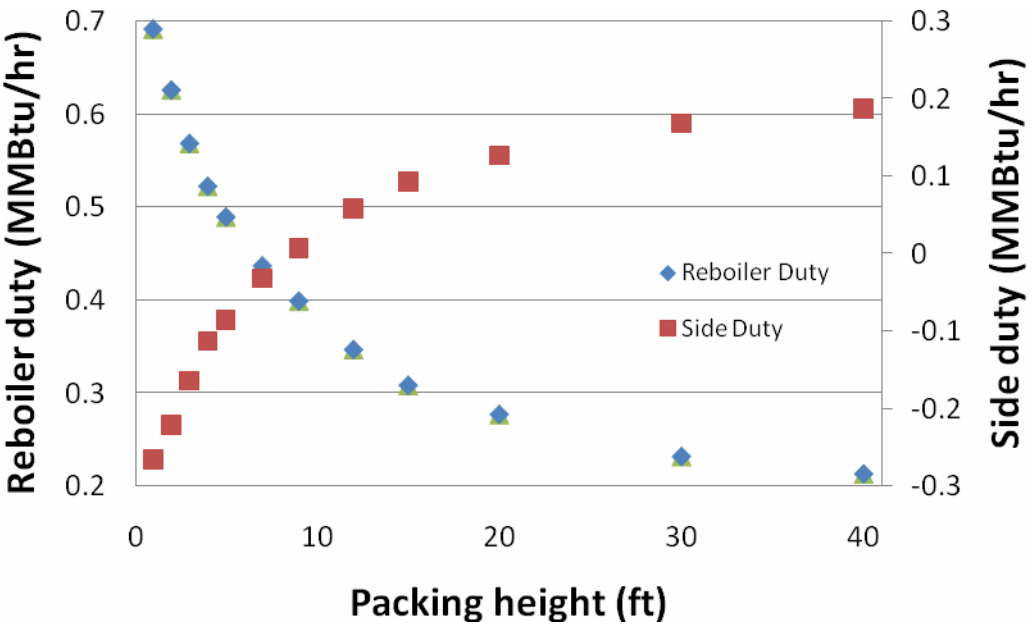

Figure 4: Heating requirement for columns with varying packing height

A summary of the relevant data from the pilot plant and Aspen simulation are displayed in Table 2. The agreement between the values demonstrates that the CO_2 removal at the pilot plant was verified with the model. The simulation predicted a nearly identical reboiler duty, and the heat loss was only 12% greater than the calculated heat loss at the pilot plant.

Table 2: Simulation/Data Agreement

	Pilot Plant	Aspen Simulation
Rich loading	0.48	0.48
Lean loading	0.36	0.36
Reboiler duty (MMBtu/hr)	0.488	0.489
Heat loss (MMBtu/hr)	0.076	0.085

The verified model can be used with the pilot plant simulation to determine how the performance can be improved. The CO_2 removal should ideally approach 90%, and the equivalent work should be around 25 kJ/mol CO_2 to rival previously optimized simple stripper simulations. The challenge for future simulations will be the method of predicting heat loss. Since the magnitude and distribution of heat loss for the pilot plant run was calculated to match the profile temperatures, the exact heat loss profile for other cases will be nontrivial.

Solar Stripping

A new stripper configuration was developed to utilize solar energy as a source for heating. A diagram is shown in Figure 5. Following the cross heat exchanger, rich solvent enters a solar

heater where it is heated to a maximum temperature, T_o. The liquid proceeds through three sequential adiabatic flashes, each with a temperature change of dT. In each step CO_2 and water vapor are flashed from the liquid, and the loading of the liquid is decreased. The liquid leaving the third flash is the lean stream to be recycled back to the absorber. The three vapor streams are sent to a compression train where most of the water is knocked out and the CO_2 is compressed to pipeline specs.

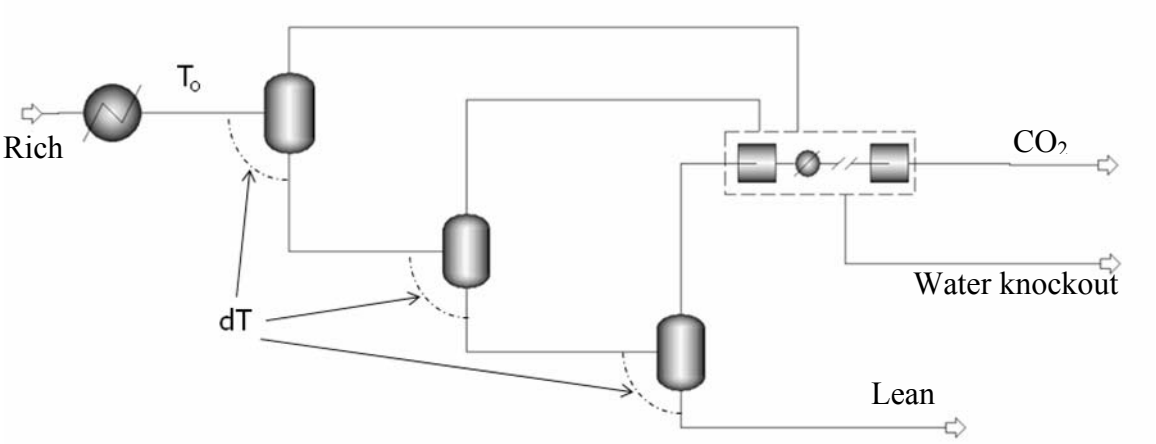

Figure 5: Flashing Stripper PFD

The model was run using 9 m MEA. Based on previous simulations, typical optimized lean streams seem to have a loading of around 0.4, so this was the initial loading selected. An absorber model by Plaza utilizing the Freguia equilibrium model was used to determine the rich stream which could be achieved by a 15 m absorber for the given lean stream. This rich stream was then used as the base specification for the stripper section. The available variables were T_o and dT, and using those variables the lean loading should be satisfied.

Optimization of this configuration had three steps. First, the appropriate temperature step between flashes was determined while holding all other variables constant. As shown in Figure 6, the temperature step, dT, can be varied to change the loading in the exiting lean stream. In the example shown in Figure 6, a lean loading of 0.4 was used in the absorber model to define the rich stream, so the correct dT was where the exiting lean loading was also 0.4. The separate curves demonstrate the impact of changing the heated temperature on the dT to reach the original lean loading. When the heated temperature was increased, the dT decreased.

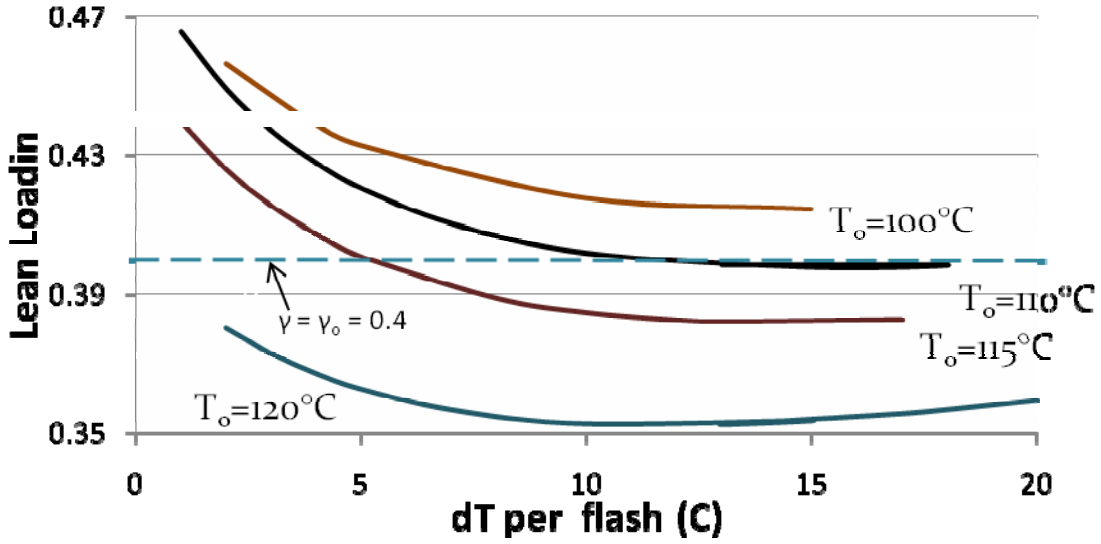

Figure 6: Lean Loading Response to Temperature Step (flashing stripping, 9 m MEA, 5° approach, lean ldg = 0.4)

After this step, the hot temperature was varied while changing the dT and maintaining an outlet lean loading to match the input from the absorber simulation. The effect of changing the hot temperature on the equivalent work of the system is shown below in Figure 7.

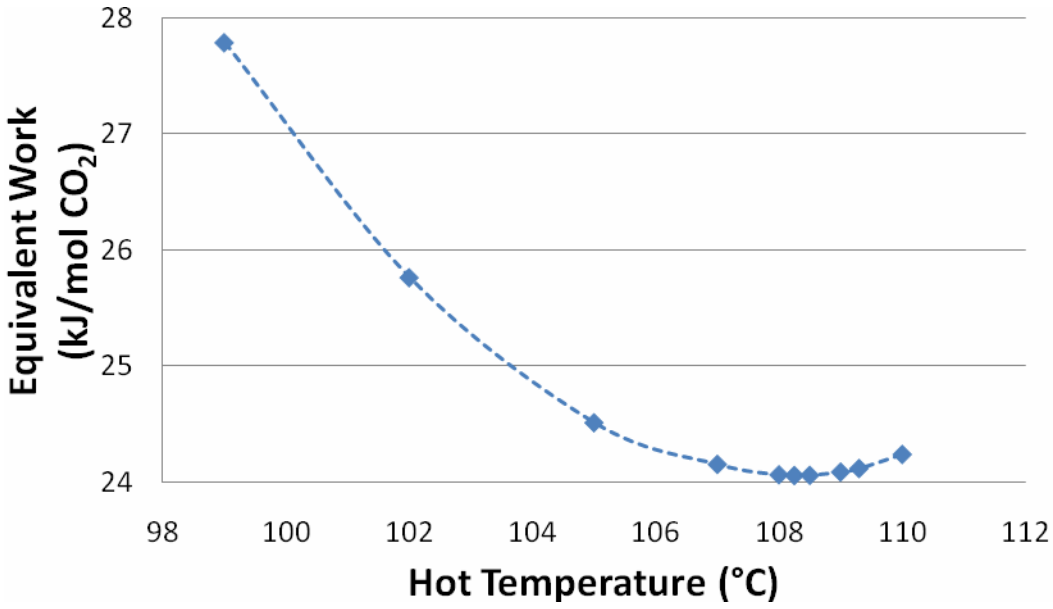

Figure 7: Effect of hot temperature on equivalent work (lean ldg = 0.4)

Following the optimization of the hot temperature, the lean loading was changed, and a new rich stream was calculated using the absorber simulation. Then the first two steps were repeated: optimizing the hot temperature while maintaining an outlet lean loading equal to the lean loading used in the absorber model. In Figure 8, the equivalent work of the system is plotted against the lean loading, and an optimum value occurs.

Figure 8: Optimization of lean loading by determination of minimum equivalent work (9m MEA, compression to 5000 kPa, 5° approach, determination of rich stream by RateSep absorber model)

The optimum lean loading was found to be 0.424, and the corresponding equivalent work with a hot temperature of 106°C was 24.47 kJ/mol CO_2. The sharp curve demonstrates the trade-off between high reflux at low lean loadings and high sensible heat requirements at high lean loadings (corresponding to high solid flow rates). However, even though these results show a clear optimum, a flaw in the specifications was realized. The rich pump was specified to reach 500 kPa, but the heated stream still vaporized before it entered the first flash tank. It would be unrealistic to expect adequate heat transfer to occur in the solar heater when the liquid is vaporizing. Additionally, a goal of the simulation was to maintain approximately equal molar flows in the vapor streams leaving the flash tanks, but the vapor leaving the first flash was greater than the other flows when the liquid vaporized before entering the tank. Therefore, the flowsheet was altered: the solar heater block was removed, and the first flash was changed to a heated as opposed to an adiabatic one. The vapor fraction of the first flash was specified, and the temperatures of the subsequent adiabatic flashes were set to change to match their vapor molar flows with that of the first tank. The last change was removing the absorber calculations from the process. It was not appropriate to simultaneously use the absorber model, based on Freguia's VLE model, and the stripper model, based on Hilliard's new VLE model. Converging the absorber model added time to the overall calculations, and approximate rich stream conditions can be calculated easily without it. Except for scenarios with very low lean loadings and solvent flow rates, the absorber had a rich end pinch, resulting in a rich loading of about 0.495. A simple material balance calculation for any given lean loading can determine the required solvent flow rate. Therefore, the absorber model will no longer be used in conjunction with this stripper model.

Conclusions

Aspen Plus was used to create a simulation of a recent pilot plant run using 35% MEA. Since data was provided for only the rich stream, lean stream, and column values, process units in addition to the stripping column were added to make the simulation complete. The stripping column used equilibrium reactions with RateSep to model mass transfer. The recently completed Hilliard Aspen VLE model for MEA-H_2O-CO_2 was implemented. The initial run using the collected data predicted correct performance in the column, but the temperatures were not accurate. After performing several regressions, an accurate portrayal of the pilot plant run could not be obtained, so a different method was utilized. Side duties were placed in the column to simulate heat loss, the sump fraction routed to the reboiler was varied to obtain the correct reboiler temperature, and the reboiler duty was varied to yield the correct lean loading. This method resulted in a temperature profile which nearly matched all of the recorded temperatures. Additionally, the reboiler duty was calculated to be 0.489 MMBtu/hr with a heat loss of 0.085 MMBtu/hr, compared to the pilot plant recorded reboiler duty of 0.488 MMBtu/hr and calculated heat loss of 0.076 MMBtu/hr.

A new flashing stripper configuration was developed to utilize solar energy for heating in the stripper section. It consisted of a three step adiabatic flash configuration with a solar powered preheater. The equivalent work of this configuration was optimized by varying the temperature step between flashes, maximum temperature, and lean loading. The optimum was found to be 24.5 kJ/mol CO_2 with a lean loading of 0.424, a maximum temperature of 106°C, and a temperature step of 0.2°C. However, this solution is not satisfactory because the rich stream was unintentionally vaporizing in the solar heater. New specifications have been developed to ensure that all three vapors leaving the flash tanks have the same molar flow.

Future Work

The three stage flash configuration will be further analyzed. It will be optimized using the new specifications. Additionally, its performance will be compared to that of a simple stripper configuration, and the effectiveness of solar heating in the three stage flash will be quantified. The difference in efficiency when using solar heat and steam heat in both the flash and simple stripper configurations will be investigated.

A new thermodynamic model is available for ROC-16. Work will begin on analyzing the performance of this solvent in previously tested configurations. ROC-16 has excellent rates, which should make it a great performer in the absorber. A key question to answer is whether it will perform well in the stripper section.

It will be determined whether rate based simulations should be used in the stripper. The kinetic reactions using the new thermodynamic model are still under development, but current simulations can be upgraded to kinetic models when they are finished.

References

Chen, E, "Carbon Dioxide Absorption into Piperazine Promoting Potassium Carbonate Using Structured Packing," Ph.D. Dissertation (2007).

Hilliard, M, "A Predictive Thermodynamic Model for an Aqueous Blend of Potassium Carbonate, Piperazine, and Monoethanolamine for Carbon Dioxide Capture from Flue Gas," Ph.D. Dissertation (2008).

Oyenekan, B, "Modeling of Strippers for CO_2 Capture by Aqueous Amines," Ph.D. Dissertation (2007).

CO_2 Absorption Modeling Using Aqueous Amines

Progress Report for January – March, 2008

by Jorge M. Plaza

Supported by the Luminant Carbon Management Program

and the

Industrial Associates Program for CO_2 Capture by Aqueous Absorption

Department of Chemical Engineering

The University of Texas at Austin

April 4, 2008

Abstract

Previous work on an absorber model for MEA that incorporates the new thermodynamic model by Hilliard (2008) was continued to obtain kinetic constants in Aspen Plus® in agreement with values calculated assuming a negligible MEA concentration gradient across the liquid film (first order approximation). Forward rates for the formation of carbamate were obtained from the previously set up absorber model that simulates the conditions of the laminar jet used by Aboudheir (2002). Two approaches were used in an effort to troubleshoot the model. Initially, the Aspen-regressed kinetic constant was compared to the number obtained directly from Aboudheir. An additional analysis was done by comparing the flux of CO_2 from Aspen ($CO_{2\ in} - CO_{2\ out}$) with the value obtained using the first order approximation. Absorber and liquid film segmentation was analyzed as part of the troubleshooting effort.

It was determined that there was an error in the first order approximation related to the application of Henry's law for this system. Once this issue was corrected it was possible to obtain Aspen values in complete concordance with the first order approximation at 293 K. Nevertheless, at higher temperatures, Aspen results deviate again from the first order approximation by as much as 25% at 333K. The difference in values might be related to the use of Fick's law in the first order approximation in contrast with the use of Maxwell-Stefan correlations by Aspen which include the effect of other diffusing species in the determination of the flux of CO_2. Results of this analysis are presented in this report.

Additionally, during this period absorber temperature profiles were revisited in an effort to establish a general criterion relating the presence of the temperature bulge and the heat carrying capacity of the liquid and the gas. It was expected that when the bulge is located in the middle of the column the heat carrying capacity of the liquid is equal to the heat carrying capacity of the gas. It was also thought that the inflection point in the solvent capacity vs. lean loading curve was related to this equality in heat carrying capacities. Both of these hypotheses appear to not be correct and results available are still inconclusive.

Description

MEA Model Development

Aboudheir (2002) generated rate data for CO_2 absorption in MEA using a laminar jet at various amine concentrations, CO_2 loadings, and temperatures. This data was used to evaluate the forward rate constants for the formation of carbamate using Aspen Plus® RateSep™. An absorber model was set up that included the new thermodynamic model developed by Hilliard (2008). Kinetics were represented using the following set of reactions:

$$2\ MEA + CO_2 \rightarrow MEAH^+ + MEACOO^- \quad (1)$$

$$MEAH^+ + MEACOO^- \rightarrow 2\ MEA + CO_2 \quad (2)$$

$$MEA + CO_2 \rightarrow HCO_3^- + MEAH^+ \quad (3)$$

$$MEAH^+ + HCO_3^- \rightarrow MEA + CO_2 \quad (4)$$

Bicarbonate reactions (3) & (4) were not included as a first approach. The reverse carbamate rate constant was obtained using the equilibrium constants by Hilliard (2008). The absorber size was based on scaled dimensions of the laminar jet reported by Aboudheir. Scaling was necessary for modeling purposes. The diameter was multiplied by 35 and the height by 20. The solvent flow rate was increased by 100. Table 1 includes the design values for the Aspen absorber model.

Table 1: Absorber design conditions for modeling cases

Variable	**Value**
Number of stages	2
	5
Packing Characteristics	
Type	CMR
Vendor	MTL
Material	Metal
Dimension	NO-1.5P

The mass transfer coefficients (k_L & k_G) were determined using a FORTRAN user subroutine included in Aspen to bypass the correlation corresponding to the CMR packing.

Work by Dugas (2007) concluded the need to correct parameters in Aspen to approach values of the density of mixture to those reported by Weiland (1998). These corrections were incorporated into the absorber model.

The gas inlet flow was set to 8.00E-05 kmol/s and the CO_2 outlet flow was calculated based on the flux reported by Aboudheir. It was set as the design specification to match while varying *k* in the power law equation.

The calculated *k* in Aspen Plus® was compared to the value found by using the pseudo-first order approximation that assumes that the MEA concentration is constant throughout the boundary layer. The resulting formula for the carbamate forward rate constant is:

$$k_2 = \left(\frac{N_{CO_2} * H_{CO_2}}{P_{CO_{2_i}} - P_{CO_2}^*}\right)^2 * \left(\frac{1}{D_{CO_2} * x_{MEA} * \tilde{\rho} * \gamma_{CO_2} * \gamma_{MEA}}\right) \quad (5)$$

where:

N_{CO2} is the flux of CO_2 – mol/s m^2 – It is calculated by dividing Aboudheir's reported CO_2 absorption rate by the interfacial area (radius * π* height)

H_{CO2} is Henry's constant for CO_2 - kPa

P_{CO2i} is the partial pressure of CO_2 at the interface – kPa

P_{CO2}^* is the equilibrium pressure of CO_2 at the loading and temperature of the system. - kPa

D_{CO2} is the diffusion coefficient for CO_2 – m^2/s

x_{MEA} is the mole fraction of MEA

γ is the activity coefficient.

$\tilde{\rho}$ is the molar density of the solution – $kmol/m^3$

In previous work (Plaza 2007) the Aspen regressed value was over four times the calculated value obtained using equation (5). Absorber stages were increased to four in an attempt to reduce discrepancies between k values. However, this had very little effect on the regressed kinetic constant. Additional analysis was done to evaluate the influence of film segmentation on the values of the regressed kinetic constant. Film segmentation is important to properly represent the enhancement effect of the carbamate reaction in the absorption of CO_2. Figure 1 shows the CO_2 concentration profiles obtained for different film segmentations. It can be observed that a few segments may not properly represent the concentration profile across the liquid film. The limitation on the number of segments is related to an increase in computation time. It may also be convenient to have smaller size segments where noticeable concentration change occurs and larger segments where concentration gradients are less dramatic. For troubleshooting purposes a fixed number of 40 segments, equally spaced, were used so as to assure proper concentration profile representation at multiple absorber conditions. Nonetheless, this did not solve the discrepancies between forward rate constants.

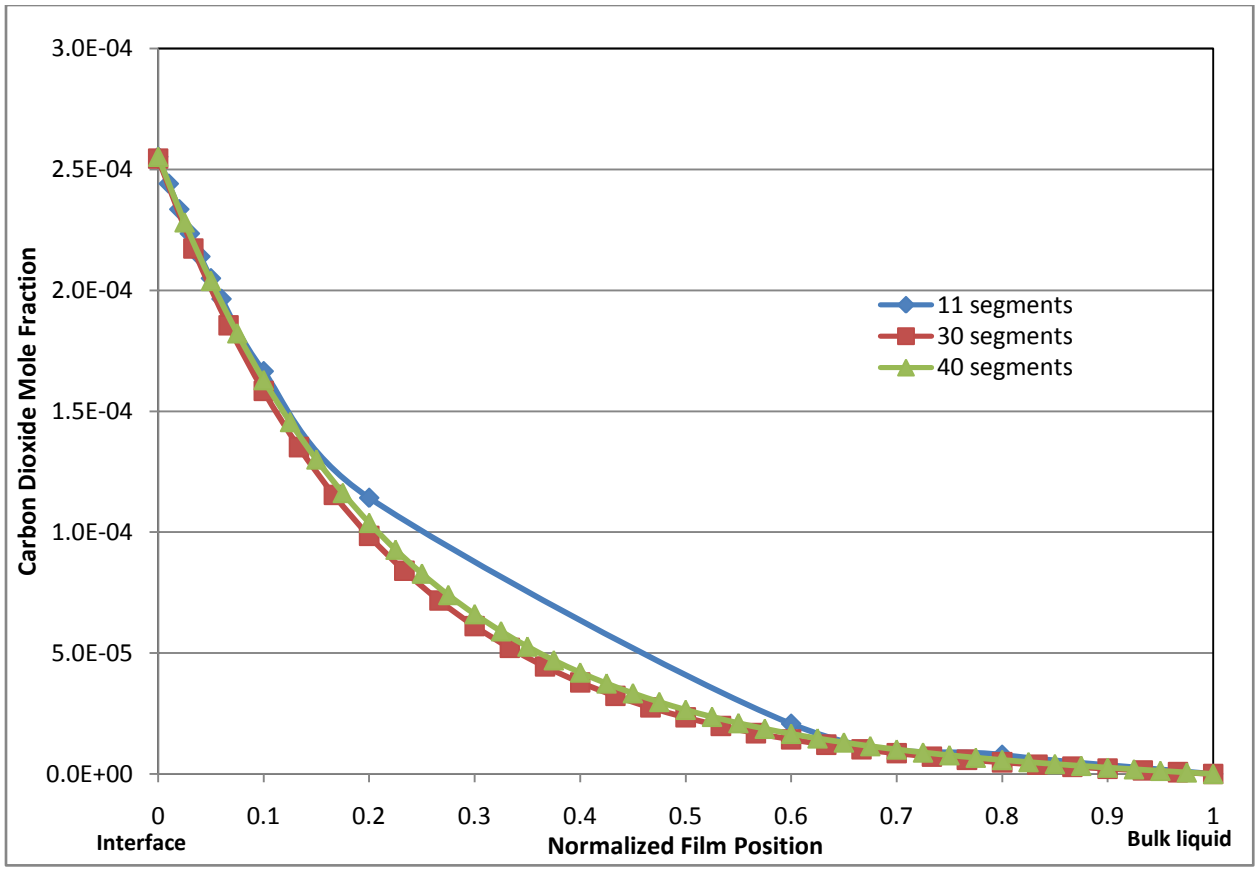

Figure 1: CO_2 concentration profiles for various equal segments in the liquid film for 3 m MEA, α = 0.27 and T = 293 K

It was observed through analysis of different temperature points that the activity coefficient for CO_2 in equation (5) changed considerably with temperature (Table 2). Aspen has three different reference states for the activity coefficients (GAMMA, GAMUS, GAMUSAQ) and there was uncertainty as to which reference state was being used for CO_2 in the flux calculation. Communication with Aspentech (Chen 2008) verified that GAMUSAQ, which is the proper activity coefficient, was being used. GAMUSAQ is the unsymmetrically normalized activity coefficient based on aqueous reference state. Aspentech recommended the inclusion of the equilibrium equations in the reactions set in Aspen. Previously they were only included in the chemistry set. A frequently used reaction mechanism for the absorption kinetics was also suggested:

$$MEA + CO_2 \rightarrow H^+ + MEACOO^- \quad (6)$$

$$H^+ + MEACOO^- \rightarrow MEA + CO_2 \quad (7)$$

$$MEA^+ \leftrightarrow MEA + H^+ \quad (8)$$

$$MEACOO^- + H_2O \leftrightarrow MEA + HCO_3^- \quad (9)$$

$$H_2O \leftrightarrow H^+ + OH^- \quad (10)$$

$$HCO_3^- \leftrightarrow H^+ + CO3^{-2} \quad (11)$$

As with the previous mechanism bicarbonate reactions were only included as equilibrium (9 & 11). There was no improvement observed with this reaction set.

Table 2: Aspen activity coefficients for CO_2 using different reference states and at various temperatures

Temperature (K)	GAMMA	GAMUS	GAMUSAQ
293	0.2431	2.4342	2.8050
313	0.6719	1.3862	1.3863
333	1.8800	1.2297	1.1548

A review of the first order approximation formula (5) showed that there was an error in the inclusion of the concentration of CO_2 as partial pressure. According to Henry's law:

$$\boldsymbol{P_{CO_2} = H_{CO_2} * \gamma_{CO_2} * x_{CO_2}} \tag{12}$$

where: P_{CO2} is the partial pressure of carbon dioxide

H_{CO2} is the Henry's constant for carbon dioxide

γ_{CO2} is the activity coefficient for CO_2 at the defined temperature

x_{CO2} is the mole fraction of CO_2

Equation (5) does not include the activity coefficient of carbon dioxide related to the molar fraction. When this value is included the first order approximation becomes:

$$k_2 = \left(\frac{N_{CO_2} * H_{CO_2}}{P_{CO_{2_i}} - P_{CO_2}^*}\right)^2 * \left(\frac{\gamma_{CO_2}}{D_{CO_2} * x_{MEA} * \tilde{\rho} * \gamma_{MEA}}\right) \tag{13}$$

Comparison between the values of k_2 obtained in equation (13) and the values regressed in Aspen (Table 3) shows less discrepancy in the rate constants.

Table 3: Carbamate formation forward kinetic rate constant for 3 m MEA, α = 0.27, T = 293 K (kmol/m^3-s)

Regressed	Equation (13)	Literature[1]
3.79E+08	3.89E+08	3.47E+08

1. Calculated using equation (13) and physical properties from literature correlations

The second approach to match kinetic constants was to compare CO_2 fluxes obtained in Aspen with the calculated using the flux version of equation (13) including the physical absorption term (k_L):

$$N_{CO_2} = \frac{\sqrt{{k_L}^2 + D_{CO_2} * x_{MEA} * \tilde{\rho} * k_2 * \gamma_{MEA} * \gamma_{CO_2}}}{H_{CO_2} * \gamma_{CO_2}} * \left(P_{CO_{2_i}} - P^*_{CO_2}\right) \quad (14)$$

Here all variables are defined as in equation (5). k_L is the physical absorption mass transfer coefficient in kmol/m^2-s. Up to this point the effects of physical absorption had been considered negligible but are included here to assure a full representation of the flux. Results show (Table 4) that there is a good match between Aspen and equation (14) at 293 K and discrepancies appear as temperature increases.

Table 4: Flux and rate constant results at various temperatures and interfacial areas for 3 m MEA

T (K)	α (molCO$_2$/mol MEA)	Interfacial area * 10^{-5} (m^2)	k_L (kmol/m^2-s)	k_2*10^8 – Aspen (kmol/m^3-s)	N_{CO2} *10^{-4} (kmol/m^2-s)		Deviation from Eq. (14) (%)
					Aspen	Eq. (14)	
293	0.27	3.06	0.0243	3.79	1.11	1.11	0.3
293	0.27	2.44	0.0271	3.97	1.15	1.14	1.3
313	0.15	4.09	0.0274	5.39	1.82	2.16	-13.2
333	0.15	3.55	0.0384	9.13		2.95	-26.7
333	0.15	2.81	0.0432	8.50	2.13	2.85	-25.4

A hypothesis for this temperature behavior is related to the fact that equations (5) and (14) use a value for the diffusion of CO_2 in the solvent that does not include the interaction with other species. Aspen calculates diffusion flux using the Maxwell-Stefan equations (Taylor 1993):

$$J = -\tilde{\rho} * [B]^{-1} * \nabla x \quad (15)$$

Where: J is the molar diffusion flux – kmol/m^2-s

$\tilde{\rho}$ is the molar density of the solution – kmol/m^3

$[B]$ is a matrix composed by the following terms:

$$\boldsymbol{B_{ij}} = \sum_{k=1}^{n} \frac{x_k}{D_{ik}} \text{ for i = 1,2,…n-1 and i} \neq \text{j}$$

$$\boldsymbol{B_{ij}} = \frac{-x_i}{D_{ij}} \text{ for i} \neq \text{j = 1,2,…, n-1}$$

D is the Maxwell – Stefan diffusivity - m^2/s

x is the composition at the point where the flux is being measured.

$\boldsymbol{\nabla x}$ is the concentration gradient in the film.

Using these equations the diffusivity of CO_2 becomes a row in the inverse B matrix that adds the effects of each of the species present in solution. For this analysis all species in equations (6) to (11) were considered with the exception of the hydroxide ion (OH^-) that was arbitrarily excluded since the matrix uses *n-1* components where *n* is the total number of species in solution. The *B* matrix was evaluated at the interface conditions (taken from Aspen) and the effect of each specie was determined by multiplying the row corresponding to CO_2 in $[B]^{-1}$ by the gradient vector $\boldsymbol{\nabla x}$. This vector is equal to the difference in concentrations between the interface and the first film segment. Dividing the result for each species by the value for CO_2 gives its fraction effect on the flux. Table 5 shows results at different temperatures. There seems to be a strong influence of the concentration of water that needs to be assessed. Since water is the predominant specie, convergence criteria in Aspen might be strongly affected by the water behavior, thus the CO_2 results may not reach adequate accuracy.

Table 5: Relative fraction effect of species in the diffusivity of CO_2 at various temperatures.

T (K)	H_2O	CO_2	MEA	MEA^+	$MEACOO^-$	HCO_3^-	CO_3^{-2}	H^+
293	0.91	1.00	0.15	0.03	0.03	2.5E-03	4.4E-03	4.8E-09
313	0.93	1.00	0.23	0.08	0.08	1.9E-03	2.2E-04	8.4E-09
333	0.96	1.00	0.28	0.12	0.12	3.4E-03	1.0E-03	3.9E-08

In a similar manner, the *B* matrix shows problems of conditioning that seem to be related to the diffusion coefficients for the hydrogen and hydroxide ions. This may have a negative effect in the calculation fluxes. Further work needs to be conducted.

Heat carrying capacities

Previous work evaluated operating conditions related to intercooling in absorbers (Plaza 2007). An optimum CO_2 loading bracket of operation for 4.5 *m* K_2CO_3/4.5 *m* piperazine solvent was defined and analysis of an absorber with split feed was carried out.

The analysis of the effects of lean loading vs. rich loading with no intercooling (Figure 2) showed the presence of an inflection where the increase in lean loading implied an increase in

rich loading. It was believed that this inflection point corresponded to equal heat carrying capacities of the liquid and the gas. The heat carrying capacity is calculated as the derivative of the enthalpy of the gas or the liquid times the flow:

$$n_i * \left(Cp_i + \frac{P^*_{H_2O}}{P_{total} - P^*_{H_2O}} * \left(Cp_{H_2O,g} + \frac{\Delta H_v^2}{R * T^2} \right) \right) = n_l * Cp_{l-mix} \quad (16)$$

Where: $Cp_{l\text{-}mix}$ is the specific heat capacity of the liquid from Aspen – kJ/kmol-K

Cp_i is the heat capacity of the inert component in the gas – 33.47 kJ/kmol-K

$Cp_{H2O,g}$ is the heat capacity of vapor water – 41.84 kJ/kmol-K

n_i are the moles of "inert" components: N_2 + O_2 + CO_2 - kmol/s

n_l are the moles of liquids – kmol/s

P^*_{H2O} is the vapor pressure of water at bulge temperature and pressure – kPa

P_{total} is the total pressure at the bulge – kPa

T is the temperature of the bulge – K

R is the gas constant – 8.314 kJ/kmol-K

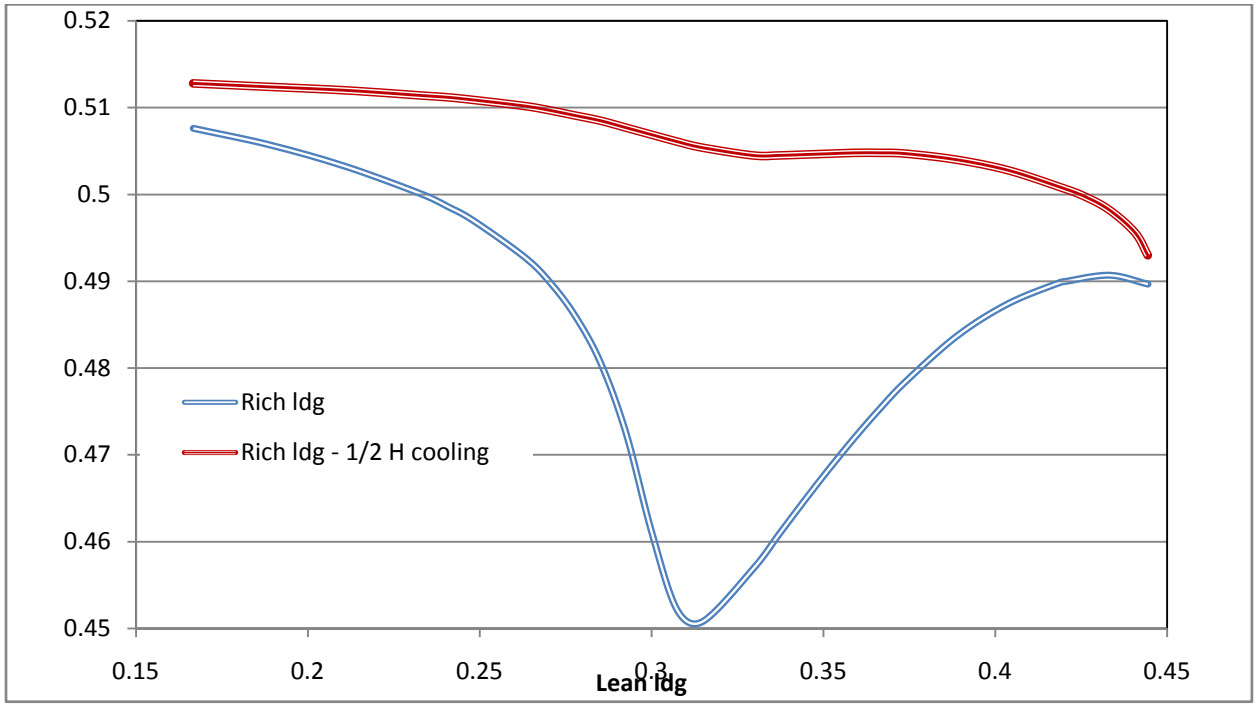

Figure 2: Change in rich loading vs. lean loading. Solvent 4.5 *m*/4.5 *m* K_2CO_3/PZ. (plug flow model)

In this expression it is assumed that the change in inert moles in the gas due to the absorption of CO_2 is negligible when compared to the total gas flow so the inlet gas flow is the same as in the temperature bulge position. The change in water content in the gas is the only variable flow. The heat carrying capacity of the gas is increased by the absorption of water which is accounted by multiplying the water moles (represented in the vapor pressure term) by the heat of absorption of water. This equality is to apply close to or at the middle of the column. Results showed that this hypothesis did not hold for the Aspen runs using a plug flow model so runs using a counter-current flow model were set up (Figure 3). It was thought that these discrepancies could be caused by back mixing effects. The latter runs showed a behavior similar to the one observed in Figure 2. The equality point for both flow models for heat carrying capacities seems to be actually located to the left of the inflection point. Further analysis is required.

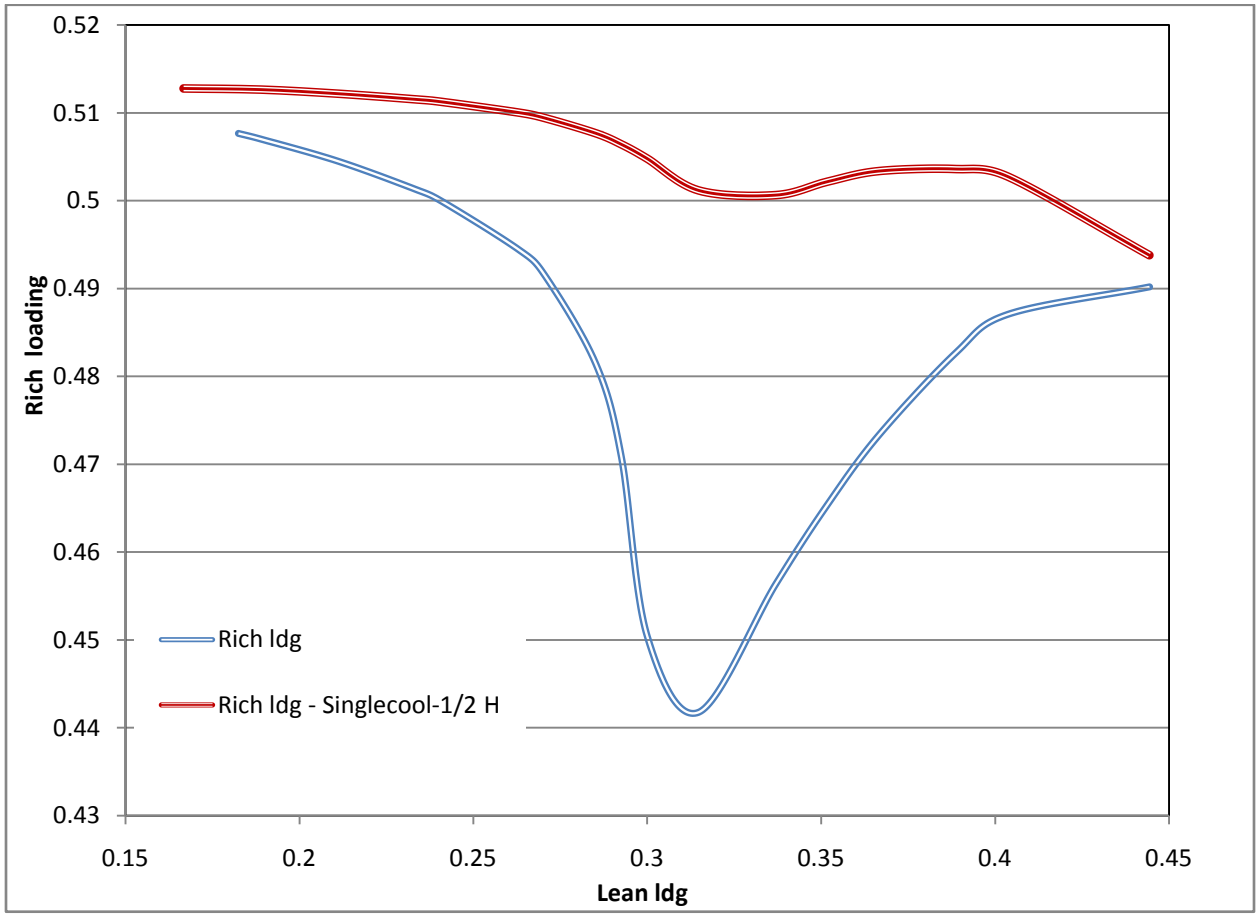

Figure 3: Change in rich loading vs. lean loading. Solvent 4.5 *m*/4.5 *m* K_2CO_3/PZ. (Countercurrent flow model)

The countercurrent model showed an additional problem at low lean loadings. As Figure 4 shows, the temperature profile shows an erratic behavior at the top of the column. In an attempt to solve this, an additional stage with minimum packing was placed at the top, mainly to correct heat exchange between incoming liquid and the gas leaving the column. However, this did not solve the problem and further work is required.

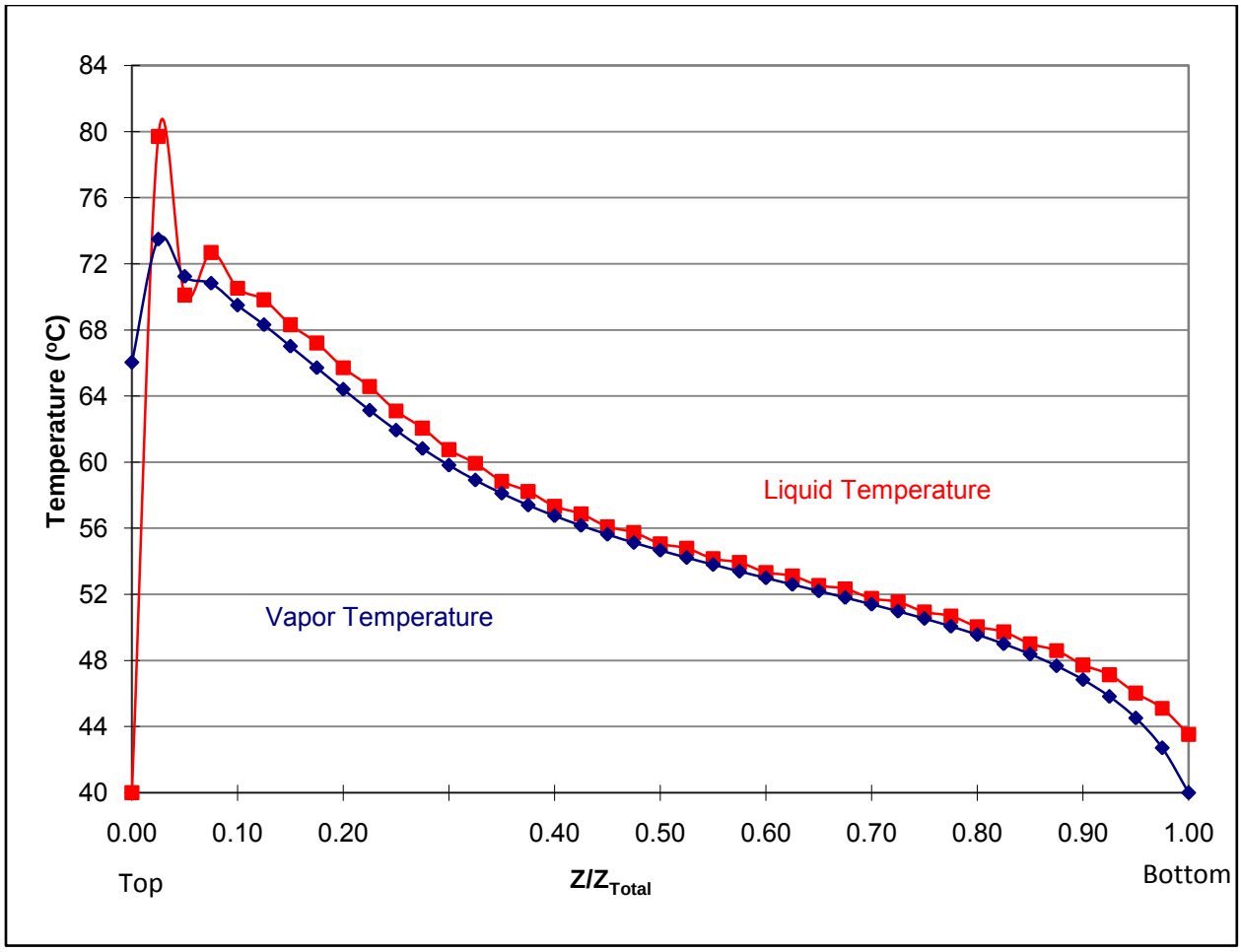

Figure 4: Temperature profiles for absorber. Solvent 4.5*m*/4.5 *m* K_2CO_3/PZ α = 0.21

Conclusions

MEA Model Development

The inclusion of the additional CO_2 activity coefficient closed the gap considerably between the values for the forward kinetic constant obtained in Aspen and the values calculated using equation (13). However there is still a discrepancy when using literature correlations to calculate physical properties.

Flux results (Table 4) show a close match between Aspen and equation (14) at 293 K. Deviation increases at higher temperatures.

The physical absorption component of the mass transfer is negligible when compared to the enhancement due to chemical reaction (maximum 0.3% of the chemical reaction term). This suggests that the approximation used in equation (13) is valid and that the laminar jet mass transfer is being modeled properly in Aspen.

Results for the Maxwell-Stefan diffusion analysis show that there is a need to evaluate the effect of water fluxes on the diffusivity of CO_2. The effect of the faster diffusing hydrogen and hydroxide ions needs to also be evaluated.

Heat carrying capacities

Results are not conclusive in this work. The proposed hypothesis related to the inflection point did not follow. It might be necessary to include the heat carrying effect related to the change in CO_2 content in the gas.

Future Work

Analysis of the temperature dependent discrepancies will be the main focus of future work. This includes determining the magnitude of the water diffusivity effect in the CO_2 flux calculation.

The effect of the hydrogen and hydroxide ions on CO_2 diffusivity will be evaluated by returning to the initial reaction set proposed for this system (equations (1) through (4)). These reactions do not include H^+ or OH^- which will allow us to establish the effect that these species have in the calculation of CO_2 diffusivity by Maxwell-Stefan equations and if it can explain the temperature behavior of the Aspen regressed forward kinetic constant. This will require definition of the equilibrium constant for reactions (1) and (2) to maintain a first order relation with all species present.

Future work will include a more thorough analysis of the relation between the Hatta number and the proper liquid film segmentation. The goal is to determine an adequate number of segments based on the value of the Hatta number.

Physical properties obtained through literature correlations will be visited to determine the need to include these in the Aspen model.

There is still a need to review the kinetics for formation of bicarbonate to evaluate their importance in CO_2 absorption modeling.

Finally, work will also be conducted to assess and compare the performance of 35-40 wt % MEA to the commonly used 30 wt %.

References

Aboudheir, A. (2002). Kinetics, Modeling and Simulation of CO2 Absorption into Highly Concentrated and Loaded MEA Solutions. Chemical Engineering. Regina, University of Regina. **Ph.D**

Chen, C.-C. (2008). J. M. Plaza. Austin, TX.

Dugas, R. (2007). J. M. Plaza. Austin, TX.

Hilliard, M. (2008). A Predictive Thermodynamic Model for an Aqueous Blend of Potassium Carbonate, Piperazine, and Monoethanolamine for Carbon Dioxide Capture from Flue Gas,. Chemical Engineering. Austin, Texas, The University of Texas at Austin. **Ph.D**.

Plaza, J. M. (2007). CO2 Absorption Modeling Using Aqueous Amines. Progress Report for October – December, 2007. Austin, Texas, The University of Texas at Austin.

Taylor, R., Krishna R. (1993). Multicomponent Mass Transfer. New York City, John Wiley & Sons.

Weiland, R. D., J.; Cronin, B.; Browning G (1998). "Density and Viscosity of Some Partially Carbonated Aqueous Alkanolamine Solutions and Their Blends." J. Chem. Eng. Data **43**: 378-382.

Reclaiming by Crystallization of Potassium Sulfate

Progress Report for January 1 – March 31, 2008

by Qing Xu

Supported by the Luminant Carbon Management Program

and the

Industrial Associates Program for CO2 Capture by Aqueous Absorption

Department of Chemical Engineering

The University of Texas at Austin

April 18, 2008

Abstract

One side reaction in CO_2 capture when using MEA/PZ is the generation of sulfate from SO_2. This sulfate has to be removed so that the MEA/PZ solution can be reused for CO_2 capture. Potassium sulfate can be crystallized and separated from MEA/PZ solvent by the addition of potassium hydroxide. In this period continuous crystallization of potassium sulfate was conducted with 7 and 11 m MEA at 0.4 CO_2 loading, 8 m PZ at 0.3 CO_2 loading, and with SO_4^{-2}/K^+ in feed from 0.185 to 1. The experiments were conducted at 25, 40, and 60℃, with residence time of 3 min, 10 min, and 20 min, with two different agitators and two different agitation rates. Crystals were vacuum filtered and oven dried and the moisture content in the filter cake varied from 4 wt % to 34 wt %. The particle size distribution was measured by a laser scanner after filtration and desiccation. The mean volume particle size ranges from 110 μm to 260 μm. SEM and light microscopy were used to analyze the crystal surface micro-morphology, particle size, crystal shape, and habit.

Introduction

In previous work, the solubility of potassium sulfate was measured with variable MEA/PZ concentration, CO_2 loading, and temperature. A model predicting empirical K_{sp} was developed. An interaction parameter set for CO_2-MEA-H_2O-K^+-$SO_4^=$ system in electrolyte-NRTL model was developed using Data Regression System in Aspen Plus®.

In this quarter continuous crystallization of potassium sulfate was conducted over a wide range of conditions and the solids were characterized by laser sizing and microscopy.

Experimental Methods

1) Continuous crystallization

The amine stock solution and KOH stock solution were prepared separately. The amine feed included CO_2 and enough K_2SO_4 to be close to K_2SO_4 saturation. Sulfuric acid was added to the amine feed to adjust $SO_4^{=}/K^{+}$. The separate KOH feed was 34 wt % or 50 wt % aqueous KOH. The apparatus is shown in Figures 1 and 2.

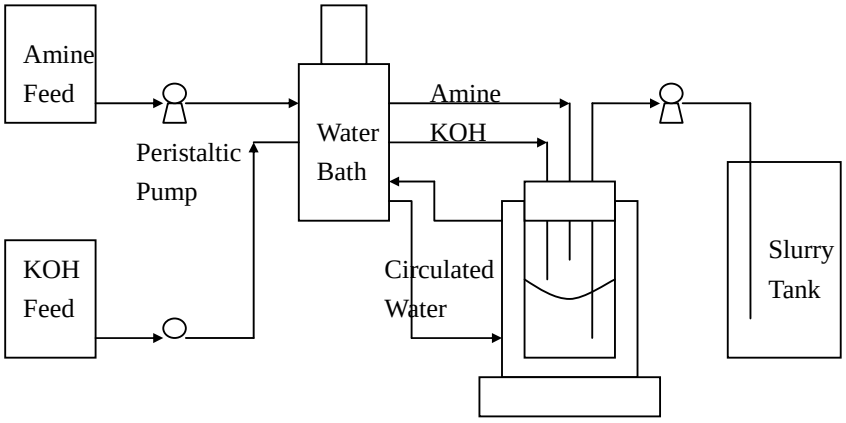

Figure 1: Continuous Crystallization Apparatus

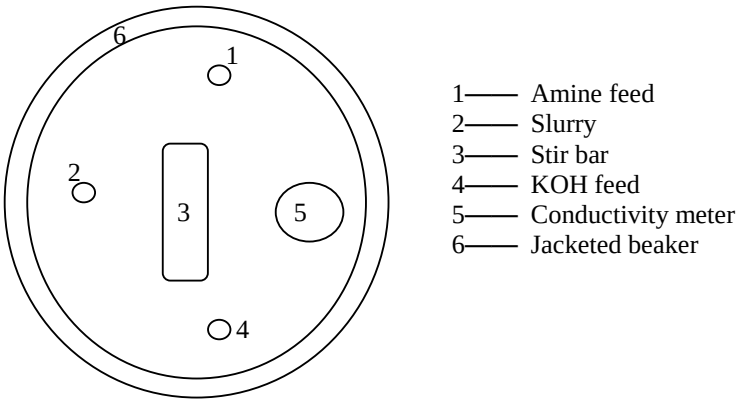

Figure 2: Top View of the Crystallizer

Before all the experiments, each peristaltic pump (amine feed, KOH, and slurry) was calibrated. Feeds were pumped into a jacketed beaker, preheated by going through the water bath. An agitator or magnetic stir bar was used for agitation. For most experiments, the agitation speed was set at 6. A conductivity meter was used to measure the electrical conductivity and temperature of the solution.. The volume of the reactor was 200 mL or 50 mL, and the residence time varied from 3 min to 20 min. The liquid level was controlled by adjusting the slurry pump.

2) Separation of solid and liquid

Slurry samples were collected during the last 2 residence times. It is assumed that the system gets to steady state around 8-10 residence times. Gravity filtration and vacuum filtration were taken for a primary separation, and then the filtered sample was dried in an oven at 105℃. The weights before and after drying were recorded.

3) Crystal analysis

a. Sizer Master

A dry sample of solids was dispersed into saturated K_2SO_4 aqueous solution by a sonicator. The size distribution was determined by a Malvern® Sizer Master.

b. Scanning Electron Microscopy (SEM)

SEM images were taken to show crystal habit, shape and surface, as well as to verify the mean crystal size result of the Sizer Master. Samples were coated with gold or silver to become conductive.

c. Light Microscopy

Light microscope images of 2 samples were taken.

4) Solution analysis

CO_2 concentration was determined with total inorganic carbon analyzer.
Total MEA, K^+, SO_4^{-2} were determined by cation and anion chromatography.

5) Settling rate

Settling rate was measured for a few samples from the reactor after experiments. In the "Jar Test", a graduated cylinder was filled with mixture from the reactor. At the time t=0, it was mixed well as a homogeneous slurry, then it settled out under the gravity into distinct zones, as illustrated in Figure 3.

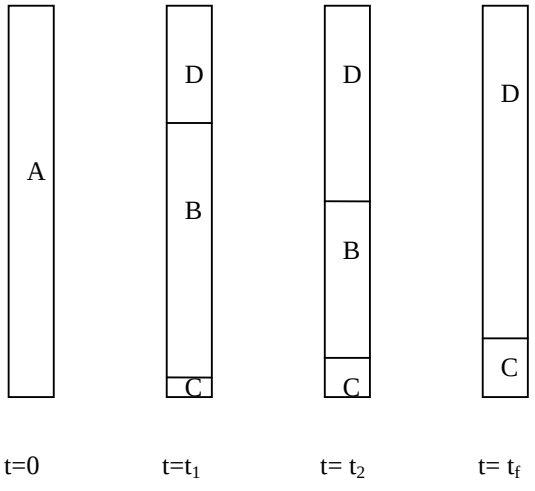

Figure 3: Sedimentation zones during slurry settling (The Jar Test)

A, initial uniform concentration; B, zone of increasing concentration; C, sediment or sludge; D, clear liquor

The changing of interface heights of D-B and B-C by time was measured.

Results

Table 1 gives the conditions for each run and the resulting particle size represented as the median volume size and as the moisture content in the filter cake. The median volume particle size varies from 110 to 260 μm with residence times of only 3 to 20 minutes. The solids filter easily and settle rapidly. It appears that greater particle sizes result from greater T, longer residence time, reduced agitation, reduced SO_4^{-2}/K^+, and reduced lower amine concentration. There appeared to be no effect of dissolved iron.

Table 1: Continuous Crystallization of Potassium Sulfate

Exp	Feed Description	τ (mi	T (℃	L* (μn	Moisture Conter in Filter cake
1	11 m MEA, a=.4, 1m SO_4^{-2}; 34% KOH, SO_4^{-2}/K^+=0.296	20	ambie	200	5.72%
2	7 m MEA, a=0.4, 1m SO_4^{-2}, 34%KOH, SO_4^{-2}/K^+=0.732	20	ambie	260	7.95%
3	7 m MEA, a=0.4, 1m SO4-2, 50%KOH, SO_4^{-2}/K^+=0.368	10	60	200	19.58%
4	7 m MEA, a=0.4, with <1mM Fe^{+2}, 1m SO_4^{-2}, 50%KOH, SO_4^{-2}/K^+=0.368	10	60	210	32.53%
5	8 m PZ a=0.3, 0.627m SO_4^{-2}, 50%KOH, SO_4^{-2}/K^+=0.185	10	40	125	18.63%
6	7 m MEA, a=0.4, 1.522m SO_4^{-2}, 50%KOH, SO_4^{-2}/K^+=1	10	40	135	4.16%
7	7 m MEA, a=0.4, 1.522m SO_4^{-2}, 50%KOH, SO_4^{-2}/K^+=1	3	40	110	13.89%
8	7 m MEA, a=0.4, 1.522m SO_4^{-2}, 50% KOH, SO_4^{-2}/K^+=1	20	40	195	12.72%
9	7 m MEA, a=0.4, 1.522m SO_4^{-2}, 50% KOH, agitation 8, SO_4^{-2}/K^+=1	10	40	150	25.22%
10	7 m MEA, a=0.4, 1.522m SO_4^{-2}, 50% KOH, doub KOH flow rate, SO_4^{-2}/K^+=0.5	10	40	260	33.77%

*: Volume Mean Particle Size.

Figure 4 gives a typical particle size distribution. The vertical axis on the left hand side is the volume percentage of certain particle size range, and the vertical axis on the right hand side is the cumulative volume percentage of particles with smaller size than certain value. As shown in the figure, the volume mean particle size L is from the intersection point of V%=50 and the curve of cumulative volume percentage.

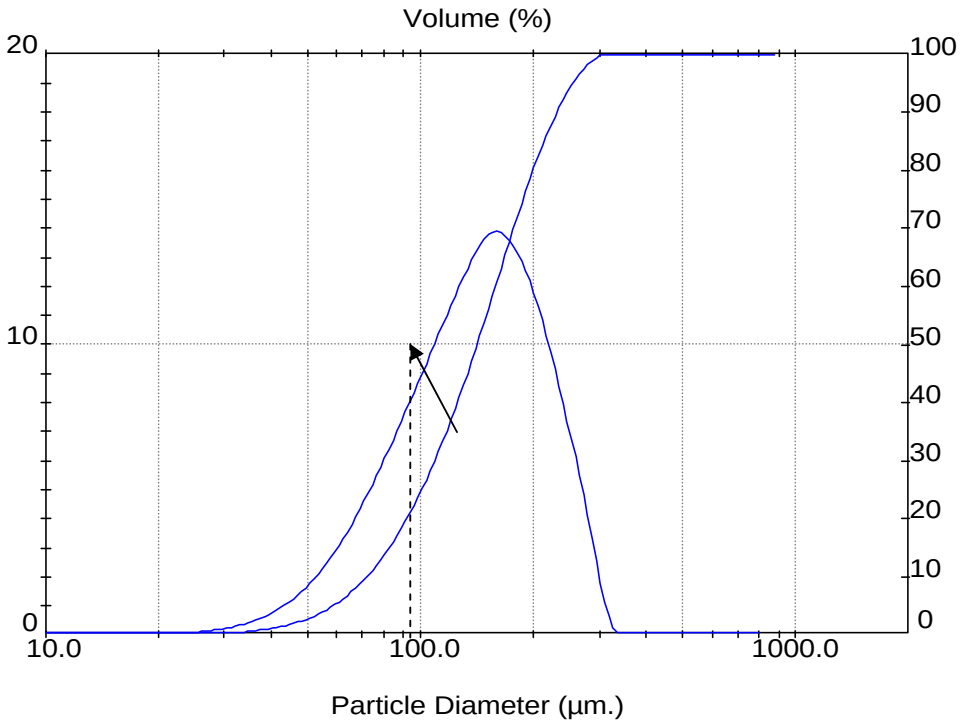

Figure 4: Typical Particle Size Distribution

Figures 5-7 give typical settling curves

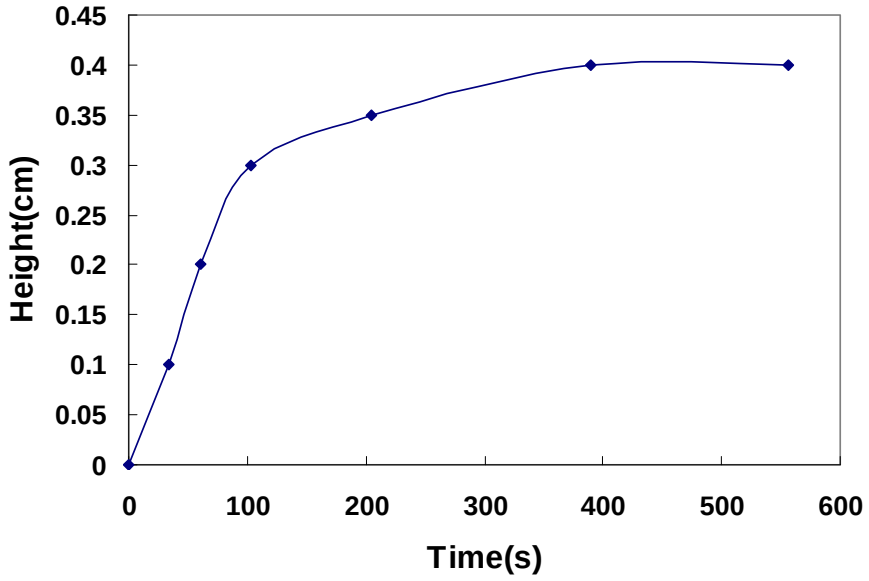

Figure 5: B-C Slurry Settling Curve of Experiment # 9

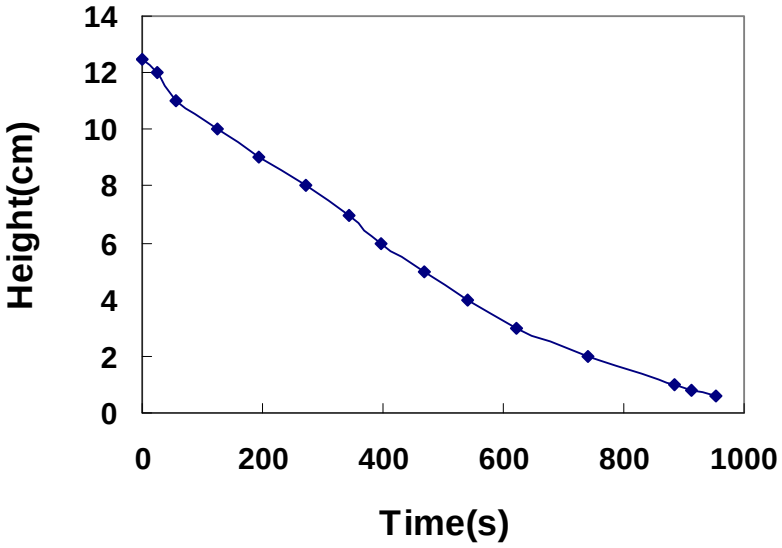

Figure 6: B-D Slurry Settling Curve of Experiment # 9

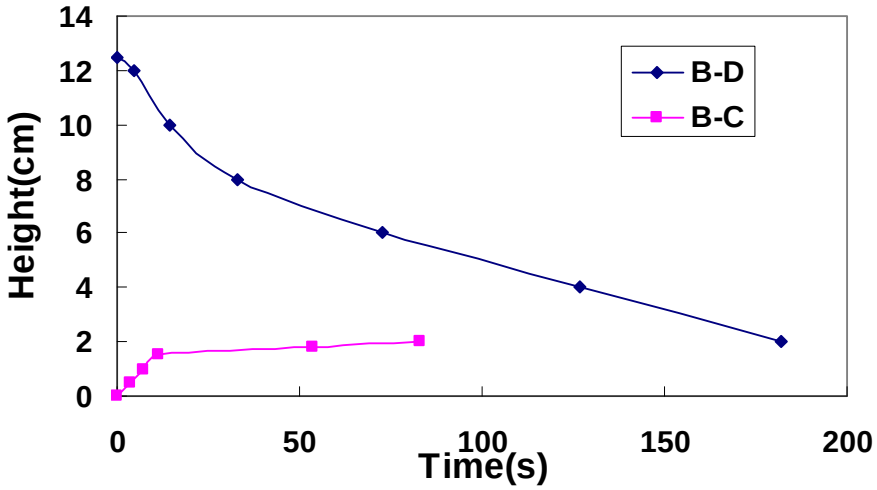

Figure 7: B-C and B-D Slurry Settling Curve of Experiment # 10

Particles from experiment # 9 have a volume mean particle size of 150 μm, while that of experiment # 10 is 260 μm. Therefore, particles with bigger size have a much faster settling rate. The final settled volume from experiment # 10 is smaller, because the slurry was more diluted. However the settling rate of # 9 was still rapid and good for industrial separation. Table 2 gives settling rate results for several experiments.

Table 2: Settling Rates

Experimen	Initial Rates (cm/mi	Final Sediment Height (c
6	7.14	0.53
7	5.11	0.52
8	3.95	0.71
9	1.42	0.40
10	7.14	2.00

1.

Figures 8- 11 give images from scanning electron microscopy. These images have a greater depth of focus than those of light microscopy. Figure 8 shows typical crystals of the baseline experiment. Figure 9 shows smaller crystals resulting from increased agitation, probably resulting in increased secondary nucleation.

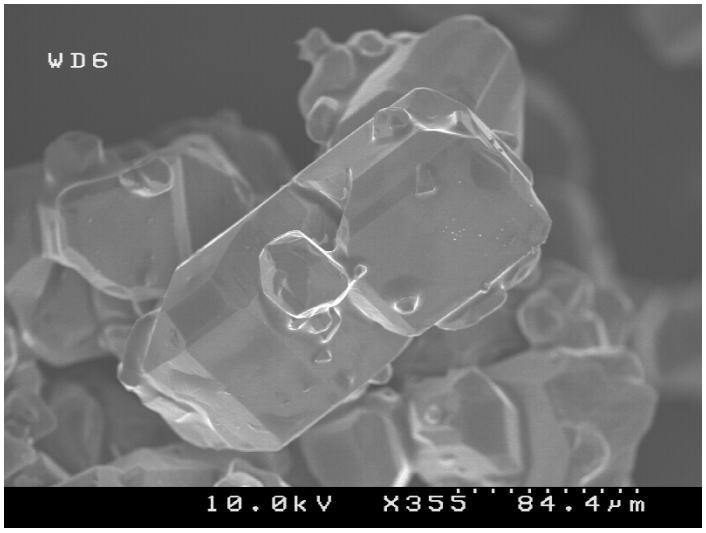

Figure 8: A Typical K_2SO_4 Crystal from experiment # 7

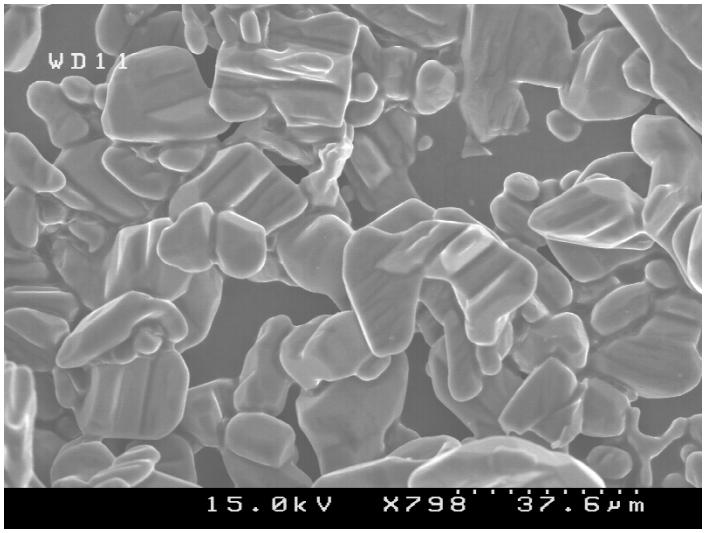

Figure 9: K_2SO_4 Crystals from experiment # 9

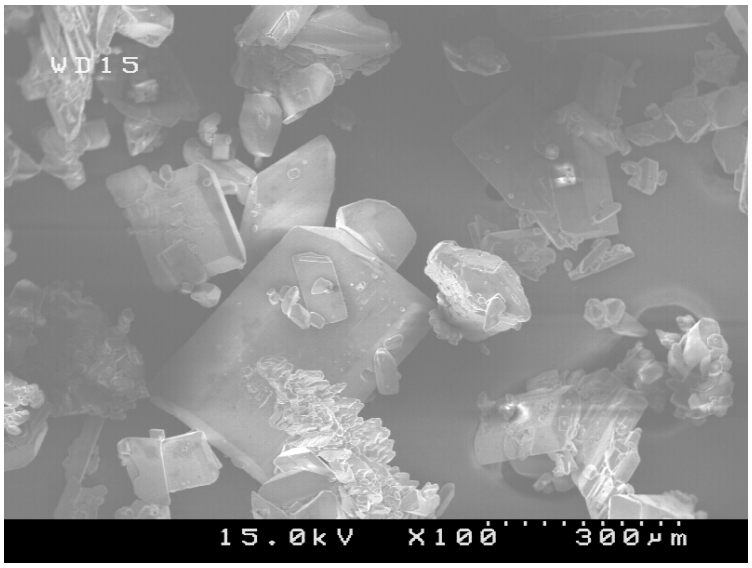

Figure 10: K_2SO_4 Crystals from Experiment # 2

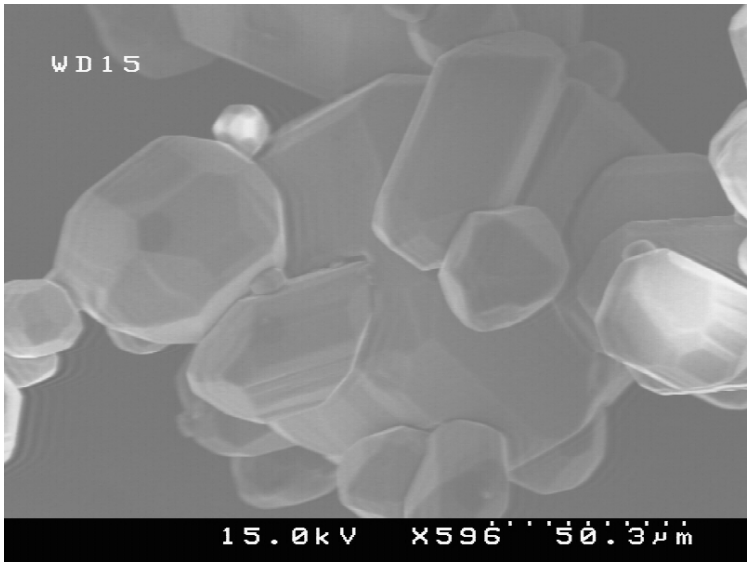

Figure 11: K_2SO_4 Crystals from Experiment # 10

Figures 12-16 give images from light microscopy. These were more difficult to focus. These images and those from SEM verify the median particle size measured by the Malvern instrument. The white bar in the figures is 100 μm.

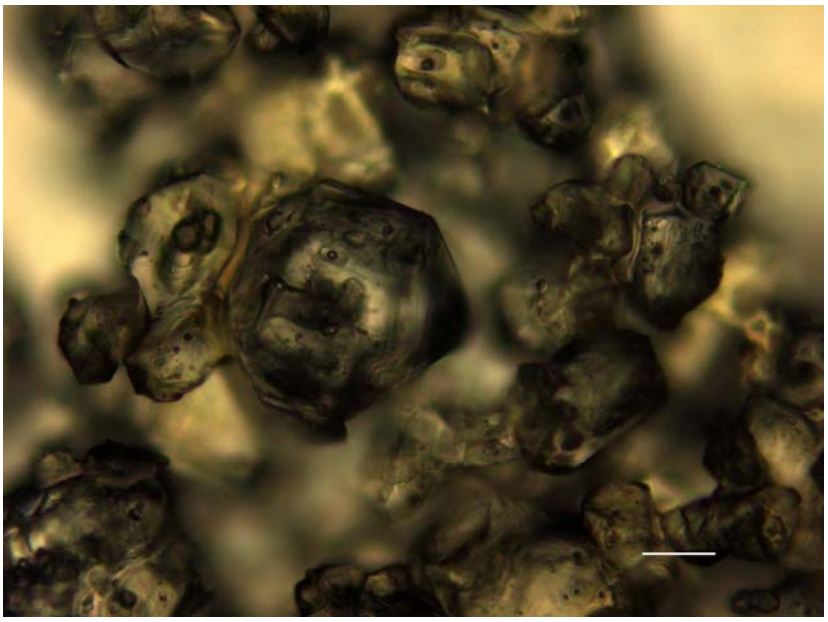

Figure 12: K_2SO_4 Crystals from Experiment # 8

Figure 13: K_2SO_4 Crystals from Experiment # 9

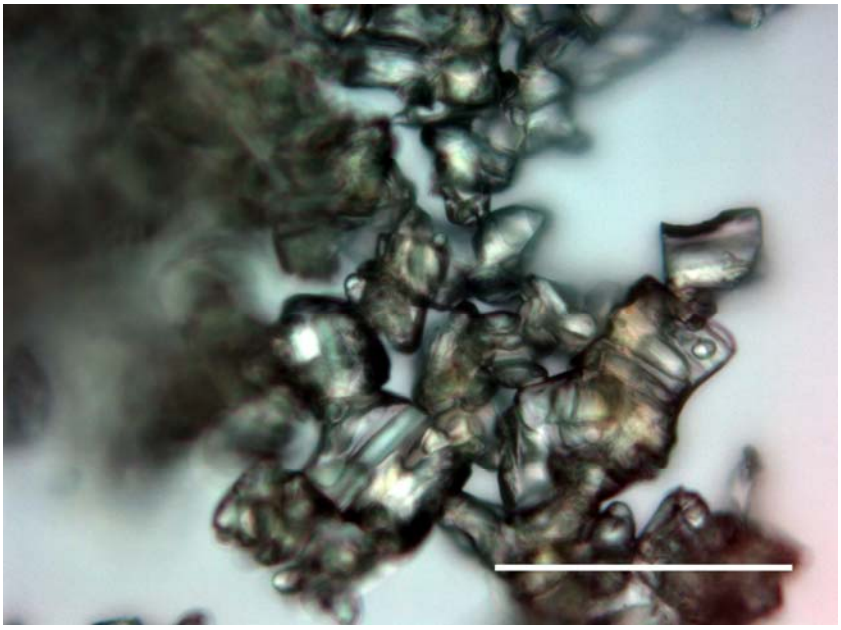

Figure 14: K_2SO_4 Crystals from Experiment # 9

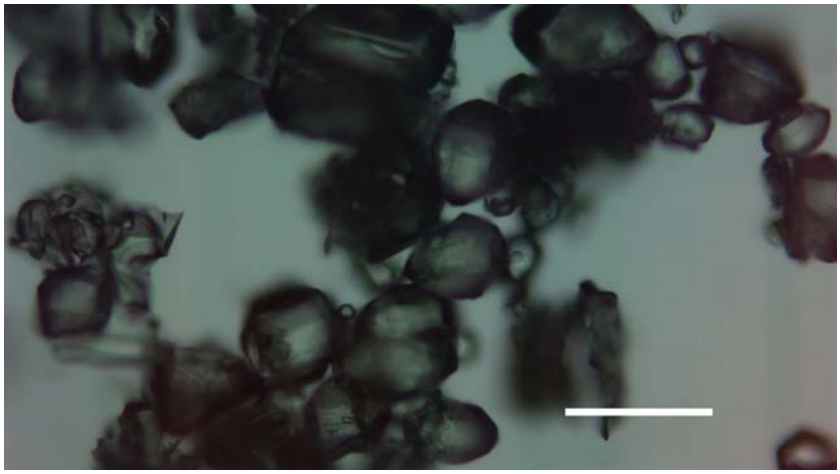

Figure 15: K_2SO_4 Crystals from Experiment # 10

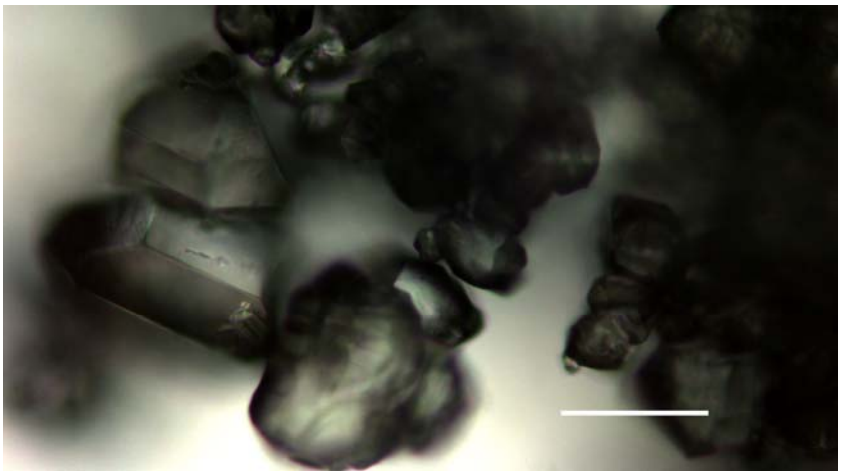

Figure 16: K_2SO_4 Crystals from Experiment # 10

Conclusion

Continuous crystallization produces particles of relatively large size; the volume mean particle size L varies from 110 to 260 μm at residence times of 3 to 20 minutes. Higher temperature gives greater L; longer residence time gives greater L; additive Fe^{+2} does not have any obvious effect on L; increasing agitation rate from 6 to 8 decreases L; lower SO_4^{-2}/K^+ ratio gives greater L. The moisture content in filter cake varies from 4 wt % to 34 wt %. The initial settling rate of concentrating slurry ranges from 1.4 to 7.2 cm/min, which illustrates that the solid-liquid separation can be roughly achieved by sedimentation. SEM and light microscope images verify the particle size given by the laser scanner. The crystal shape and habit varies a little from sample to sample: the reason for this may be agitation, total SO_4^{-2}/K^+ ratio in feed, and residence time, or a combination of these.

Future Work

- Continuous crystallization with 11 m MEA, 7 m MEA/2 m PZ feed.
- Continuous crystallization with oxidation and thermal degradation products as additives, including Fe^{+2}, Cr^{+2}/Cr^{+3}, Cu^{+2}, Ni^{+2}, HEEDA, HEIA, inhibitor A, etc. Study the effects of these additives.
- Variable pressure SEM imaging without coating.
- Select proper method of crystal imaging for following each experiment sample.
- X-ray diffraction of solid samples to analyze impurities that might exist in the product samples.
- K_2SO_4 solubility measurement at high extra SO_4^{-2} or K^+ concentration. This is to complete the previous empirical model for K_2SO_4 solubility prediction.
- Develop the K_2SO_4 crystal nucleation and crystal growth model, and regress parameters from experimental data.
- Develop the model of reclaiming process to remove sulfate by potassium sulfate

crystallization in Aspen Plus®.

- Mass balance and population balance calculation based on the results from interaction parameter regression and crystallization kinetics data.

Degradation of Concentrated Aqueous Piperazine

Quarterly Report for January 1 – March 31, 2008

by Stephanie Freeman

Supported by the Luminant Carbon Management Program

and the

Industrial Associates Program for CO_2 Capture by Aqueous Absorption

Department of Chemical Engineering

The University of Texas at Austin

April 18, 2008

Background

My work this quarter focused on oxidative and thermal degradation of 8 m piperazine (PZ). Addition of 4.0 mM of copper was confirmed to catalyze degradation of PZ primarily producing formate, piperazine formamide, ethylenediamine (EDA), oxalate, and oxamide. Small concentrations of iron and vanadium, 0.1 mM each, did not catalyze PZ degradation to a significant degree. The addition of inhibitor A to 8 m PZ solution with copper and iron effectively inhibited the degradation catalyzed by copper. PZ showed appreciable degradation at 175°C while negligible degradation was observed at 135 and 150°C. Copper, iron, inhibitor A, nickel, and chromium do not further catalyze the thermal degradation of 8 m PZ at 175°C.

Introduction

Concentrated aqueous piperazine (PZ) is being investigated as a possible alternative to the standard 30 wt % (or 7 m) MEA in absorber/stripper systems to remove CO_2 from coal-fired power plant flue gas. Aqueous PZ has been given a proprietary name of ROC20 for 10 m PZ and ROC16 for 8 m PZ. The two names are used interchangeably in this document.

Preliminary investigations of PZ have shown numerous advantages over 7 m MEA systems. Aqueous concentrated PZ produces less degradation both thermally and oxidatively as previously shown at concentrations of 5 and 8 m. The kinetics of CO_2 absorption are faster in concentrated PZ, as shown by Tim Cullinane, and are currently being measured by Ross Dugas. The capacity of PZ is higher than that of MEA while the heat of absorption and volatilities are comparable.

Oxidative degradation of amine solvents in these systems can occur in the absorber where oxygen is present from the flue gas. It can also occur in the sump of the absorber or in the lines of the cross exchanger before the rich solvent enters the stripper. Thermal degradation primarily occurs in the stripper where high pressure and temperature steam is used to strip the rich solvent. Temperatures in the stripper are usually up to 120°C, but degradation of PZ has been investigated at 135, 150, and 175°C. Both oxidative and thermal degradation of PZ was

investigated this quarter. In addition, some work has been completed on building an apparatus to test the foaming characteristics of solvents.

Materials and Methods

Experimental Methods

Low Gas Flow Apparatus: The low gas flow apparatus is used to measure oxidative degradation through the exposure of an amine solution to an oxygen rich environment. The apparatus has been detailed previously in the progress reports of Andrew Sexton. No major modifications have been made. Overall, the apparatus consists of a glass vessel that is maintained at 55°C using a recirculating, heated water bath. The amine solution is mechanically agitated at 1400 RPM and the vessel is loosely sealed with a large rubber stopper. A gas flow of 100 mL/min of 98%/2% O_2/CO_2 is introduced at the top of the gas liquid interface during agitation.

Thermal Degradation: Thermal degradation experiments are performed as detailed previously in the progress reports of Jason Davis. No major modifications have been made. In summary, 2 mL of amine solution is loaded into an airtight, stainless steel bomb made of Swagelok connections. The bombs are placed in forced convection ovens for extended periods of time and removed for analysis.

Foaming Apparatus: An apparatus to measure the foaming characteristics of various solvents is being built. The apparatus is modeled after ASTM method D 892 and the work of Bhurisa Thitakamol at University of Regina[1]. The apparatus is in the initial stages of testing and data should be reported in the next quarter on this test apparatus.

Analytical Methods

Anion Chromatography: Anion chromatography was used to determine the concentration of glycolate, acetate, formate, nitrite, oxalate, and nitrate in experimental samples. A Dionex ICS3000 instrument with AS15 IonPac column and ASRS 4-mm self-regenerating suppressor was used as previously described by Andrew Sexton using a linear sodium hydroxide eluent gradient ranging from 2 to 45 mM. No major modifications have been made to the method in this quarter.

Cation Chromatography: The cation chromatography was used to determine the concentration of PZ and EDA in experimental samples. A Dionex ICS2500 instrument with CS17 IonPac column with CSRS 4-mm self-regenerating suppressor was used as previously described by Jason Davis with 55 mM methanesulfonic acid (MSA) eluent. No major modifications have been made to the method in this quarter.

NaOH Treatment for Amides: The analytical test for the formation of amides as developed by Andrew Sexton in 4th quarter 2007 is in continued use since last quarter. Experimental samples are treated with an equal mass of 5 N NaOH and allowed to sit overnight. Then the anion chromatography analytical method is used to quantify increases in the concentrations of analytes as compared to the original samples. In most cases, the main increases are shown in the production of formate and oxalate following NaOH treatment.

Total Inorganic Carbon Analysis (TIC): Quantification of CO_2 loading is performed using a total inorganic carbon analyzer. In this method, a sample is acidified with 30 wt % H_3PO_4 to release the CO_2 present in solution. The CO_2 is carried in the nitrogen carrier gas stream to the detector.

PicoLog software is used to record the peaks that are produced from each sample. A calibration curve is prepared at the end of each analysis using a TIC standard mixture of K_2CO_3 and $KHCO_3$. The TIC method quantifies the CO_2, CO_3^{-2}, and HCO_3^- present in solution. These species are in equilibrium in the series of reactions shown below.

$$CO_3^{2-} + 2H^+ \leftrightarrow HCO_3^- + H^+ \leftrightarrow H_2CO_3 \leftrightarrow CO_2 + H_2O$$

Acidification of the sample shifts the equilibrium toward CO_2 which bubbles out of solution and is detected in the analyzer.

Acid pH Titration: Titration with 0.2 N H_2SO_4 is used to determine the concentration of amines in experimental samples. The automated Titrando apparatus is used for this method. A known mass of sample is diluted with water and the autotitration method is then used. The Titrando titrates the sample with acid while monitoring the pH. The equivalence points are recorded. The equivalence point around a pH of 3.9 corresponds to basic amine species in solution. The test is not sensitive to the type of amine, so if PZ has degradated to EDA, the titration test will detect the sum of contributions from the species.

Methanolic KOH Titration: A method for the determination of CO_2 loading in amine solutions using methonolic KOH titration is being developed. The method is based on a proprietary method from Dow Chemical Company currently used at the Pickle Pilot Plant and on a UOP method obtained from Dr. Asha Masohan of the Indian Institute of Petroleum[2, 3].

Viscosity Measurements: Viscosity of solutions was measured using a Physica MCR 300 cone and plate rheometer (Anton Paar, Graz, Austria). The apparatus allows for precise temperature control for measuring viscosity at temperatures ranging from 25 to 70°C. To take a measurement, 700 mL of solution is loaded onto the measurement disk. The instrument accelerates the top disk at a predetermined angular speed and measures the shear stress over time. The program that is used increases the angular speed from 100 to 1000 over a period of 100 seconds, measuring shear stress every 10 seconds. Viscosity is calculated for each sampling instance and an average and standard deviation are calculated from the 10 individual measurements.

Results

The results of oxidative and thermal degradation experiments performed in the fourth quarter 2007 were reported with partially incomplete data sets in the prior report. This includes oxidative experiment 02 and thermal experiments 01, 02, and 03. The analysis of the experiment samples has been completed this quarter and those results are reported.

New experiments on both oxidative and thermal degradation of PZ solutions have been performed this quarter and are reported.

Summary of Oxidation Degradation Experiments Performed to Date:

1. ROC20 with 0.6 mM chromium (Cr^{2+}), 0.1 mM nickel (Ni^{2+}), and 0.1 mM iron (Fe^{2+}) (loading of 0.4, 55°C, 1400 RPM agitation)
2. ROC20 with 4.0 mM copper (Cu^{2+}) (loading of 0.4, 55°C, 1400 RPM agitation)
3. ROC16 with 0.1 mM Fe^{2+} and 0.1 mM V^{5+} (loading of 0.3, 55°C, 1400 RPM agitation)
4. ROC16 with 5.0 mM Cu^{2+}, 0.1 mM Fe^{2+}, and 100 mM Inhibitor "A" (loading of 0.3, 55°C, 1400 RPM agitation)

Summary of Thermal Degradation Experiments Performed to Date:

1. ROC20 at 135°C (loadings of 0.3 and 0.4, 2 mL bombs)
2. ROC20 at 150°C (loadings of 0.3 and 0.4, 2 mL bombs)
3. ROC30 and ROC40 at 150°C (loading of 0.3, 2 mL bombs)
4. ROC16 at 175°C (loading of 0.3, 2 mL bombs)
5. ROC16 at 175°C with 5.0 mM Cu^{2+} and 0.1 mM Fe^{2+} (loading of 0.3, 2 mL bombs)
6. ROC16 at 175°C with 5.0 mM Cu^{2+}, 0.1 mM Fe^{2+}, 100 mM Inhibitor "A" (loading of 0.3, 2 mL bombs)
7. ROC16 at 175°C with 1.0 M formate, 100 mM oxalate, and 150 mM EDA (loading of 0.3, 2 mL bombs)
8. ROC16 at 175°C with 0.6 mM Cr^{2+}, 0.1 mM Fe^{2+}, 0.1 mM Ni^{2+} (loading of 0.3, 2 mL bombs)

Results of Oxidative Degradation

A majority of the results for the first (OE1) and second (OE2) oxidative degradation experiments was reported last quarter. One data point for OE1 was reanalyzed for amide production this quarter. The sample at t=13 days (316 hours) was treated with NaOH again and reanalyzed for post NaOH formate concentration. The concentration of formate was found to be lower and to fit the trend of the data before and after this sample. The old concentration profiles reported in the previous quarterly report (4^{th} quarter, 2007) are shown in Figure 1 while the corrected data are shown in Figure 2.

Figure 1: Concentration Profiles for OE1 (0.6 mM Cr^{2+}, 0.1 mM Ni^{2+}, 0.1 mM Fe^{2+}, 55°C, α=0.4)

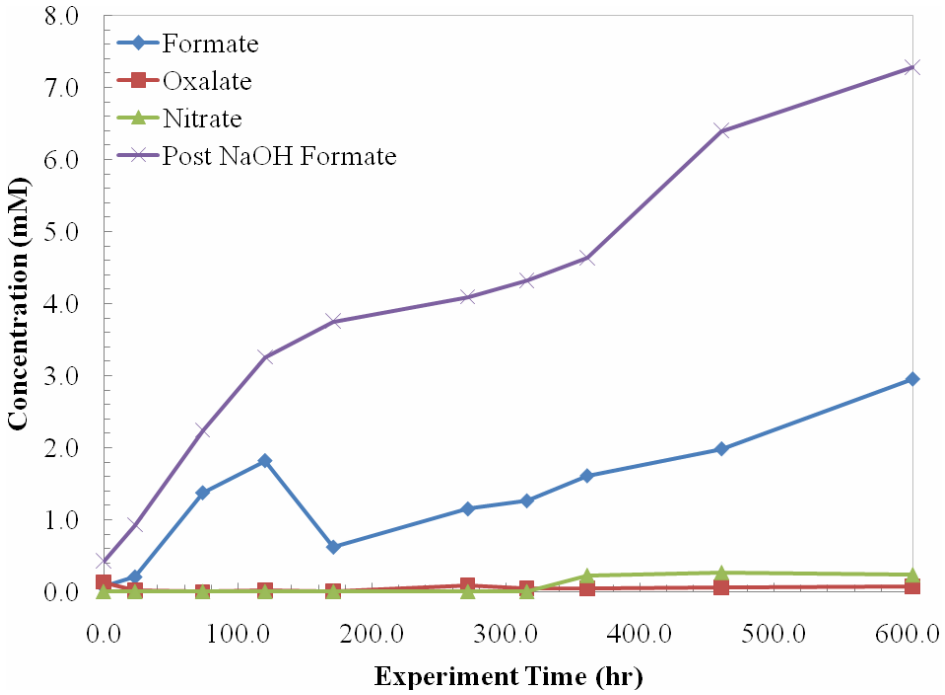

Figure 2: Concentration Profiles for OE1 with corrected data point at 316 hours (0.6 mM Cr^{2+}, 0.1 mM Ni^{2+}, 0.1 mM Fe^{2+}, 55°C, α=0.4)

The analysis for amides for OE2 has been completed this quarter and the data are presented in Figure 4 below. In addition, an error was found in the manner in which the EDA concentration was calculated from the cation chromatography results. This error has been fixed and the EDA concentrations throughout the experiment are actually higher than reported last quarter. The incorrect results reported previously are shown in Figure 3 as a comparison to the corrected results shown in Figure 4.

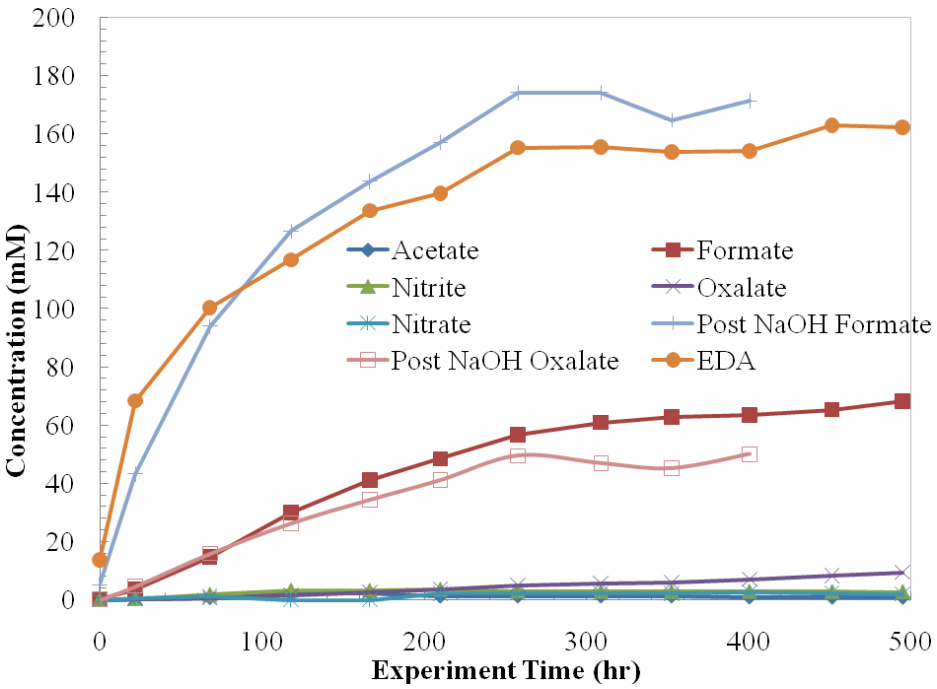

Figure 3: Concentration Profiles for OE2 as Reported Last Quarter (4.0 mM Cu^{2+}, 55°C, α=0.4)

Figure 4: Concentration Profiles for OE2 (4.0 mM Cu^{2+}, 55°C, α=0.4)

The concentration of formate following NaOH treatment continued to grow in the final two samples, maintaining the overall trend. The concentration of oxalate following NaOH treatment, on the other hand, decreased in the final two samples. This may reflect the fact that the final two samples were treated with NaOH and analyzed one month after the experiment ended. This may have allowed time for changes in the sample because it was left out for an extended period of time.

The third oxidative experiment listed above (OE3) was completed this quarter. This low gas flow experiment was performed on 8.0 m PZ (ROC16) with 0.1 mM Fe^{2+} and 0.1 mM V^{5+}. The concentration profiles of degradation products are shown in Figure 5.

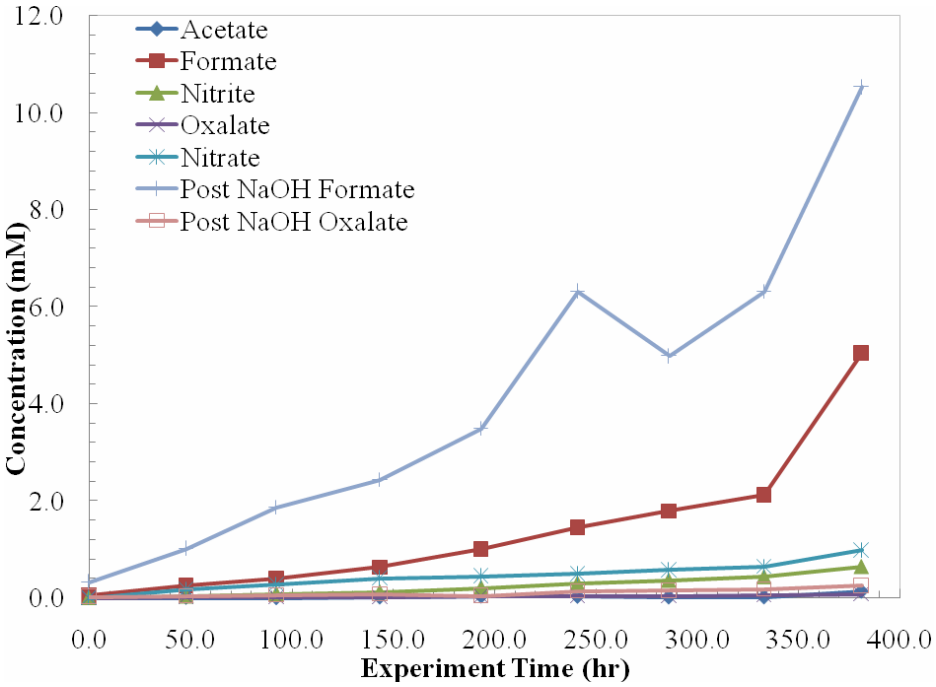

Figure 5: Concentration Profiles for OE3 (0.1 mM Fe^{2+}, 0.1 mM V^{5+}, 55°C, α=0.3))

The fourth oxidative degradation experiment (OE4) was completed this quarter as well. This low gas flow experiment was performed on 8.0 m PZ (ROC16) at 55°C with 5.0 mM Cu^{2+}, 0.1 mM Fe^{2+}, and 100 mM Inhibitor A. The concentration profiles of the degradation products and piperazine are shown in Figure 6.

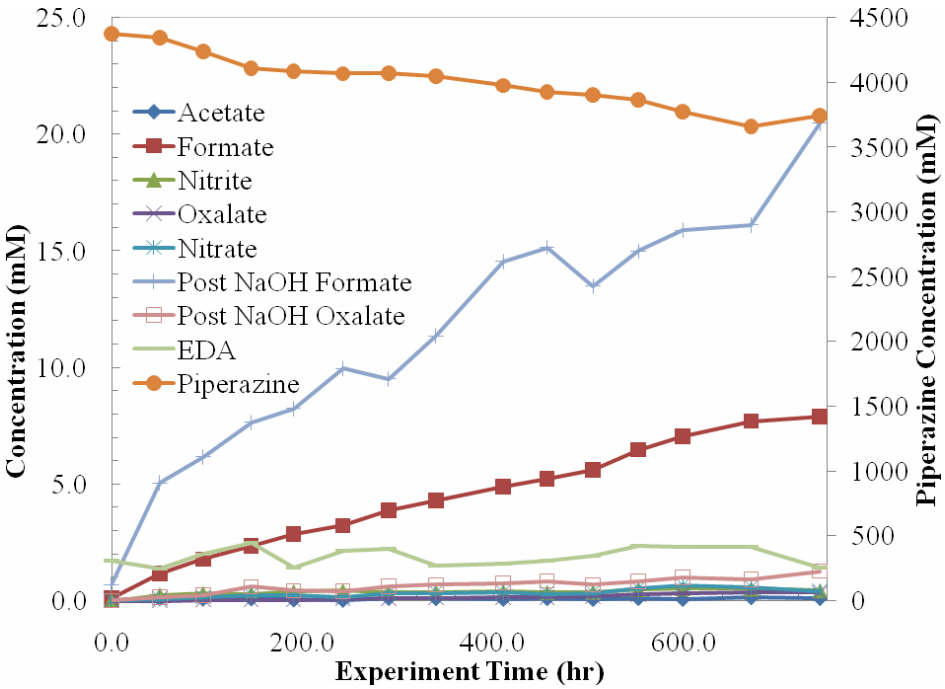

Figure 6: Concentration Profiles for OE4 (5.0 mM Cu^{2+}, 0.1 mM Fe^{2+}, 100 mM "A", 55°C, α=0.3)

Results of Thermal Degradation

The first thermal degradation experiment (TE1) investigated the degradation of 10 m PZ (ROC20) solutions with loadings 0.3 and 0.4 mol CO_2/2 mol ROC20 at 135°C. This experiment was started in the 4th quarter of 2007 and was conducted for 15 weeks. The concentration profiles of the degradation products detected are shown in Figure 7 and Figure 8. The experiment with α=0.3 is designated TE1-A (Figure 9Figure 7) while the experiment with α=0.4 is TE1-B (Figure 10Figure 8). TE1-A did not have a bomb to analyze at 15 weeks because it was empty when removed from the oven.

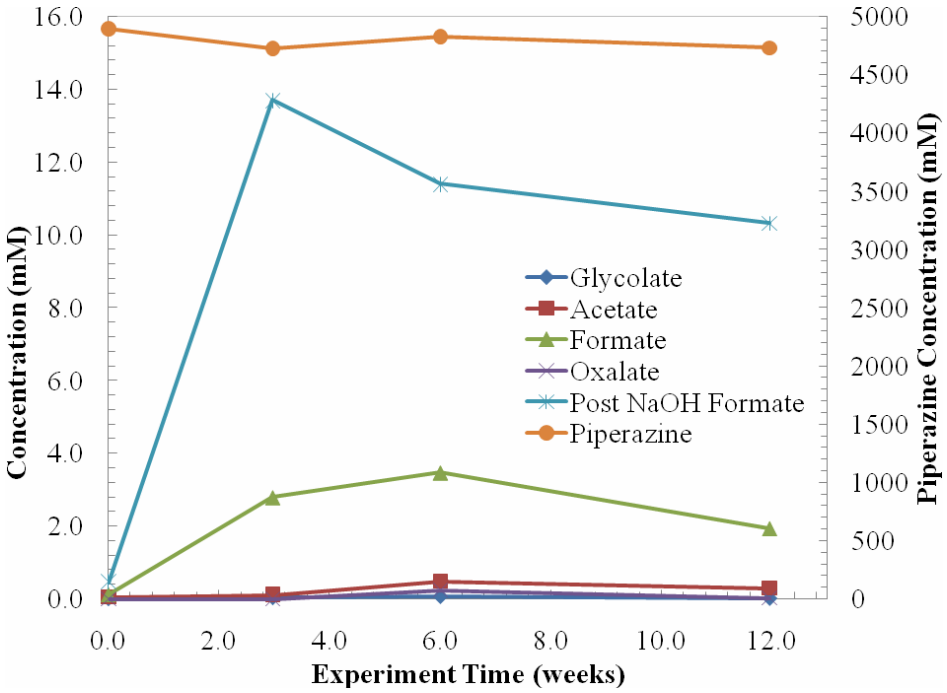

Figure 7: Concentration Profiles for TE1-A (ROC20, α=0.3, 135°C, 2 mL bombs)

Figure 8: Concentration Profiles for TE1-B (ROC20, α=0.4, 135°C, 2 mL bombs)

The second (TE2) and third (TE3) thermal degradation experiments tested the degradation of ROC20, ROC30, and ROC40 solutions with loadings of either 0.3 or 0.4, at the elevated

temperature of 150°C. Preliminary results for both experiments were reported in the preceding quarterly report (4th quarter, 2007) and the completed data analysis is presented here.

Both experiments were conducted for 5 weeks and the concentration profiles of degradation products detected are shown in Figure 9-12 below. The ROC20 experiment with α=0.3 is designated TE2-A (Figure 9) while the ROC20 experiment with α=0.4 is TE2-B (Figure 10). The experiment with ROC30, α=0.3, is designated TE3-A (Figure 11) and with ROC40, α=0.3, is designated TE3-B (Figure 12).

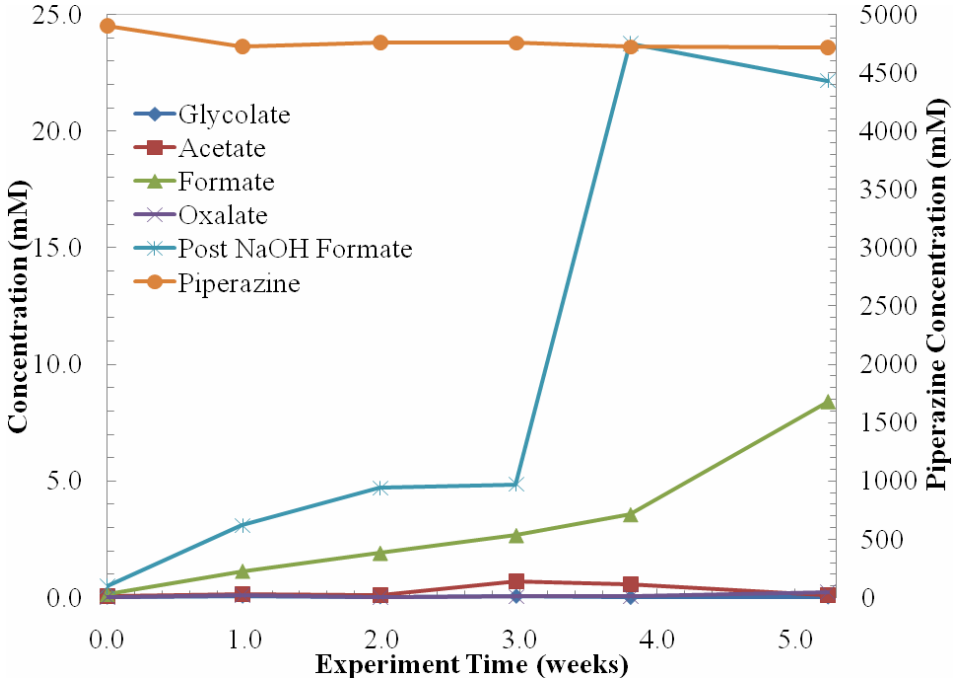

Figure 9: Concentration Profiles for TE2-A (ROC20, α=0.3, 150°C, 2 mL bombs)

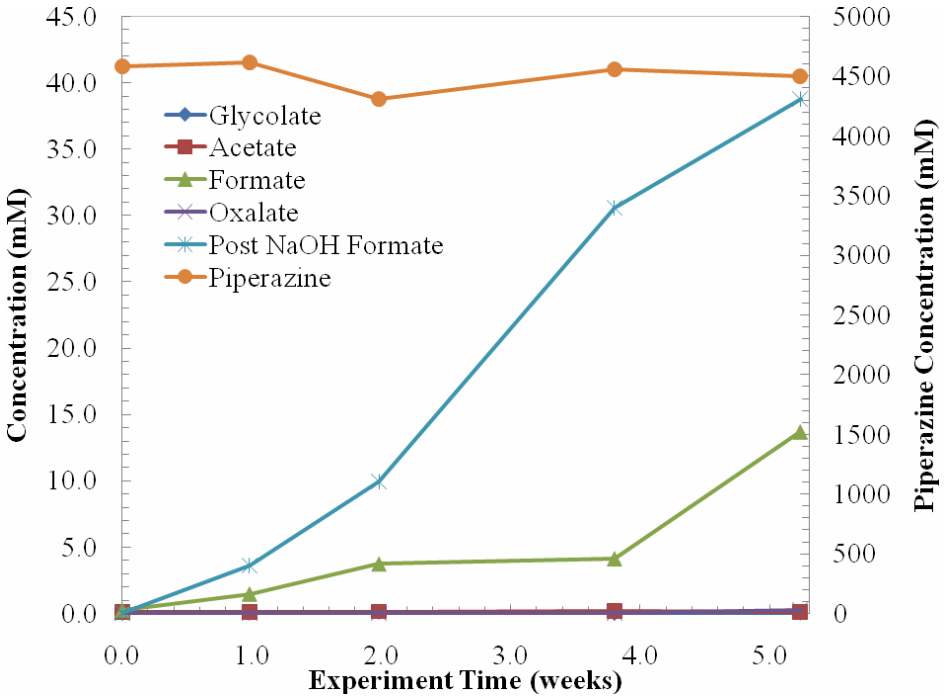

Figure 10: Concentration Profiles for TE2-B (ROC20, α=0.4, 150°C, 2 mL bombs)

Figure 11: Concentration Profiles for TE3-A (ROC30, α=0.3, 150°C, 2 mL bombs)

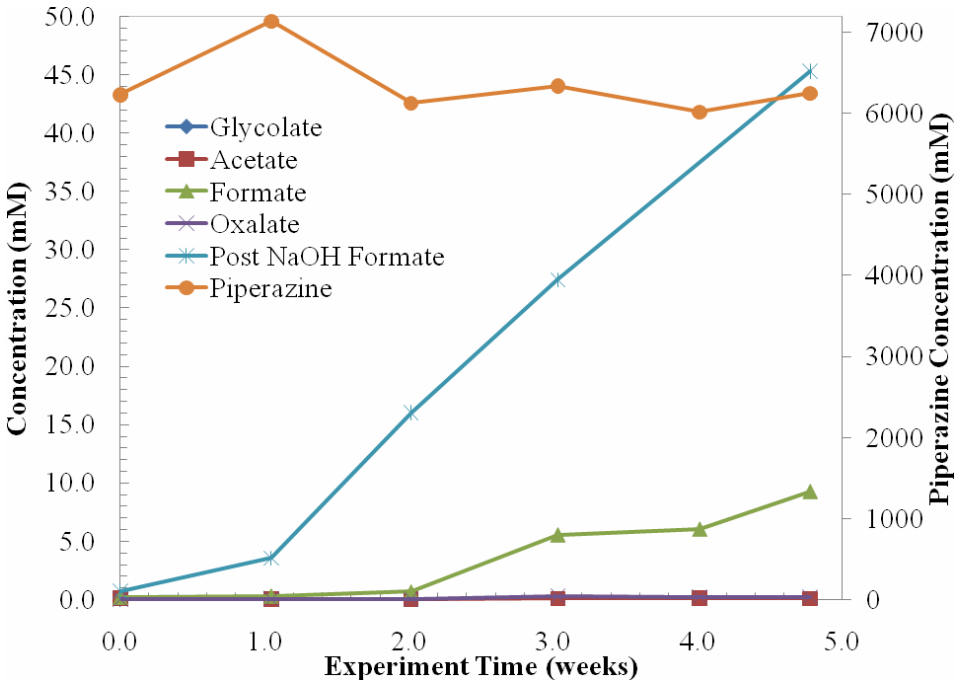

Figure 12: Concentration Profiles for TE3-B (ROC40, α=0.3, 150°C, 2 mL bombs)

Similar to the results of TE1, all the conditions of TE2 and TE3 produced formate as a degradation product. Little PZ degradation was seen overall, as demonstrated by the minimal change in the PZ concentration profile, but a small amount of formate was made in each instance, ranging from 22.1 to 45.3 mM. Even less formate, only 10.6 mM and 6.5 mM for 0.3 and 0.4 loading, respectively, was produced at the lower temperature of 135°C in TE1.

Five additional thermal degradation experiments were started during this quarter. All of these, TE4 through TE8, investigate the degradation of 8.0 m PZ (ROC16) with 0.3 CO_2 loading at the very high temperature of 175°C. Since very little degradation has been seen in 10.0 m PZ at 135 and 150°C, 175°C was chosen to see if we could get the PZ to degrade. This temperature is higher than would be seen in real strippers, but was chosen in order to force the PZ to degrade. The concentration profiles of the degradation products and PZ are shown in the figures below. TE4 has no further additives (Figure 13). TE5 contains 4.0 mM Cu^{2+} and 0.1 mM Fe^{2+} to investigate high copper concentrations on thermal degradation (Figure 14). TE6 has 4.0 mM Cu^{2+}, 0.1 mM Fe^{2+}, and 100 mM Inhibitor A to test the presence of Inhibitor A on thermal degradation (Figure 15). TE7 has 1.0 M formate, 100 mM oxalate, and 150 mM EDA to determine the effect of the presence of oxidative degradation products in solution (Figure 16). Finally, TE8 has 0.6 mM Cr^{2+}, 0.1 mM Fe^{2+}, and 0.1 mM Ni^{2+} to test the effect of stainless steel metals on thermal degradation (Figure 17).

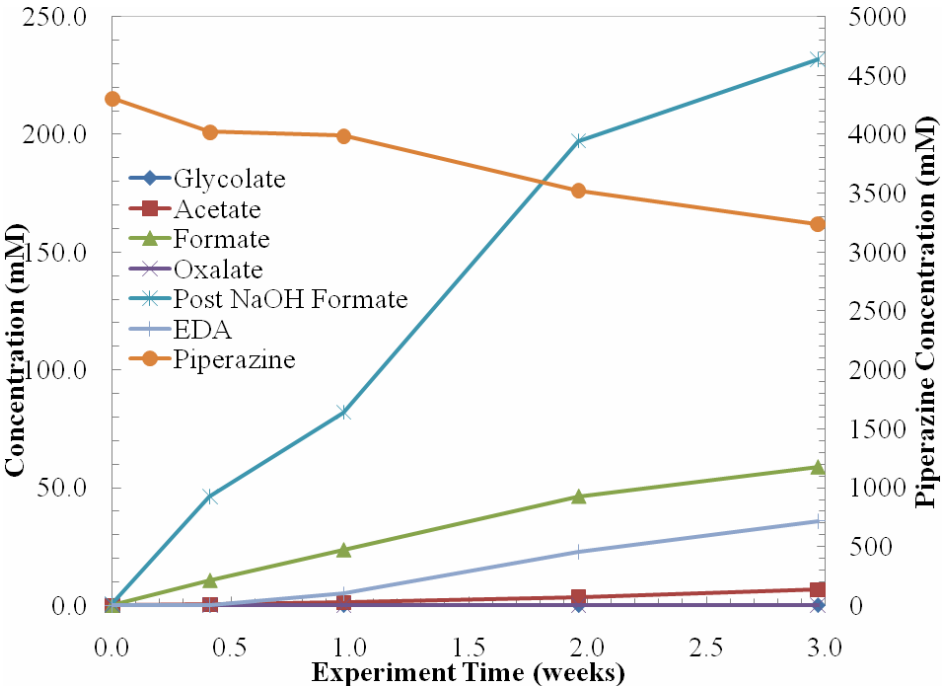

Figure 13: Concentration Profiles for TE4 (ROC16, α=0.3, 175°C, 2 mL bombs)

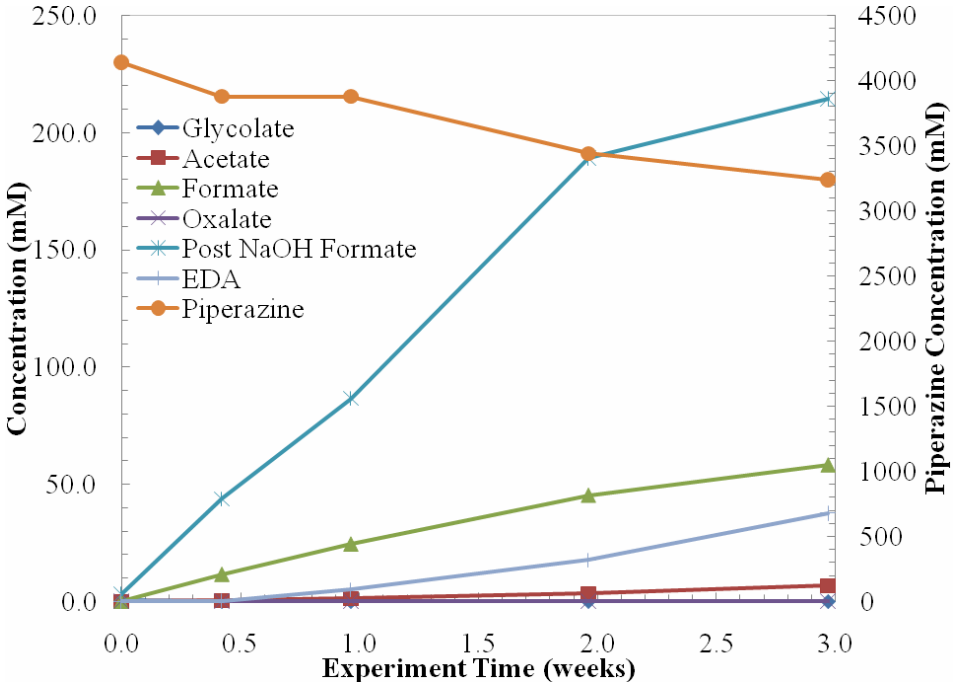

Figure 14: Concentration profile for TE5 (ROC16, 5.0 mM Cu^{2+}, 0.1 mM Fe^{2+}, α=0.3, 175°C, 2 mL bombs)

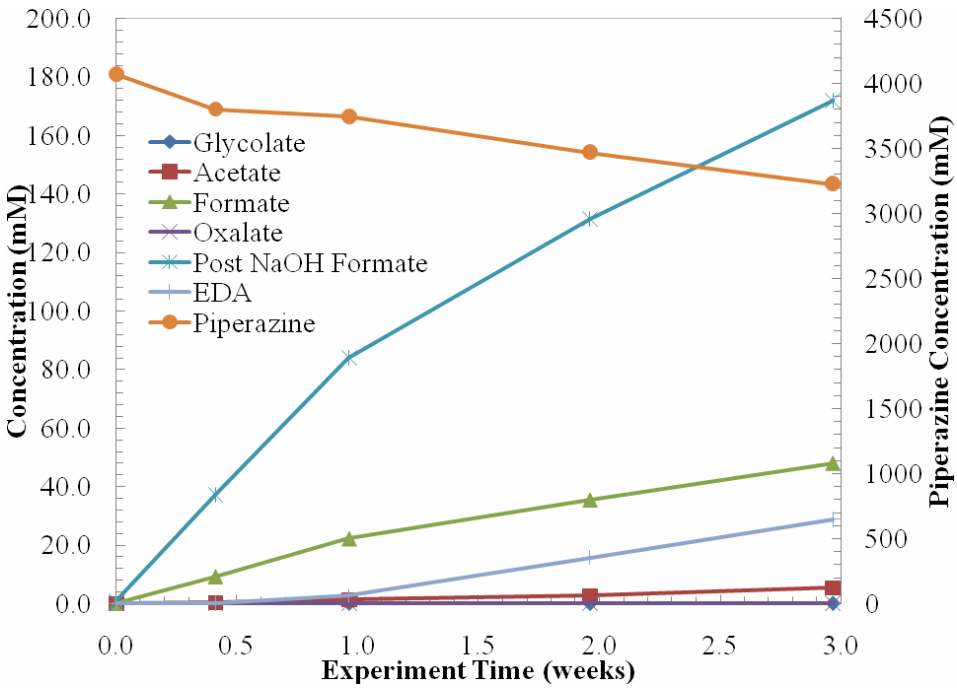

Figure 15: Concentration Profile for TE6 (ROC16, 5.0 mM Cu^{2+}, 0.1 mM Fe^{2+}, 100 mM "A", α=0.3, 175°C, 2 mL bombs)

Figure 16: Concentration Profiles for TE7 (ROC16, 1.0 mM formate, 100 mM oxalate, 150 mM EDA, α=0.3, 175°C, 2mL bombs)

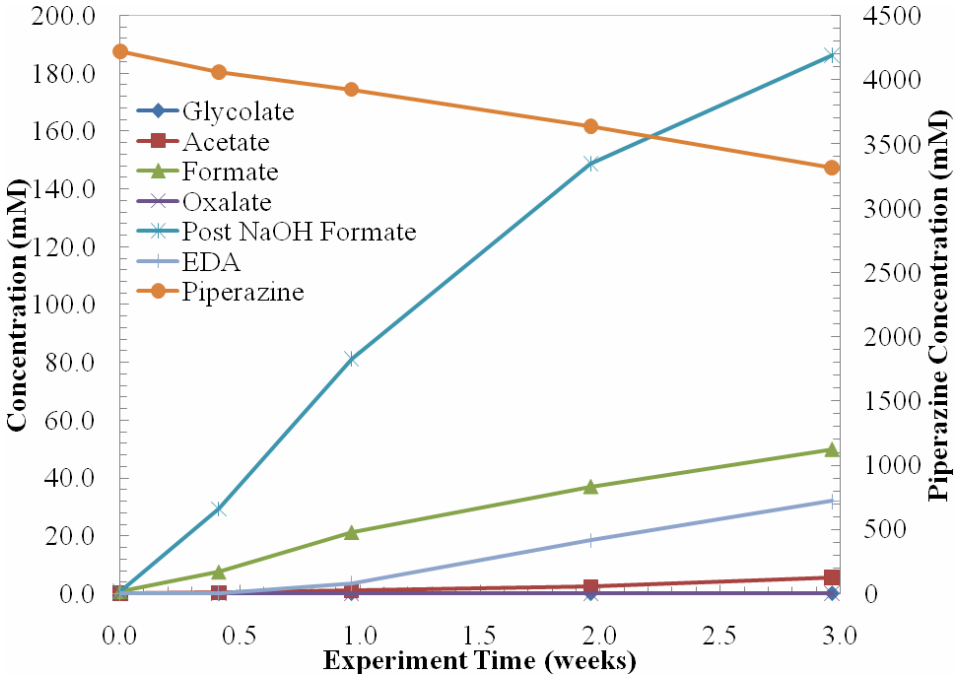

Figure 17: Concentration Profiles for TE8 (ROC16, 0.6 mM Cr^{2+}, 0.1 mM Fe^{2+}, 0.1 mM Ni^{2+}, α=0.3, 175°C, 2mL bombs)

These thermal degradation experiments are only 3 weeks into a 5-week experiment. The complete results will be reported in the next quarterly report.

The analytical results of TE7 have proved difficult to interpret. The original intent was to add 100 mM of formate to TE7 to match the amounts of oxalate and EDA added, but a mistake in the calculations was made. Ten times the amount was added to make the initial concentration approximately 1.0 M. The mistake was not noticed until two weeks into the experiment, so the results may not be entirely useful because the concentration of formate is so much higher than ever seen in oxidative degradation experiments. In addition, the concentration determined from the anion chromatography does not seem to meet the expected 1.0 M that was added based on mass in the setup of the experiment. Usually, samples are diluted 100X for anion analysis. For TE7, a variety of dilutions have been used to have the formate ion concentration between the 10 and 50 ppm standards used in the anion IC. Multiple dilutions are therefore used to get data on formate (2000X) and the rest of the anions (100X). The initial formate concentrations (both pre- and post-NaOH treatment) are slightly higher than the expected 1.0 M concentration. It is unknown why there is an additional 300 mM of formate detected by the anion chromatography. Furthermore, the oxalate originally present in the experiment bombs disappears after the initial sample. It is not known what the oxalate is being converted to since formate is the only other degradation product identified in a sizeable quantity and it does not increase significantly through the first two weeks, as shown in Figure 16).

Discussion

Oxidative Degradation Experiments

Oxidative degradation experiments performed to date have began to explore the possible degradation in high concentration aqueous PZ. A summary of the four low gas flow experiments performed to date is shown in Table 1.

Table 1: Summary of Oxidative Degradation Experiments on PZ

	OE1	OE2	OE3	OE4
Duration	25 days	21 days	16 days	31 days
Amine	PZ	PZ	PZ	PZ
Amine Conc. (m)	10	10	8	8
CO_2 Loading	0.3	0.3	0.3	0.3
Temperature (°C)	55	55	55	55
Additives (Conc. in mM)	Cr^{2+} (0.6) Fe^{2+} (0.1) Ni^{2+} (0.1)	Cu^{2+} (4.0)	Fe^{2+} (0.1) V^{5+} (0.1)	Cu^{2+} (5.0) Fe^{2+} (0.1) "A" (100)
Final Total Formate Conc. (mM)	7.3	184.7	10.5	20.5
Final EDA Conc. (mM)	0	232.8	0	6.7
Final Nitrate+Nitrite Conc. (mM)	0.2	4.8	1.6	0.8
Final Total Oxalate Conc. (mM)	0.2	25.8	0.3	0.5

Concentrated solutions of PZ are highly susceptible to oxidative degradation in the presence of copper, as with most amines such as MEA. In the presence of the stainless steel metals, chromium, iron, and nickel, very little degradation is observed through little production of degradation products and from the maintained presence of PZ. Very little degradation was also observed in the experiment with iron and vanadium. Although the experiments were performed at two different PZ concentrations, it is assumed that the catalytic effect of each metal would be maintained at varying concentrations of PZ. The effect of inhibitor A was also tested in OE4 and was shown to significantly reduce the oxidative degradation seen in OE2 in the presence of copper. The inhibitory effect of A has been observed in other amine systems and the beneficial properties are demonstrated in PZ solutions as well.

One ongoing issue related to the low gas flow experiments is a loss of CO_2 loading that has been observed. The loading of samples was not measured for OE1, OE2, or OE3, but the measurements made for OE4 reveal a possible issue with our experimental setup. The CO_2 loading was measured throughout the experiment using the Total Inorganic Carbon analyzer (TIC) and the results are shown in Figure 18 with experimental error bars. The original solution created for OE4 was loaded to 0.3, as verified by the first point on the graph. Then, the solution appears to lose CO_2 loading during the course of the experiment.

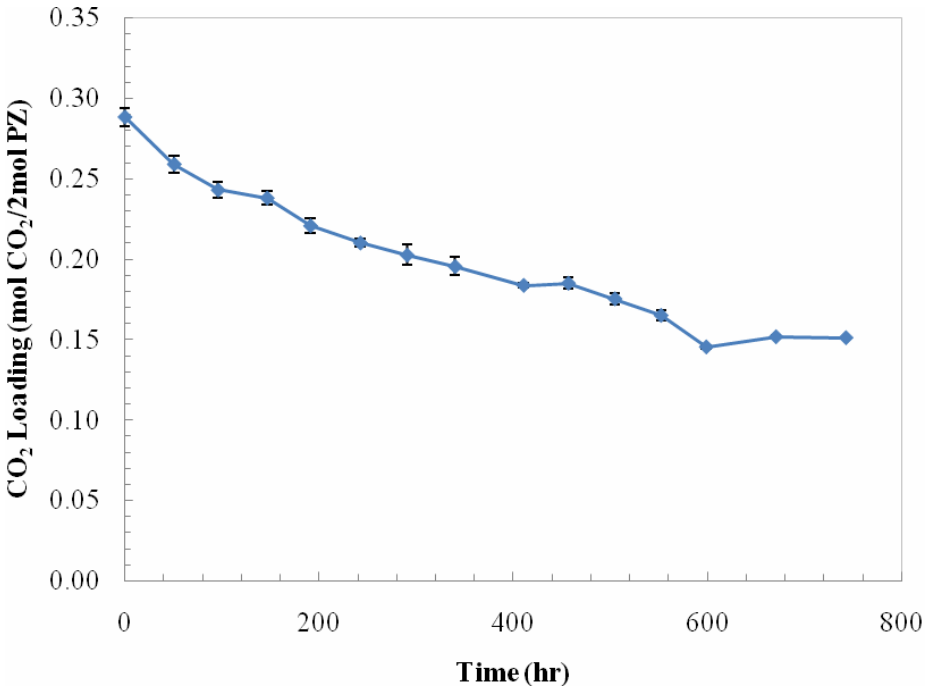

Figure 18: Change in CO_2 Loading in OE4

Using the work of Marcus Hilliard as a reference, the expected CO_2 loading for this solution should be known. A figure from Hilliard's thesis is included below as a reference to this system (Figure 14.5-5). This graph is for 5.0 m PZ, but I assumed that the range of CO_2 solubility values would be similar, at least in this general comparison. For the low gas flow system at 55°C, the expected CO_2 solubility can be interpolated for a headspace of 2% CO_2 (~2kPa CO_2). At this approximate partial pressure, the equilibrium CO_2 loading should be roughly 0.33. The loading in the reactor falls to almost 0.15 from the initial loading of 0.3, instead of maintaining its loading or rising close to 0.33. A few possibilities can explain this phenomenon. First, the CO_2 flow controller might be malfunctioning and not delivering the desired amount of CO_2 and the decrease in the loading demonstrates the loss of CO_2 when the headspace is pure oxygen. Second, the headspace is not being maintained at 2% CO_2, but falling below 2%, causing the equilibrium loading to be below the expected 0.33. It is not known at this time why the headspace would be far below the expected 2% CO_2.

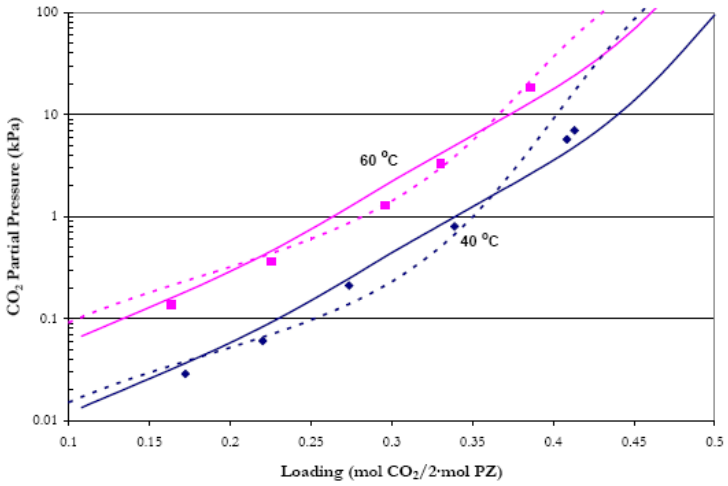

Figure 14.5-5. Comparison between Experimental and Predicted CO_2 Solubility in 5.0 m PZ at 40 and 60 °C. Points: ♦, 40 °C, ■, 60 °C, this work. Lines: - - -, Hilliard (2005), —, this work.

Thermal Degradation Experiments

All of the data analysis for the initial set of thermal degradation experiments on ROC20, ROC30, and ROC40 has been completed this semester (TE1 through TE3). A further analysis of degradation of ROC16 at 175°C was started this semester and will continue into the 2nd quarter of 2008.

Overall, solutions of 10 m PZ did not significantly degrade at 135 and 150°C. At 135°C, the production of formate was noticeably higher with a loading of 0.4 (TE1-B, Figure 8) than with a loading of 0.3 (TE1-A, Figure 7). TE1-B reached nearly 40 mM of formate while TE1-A had less than 15 mM of formate detected. At 150°C, the formate production followed the same trend with formate levels reaching 20 and 45 mM at 0.3 and 0.4 loading, respectively. EDA was noticeably absent from both experiments. Based on these results, it seems that higher loadings lead to slightly higher levels of formate in thermal degradation.

Solutions of 15 and 20 m PZ also did not significantly degrade at 150°C. EDA was not found in the degraded samples of either concentration of PZ. The final, total formate concentration was slightly higher in the 20 m PZ at 45 mM compared to 30 mM for the 15 m solution.

The goal of TE4 through TE8 was to see if raising the temperature could force PZ to thermally degrade. A side goal is to see if the addition of either metals andor oxidative degradation products would catalyze thermal degradation. At this point in the experiments, the main observation for TE4 through TE8 (excluding TE7) is that the addition of various metal catalysts does not affect the rate of thermal degradation of PZ. All four experiments had very similar concentration profiles for the primary degradation products (total formate, EDA, oxalate, etc) and reached similar total concentrations after 3 weeks at 175°C. These experiments provide a crucial finding: that the presence of metals that catalyze oxidative degradation does not affect the mechanisms at work at high temperature thermal degradation.

Table 2: Summary of Thermal Degradation Experiments on PZ

Experiment	TE1	TE2	TE3	TE4	TE5	TE6	TE7	TE8
Duration[1]	15 wks	5 wks	5 wks	3 wks	3 wks	3 wks	3 wks	3 wks
Amine	PZ	PZ	PZ	PZ	PZ	PZ	PZ	PZ
Amine Conc. (m)	10	10	12/15	8	8	8	8	8
CO_2 Loading	0.3/0.4	0.3/0.4	0.3	0.3	0.3	0.3	0.3	0.3
Temperature (°C)	135	150	150	175	175	175	175	175
Additives (Conc. in mM)	-	-	-	-	Cu^{2+} (4.0) Fe^{2+} (0.1)	Cu^{2+} (4.0) Fe^{2+} (0.1) "A" (100)	Formate (1000) Oxalate (100) EDA (150)	Cr^{2+} (0.6) Fe^{2+} (0.1) Ni^{2+} (0.1)
Final Total Formate Conc. (mM)[2]	10.3/36.5	22.2/38.8	29.3/45.3	186.5	173.3	141.6	566.6	151.9
Final EDA Conc. (mM)	0	0	0	35.8	37.5	28.8	33.4	32.0
Unidentified degradation products?	No	No	No	Yes	Yes	Yes	Yes	Yes
Degradation?	No	No	No	Yes	Yes	Yes	Yes	Yes

[1] TE4 through TE8 are ongoing. Currently week 3 of 5 total

[2] Different formate concentrations refer to different loading or PZ concentration

Conclusions and Future Work

Oxidative and thermal degradation experiments were the focus of this quarter. The combination of low concentrations of iron and vanadium do not catalyze degradation in 8 m PZ. Additionally, inhibitor A was shown to inhibit oxidative degradation in 8 m PZ in OE4 as compared to OE2, where a high concentration of copper (4 mM) catalyzed the production of formate and EDA. Although the mechanism is not clear in PZ solutions, it appears that inhibitor A works as well in PZ as has been previously demonstrated in MEA (work of A. Sexton).

For thermal degradation, it has been demonstrated that PZ will degrade at 175°C. An important finding is that the addition of copper, iron, chromium, nickel, and chromium does not significantly affect the concentration profiles of the degradation products or the PZ. Unfortunately, the experiment meant to test the degradation of PZ in the presence of oxidative degradation products (formate, oxalate, and EDA) was not properly prepared and the results are unclear.

During the next quarter, my work will focus on characterizing the foaming tendency and solubility of PZ solutions. A foaming apparatus has been constructed this quarter and testing will begin next quarter. The first step will be to attempt to recreate some of the work of Thitakamol of University of Regina to validate the design of the apparatus[1]. Then, the foaming of 8 m PZ and various loadings with metal additives will be investigated. The goal of the solubility experiments will be to find the solubility envelop for PZ in terms of concentration, loading, and temperature. Initial work will focus on 8 m PZ at 25 and 40°C.

References

Thitakamol B & A Veawab. "Foaming Behavior in CO_2 Absorption Process Using Aqueous Solutions of Single and Blended Alkanolamines." *Industrial & Engineering Chemistry Research* **2007,** 47, 216-225.

Method 829-82: Titrimetric Determination of CO_2 in Ethanolamines; UOP: 1982.

Weight Percent Amine and CO_2 Loading Calculations; The Dow Chemical Company: 2007.

Thermodynamics of Piperazine

Quarterly Report for January 1 – March 31, 2008

by Bich-Thu Nguyen

Supported by the Luminant Carbon Management Program

and the

Industrial Associates Program for CO_2 Capture by Aqueous Absorption

Department of Chemical Engineering

The University of Texas at Austin

April 18, 2008

Abstract

This report presents (1) CO_2 solubility and (2) piperazine volatility data for the PZ-CO_2-H_2O system. CO_2 solubility, measured in terms of partial pressure, is explored as a function of temperature, loading, and amine concentration for systems ranging from 0.9 m to 8.0 m PZ at temperatures of 40ºC, 60ºC, and 120ºC. New data are included for 8 m PZ. CO_2 partial pressure follows practically the same dependence on loading (mol CO_2/2*mol PZ) with all piperazine concentrations. These data are represented by the empirical equations: ln (P_{CO2}) = 18.54 - 8160.59*(1/T) + 22.32*(Loading) at 40ºC and 60ºC; and ln (P_{CO2}) = -1.12 + 28.82*(Loading) - 34.53*(Loading^2) at 120ºC due to the quadratic shape of the data. PZ partial pressure is higher with greater PZ concentration and with higher system temperature. PZ volatility decreases as CO_2 loading increases because free piperazine is converted to other species. PZ partial pressure is given by ln (P_{PZ}/[PZ]) = 6.73 – 4045.05*(1/T) – 4.21*(Loading).

Introduction

VLE experimental data for systems ranging from 0.9 m-5.0 m PZ were obtained by Hilliard using the Gasmet FTIR analyzer. PZ volatility data for 8.0 m PZ was also obtained with this analyzer (this work) while CO_2 solubility at this concentration was gathered using a wetted wall column (Dugas, 2008). Additionally, CO_2 solubility data at 120ºC, collected by the use of headspace chromatography, was also considered in the analysis (Ermatchkov, 2006). Ultimately, regression analyses are carried out using Excel to arrive at a model relating the parameters of interest, namely CO_2 solubility and PZ volatility, to temperature, loading, and PZ concentration, respectively.

Data and Experimental Procedure

The equilibrium partial pressures of CO_2 and PZ were measured in a stirred reactor coupled with FTIR analysis (Figure 1).

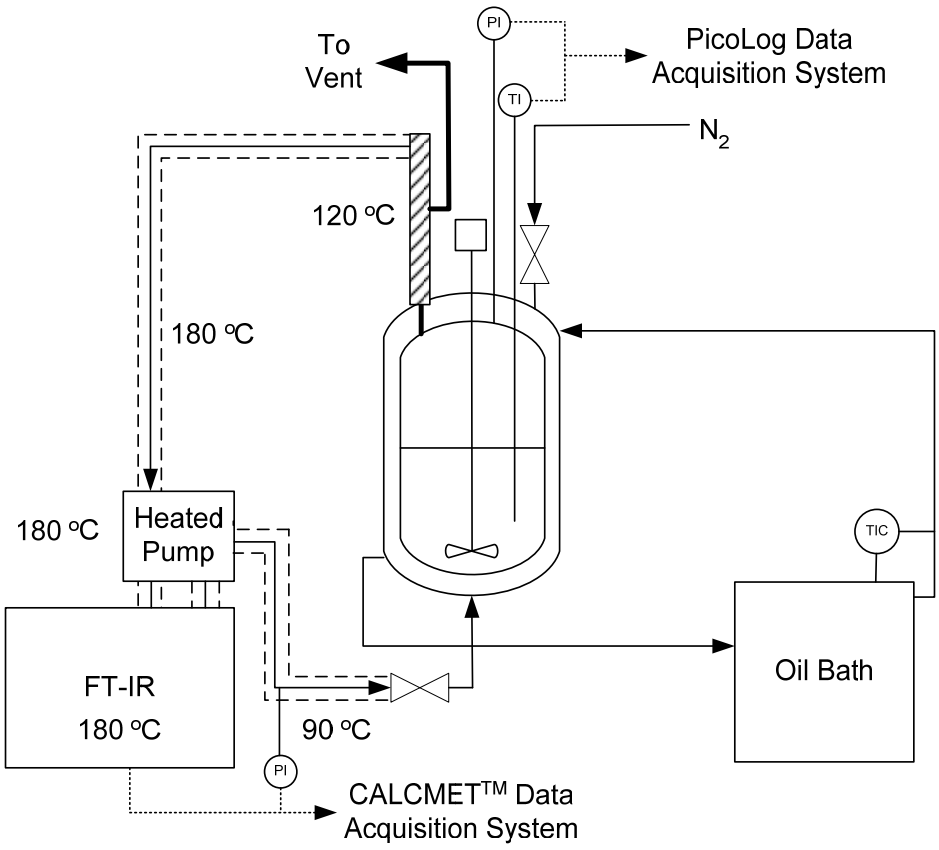

Figure 1: Schematic of Vapor-Liquid Equilibrium FTIR Apparatus

This VLE apparatus allows simultaneous measurements of CO_2 solubility and amine volatility. The heated sample is introduced at 180ºC to a hot gas FTIR at the same temperature. The elevated operating temperature serves to eliminate condensation and adsorption of vapor amine to any apparatus surface; thus, low vapor concentrations of amine can be analyzed more accurately.

The FTIR equipment has the capability of performing a multi-component analysis by combining complete calibration spectra of each component to make up the measured spectrum of the unknown gas. Once FTIR analysis is complete, gas is recycled back to the reactor at a temperature that is ~55ºC higher than the reactor temperature to preserve low amine concentrations. Note that it takes roughly 1.5-2.0 hours for the system to reach equilibrium before a data point can be taken.

Solution loading is prepared gravimetrically by weighing the total contents of the system before and after sparging with CO_2. CO_2 content of the solution is also determined by acidification and evolution into an IR analyzer. The total amine concentration in solution is determined by acid titration to an inflection point.

The table below captures experimental data from different sources considered for this analysis.

Table 1: Experimental Data for 0.9 m-8.0 m PZ-CO_2_H_2O Systems

PZ (m)	Temp (C)	Temp (K)	Loading	P_{CO2} (kPa)	P_{PZ} (kPa)
0.890	39.977	313.127	0.208	4.400E-02	8.300E-04
0.910	40.089	313.239	0.217	7.050E-02	8.900E-04
0.930	39.987	313.137	0.241	1.030E-01	8.500E-04
0.910	40.000	313.15	0.284	2.340E-01	7.200E-04
0.910	40.012	313.162	0.344	9.870E-01	6.600E-04
0.900	40.024	313.174	0.418	4.850E+00	5.300E-04
0.910	60.051	333.201	0.111	2.900E-02	3.250E-03
0.910	60.001	333.151	0.217	2.990E-01	1.970E-03
0.910	60.016	333.166	0.242	8.410E-01	1.570E-03
0.890	60.003	333.153	0.325	1.930E+00	1.080E-03
0.890	60.032	333.182	0.370	8.290E+00	8.500E-04
0.910	59.948	333.098	0.383	1.470E+01	8.000E-04
2.030	60.058	333.208	0.132	9.240E-02	5.550E-03
2.020	60.039	333.189	0.193	2.960E-01	4.800E-03
2.030	59.999	333.149	0.275	1.400E+00	2.930E-03
2.020	59.998	333.148	0.330	3.950E+00	2.240E-03
2.020	60.037	333.187	0.370	9.910E+00	1.770E-03
2.000	59.951	333.101	0.412	2.470E+01	1.280E-03
1.900	59.945	333.095	0.169	1.420E-01	5.130E-03
2.070	59.965	333.115	0.383	1.370E+01	1.870E-03
2.030	40.050	313.2	0.146	2.150E-02	2.120E-03
2.080	40.013	313.163	0.227	1.060E-01	1.800E-03
2.020	40.072	313.222	0.257	1.840E-01	1.680E-03
2.050	40.007	313.157	0.309	5.260E-01	1.490E-03
2.030	40.090	313.24	0.372	1.950E+00	1.380E-03
1.990	40.058	313.208	0.431	1.010E+01	1.090E-03
2.570	40.007	313.157	0.166	3.170E-02	2.290E-03
2.500	39.969	313.119	0.228	8.840E-02	2.080E-03
2.490	39.975	313.125	0.278	2.470E-01	1.840E-03
2.500	39.966	313.116	0.328	6.620E-01	1.520E-03
2.490	40.014	313.164	0.423	7.510E+00	1.250E-03
2.480	40.011	313.161	0.437	1.060E+01	1.150E-03
2.510	59.974	333.124	0.164	1.410E-01	6.180E-03
2.500	60.029	333.179	0.196	2.630E-01	5.270E-03
2.530	59.980	333.13	0.251	7.250E-01	4.560E-03
2.520	60.018	333.168	0.341	3.960E+00	3.110E-03
2.530	60.028	333.178	0.400	1.690E+01	2.450E-03
2.450	60.021	333.171	0.443	2.740E+01	2.240E-03
3.630	59.991	333.141	0.158	1.290E-01	7.470E-03
3.580	60.016	333.166	0.217	4.310E-01	6.420E-03
3.580	60.013	333.163	0.277	1.050E+00	4.930E-03
3.600	60.009	333.159	0.338	3.490E+00	3.820E-03
3.670	60.006	333.156	0.385	1.360E+01	3.090E-03
3.660	60.128	333.278	0.400	1.930E+01	2.770E-03
3.630	40.031	313.181	0.146	2.110E-02	3.310E-03
3.590	40.017	313.167	0.217	6.280E-02	2.510E-03

3.650	40.009	313.159	0.272	2.110E-01	2.120E-03
3.610	39.995	313.145	0.318	6.870E-01	1.830E-03
3.650	40.043	313.193	0.384	4.370E+00	1.440E-03
3.580	40.024	313.174	0.412	8.420E+00	1.410E-03
5.090	40.028	313.178	0.172	2.870E-02	3.120E-03
4.830	40.049	313.199	0.220	6.050E-02	2.880E-03
5.070	40.029	313.179	0.274	2.110E-01	2.200E-03
4.970	39.997	313.147	0.339	7.980E-01	1.030E-03
4.960	40.029	313.179	0.409	5.710E+00	8.200E-04
5.020	40.051	313.201	0.413	6.990E+00	8.600E-04
5.180	60.023	333.173	0.164	1.370E-01	1.020E-02
5.050	60.020	333.17	0.226	3.650E-01	7.450E-03
5.080	60.042	333.192	0.296	1.290E+00	5.590E-03
5.050	60.075	333.225	0.330	3.310E+00	4.860E-03
5.020	60.046	333.196	0.386	1.830E+01	2.860E-03
4.960	60.061	333.211	0.417	5.140E+01	2.230E-03
8.000	40.000	313.15	0.300	7.204E-03	1.187E-03
8.000	60.000	333.15	0.300	1.781E+00	8.242E-03
8.000	40.000	313.15	0.400	3.250E+00	4.773E-04
8.000	60.000	333.15	0.400	5.769E+00	6.680E-03
8.000	40.000	313.15	0.305	5.300E-01	
8.000	60.000	333.15	0.305	2.407E+00	
8.000	40.000	313.15	0.405	8.153E+00	
8.000	60.000	333.15	0.405	3.078E+01	
2.046	120.000	393.15	0.047	1.150E+00	
2.013	120.000	393.15	0.102	4.810E+00	
2.013	120.000	393.15	0.137	8.930E+00	
2.046	120.000	393.15	0.165	1.394E+01	
2.046	120.000	393.15	0.217	2.914E+01	
2.013	120.000	393.15	0.242	4.123E+01	
3.837	120.000	393.15	0.026	5.340E-01	
4.443	120.000	393.15	0.037	9.000E-01	
3.972	120.000	393.15	0.063	2.180E+00	
3.972	120.000	393.15	0.111	5.990E+00	
3.837	120.000	393.15	0.147	1.094E+01	
4.443	120.000	393.15	0.201	2.532E+01	
3.837	120.000	393.15	0.240	4.293E+01	
4.443	120.000	393.15	0.245	4.693E+01	
3.972	120.000	393.15	0.294	9.530E+01	
1.167	40.000	313.15	0.318	5.700E-01	
1.167	40.000	313.15	0.336	8.500E-01	
1.167	40.000	313.15	0.360	1.490E+00	
0.989	40.000	313.15	0.370	1.670E+00	
0.989	40.000	313.15	0.399	3.300E+00	
0.989	40.000	313.15	0.429	6.550E+00	
0.989	40.000	313.15	0.449	1.262E+01	
0.989	40.000	313.15	0.461	1.750E+01	
1.167	40.000	313.15	0.473	3.009E+01	

1.167	40.000	313.15	0.473	3.017E+01	
2.750	40.000	313.15	0.240	1.150E-01	
2.750	40.000	313.15	0.326	7.200E-01	
2.091	40.000	313.15	0.348	1.140E+00	
2.091	40.000	313.15	0.393	3.600E+00	
2.750	40.000	313.15	0.418	8.670E+00	
2.044	40.000	313.15	0.441	2.041E+01	
2.091	40.000	313.15	0.451	2.056E+01	
2.044	40.000	313.15	0.457	2.422E+01	
2.044	40.000	313.15	0.473	4.842E+01	

Results

CO_2 solubility data, measured in terms of its partial pressure, is explored as a function of temperature, loading, and amine concentration for PZ-CO_2-H_2O systems ranging from 0.9 m-8.0 m PZ. The following plot shows the behavior of CO_2 partial pressure with respect to the parameters mentioned.

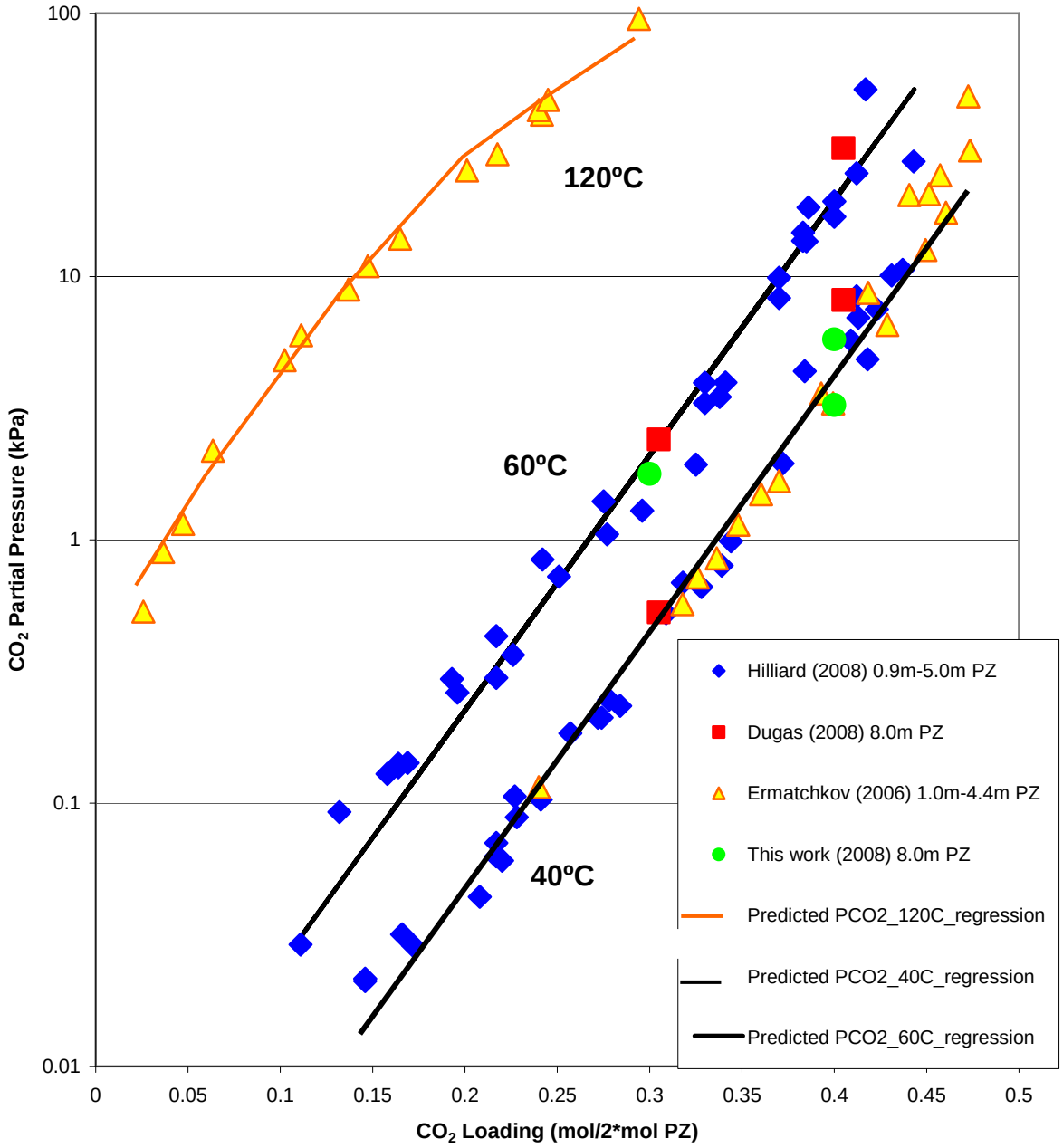

Figure 2: CO_2 Solubility in 0.9 m-8.0 m PZ-CO_2-H_2O Systems

The plot shows that CO_2 partial pressure increases with greater loading. This is because more CO_2 is introduced to the system with greater loading, thereby increasing the partial pressure. Secondly, CO_2 partial pressure is greater at higher temperatures. The reason for this behavior is that higher temperatures give rise to higher CO_2 vapor pressures which contribute to greater partial pressure in the headspace. Nevertheless, there appears to be a lack of correlation between CO_2 partial pressure and amine concentration. This observation was first noted by Hilliard and is clearly supported by data from other authors as well.

A model which relates CO_2 partial pressure to temperature and loading is regressed using a total of 81 experimental points. The following regression results are obtained:

$$\ln (P_{CO2}) = 18.54 - 8160.59*(1/T) + 22.32*(\text{Loading}) \text{ at } 40^oC \text{ and } 60^oC \ (R_{square} \sim 0.94)$$

$$\ln (P_{CO2}) = -1.12 + 28.82*(\text{Loading}) - 34.53*(\text{Loading}\hat{}2) \text{ at } 120^oC \ (R_{square} \sim 0.99)$$

Note that predicted model values are also shown in the above plot. It is clear that the model predictions agree very well with experimental data.

A smaller subset of the data is now plotted to show CO_2 solubility for PZ-CO_2-H_2O systems within the loading range of industrial interest: 0.2-0.5 mol CO_2/mol PZ.

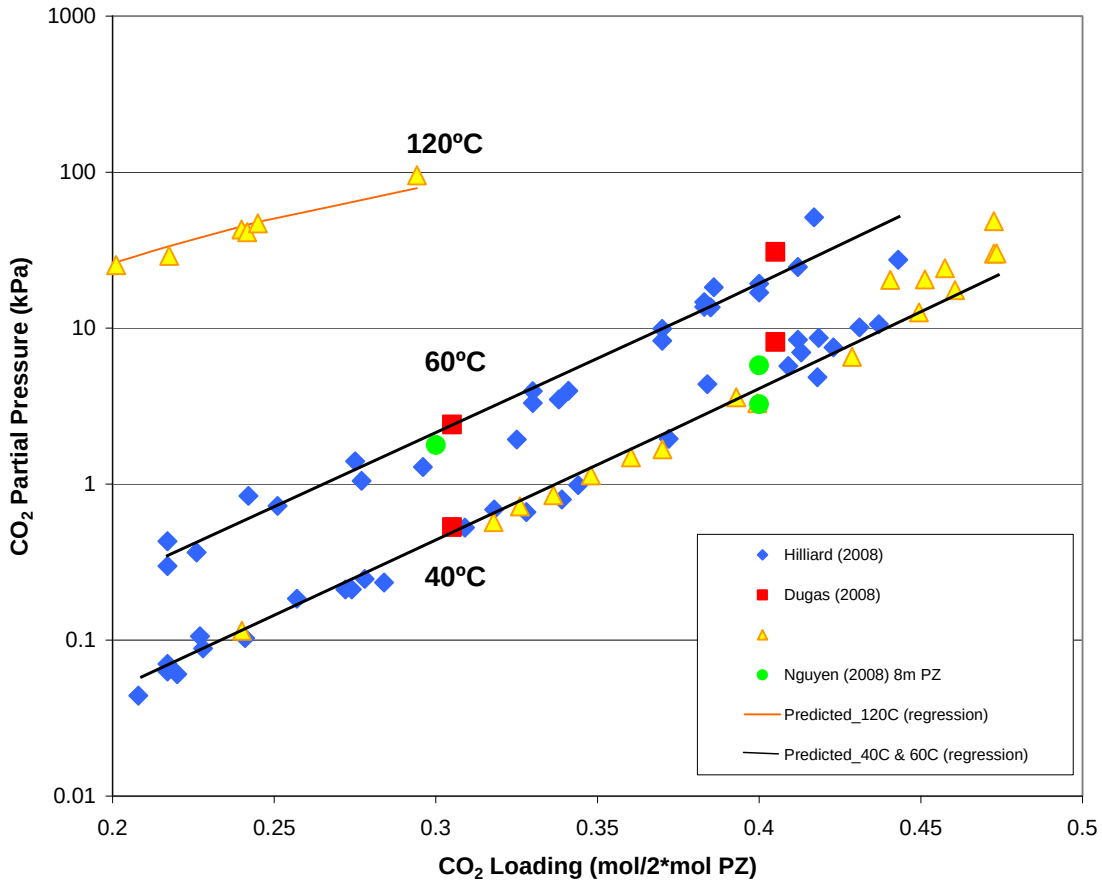

Figure 3: CO_2 Solubility for Loading Range of Industrial Interest 0.2-0.5

Again, the partial pressure increases with higher loading and temperatures with very little correlation to amine concentration. Also, predicted CO_2 partial pressures are also shown for this loading range of interest at 40ºC, 60ºC, 120ºC.

PZ volatility is now presented in terms of its partial pressure response to changes in temperature, loading, and amine concentration. The following plot illustrates PZ volatility versus loading and temperature.

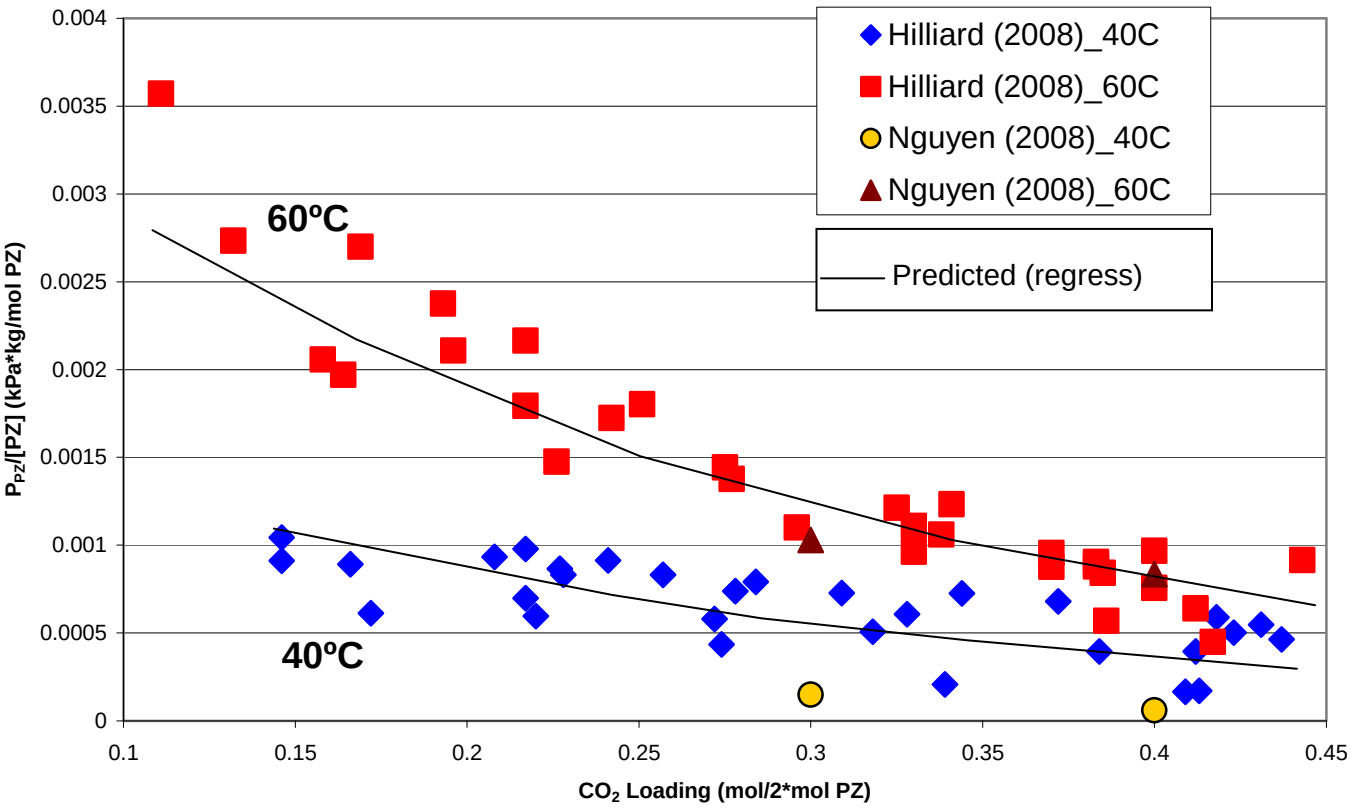

Figure 4: Piperazine Volatility for 0.9 m-8.0 m PZ-CO_2-H_2O Systems

PZ partial pressure decreases with higher loading as more free PZ is converted into reaction products. Secondly, higher PZ partial pressures are seen at higher temperatures as greater PZ vapor pressures are expected and thereby resulting in greater contribution to partial pressure. Lastly, one should reasonably expect a correlation between PZ partial pressure and amine concentration even though this relationship isn't clear from the plot due to experimental error and inconsistency observed with a few of the data points.

A model relating PZ partial pressure to loading and temperature is regressed using all but two of the questionable data points seen. The equation obtained is:

$$\ln (P_{PZ}/[PZ]) = 6.73 - 4045.05*(1/T) - 4.21*(\text{Loading}) \qquad (R_{square} \sim 0.8)$$

A smaller subset of the data is now presented for systems of 5m and 8m PZ only. The below plot illustrates PZ partial pressure as a function of loading, temperature, and amine concentration for the mentioned systems.

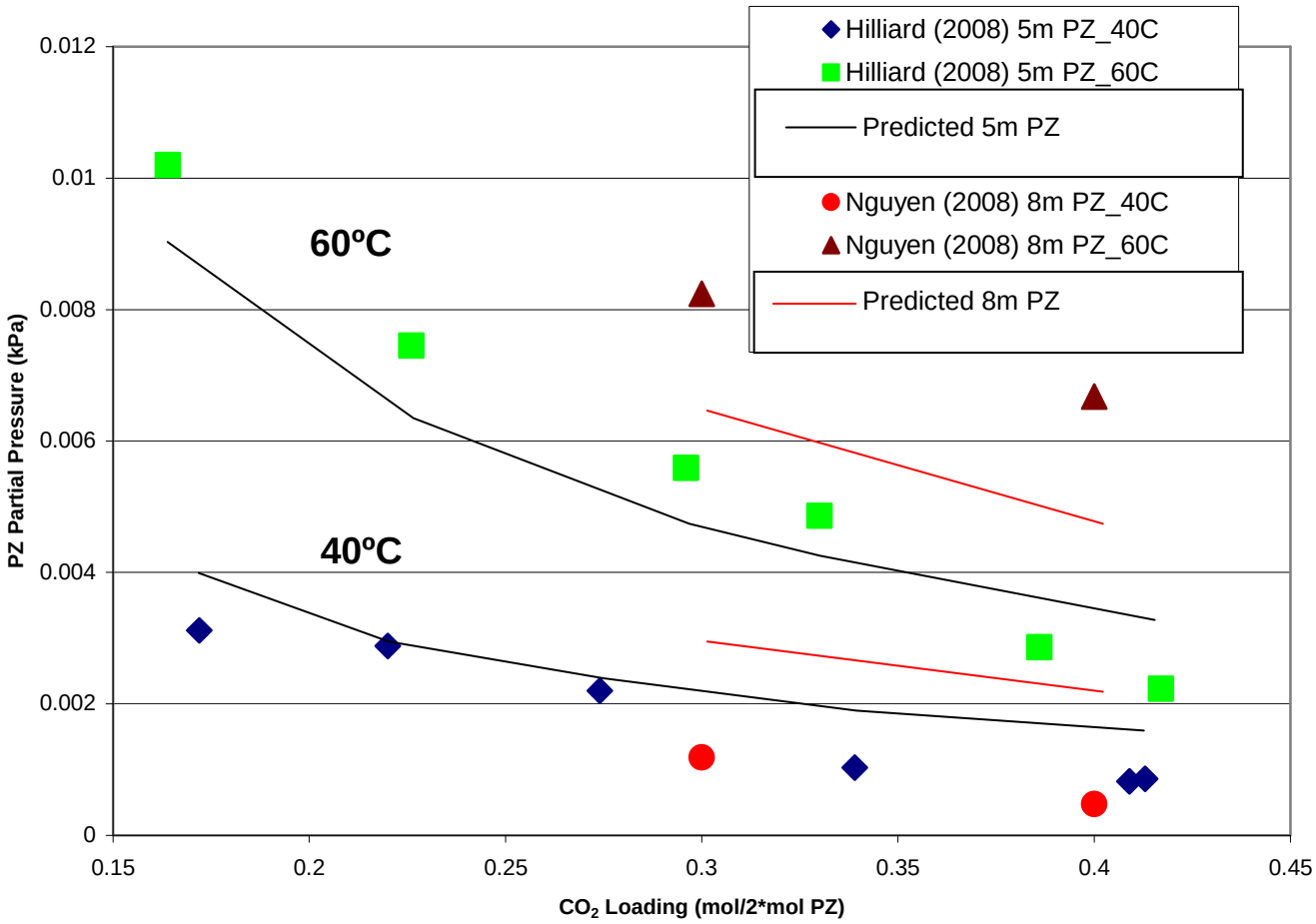

Figure 5: Piperazine Volatility for 5 m and 8 m PZ-CO_2-H_2O Systems

Again the same trends are seen with PZ partial pressure decreasing at higher loadings while increasing with higher temperatures. Also, at a given temperature, systems with higher amine concentration naturally show higher partial pressure than those with lower concentrations as there are more PZ present in the former. Also, predicted PZ partial pressure trends for the systems of interest are also shown using the experimentally regressed model. It appears that there is a decent agreement between experimental and predicted results for the most part without taking into account experimental inconsistency with the 8 m data.

Conclusion

CO_2 solubility is seen to increase with higher loading and temperatures. However, it is also concluded that there is no apparent correlation between CO_2 solubility and amine concentration given the data analyzed to date. In regard to PZ volatility, it is expected and also clearly seen that PZ partial pressure increases with greater amine concentration and higher temperatures. Conversely, the volatility decreases as loading is increased due to the fact that more amine is taken up by CO_2 in reaction. Finally, equations have also been regressed using the bulk of the experimental data available to correlate the effects of temperature and loading on solubility and volatility individually.

References

Hilliard, MD. A Predictive Thermodynamic Model for an Aqueous Blend of Potassium Carbonate, Piperazine, and Monoethanolamine for Carbon Dioxide Capture from Flue Gas. Ph.D. Dissertaton, The University of Texas at Austin, 2008.

Dugas, R. First Quarter 2008 Progress Report Austin, TX, 2008.

Ermatchkov, V, AP Salado Kamps, D Speyer, G Maurer. Solubility of Carbon Dioxide in Aqueous Solutions of Piperazine in the Low Gas Loading Region. *J. Chem. Eng. Data* 2006, 51, 1788-1796.

Dynamic Modeling of the Stripper with Monoethanolamine in Aspen Custom Modeler®

Quarterly Report for January 1 – March 31, 2008

by Sepideh Ziaii Fashami

Supported by the Luminant Carbon Management Program

and the

Industrial Associates Program for CO_2 Capture by Aqueous Absorption

Department of Chemical Engineering

The University of Texas at Austin

April 18, 2008

Abstract

This quarter's work focuses on rate-based dynamic modeling of the stripper with 30% monoethanolamine in a flow sheet of Aspen Custom modeler®. The rigorous model of one segment in the stripper is run in steady state mode successfully and the results look reasonable, however it does not match exactly with simulation results from Aspen Plus® because the respective thermodynamic models do not predict the same CO_2 solubility. In addition, a new strategy for on/off operation of CO_2 capture is proposed in which no amine inventory is needed and the dynamic behavior of the stripper can be studied independently.

Introduction

On/off operation of CO_2 capture in coal-fired power plants has been proposed as a policy to operate the capture at a lower cost. Turning CO_2 capture "off" at periods of high electricity demand can recover plant generation capacity lost due to CO_2 capture, thereby eliminating the capital cost of installing additional capacity. Over the last quarter, we have introduced different dynamic strategies for CO_2 capture operation and evaluated their advantages and disadvantages.

For dynamic analysis of the CO_2 capture operation we need to have a dynamic model of the process which should be rigorous enough to reflect the dynamic information of the system and simple enough to be modeled mathematically and solved in available modeling tools.

As the dynamic evaluation of the new proposed strategy is dependent on the dynamic model of the stripper, in this work the dynamic model of a segment of the packed column

stripper is carefully studied and the mathematical model is created in a flow sheet of Aspen Custom Modeler®.

A Dynamic Strategy For On/Off Operation of CO_2 Capture

In this strategy, the absorber is operated at a variable lean loading or variable level of CO_2 removal and the stripper is operated at a reduced flow rate during the peak load. In this strategy, we keep the rich loading of the rich solution entering the top of the stripper constant while the stripper is operated at reduced or full load. Thereby the stripper can be isolated from absorber in dynamic analysis. In other words, we are able to study this strategy by just examining the dynamic model of the stripper and control without needing to develop a dynamic model for the absorber. In addition, by implementing this strategy, we do not lose the CO_2 value by continuing operation of the absorber and we avoid the capital investment for amine inventory and storage tanks.

The mathematical model of one segment in the stripper

For this model, it is assumed a packed column is divided into several segments vertically and the radiant gradients are ignored in each segment.

The main assumptions made in this model are:

1. Liquid and vapor phase are both mixed (mixed flow model).
2. Liquid-vapor equilibrium forms at the interface (simplified rate-based modeling).
3. The solvent is 7 m MEA and is assumed to be a nonvolatile solvent. Therefore, the vapor phase is a binary mixture of CO_2 and water.
4. Mellapak 250Y is the type of packing used in this model.
5. The model includes following two equilibria in the liquid phase:

$$2MEA + CO_2 \underset{\leftarrow}{\longrightarrow} MEACOO^- + MEA^+$$

$$H_2O + MEA + CO_2 \underset{\leftarrow}{\longrightarrow} MEA^+ + HCO_3^-$$

The model consists of a set of differential and algebraic equations, which are solved simultaneously. The differential equations are associated with component mass balance and total energy balance in each phase.

The algebraic equations are:

- Component mass hold up in the liquid and gas phase;
- Energy hold up for each phase;
- Steady state energy balance at the interface;
- Binary diffusion of components between liquid and gas phases;
- Hydraulic relations;
    - Pressure drop along the structured packing using “Generalized Method”
    - Liquid holdup using Spiegel correlation for Mellapak packing
- Equation-based calculation of physical properties for loaded aqueous MEA and vapor phase;
- Mass and heat transfer coefficients using Onda’s correlation and Chilton-Colburn analogy;
- Enthalpy calculation relations (reference state: vapor at 100°C);
- Mass balance and charge balance equations for speciation in the liquid phase.

Figure 1 shows the energy model used for a segment. In this model, the segment is divided into three sections: liquid, vapor, and interface.

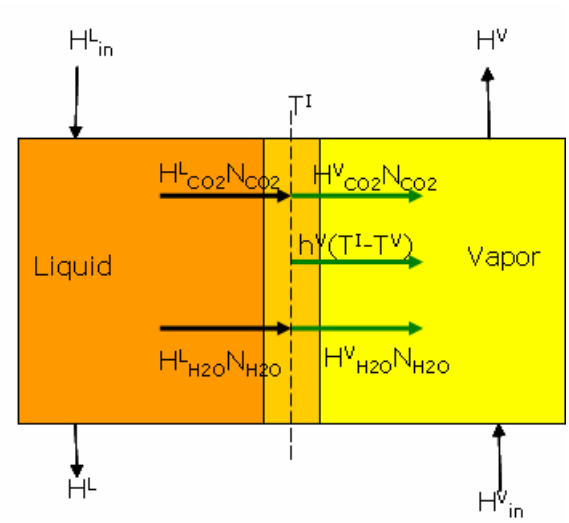

Figure 1: An Energy model for a segment

As shown in Figure 1, the energy streams entering and coming out of the liquid phase are the enthalpies of liquid inlet and outlet streams besides the partial enthalpies associated with CO_2 and water fluxes. For the vapor we have similar enthalpy balance, however an additional heat stream should be considered because of temperature driving force between the interface and vapor bulk.

As the liquid phase is mostly water and the thermal conductivity of water is much higher than that of the vapor, we assume that the liquid heat transfer coefficient is much larger than the vapor coefficient, so the interface temperature is equal to liquid bulk temperature.

Simulation of One Segment in Aspen Custom Modeler®

The above-described dynamic model of a segment in the stripper is programmed in the coding environment of Aspen Custom Modeler® and after debugging, was run in a flow sheet of this software.

Aspen Custom Modeler® is able to run a dynamic model in both steady state and dynamic modes. The current model is successfully simulated in the steady state mode and the results are presented in next section of this report. For the dynamic simulation, we are trying to identify and solve the numerical problems appearing during dynamic simulation. We may simplify the model to get it converged in the dynamic mode.

Steady State Simulation Results

In order to check the correctness of the created model, the conditions of the inlet liquid and vapor streams to the segment are fixed in the flow sheet and the model is run. The results of the model look reasonable compared to an Aspen Plus® model. At this examination, the conditions of the inlet streams are selected arbitrarily. As the inlet vapor and liquid streams are not independent physically, we need to find more reasonable

inlet conditions which are matched with the physical nature of the absorption/stripping process.

The preliminary results of the steady state simulation of a segment are shown in Figure 2. The output of the simulation is the condition of liquid and vapor streams coming out of the segment. The packing of this segment is Mellapak 250Y.

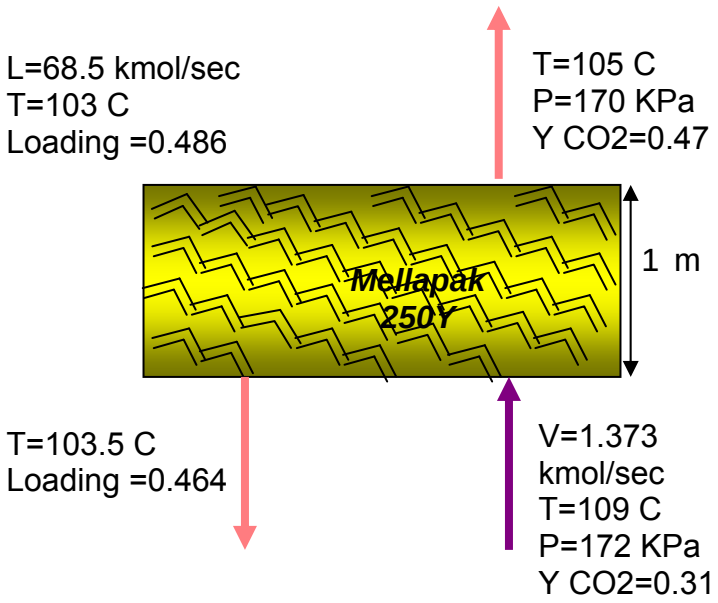

Figure 2: Preliminary results of steady state simulation

Conclusions and Future Work

In this quarter, a new dynamic strategy was proposed for on/off operation of CO_2 capture in which the dynamic behavior of the stripper can be analyzed independently and there is no amine inventory cost associated with this option.

In addition, the dynamic model of one segment of the stripper with MEA solvent was created in ACM® and the model was successfully run in steady state mode and the results of this simulation looks reasonable.

In the next quarter, the steady state model will be checked with typical inlet conditions, and a sensitivity analysis will be done for the length of the packing. The numerical problems in running the dynamic model will be identified and solved. After finalizing the model for one segment and developing a model for a reboiler we will be able to build the entire model of the stripper by connecting a number of segments and reboiler models in the flow sheet.

Finally, the dynamic analysis and estimation of the response time of the stripper in the proposed on/off strategy will be done by using the dynamic model of the stripper.

References

Onda K, H Takeuchi & Y Okumoto, "Mass Transfer Coefficients Between Gas and Liquid Phases in the Packed Column," *J Chem Eng Japan*, **1**, 56-62(1968).

Peng J, S Lextrait, TF Edgar & RB Eldridge, “A Comparison of Steady-State Equilibrium and Rate-Based Models for Packed Reactive Distillation Columns,” *Ind Eng Chem Res*. **41**, 2735-2744 (2002).

Peng J, TF Edgar & RB Eldridge, “Dynamic Rate-Based and Equilibrium Models for a Packed Reactive Distillation Column,” *Chem Eng Sci* **58**, 2671-2680 (2003).

Snijder ED, MJM te Riele, GF Versteeg & WPM van Swaaij, “Diffusion Coefficients of Several Aqueous Alkanolamine Solutions,” *J Chem Eng Data*, **38**, 475-480 (1993).

Weiland RH, JC Dingman, DB Cronin & GJ Browning, “Density and Viscosity of Some Partially Carbonated Aqueous Alkanolamine solutions and Their Blends.” J Chem Eng Data, **43**, 378-382 (1998).

System Level Implications of Flexible CO_2 Capture Operation

Progress Report for January 1 – March 31, 2008

by Stuart Cohen

Supported by the Luminant Carbon Management Program

and the

Industrial Associates Program for CO_2 Capture by Aqueous Absorption

Department of Chemical Engineering

The University of Texas at Austin

April 18, 2008

Abstract

To investigate the implications of flexible CO_2 capture, a system model was created to calculate the performance, economics, and CO_2 emissions in the Electric Reliability Council of Texas (ERCOT) grid for several operational strategies of flexible CO_2 capture. The model compares cases with no CO_2 capture and "always on" CO_2 capture with scenarios when capture is "off" during: 1) peak load hours every day of the year; 2) the entire season of system peak load; and 3) system peak load hours only on seasonal peak load days. Assuming installation of MEA absorption at all coal plants in ERCOT and using 2006 grid conditions, flexible operation prevents the need for over 4400MW of new capacity, which amounts to several billion dollars in capital cost savings. CO_2 capture must be "off" for only 99 hours throughout the year, resulting in a 52% system-wide CO_2 emissions reduction that is within 1% of that achieved in the "always on" scenario. A system that must remain "off" for the entire peak load season will do so for 76 days, which still reduces emissions by 41%. Average generation costs rise by up to 38% for the "always on" scenario. Costs grow due to the added cost of CO_2 capture as well as the increased use of expensive natural gas generators to replace the base load capacity lost when CO_2 capture is "on." Flexible CO_2 capture is not shown to have a large effect on annual average generation costs or CO_2 avoidance costs, which are calculated as \$44-\$45 per metric ton of CO_2 in every scenario that uses CO_2 capture. A clear reserve margin specification is important from a policy standpoint because it can be used to define the threshold load above which CO_2 capture must be "off." Future work will investigate tradeoffs between grid performance, economics, and CO_2 emissions when electricity price variation and CO_2 emissions costs are used to determine operational strategies for flexible CO_2 capture. Much of the results and analysis contained in this report have been submitted to the American Society of Mechanical Engineers 2nd International Conference on Energy Sustainability for dual peer review for publication in the ASME Conference Proceedings and the ASME Journal of Energy Resources Technology.

Introduction

Major barriers to the implementation of CO_2 capture technologies include its high capital cost and the operation and maintenance (O&M) costs associated with the energy used to operate CO_2 capture systems. A post combustion capture system using aqueous absorption is estimated to require anywhere from 11-40% of base plant output without CO_2 capture, with a typical value of around 30% (Metz, 2005; Bergerson and Lave, 2007; Davidson, 2007). The energy required for CO_2 capture is dominated by the heat used for solvent regeneration and the energy needed compress CO_2 to a pressure suitable for pipeline transport. This energy is typically assumed to be supplied by steam diverted from power generating turbines, which results in the aforementioned reduction in net generation capacity.

The inherent flexibility of post-combustion CO_2 capture affords the possibility of recovering some or all of the energy required by CO_2 capture systems for use in electricity generation when this practice is economical. At its extreme, flexible CO_2 capture may consist of two modes of operation, a capture "on" configuration with all capture systems running at maximum design capacity and an "off" position where most or all process steam is used for electricity generation. An "off" configuration does not necessarily suggest that all components involved with CO_2 capture are brought to a complete stop; it simply implies that the energy intensive capture systems are operated at loads such that plant power output is at or near its capacity without CO_2 capture.

This practice can ease capacity planning and save capital costs by eliminating the need to build generating capacity to replace that lost to CO_2 capture (J.R. Gibbins, R.I. Crane et al., 2005). Capture systems could also be turned "off" during periods of high electricity prices, allowing generators to increase electricity output and use these high priced electricity sales to allow faster recovery of an investment in CO_2 capture relative to an "always on" capture scenario.

This study uses the perspective of the electric grid to consider the system level performance, economics, and environmental effects of flexible or "on/off" CO_2 capture. In contrast to typical techno-economic analyses of CO_2 capture systems that consist of bottom-up plant analyses or top-down macro-scale energy analyses, this body of work considers diurnal and seasonal variations in electricity demand and the associated effects on plant dispatch and electricity costs (Rao and Rubin, 2002; Katzer, 2007).

Configurations for Flexible CO_2 Capture

While there may be several ways to design and control a flexible CO_2 capture system, two general concepts are considered below. For basis of comparison, a standard CO_2 absorption/stripping unit assumes that steam is extracted between the base plant's intermediate and low pressure turbines and expanded in a let-down turbine to the desired stripper conditions for use in solvent regeneration. This let-down turbine also drives the CO_2 compressor train.

Figure 1 displays the option of venting CO_2 in an "off" configuration. In this case, the steam being used to regenerate rich solvent and drive CO_2 compression is redirected back to the base plant's power train without any provisions to continue capturing CO_2 in the absorber. Whether the flue gas in an "off" configuration bypasses the capture system entirely or continues to flow through the absorber/stripper until all solvent is loaded to maximum CO_2 capacity, the net result will be the venting of CO_2 to the atmosphere.

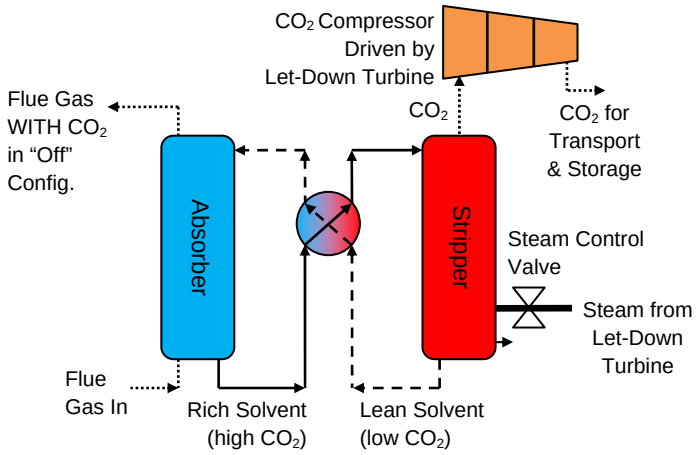

Figure 1: CO_2 absorption/stripping unit that vents CO_2 in an "off" configuration

In a regulatory environment where there is a value placed on CO_2 emissions, venting CO_2 in an "off" configuration would incur additional costs to generation. This added cost is avoided if a system is designed with enough solvent storage capacity to allow the absorber to run continuously when the stripper and CO_2 compressors are not operating (Figure 2). With this design, additional capital costs are required for solvent storage systems and greater stripping capacity. Since an "on" configuration requires regeneration of stored solvent along with that loaded by current flue gas, and because the corresponding volume flow rates of CO_2 sent to a compression train will increase relative to a standard absorption/stripping system, the stripper and CO_2 compressors require more energy than in a standard process configuration.

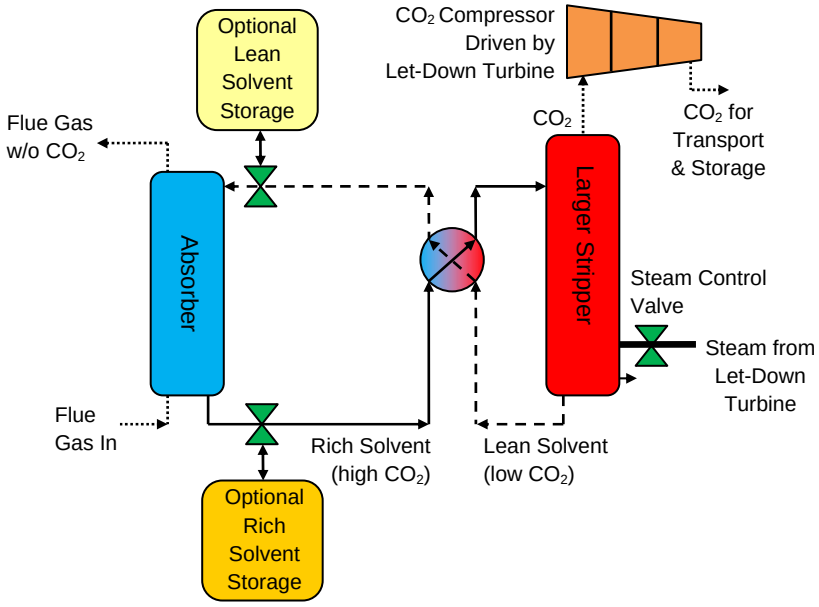

Figure 2: CO_2 absorption/stripping unit with solvent storage to prevent from venting CO_2 in an "off" configuration

Modeling Methodology

A MATLAB model has been created to make baseline estimates of the impact that flexible CO_2 capture may have on the performance, economics, and CO_2 emissions of the Electric Reliability Council of Texas (ERCOT) electric grid. Rather than attempt to optimize the economics of flexible CO_2 capture operation under a particular CO_2 emissions regulatory scheme, the model defines specific strategies for operating capture systems in order to better understand how flexible CO_2 capture can affect widespread implementation of CO_2 capture in the ERCOT grid. Based on ERCOT hourly load data, the relative generation costs and emissions of each plant type (coal, natural gas, nuclear, etc.), and the desired strategy for capture operation, the model decides how much of electricity demand is met by each generation source. These data display usage patterns of flexible CO_2 capture and allow calculation of average generation costs and system-wide CO_2 emissions.

Scenarios that implement CO_2 capture consider the conditions where all 15 coal plants in the ERCOT grid are retrofitted with CO_2 capture using aqueous MEA absorption. A capture "on" configuration requires a certain percentage of original coal capacity while capturing a specified fraction of CO_2 emissions from coal plants. An "off" configuration allows full recovery of original coal capacity at a generation cost equal to that if no CO_2 capture system is installed. Full recovery of base plant performance and cost may not be likely, but residual energy requirements are not considered in this baseline analysis. Current results assume that CO_2 is vented in the "off" position, because this practice will represent the worst case environmental effects of flexible CO_2 capture.

For comparison with studies that assume full replacement of the generating capacity lost to CO_2 capture, the model's baseline assumption is that whenever CO_2 capture is turned "off" due to system capacity constraints, the load threshold above which capture is turned "off" is taken as the annual peak load minus the energy required for CO_2 capture.

Model Input Parameters

Due to the availability of data, all values used to represent the ERCOT grid are from 2006. In 2006, ERCOT's installed capacity was 71,812MW, which is broken down by source in Figure 3 below (ERCOT, 2006). NGCC refers to natural gas combined cycle, NG boilers use natural gas for heat in a steam cycle, and NGGT are simple gas turbines. Because generation sources other than fossil fuels and nuclear power contribute relatively little to ERCOT generation, these are grouped into an "Other" category. In this category, wind turbines account for 75% of actual generation, so any model parameters associated with this category correspond to appropriate values for wind power.

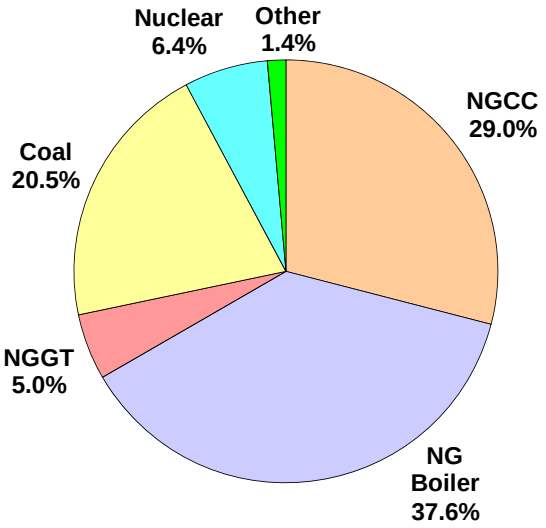

Figure 3: ERCOT installed capacity by generation source (ERCOT 2006; 2007)

MEA absorption systems are assumed to require 30% of ERCOT's coal capacity and capture 90% of the CO_2 emitted at coal facilities. These values are chosen as those typical of techno-economic studies of CO_2 capture (Rao and Rubin, 2002; Metz, 2005; Davidson, 2007).

Emissions rates for each plant type, expressed in metric tons of CO_2 per Megawatt-hour (tCO_2/MWh), are determined by calculating average emissions rates of ERCOT plants of each type, weighted by that plant's actual generation. Values expressed in units *Mt* indicate emissions in millions of metric tons.

Generation costs for each plant type include fuel costs and operation and maintenance (O&M) costs. While capital charges are critical when considering new plant investment, the immediate costs of generating electricity are most important in the dispatch decisions that affect a grid level analysis. The model assumes that plant types are dispatched in the order of least to most expensive generation costs. Conventional coal and natural gas generation costs are calculated using average ERCOT plant heat rates weighted by actual generation, average 2006 fuel costs in Texas, and published O&M costs. Nuclear generation cost and the cost of coal generation with MEA absorption are determined from the literature. All costs are shown in 2006 dollars. The following tables summarize model input parameters.

Table 1: Summary of MEA system parameters and fuel costs (USEIA, 2007; USEIA, 2008)

MEA Absorption System Parameters	*Value*
Capture Energy Penalty	30%
CO_2 Capture Efficiency	90%
Fossil Fuel Costs ($/MMBtu)	
Coal	1.48
Natural Gas	6.60

Table 2: Summary of parameters related to each generation source (Rao and Rubin, 2002; IEA and NEA, 2005; Rao and Rubin, 2006; NEI, 2007; USEIA, 2007; USEPA, 2007)

Generation Source	*Fossil Fuel Heat Rate (MMBtu/MWh)*	*Generation Cost ($/MWh)*	*CO_2 Emissions Rate (tCO_2/MWh)*
Coal	11.0	21.68	1.04
Coal + CCS	n/a	52.75	0.10
NGCC	8.98	64.45	0.48
NG Boiler	11.8	83.14	0.63
NGGT	13.1	91.83	0.69
Nuclear	n/a	17.15	0
Other	n/a	10.52	0

Operational Scenario Descriptions

Scenario A

This scenario represents a status quo ERCOT grid without CO_2 capture.

Scenario B

CO_2 capture operates continuously throughout the year at maximum design capacity. If electricity demand exceeds the threshold load defined by CO_2 capture energy requirements, new generation capacity is required. Any new required capacity is assigned the characteristics of NGCC generation because such instances occur only at the highest peak loads, and any new peaking capacity is unlikely to consist of NG boilers or simple gas turbines.

Scenario C

CO_2 capture is turned off every day of the year when load exceeds the daily peak minus CO_2 capture energy requirements. This criterion establishes a moving "capture off" threshold load such that CO_2 capture is turned off for some amount of time every day regardless of the absolute level of the daily peak. Figure 4 gives an example of how this strategy would be used on a winter day with a relatively low electricity demand. While this strategy of operation may appear cost prohibitive from a capital expenditure standpoint due to extended capital recovery times for CO_2 capture systems, it is taken as a worst case environmental scenario should the economics of the real time electricity market dictate its attractiveness.

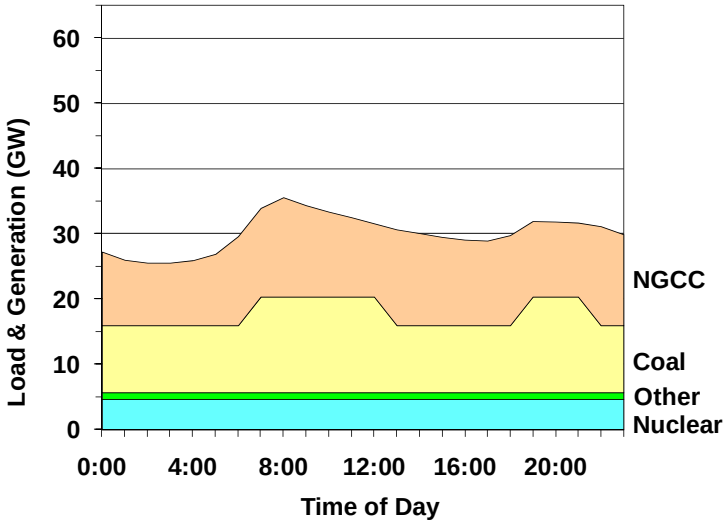

Figure 4: Scenario C load & generation on January 6, 2006

Scenario D

The "capture off" threshold load is set as the annual peak load less the energy requirement for capture. Once in the "off" configuration, this scenario assumes that capture systems cannot be turned "on" again until the entire peak load season has passed (Figure 5). This scenario places an upper limit on the minimum downtime that CO_2 capture systems must remain "off," which may also be thought of as a maximum system response time.

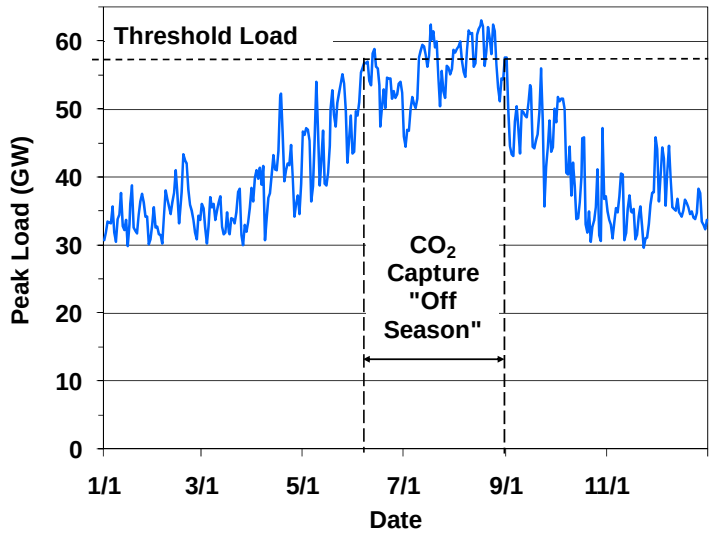

Figure 5: ERCOT daily peak load in 2006 with possible CO_2 capture "off season" shown

Scenario E

The CO_2 "capture off" load threshold is the same as in Scenario D, but Scenario E represents the opposite end of the range of system response time by assuming that CO_2 capture can be turned "off" and "on" as fast as is necessary. Thus, CO_2 capture is only "off" during the specific hours of the year when system load exceeds the threshold load. Figure 6 gives an example of this scenario for August 17, 2006, the day in 2006 when the annual peak load occurred.

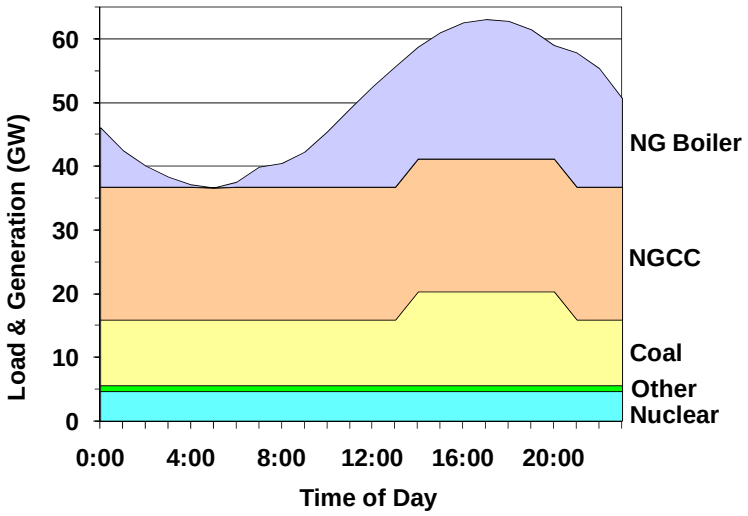

Figure 6: Scenario E load & generation on August 17, 2006

Model Validation

The model was validated by comparing actual generation and emissions data with those computed for Scenario A. Total generation remains the same because system load is always assumed to be met. The primary discrepancy is an overestimate of coal generation and emissions because the model does not account for variation in plant availability such as plant downtime during scheduled maintenance activities. This effect corresponds to an underestimate of natural gas generation and emissions.

Table 3: Model validation parameters

Generation (million MWh)	*Model Calculation*	*Actual Data*	*% Difference*
Coal	129	116	+11
Natural Gas	133	144	-7.7
Nuclear	40	42	-5
Other	8.8	8.7	+1.1
Total	311	311	0
CO_2 Emissions (Mt)			
Coal	133	121	+10
Natural Gas	66	73	-10
Total	200	197	+1.3

Model Results & Discussion

Figure 7 displays calculated total generation for each plant type in 2006. Because plant availability is not accounted for in the model, system load never exceeds the point at which NGGT units must come online. The graph shows the obvious result that coal-fired generation decreases with an increased use of CO_2 capture, and this lost generation capacity must be

replaced by greater use of natural gas. Scenario E has nearly the same amount of coal-fired generation as the "always on" Scenario B because there are very few hours throughout the year when CO_2 capture must be turned off. This result is reinforced in Figure 8, which shows that Scenario E utilizes CO_2 capture during 99% of the hours in 2006, corresponding to a total "off" time of only 99 hours spread out over 25 days. Scenario D requires the CO_2 capture system to be "off" for 76 days between June 11 and August 26.

Despite the venting of CO_2 in the "off" configurations of Scenarios C, D, and E, system-wide CO_2 reductions are dramatic in every case. Even Scenario C, which vents CO_2 every day, reduces emissions by 29%. Scenario D reduces CO_2 emissions by 41%, and Scenario E's 52% reduction is within 1% of the "always on" case of Scenario B. Some of the captured CO_2 is offset by increased natural gas emissions, but lower emissions rates of NG units allow for the net effect of substantial CO_2 emissions reductions.

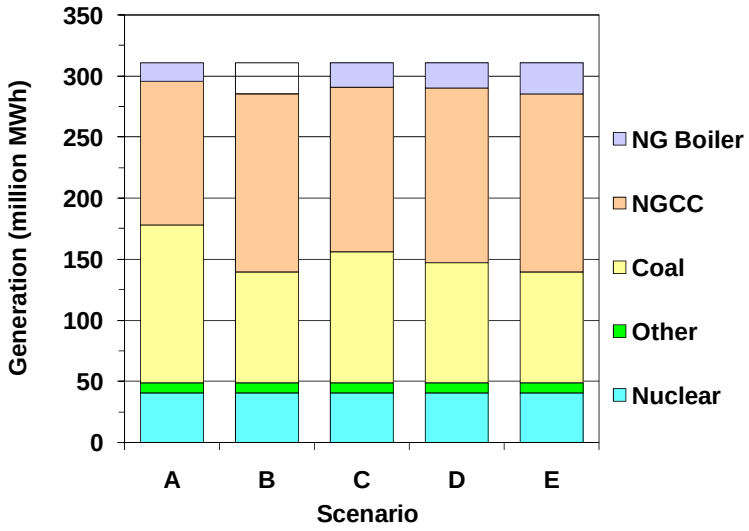

Figure 7: Generation mix for each scenario

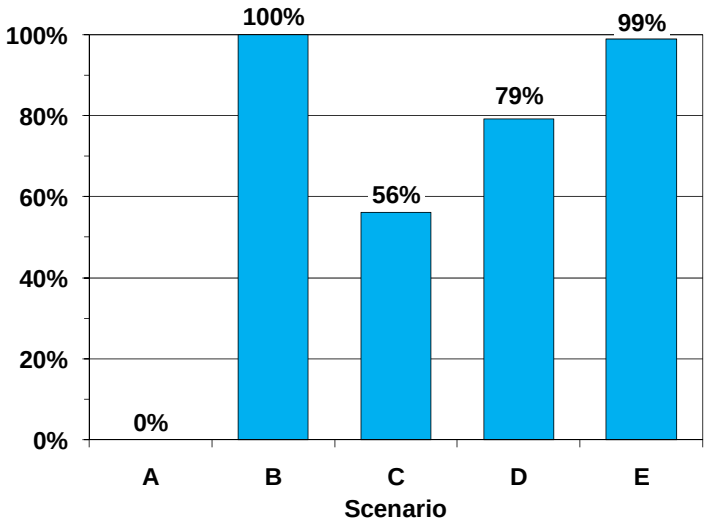

Figure 8: Percent of time CO_2 capture is "on" for each scenario

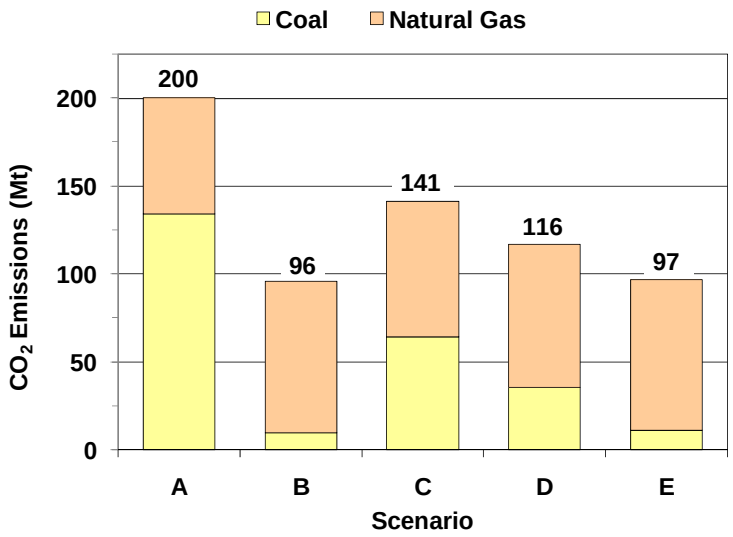

Figure 9: CO_2 emissions for each scenario

System average generation and CO_2 avoidance costs are shown in Figure 10 below. Average generation cost increases by 37.5% from Scenario A to Scenario B, and other generation costs follow the predictable pattern where increased use of CO_2 capture leads to higher average generation costs. This result is due to the cost of coal generation with CO_2 capture as well as the increased use of expensive natural gas units for base load generation when CO_2 capture is "on." Thus, high natural gas prices contribute significantly to any increase in average generation costs.

Amongst scenarios where CO_2 capture is implemented, average generation costs do not differ greatly, resulting in CO_2 avoidance costs that stay between \$44-45/tCO_2 for each scenario. This outcome suggests that flexible CO_2 capture may offer little economic benefit in terms of system average operating costs.

The primary economic benefit of using flexible CO_2 capture to alleviate capacity constraints is the elimination of a need for new capital investment to replace the capacity lost to energy used by CO_2 capture systems. Scenario B requires over 4,400MW of new capacity; if a new subcritical coal plant costs \$1550/kW, flexible CO_2 capture can save \$6.82 billion (USNETL, 2007). If the minimum downtime associated with a CO_2 capture system response time is short, these cost savings can be achieved with very infrequent use of the "off" configuration, resulting in CO_2 emissions reductions near those of an "always on" scenario. If the capital cost of an MEA system is \$880/kW, utilization of CO_2 capture must drop below 57% to justify building replacement capacity (USNETL, 2007). The usage of CO_2 capture in Scenarios D and E suggest that regardless of the expected downtime associated with turning capture systems "off," flexible operation is preferable to building replacement capacity.

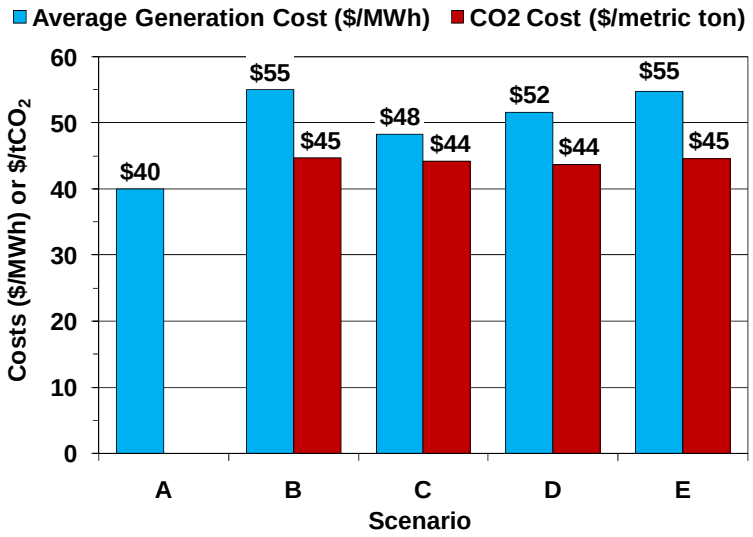

Figure 10: Average generation costs and CO_2 avoidance costs for each scenario

Sensitivity to Reserve Margin

A particularly important parameter related to capacity planning is the reserve margin, which ERCOT defines as the percent of total installed capacity that must be available during the maximum peak load of the year. This value is currently specified as 12.5%. The observed 2006 reserve margin of 14.6%, coupled with projections for increased electricity demand in TX, suggests that capacity constraints and their associated reliability issues will be important for ERCOT in upcoming years (ERCOT, 2006).

The reserve margin specification is relevant to flexible CO_2 capture because it may also be used to set a load threshold above which capture systems should be in the "off" configuration. In fact, if the 12.5% reserve margin is used to determine when additional capacity should be added due to CO_2 capture installation, the new capacity required in 2006 in an "always on" CO_2 capture scenario would only be 220MW. The figure below indicates that requiring full replacement of CO_2 capture energy is equivalent to an 18.3% reserve margin based on installed capacity and peak load in 2006.

Using reserve margin instead of total CO_2 capture energy to determine a threshold "off" load has a strong effect on the operation of a flexible CO_2 capture system, as is indicated in Figure 12. While Scenario E maintains a relatively small total "off" time even with a large reserve margin specification, the "off season" in Scenario D expands quickly with increased reserve margin specification as the operational strategy finds atypically high peak loads further from the primary season of high peak loads.

A clearly defined reserve margin specification that considers the possibility of flexible CO_2 capture operation will be essential to effectively plan when capture systems should be turned "on" and "off."

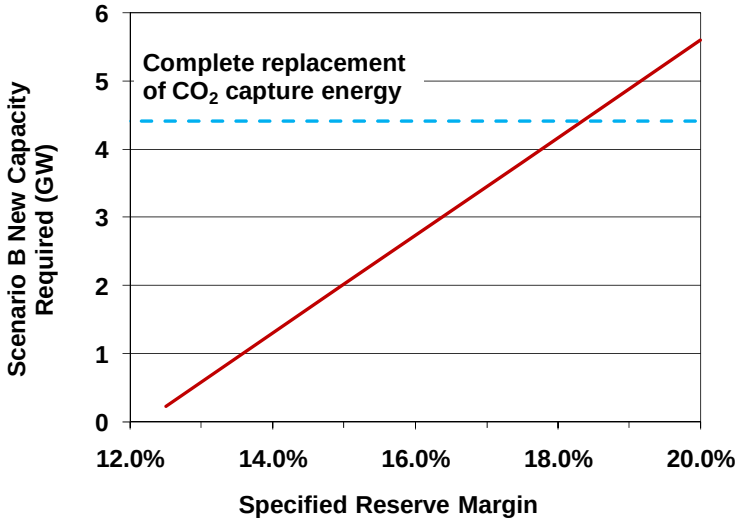

Figure 11: New capacity required in Scenario B vs. specified reserve margin

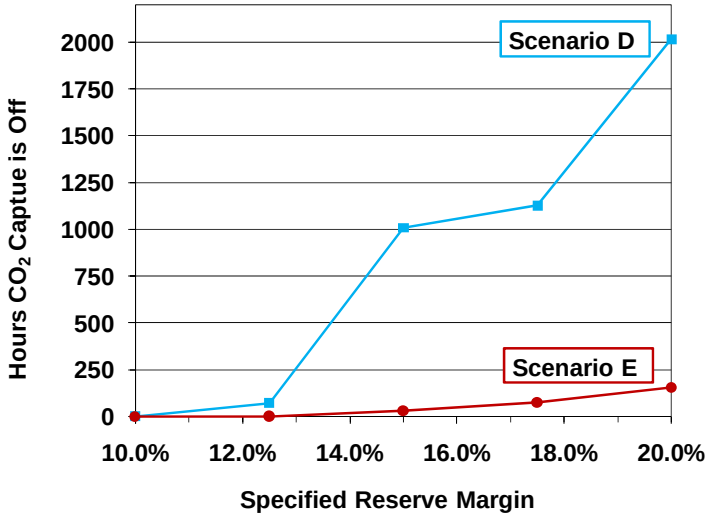

Figure 12: Number of hours CO_2 capture is off for Scenarios D and E vs. specified reserve margin

Interactions Between the Values of CO_2 and Electricity

The next step in modeling efforts is to examine how different configurations of flexible CO_2 capture may be economically operated in response to varying electricity prices when there is also a value attached to CO_2 emissions.

If an "off" configuration results in the venting of CO_2, an electricity price can be defined above which the additional revenue from selling more electricity at higher prices outweighs the costs incurred by additional CO_2 emissions. If a system is designed to capture CO_2 in an "off" configuration by utilizing solvent storage, the strategy for switching between an "on" and "off" configuration must be investigated at the design stage. Solvent storage capacity and stripper size will determine how long the stripper and CO_2 compressor may remain off, and this constrained "off" time will determine the length of time that a generator can benefit from high electricity prices. There is no added cost to emitting CO_2 in an "off" configuration using solvent storage,

but the added operational cost of running larger stripping/compression systems in the "on" position must be weighed against profits collected when the system is "off." Alternatively, different components of a CO_2 absorption/stripping system could be run at part load to allow variation in the amount of time that solvent storage is used. In this case, detailed attention must be paid to the load-efficiency relationships of CO_2 capture systems and other plant components. Another option is a system that is designed for an "off" configuration that stores solvent until maximum storage capacity is reached, after which CO_2 is vented to the atmosphere.

For proper analysis of the interactions between the values of CO_2 and electricity, the effect of CO_2 prices on electricity prices must be considered. In the ERCOT grid, the value of electricity at any time is typically determined by the least expensive available natural gas generator, because natural gas units are utilized almost exclusively to balance electricity demand and generation. Over the course of the day, as electricity demand increases, less efficient and higher emissions natural gas units must be brought online, meaning that the contribution of CO_2 emissions costs to total generation costs will increase in periods of higher demand. In ERCOT's current grid arrangement, implementation of CO_2 capture will add to this effect by requiring use of additional natural gas generation for base load. A graphical representation of the possible effect of CO_2 price on ERCOT balancing energy prices is shown in Figure 13 below.

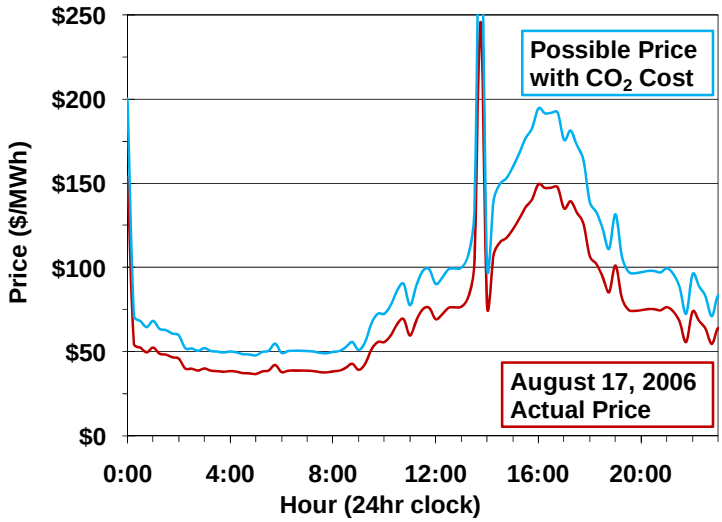

Figure 13: Possible effect of CO_2 emissions cost on ERCOT energy prices

Conclusions

A MATLAB model allows investigation of the impacts of widespread implementation of flexible CO_2 capture in the ERCOT grid. Flexible operation prevents the need to replace over 4400MW of capacity lost to the energy requirement of CO_2 capture, which saves several billion dollars in capital investment. Since the highest electricity demands occur very infrequently, a flexible CO_2 capture system is only required to be in the "off" configuration for a total of 99 hours in 2006, allowing system-wide CO_2 reductions of 52%. This emissions reduction is nearly the same as when CO_2 capture runs continuously at maximum design capacity. If a long system downtime requires CO_2 capture systems to remain off for the entire season of high system loads, CO_2 capture will remain off for 76 days between June 11 and August 26, but CO_2 is still reduced by 41% relative to emissions without CO_2 capture.

Average generation costs and CO_2 avoidance costs are not largely affected by flexible CO_2 capture. However, these costs will increase as CO_2 capture is used more often because of the higher cost of coal-fired generation with CO_2 capture and the increased use of expensive natural gas for base load generation when CO_2 capture is "on." Because the grid reserve margin specification is important for defining the threshold load above which CO_2 capture should be turned "off," a clear definition of this parameter will be important to ensure proper planning and operation of flexible CO_2 capture systems.

Future Work

The primary focus of future work in the near term will be modeling and characterizing the effects that the values of energy and CO_2 emissions have on the operation of flexible CO_2 capture systems. Venting CO_2 in the "off" configuration as well as continuous capture with solvent storage will be considered in these analyses. The goal of these efforts is to understand the performance, economic, and environmental tradeoffs associated with various flexible CO_2 capture configurations when real time variation in the electricity prices is used to determine strategies for flexible CO_2 capture operation.

Collaboration with S. Ziaii will allow refinement of model performance specifications and a more detailed characterization of CO_2 capture performance at the "on" and "off" operating points as well as transition behavior between the two configurations.

Once the above baseline analyses are completed, attention will focus towards more rigorous efforts to consider technical and policy based constraints on a flexible CO_2 capture system. A possible direction includes a more detailed consideration of the effects of multiple operating points on other power plant components. Efforts may also turn to more detailed grid modeling that considers geographical constraints and a realistic dispatch order based on individual plant characteristics. More policy focused work could investigate the issues surrounding logistical implementation of flexible CO_2 capture from the perspectives of electricity generators and electric grid operators.

References

(2007). 2006 State of the Market Report for the ERCOT Wholesale Electricity Markets, Potomac Economics, Ltd.

Bergerson JA & LB Lave (2007). "Baseload Coal Investment Decisions under Uncertain Carbon Legislation." Environ. Sci. Technol. **41**(10): 3431-3436.

Davidson RM (2007). Post-combustion carbon capture from coal fired plants – solvent scrubbing, IEA Clean Coal Centre.

ERCOT (2006). 2006 Annual Report.

IEA and NEA (2005). Projected Costs of Generating Electricity: 2005 Update. Paris, France, OECD.

Gibbins JR, RI Crane, et al. (2005). Maximising The Effectiveness of Post Combustions CO_2 Capture Systems. The Seventh International Conference on Greenhouse Gas Control Technologies: GHGT-7. ES Rubin, DW Keith & CF Gilboy. Vancouver, Canada, Oxford, UK. **I:** 139-146.

Katzer J, et. al. (2007). The Future of Coal: Options for a Carbon Constrained World. Cambridge, Massachusetts Institute of Technology.

Metz B, O Davidson, et.al. (2005). IPCC Special Report on CO_2 Capture and Storage.

NEI (2007). U.S. Electricity Production Costs and Components. u.s._electricity_production_costs_and_components.xls. Washington, D.C.

Rao AB & ES Rubin (2002). "A Technical, Economic, and Environmental Assessment of Amine-Based CO_2 Capture Technology for Power Plant Greenhouse Gas Control." Environ. Sci. Technol. **36**(20): 4467-4475.

Rao AB & ES Rubin (2006). "Identifying Cost-Effective CO_2 Control Levels for Amine-Based CO_2 Capture Systems." Ind. Eng. Chem. Res. **45**(8): 2421-2429.

USEIA (2007). Average Cost of Coal Delivered for Electricity Generation by State, Year-to-Date through October 2007 and 2006. epmxlfile4_10_b.xls, USDOE.

USEIA (2008). Texas Natural Gas Wellhead Price, USDOE.

USEPA (2007). Emissions & Generation Resource Integrated Database (eGRID). eGRID2006_Version_2_1.

USNETL (2007). Cost and Performance Baseline for Fossil Energy Plants. Bituminous Coal and Natural Gas to Electricity. J. M. Klara. **1**.

Oxidation-Reduction Potential and Thermal Degradation Experiments

Quarterly Report for January 1 – March 31, 2008

by Fred Closmann

Supported by the Luminant Carbon Management Program

and the

Industrial Associates Program for CO_2 Capture by Aqueous Absorption

Department of Chemical Engineering

The University of Texas at Austin

April 18, 2008

Abstract

In this quarter we performed oxidation-reduction potential (ORP) experiments on ROC16 solution at a loading of 0.4 moles CO_2/mol PZ. The ORP studies were performed to establish baseline ORP response in PZ solutions under quiescent conditions, and in the presence and absence of reactor agitation and sparging with oxygen and nitrogen. The absence of nitrogen sparging and/or reactor mixing delays ORP response following rapid shutdown of oxygen. When the reactor was brought from a quiescent state to an oxygenated state in rapid fashion, the recovery (increase) of ORP was delayed in the absence of reactor mixing. Thermal degradation of MDEA/PZ (7 m/2 m) occurs at 135°C, with more rapid degradation occurring at 150°C. Within two weeks, over 96% of PZ mass degraded in the presence of MDEA. MDEA and PZ may degrade in an equimolal relationship when thermally degraded as a blended solvent.

In the first quarter of 2008, experiments were performed to investigate the oxidation-reduction potential (ORP) of ROC16 solvent. Knowledge of ORP in this solvent will enable the group to better understand the potential for oxidative degradation of amines to occur in the absorption/stripping process. We also performed thermal degradation studies on an MDEA/PZ solvent blend at temperatures of 135°C and 150°C. The degradation studies were performed using Swagelok sample bombs in temperature-controlled ovens. Data tables are included with this report in Appendix A, and figures are included in Appendix B.

Oxidation-Reduction Potential (ORP) Measurements

ORP measurements in aqueous amine solutions were made with an off-the-shelf ORP probe (Accumet 13-620-81). This probe is a platinum Ag/AgCl combination electrode (with reference) designed for measurements of ORP in aqueous solutions, and was used in conjunction with an Altex 41 pH meter. ORP measurements were conducted following ASTM Method D1498-07 (Standard Test Method for Oxidation-Reduction

Potential of Water). Temperature was recorded during each experiment to allow for any corrections in ORP measurements needed (none were made). The electrode is stored in a dilute aqueous solution of Ag/AgCl as recommended by the manufacturer. Quinhydrone/water reference solutions of pH 4 and 7 were created and utilized each day that ORP measurements were collected on reactor solutions. The standards were used as described in the ASTM standard for checking instrument response prior to use each day. For the pH 4 solution at 25°C, the ORP reading should be 263 mV +/- 30 mV.

Reactor Set-up

A jacketed glass reactor with a nominal capacity of approximately 350 ml was used in this series of experiments. The jacket side of the reactor was fitted with flexible tubing to a Lauda E100 circulating temperature control water bath; jacket side temperature was set at 55°C. The reactor lid was fitted with rubber stoppers sized to allow entry of the ORP probe, thermometer, and a stainless steel line fitted with a sparge stone at the end with Swagelok fittings for submergence into the amine solvents being tested. The stainless steel line was plumbed to N_2 and O_2 gases supplies with Cole-Parmer rotameters in-line to measure and vary the amount of each gas supplied to the reactor during measurements. The reactor was stirred with a magnetic stir bar, and the glass reactor was placed directly on a magnetic stir plate.

Experimental Series

An aqueous ROC16 solution was formulated at a CO_2 loading of 0.3 m/m based on total alkalinity of amine. After the reactor was loaded and operated for several hours to establish a steady state condition and ORP response, a series of eleven experiments were performed on the 8 m PZ solution as described below.

(1) Reactor oxygen shut down – the reactor was brought to steady state conditions with mixing, O_2 and N_2 introduction, then the O_2 was shut down while mixing and sparging of N_2 was continued; ORP response was measured over time until new steady state conditions were achieved.

(2) Reactor O_2 and N_2 shut down – the reactor was brought to steady state conditions with mixing and oxygenation, then the O_2 and N_2 were shut down while mixing was continued; ORP response was measured over time until new steady state conditions was achieved.

(3) Reactor O_2, N_2, and mixing shut down – the reactor was brought to steady state conditions with mixing, O_2 and N_2 flow, then both gases and mixing were shut down in a rapid fashion; ORP response was measured over time until new steady state conditions were achieved.

(4) Reactor rapid start-up – the reactor was allowed to achieve quiescent conditions, then brought back to steady state conditions with the rapid introduction of mixing, and gases; ORP response was measured over time until new steady state conditions were achieved.

(5) Reactor rapid start-up – the reactor was allowed to achieve quiescent conditions, then brought back to steady state conditions with the rapid introduction of mixing, O_2, and N_2; ORP response was measured over time until new steady state conditions are achieved; (collected Sample No. 3A-4).

(6) Reactor rapid start-up – the reactor was allowed to achieve quiescent conditions, then brought back to steady state conditions with the rapid introduction of O_2 only (no mixing); ORP response was measured over time until new steady state conditions were achieved.

(7) Reactor rapid start-up – the reactor was allowed to achieve quiescent conditions, then brought back to steady state conditions with the rapid introduction of O_2 and mixing only (no N_2); ORP response was measured over time until new steady state conditions were achieved.

(8) Reactor rapid start-up (repeat of No. 7) – the reactor was allowed to achieve quiescent conditions, then brought back to steady state conditions with the rapid introduction of O_2 and mixing only (no N_2); ORP response was measured over time until new steady state conditions were achieved.

(9) Reactor rapid start-up – the reactor was allowed to achieve quiescent conditions, then brought back to steady state conditions with the rapid introduction of O_2, N_2, and mixing, but with a lower O_2 gas flow rate (<"10" on rotameter; q<8.4 mL/min); ORP response was measured over time until new steady state conditions were achieved.

(10) Reactor rapid start-up – the reactor was allowed to achieve quiescent conditions, then brought back to steady state conditions with the rapid introduction of mixing, O_2, and N_2; ORP response was measured over time until new steady state conditions were achieved; (collected Sample No. 3A-4); in this case, the ROC16 was augmented with NaO_3V at 0.01 mM.

(11) Reactor rapid start-up – the reactor was allowed to achieve quiescent conditions, then brought back to steady state conditions with the rapid introduction of mixing, O_2, and N_2; ORP response was measured over time until new steady state conditions were achieved; (collected Sample No. 3A-4); in this case, the ROC16 was augmented with NaO_3V at 0.1 mM.

Results - Oxidation-Reduction Potential

Data collected during the ORP studies are presented in Tables 1 through 11 (Appendix A) and Figures 1-11 (Appendix B), with the number in each figure/table series corresponding to each of the experiments described above.

As presented in 2007, the Experiment No. 1 ORP data indicate that a new steady state ORP in the solvent was reached 25 minutes after shutdown of oxygen (ORP of -290 mV), but with continued nitrogen sparging and mixing (stir bar) (Figure 1). Experiment No. 2 was conducted in the same fashion, with the exception that nitrogen was also shut down immediately, but mixing of the reactor continued. Very little change in ORP in the system was observed. The nitrogen sparging was then continued, resulting in an immediate reduction in solvent ORP starting at approximately 1800 seconds (30 minutes). A new steady state condition was reached at approximately 2150 seconds (36 minutes). Figure 3 is a plot of the data for Experiment 3 wherein both gases as well as mixing were rapidly shut down. The data indicate that the system was delayed in reaching the new steady state (more reduced) when compared to Figure 1, which represents the oxygen shutdown only experiment. These data suggest that the continued sparging of nitrogen in the solvent lowers the ORP by removing (stripping) oxygen.

Figures 4 through 8 present the data for rapid start-up experiments, conducted after the solvent ORP had remained at a steady state for an extended period of time. However, the experiment represented by data plotted in Figure 5 was shut down after approximately 40 minutes (2400 s), resulting in a drift downward in ORP from a high of -120 mV, to a new steady state at shutdown of approximately -220 mV. However, during Experiment No. 7, the stir bar was restarted approximately 33 minutes (2000 seconds) into the experiment, resulting in the downward trend in ORP to a new steady state with oxygen and mixing of approximately -185 mV. This observation reflects the agitation of the solvent system and resultant removal of oxygen; the quiescent solvent retains dissolved oxygen, thereby exhibiting a higher ORP.

Experiment No. 9 was conducted in a similar fashion to Experiment No. 4, with the exception that the oxygen sparge rate was reduced to one tenth of its original rate (<8.4 mL/min). The trendlines were similar, with a new steady state condition for ORP reached after approximately 1200 to 1500 seconds; for Experiment No. 4, this same steady state condition was reached in less than 300 seconds (5 minutes).

The effects on ORP of sodium metavanadate are not clear at this time. In both Experiment No. 10 and No. 11, a new steady state ORP condition was reached in less than 500 seconds, which compares favorably with the results of Experiment No. 4, conducted in the absence of sodium metavanadate. However, ORP did drift slightly downward after a period of time (250 and 900 seconds, respectively) in Experiments No. 10 and 11.

Thermal Degradation of MDEA/PZ

The results of thermal degradation studies performed on a 7 m/2 m MDEA/PZ solvent are presented in Table 12 and Figure 12. The data in Table 12 have been corrected for gravimetric dilutions. Those data indicate that after two weeks of degradation in 135°C and 150°C ovens, most of the PZ was degraded, with an equivalent amount of the MDEA also degraded. After two weeks at 150°C, over 96% of the PZ was degraded, which represents a loss of 2 moles of PZ/kg water (2 molal). The loss in PZ and MDEA was close to equimolal. In comparison, only 56% of the starting mass of PZ was degraded in the solvent blend held at 135°C. This PZ loss corresponded to approximately 1.1 moles of PZ/kg water (1.1 molal). The corresponding MDEA loss was approximately 1.3 moles/kg water (1.3 molal), indicating that a correlation in losses between the two amines in the thermally degraded samples may exist. The relationship between PZ and MDEA thermal degradation in the solvent blend will be investigated further in future studies.

Future Work

The ORP data reported herein will undergo a more rigorous analysis to determine predictive correlations between loading, amine concentrations, and ORP in solution, or to use ORP measurements as a parameter for measuring oxidation of solvent species and solution degradation in general. Follow-on ORP experiments will be performed with metals species (iron, cobalt, or nickel) in the solvent to determine whether catalytic effects exist with ORP.

Other work to be performed includes further investigation into possible polymerization activity in solution, as possibly evidenced by ROC20 solution augmented with copper in

2007. To date, the latest experiments have not exhibited polymerization, as evidenced by increased viscosity.

Additional thermal degradation studies will be performed on MDEA and MDEA/PZ solvents at temperatures of 100°C and 120°C. Experiments will be performed on these solutions at loadings of 0.1 through 0.3 moles/mol amine equiv. These experiments will enable the group to understand the lower limit in temperature tolerance of these amine solvents over practical loading ranges.

Appendix A - Tables

Experiment No. 1 – O_2 Shutdown		
Time (sec)	**ORP (mV)**	**Temp (°C)**
2	-136	54
16	-141	54
25	-145	54
35	-150	54
45	-157	54
55	-164	54
65	-170	54
80	-180	54
100	-192	54
120	-203	54
135	-211	54
150	-218	54
180	-231	54
210	-241	54
240	-249	54
300	-260	54
360	-268	54
420	-273	54
480	-277	54
540	-280	54
600	-283	54
720	-287	54
900	-291	54
1200	-295	54
1500	-298	54
1800	-298	54

Experiment No. 2 – O_2 and N_2 Shutdown		
Time (sec)	**ORP (mV)**	**Temp (°C)**
0	-116	53.5
10	-116	53.5
25	-114	53.5
40	-114	53.5
60	-114	53.5
90	-114	53.5
120	-114	53.5
180	-114	53.5
300	-115	53.5
600	-118	54
900	-120	54
1500	-125	54
1800	-127	54
1868	-150	54
1885	-165	54
1905	-175	54
1920	-183	54
1935	-191	54
1950	-197	54
1980	-208	54
2010	-215	54
2040	-219	54
2100	-225	54
2160	-227	54
2460	-220	54
2700	-213	54
3300	-203	54
3600	-199	54

Experiment No. 3 – Rapid Shutdown of N_2, O_2 and Stirring		
Time (sec)	**ORP (mV)**	**Temp (°C)**
0	-132	54
20	-120	54
30	-120	54
45	-120	54
60	-122	54
180	-122	54
240	-124	54
300	-124	54
420	-125	54
540	-125	54
720	-126	53
900	-127	53
1080	-129	53
1410	-134	53
1560	-137	53
1800	-143	53
2160	-153	53
2520	-164	53
2880	-178	53
3240	-193	53
3600	-205	53
4200	-221	53
4700	-220	53
4800	-220	53
5100	-220	52.5

Experiment No. 4 – Rapid Start-up of N_2, O_2, and Stirring		
Time (sec)	**ORP (mV)**	**Temp (°C)**
0	-294	52
5	-290	52.5
10	-260	52.5
15	-213	52.5
20	-196	52.5
30	-173	52.5
45	-155	52.5
60	-148	52.5
90	-144	52.5
120	-141	52.5
150	-140	52.5
180	-139	52.5
210	-138	52.5
240	-137	52.5
300	-137	52.5
360	-136	52.5
480	-134	52.5
600	-132	52.5
900	-126	52.5
1200	-121	52.5
1800	-119	52.5

Experiment No. 5 – Rapid Start-up of N_2, O_2, and Stirring		
Time (sec)	**ORP (mV)**	**Temp (°C)**
0	-294	53
5	-258	53
10	-224	53
20	-178	53
30	-164	53
45	-155	53
60	-151	53
75	-148	53
90	-147	53
105	-146	53
120	-146	53
135	-145	53
150	-144	53
165	-144	53
180	-142	53
210	-142	53
240	-140	53
300	-137	53.5
360	-135	53.5
480	-131	53.5
600	-129	54
720	-127	54
900	-125	54
1200	-122	54
1800	-119	54
2400	-117	54
2520	-118	54
2700	-121	53.5
3000	-125	53
3660	-137	53
4200	-149	53
4800	-165	53
5400	-184	53
6600	-206	52.5
7200	-207	52.5
7220	-212	53
7235	-212	53

Experiment No. 6 – Rapid Start-up of O_2 only		
Time (sec)	**ORP (mV)**	**Temp (°C)**
0	-214	53
5	-216	53
10	-212	53
20	-190	53
30	-178	53
45	-164	53
60	-154	53
75	-149	53
90	-145	53
120	-139	53
150	-135	53
180	-132	53
210	-130	53
240	-128	53
300	-126	53
360	-124	53
480	-122	53
600	-122	53
900	-120	53
1200	-119	53
1800	-114	53
2400	-105	53
3000	-100	53
3600	-99	53

Experiment No. 7 – Rapid Start-up of O_2 and mixing only		
Time (sec)	**ORP (mV)**	**Temp (°C)**
0	-230	53
10	-203	53
15	-194	53
20	-182	53
30	-170	53
45	-158	53
70	-141	53
75	-139	53
90	-134	53
120	-130	53
150	-129	53
180	-128	53
210	-127	53
270	-125	53.5
360	-122	54
660	-114	54
900	-106	54
1200	-99	54
1500	-96	54
1800	-95	54
1860	-94	54
1980	-94	54
2100	-96	54
2400	-99	54
3000	-106	54
3960	-119	54
4500	-128	54
5100	-138	54
7000	-168	54
9000	-163	54
9540	-182	54
9900	-185	54
10200	-185	53

Experiment No. 8 – Rapid Start-up of O_2 and mixing only		
Time (sec)	**ORP (mV)**	**Temp (°C)**
0	-184	53
10	-160	53
20	-149	53
30	-138	53
45	-132	53
60	-130	53
75	-128	53.5
90	-128	53.5
120	-127	53.5
180	-127	53.5
300	-126	53.5
420	-125	53.5
600	-124	54
900	-121	54
1200	-118	54
1800	-100	54
2700	-98	54

Experiment No. 9 - Rapid Start-up of N_2, O_2, and Stirring (O_2 set at <10 rotameter settting)		
Time (sec)	**ORP (mV)**	**Temp (°C)**
0	-197	53
10	-171	53
20	-166	53
30	-160	53
45	-151	53
60	-143	53
75	-137	53
90	-134	53
120	-130	53.5
150	-127	53.5
180	-124	53.5
240	-120	54
300	-114	54
360	-110	43
480	-105	43
600	-102	54
720	-100	54
900	-98	54
1200	-96	54
1500	-96	54
1800	-96	54

Experiment No. 10 – Rapid Start-up of N_2, O_2, and Stirring w/ 0.01 mM NaO_3V		
Time (sec)	**ORP (mV)**	**Temp (°C)**
0	-193	53
5	-157	53
10	-148	53
20	-142	53
30	-140	53
45	-139	53
60	-139	53
75	-139	53
90	-138	53
120	-137	53
150	-136	53
180	-136	53
270	-137	53.5
360	-138	54
480	-140	54
600	-141	54
720	-141	54
900	-142	54
1200	-144	54
1500	-145	54
1800	-145	54

Experiment No. 11 – Rapid Start-up of N_2, O_2, and Stirring w/ 0.1 mM NaO_3V		
Time (sec)	**ORP (mV)**	**Temp (°C)**
0	-176	53
0	-162	53
10	-154	53
20	-150	53
30	-147	53
45	-146	53
60	-145	53
90	-144	53
120	-144	53
120	-144	53.5
150	-144	53.5
180	-143	53.5
240	-142	53.5
300	-142	53.5
420	-141	53.5
600	-141	54
900	-141	54
1200	-144	54
1920	-144	54

Table 12 - Thermal Degradation of MDEA/PZ

Time	MDEA			PZ		
(Days)	**Undegraded**	**135°C**	**150°C**	**Undegraded**	**135°C**	**150°C**
0	7.00	7.00	7.00	2.00	2.00	2.00
3	7.22	6.79	6.20	2.06	1.90	1.22
9	7.00	6.23	5.28	1.93	1.20	0.18
11	8.22	5.99	4.94	2.50	1.01	0.06
14	6.89	5.72	5.70	1.95	0.88	0.07

Appendix B - Figures

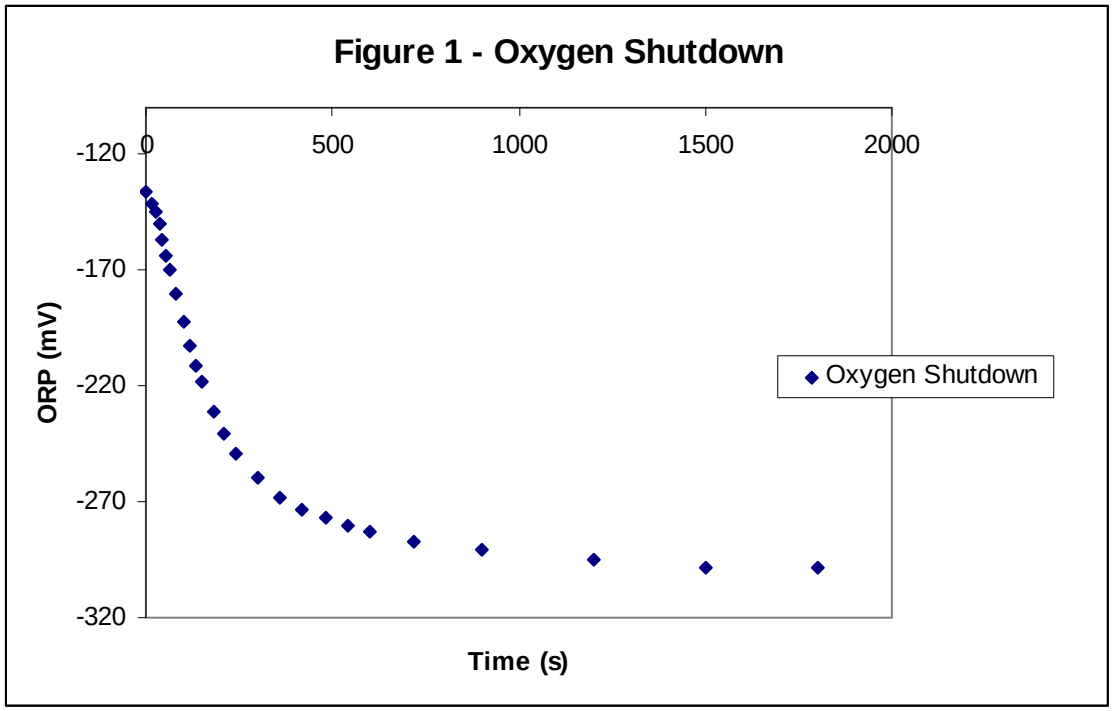

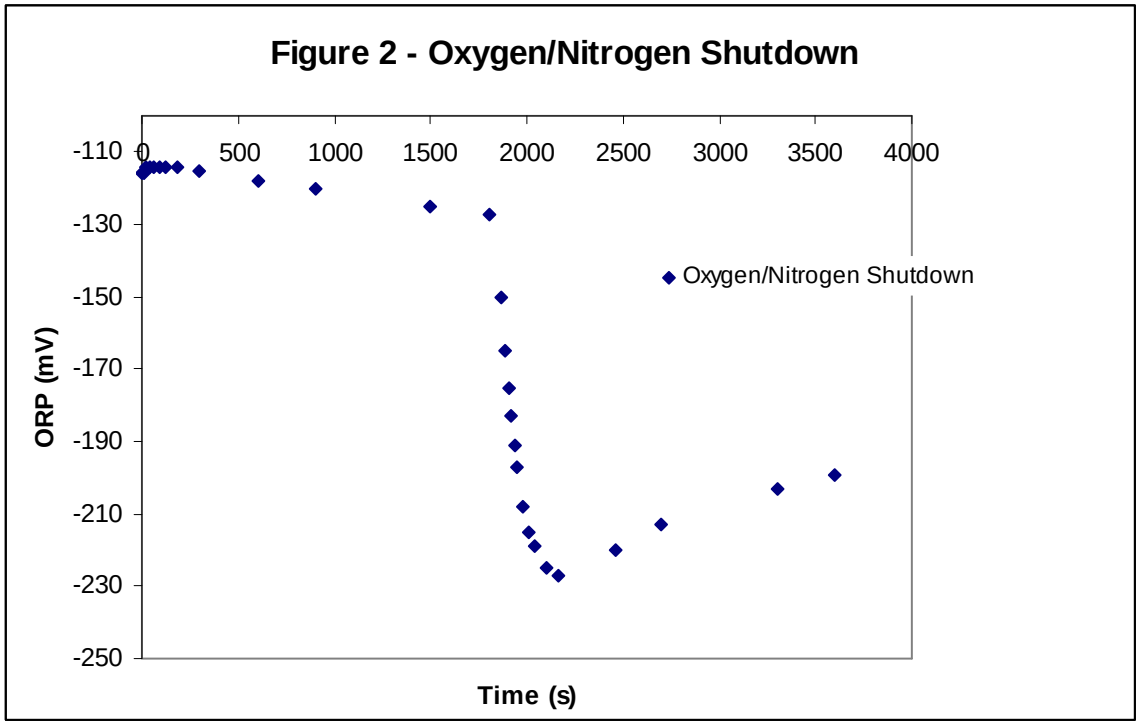

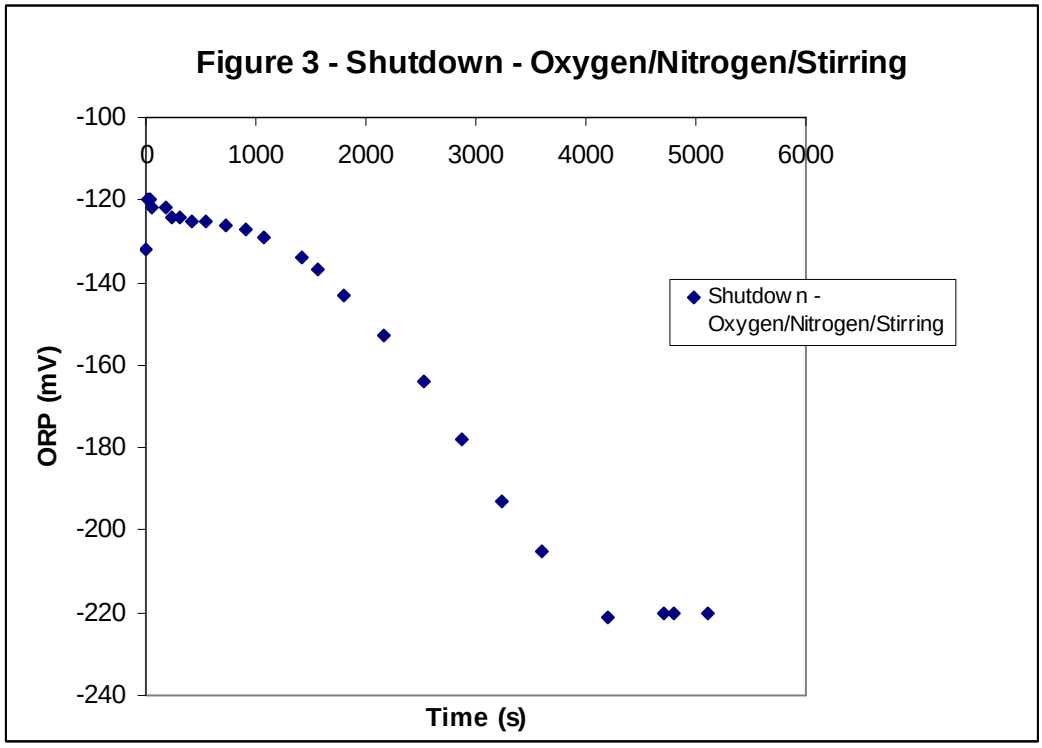
Figure 3 - Shutdown - Oxygen/Nitrogen/Stirring
-100
-120
-140
-160
-180
-200
-220
-240
0
1000
2000
3000
4000
5000
6000
ORP (mV)
Time (s)
Shutdow n - Oxygen/Nitrogen/Stirring

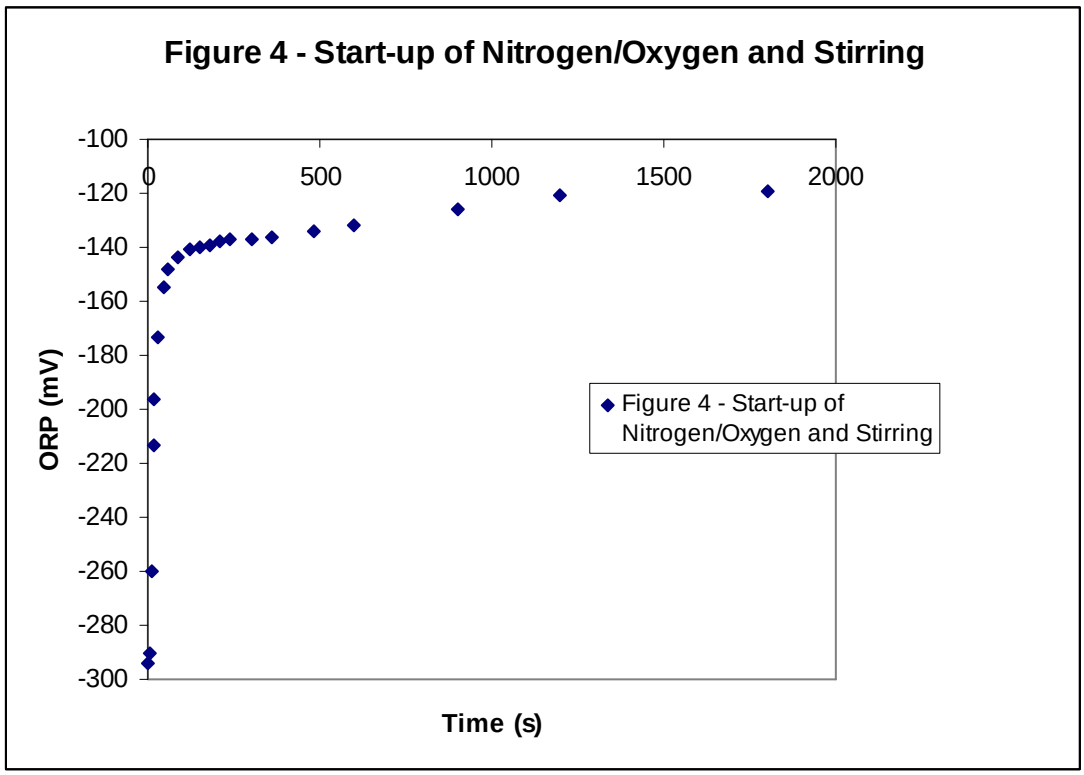
Figure 4 - Start-up of Nitrogen/Oxygen and Stirring
-100
-120
-140
-160
-180
-200
-220
-240
-260
-280
-300
0
500
1000
1500
2000
ORP (mV)
Time (s)
Figure 4 - Start-up of Nitrogen/Oxygen and Stirring

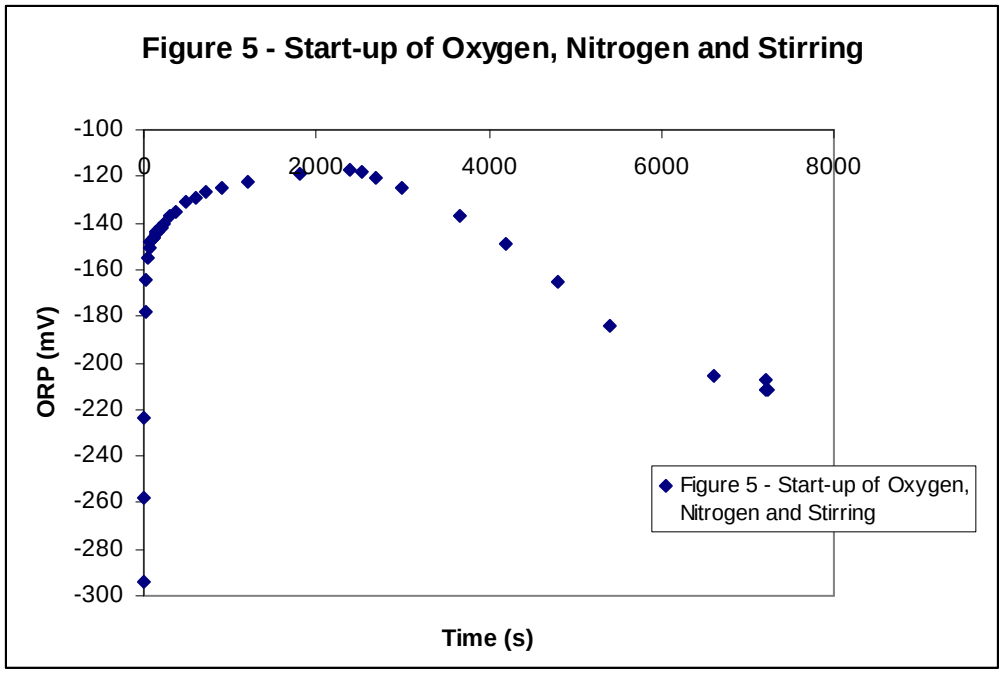
Figure 5 - Start-up of Oxygen, Nitrogen and Stirring
-100
-120
-140
-160
-180
-200
-220
-240
-260
-280
-300
0
2000
4000
6000
8000
ORP (mV)
Time (s)
Figure 5 - Start-up of Oxygen, Nitrogen and Stirring

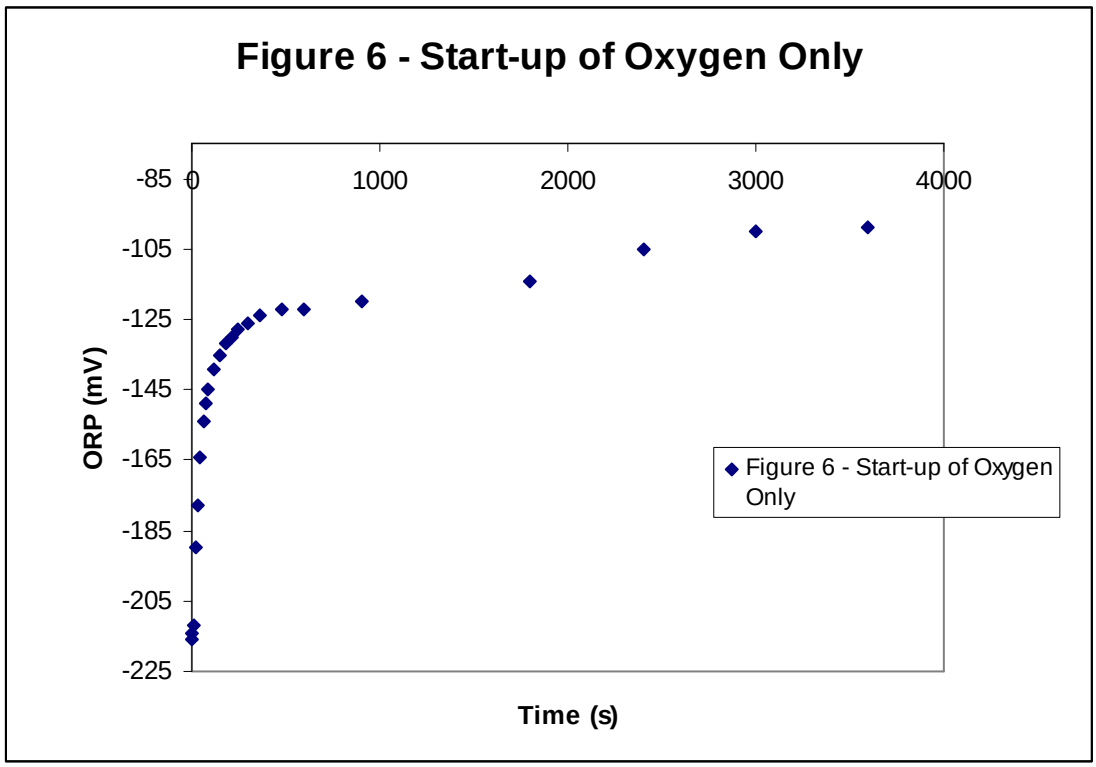
Figure 6 - Start-up of Oxygen Only
-85
-105
-125
-145
-165
-185
-205
-225
0
1000
2000
3000
4000
ORP (mV)
Time (s)
Figure 6 - Start-up of Oxygen Only

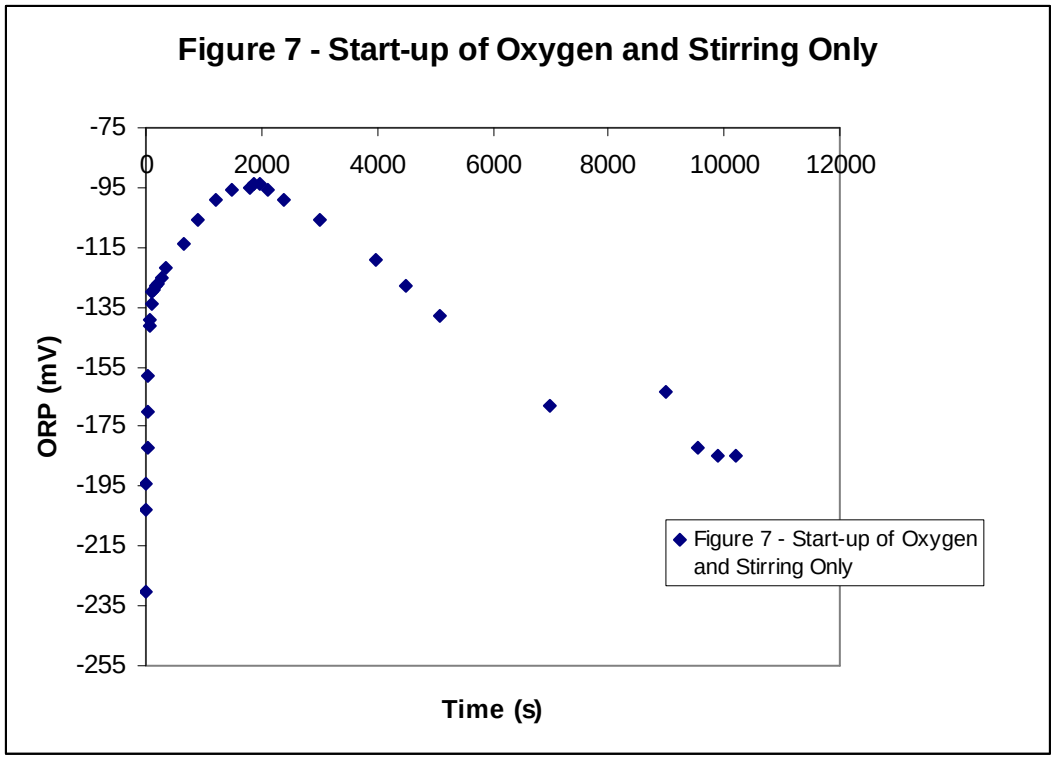
Figure 7 - Start-up of Oxygen and Stirring Only
-75
-95
-115
-135
-155
-175
-195
-215
-235
-255
0
2000
4000
6000
8000
10000
12000
ORP (mV)
Time (s)
Figure 7 - Start-up of Oxygen and Stirring Only

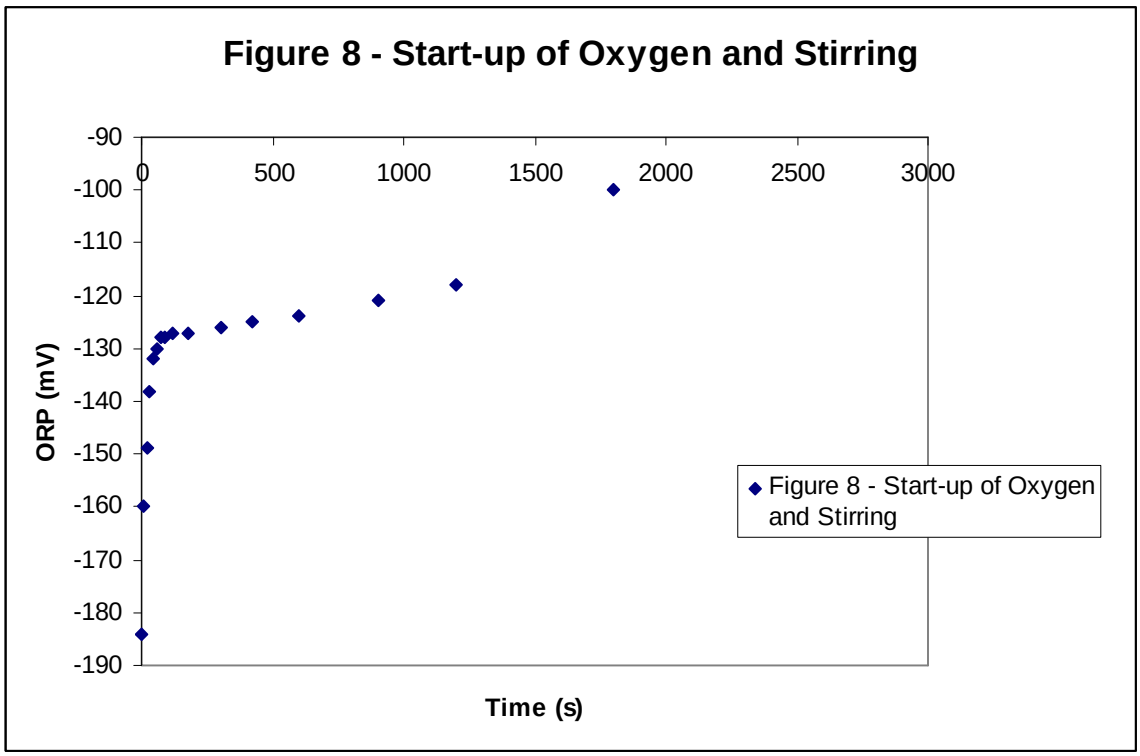
Figure 8 - Start-up of Oxygen and Stirring
-90
-100
-110
-120
-130
-140
-150
-160
-170
-180
-190
0
500
1000
1500
2000
2500
3000
ORP (mV)
Time (s)
Figure 8 - Start-up of Oxygen and Stirring

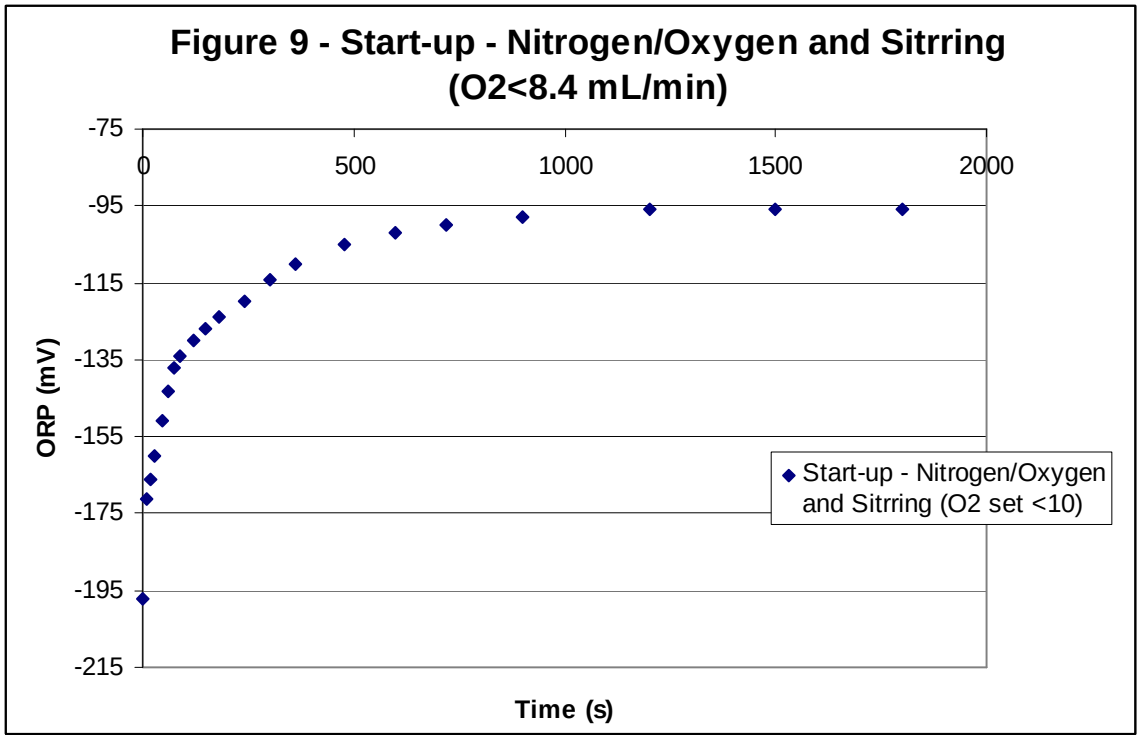
Figure 9 - Start-up - Nitrogen/Oxygen and Sitrring (O2<8.4 mL/min)
-75
-95
-115
-135
-155
-175
-195
-215
0
500
1000
1500
2000
ORP (mV)
Time (s)
Start-up - Nitrogen/Oxygen and Sitrring (O2 set <10)

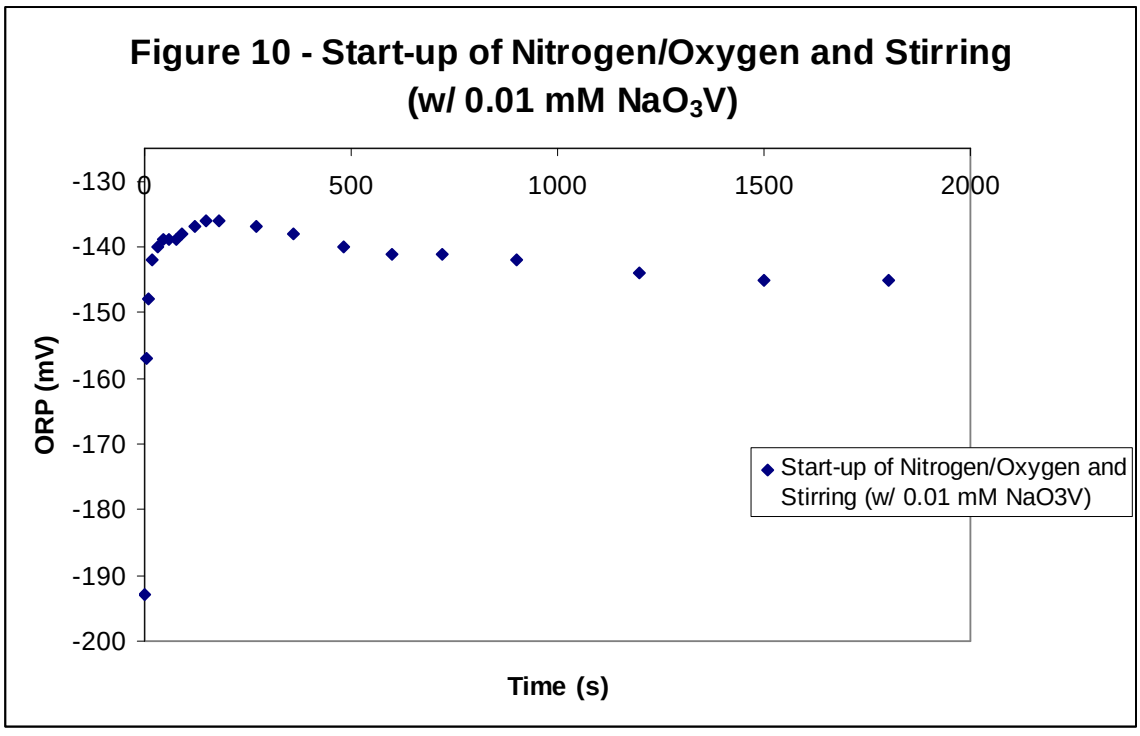
Figure 10 - Start-up of Nitrogen/Oxygen and Stirring (w/ 0.01 mM NaO3V)
-130
-140
-150
-160
-170
-180
-190
-200
0
500
1000
1500
2000
ORP (mV)
Time (s)
Start-up of Nitrogen/Oxygen and Stirring (w/ 0.01 mM NaO3V)

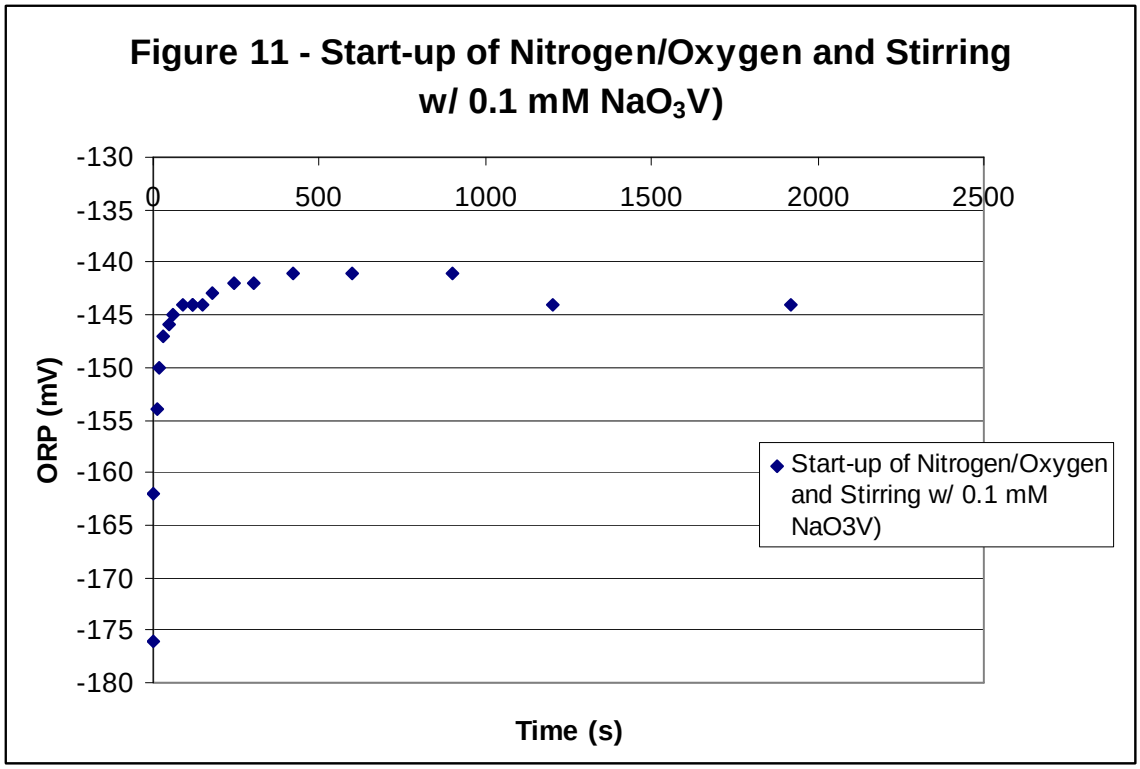
Figure 11 - Start-up of Nitrogen/Oxygen and Stirring w/ 0.1 mM NaO3V)
-130
-135
-140
-145
-150
-155
-160
-165
-170
-175
-180
0
500
1000
1500
2000
2500
ORP (mV)
Time (s)
Start-up of Nitrogen/Oxygen and Stirring w/ 0.1 mM NaO3V)

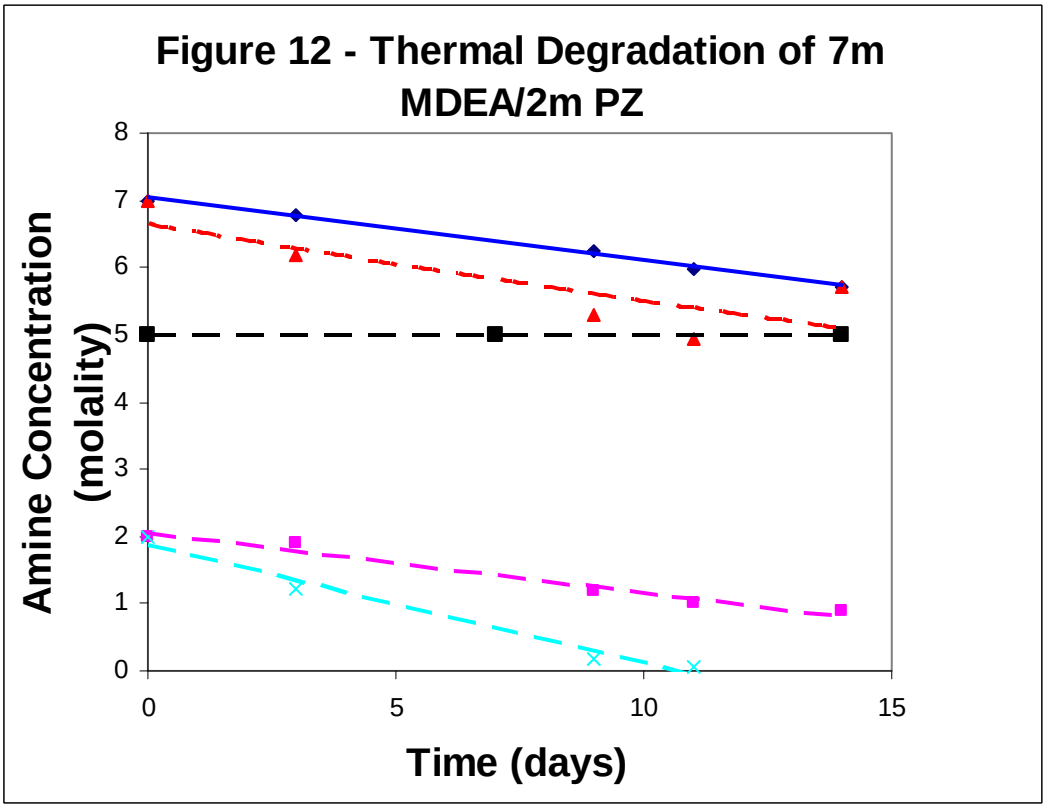
Figure 12 - Thermal Degradation of 7m MDEA/2m PZ
Amine Concentration (molality)
8
7
6
5
4
3
2
1
0
0
5
10
15
Time (days)